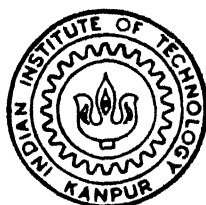


**NMR STUDIES OF LECITHIN AND DEOXYCHOLATE
REVERSE MICELLES AND CONSTRUCTION OF A VERSATILE
MAGNETIC FIELD GRADIENT CONTROLLER**

By

V. GOVINDARAJU



DEPARTMENT OF CHEMISTRY

INDIAN INSTITUTE OF TECHNOLOGY KANPUR

FEBRUARY, 1993

TH
543.0877
G7477
CHM
1993
D
Gov
NMR

**NMR STUDIES OF LECITHIN AND DEOXYCHOLATE
REVERSE MICELLES AND CONSTRUCTION OF A VERSATILE
MAGNETIC FIELD GRADIENT CONTROLLER**

A thesis Submitted
in Partial Fulfilment of the Requirements
for the Degree of
DOCTOR OF PHILOSOPHY

by
V. GOVINDARAJU

to the
**DEPARTMENT OF CHEMISTRY
INDIAN INSTITUTE OF TECHNOLOGY KANPUR**

February, 1993

1 3 JUN 1994 /chem
CENTRAL LIBRARY
I I T, KANPUR

Ser. No. A. 117871

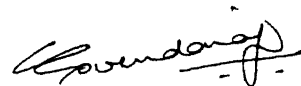
6/2/94

Dedicated
to
My Parents

STATEMENT

I hereby declare that the work embodied in this thesis entitled, 'NMR STUDIES OF LECITHIN AND DEOXYCHOLATE REVERSE MICELLES AND CONSTRUCTION OF A VERSATILE MAGNETIC FIELD GRADIENT CONTROLLER' is the result of investigations carried out by me in the Department of Chemistry, Indian Institute of Technology Kanpur, India, under the supervision of Professor P. Raghunathan.

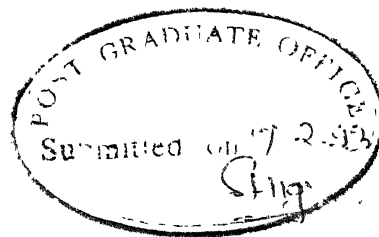
In keeping with scientific tradition, wherever work done by others has been utilized, due acknowledgement has been made.



V. Govindaraju

Kanpur


February, 1993



ii

CERTIFICATE I

Certified that the work presented in this thesis entitled, 'NMR STUDIES OF LECITHIN AND DEOXYCHOLATE REVERSE MICELLES AND CONSTRUCTION OF A VERSATILE MAGNETIC FIELD GRADIENT CONTROLLER' by *Mr. V. Govindaraju* has been carried out under my supervision and has not been submitted elsewhere for a degree.


(Professor P. Raghunathan)
Thesis Supervisor
Department of Chemistry
I.I.T. Kanpur

Kanpur
February, 1993

DEPARTMENT OF CHEMISTRY
INDIAN INSTITUTE OF TECHNOLOGY KANPUR, INDIA

CERTIFICATE II

This is to certify that Mr. V. Govindaraju has satisfactorily completed all the courses required for the Ph.D. degree program. The courses include :

Chm 505	Principles of Organic Chemistry
Chm 521	Chemical Binding
Chm 524	Modern Physical Methods in Chemistry
Chm 525	Principles of Physical Chemistry
Chm 545	Principles of Inorganic Chemistry
Chm 526	Solid State Chemistry
Chm 534	Symmetry and Molecular Structure
Chm 800	General Seminar
Chm 801	Special Seminar
Chm 900	Ph.D. Thesis

Mr. V. Govindaraju was admitted to the candidacy for the Ph.D. degree in February 20, 1987 after he successfully completed the written and oral qualifying examinations.



(Prof. P.K. Ghosh)
Head
Department of Chemistry
I.I.T. Kanpur



(Prof. Y.D. Vankar)
Convener
Departmental Postgraduate Committee
I.I.T. Kanpur

ACKNOWLEDGEMENTS

It is a great pleasure to express my gratitude to Prof.P. Raghunathan who introduced me to the area of magnetic resonance in general and NMR in particular. My close association with him for past several years has helped me to shape my attitudes towards academic as well as non academic issues. Without his inspiring guidance, constant encouragement and many stimulating discussions that I have had with him, I would not have imagined the successful completion of this work. I shall remember his excellent cooperation extended to me during the preparation of this thesis.

I am deeply indebted to Prof. N. Sathyamurthy who guided me as Programme Advisor towards the completion of this thesis after Prof. Raghunathan's deputation to AIIMS, New Delhi.

I am very much thankful to Mr.Arun Bhavsar who has helped me at innumerable stages of Chapter V work, many times at odd hours. His knowledge and experience in electronics and NMR instrumentation have been indispensable to me.

I humbly express my sincere thanks to Prof.S. Subramanian, RSIC, IIT, Madras and Dr.Raja Roy, RSIC, CDRI, Lucknow for allowing me to utilize their NMR facilities whenever I needed them for my experimental work.

My association with the colleagues in the laboratory will remain unforgettable. This includes Drs. Narasimha Reddy, S.C.Sivasubramanian, A.Ramamoorthy, A.K.Dubey and S.S.Ray ; also Messrs U.Ilangovan and A.Kasi Viswanathan.

I would like to thank a number of individuals who have been helpful and encouraging during the long, seemingly endless, process of writing this thesis. Many friends and colleagues were kind to proof read many incarnations of typed version of this thesis material and offer advice as well as point out errors. I would like to thank the following : U.Ilangovan, A.Kasi Viswanathan, Immanuvel Selvaraj, K.Srinivasan, 'Malayala' Tamilarasu and Murali.

I also thank and appreciate Mr. Bhagwat Prasad Pant for the neat and efficient typing and Mr. Gouri Singh Thapa for the careful drawings of figures.

Finally, I respectfully thank my parents who have sweat out in farming work to educate me. I also place on record the encouragement and constant support provided by my parents, grand parents and my brothers to pursue higher studies.

V. Govindaraju

SYNOPSIS

Reverse micelles are the aggregates of amphipathic molecules such as synthetic surfactants and phospholipids in nonpolar media. These aggregates are capable of solubilizing large amounts of water in their polar interior, which is then called a 'water pool'. The surfactants are located only at the interface, with their polar head-groups directed towards the water pool and their tails sticking out into the nonpolar continuous phase. Such structures have received much attention in recent years as they constitute suitable working models for exploring physico-chemical properties of cell membranes, and also because of the potential use of the water pool as a microreactor for many enzymatic and nonenzymatic reactions.

The surfactant chosen for the work embodied in this thesis is lecithin (phosphatidylcholine or PC) - one of the most commonly found glycerophospholipids which constitutes the bulk of the phospholipid content in animal cell and bacterial membranes. Reverse micelles of PC have been formed with cyclohexane and carbon tetrachloride(CCl_4) as two typical nonpolar media. In the first part of this work, attention has been mainly focused on a variety of NMR studies of the pool water and the polar head-groups⁺ ($-\text{N}(\text{CH}_3)_3$ and phosphate) of lecithin. In the second part, the design and construction of a versatile magnetic field gradient controller (MFGC) is reported for making NMR measurements.

In Chapter I, the present state-of-the-art pertaining to research in phospholipid reverse micelles is presented.

In Chapter II, we report a new lecithin-based reverse micelle with dicyclohexyl carbodiimide (DCC), a popular 'peptide condensing agent', as co-surfactant. Systematic water uptake of this reverse micelle at the chosen molar ratio of 5 : 1 of PC to DCC in cyclohexane shows that a maximum of 15.8 moles of water can be solubilized per mole of PC. Based on ^1H and ^{31}P NMR chemical shift studies, a suitable model is proposed for the interaction of water with the polar heads of lecithin and DCC. Water proton T_1 's recorded as a function of water addition are analyzed theoretically with the help of the well-known Bloembergen- Purcell- Pound model, and a rationalization is made of the rotational correlation time (τ_c) and microviscosity (η) of water calculated from our experiments. The water proton T_2 measured from the experimental spectral linewidth is analyzed theoretically assuming that only dipole-dipole relaxation is dominant. A suitable explanation is also given for the observation of a contrasting trend in the ^{31}P T_1 values observed for this reverse micelle.

Chapter III describes our studies of intramolecular water dynamics and exchange of water between two different types of sites ('bound' and 'free') through deuterium magnetic resonance (DMR) spectroscopy. For these studies we have used the PC/DCC/cyclohexane with D_2O in place of H_2O , as well as its non-DCC counterpart for comparison, and have performed our experiments at two different temperatures (263 K and 296 K). Also presented in this chapter are (i) a general DMR theory, (ii) a very brief quantum mechanical background for calculating nuclear spin systems' response to radio-frequency (rf) pulse(s) and to the

quadrupolar echo pulse sequence used for recording DMR spectra, and (iii) a computational method used for simulating experimental spectra. The two-line DMR spectrum observed in both the reverse micellar systems at all D_2O concentrations is correctly assigned. Our computed lineshape fittings show that the exchange rates of water between the 'bound' and 'free' sites are nearly 10^3 times less at 263 K than at 296 K, the T_2 values of 'bound' water being 10^2 times less than those of 'free' water. Interesting results obtained from both the reverse micellar systems at 263 K are also discussed. A tentative conclusion is drawn at the end of this chapter about water 'freezing over' at one of these sites at 263 K, in comparison with analogous hydration studies of lipid head-groups.

Chapter IV briefly reviews a recent technique for using the one-dimensional analog of a 2-D proton multiple quantum (MQ) filtered correlation spectroscopy for observing 'forbidden' cross peaks and extracting therefrom some useful cross-relaxation effects among coupled nuclear spins in a molecular aggregate. We have shown that, by fitting the MQ-filtered profiles of forbidden peak-intensities versus evolution time to our theoretical equations, valuable structural and dynamical parameters can be obtained for a specific molecular group in a macromolecule. However, calculations of the theoretical response for a group as large as the $-N(CH_3)_3$ (which is a coupled A_9 case) turn out to be too complicated, as shown in this chapter. This has constrained us to use the simpler, well-studied sodium deoxycholate (DOC) as a surfactant for forming reverse micelles. The results of our zero- and double-quantum filtered 1-D experiments of this reverse

micelle have been interpreted using a suitable motional model for the $-\text{CH}_3$ group of the DOC molecule, which provides a good illustrative support for the theory developed in this chapter.

Chapter V comprises work on instrumentation development. In the first part of this chapter, we review the different types of the magnetic field gradients (MFG) and the methods for generating them. The design of a versatile magnetic field gradient controller, adapted from the work of Fitzsimmons [Rev.Sci. Instrum. 53, 1338 (1982)], with detailed circuit diagrams and performance results for two types of applied MFG, are given. The improved features of our magnetic field gradient controller over those of Fitzsimmons' are summarized. In the second part of this chapter, the results of our experimental measurements of the self-diffusion coefficient (D) of 'pool' water in two reverse micellar systems (PC/cyclohexane/ H_2O and $\text{PC}/\text{CCl}_4/\text{H}_2\text{O}$) using a commercial NMR equipment are presented. The D -value trends for the 'pool' water trapped in these reverse micelles substantiate some earlier findings of our laboratory.

In Chapter VI we summarize the results of this thesis, and suggest some further work which should be done on phospholipid-based reverse micelles for an enhanced understanding of these fascinating molecular assemblies.

The Appendix contains a listing of our FORTRAN 77 program which simulates the experimental DMR lineshape discussed in Chapter III.

LIST OF CONTENTS

	Page
STATEMENT	i
CERTIFICATE I	ii
CERTIFICATE II	iii
ACKNOWLEDGEMENTS	iv
SYNOPSIS	v
LIST OF FIGURES	xiii
LIST OF TABLES	xx
CHAPTER I	
GENERAL INTRODUCTION	1
I.1	Reverse Micelles 1
I.2	Phospholipids : Source and Structure 2
I.3	Lipid Polymorphism 6
I.4	Existence of Reverse Micellar Structures in Biological Membranes 6
I.5	Thermodynamics and Phase Diagrams 8
I.6	Reverse Micellar 'Water Pool' 11
I.7	Experimental Methods Used to Probe Reverse micelles 13
REFERENCES	26
CHAPTER II	
PREPARATION AND ^1H AND ^{31}P NMR STUDIES OF A NEW REVERSE MICELLE, LECITHIN/DCC/CYCLOHEXANE/ H_2O	35
II.1	Introduction 35
II.2	Experimental Details 36
II.2.1	Materials used 36
II.2.2	Maximum Water Uptake Measurement 37

II.2.3	NMR Studies	39
II.3	Results and Discussion	40
II.4	Conclusions	65
	REFERENCES	67
CHAPTER III	DEUTERIUM NMR LINESHAPE ANALYSIS OF REVERSE MICELLAR POOL WATER	69
III.1	Introduction	69
III.2	DMR Spectroscopy	70
III.2.1	General Theory	70
III.2.2	DMR in D ₂ O	72
III.2.3	System Response to the Quadrupolar Echo Sequence	73
III.2.4	Theoretical Background	73
III.3	DMR Measurements	85
III.3.1	Solid Echo or Quadrupolar Echo Pulse Sequence	85
III.3.2	Quadrupolar Echo Pulse Sequence and the Spin System's Response	86
III.3.3	Computational Method For Lineshape Calculation	90
III.4	Results and Discussion	97
III.5	Conclusions	122
	REFERENCES	124
CHAPTER IV	PROTON MULTIPLE QUANTUM RELAXATION OF A DEOXYCHOLATE METHYL GROUP IN REVERSE MICELLE	128
IV.1	Introduction	128
IV.2	Cross-relaxation Times	129
IV.3	Extraction of Cross-correlation Spectral Density Terms Using Multiple Quantum NMR	133
IV.4	The A ₉ Spin System (e.g. : the -N (CH ₃) ₃ Head group) : Derivation of Pure State Basis Functions and Demonstration of Difficulties in Mathematical Tractability	145

IV.5	Studies on the Deoxycholate (DOC) Reverse Micelles	146
IV.5.1	Experimental Details	146
IV.5.2	Results and Discussion	148
IV.6	Conclusions	157
	REFERENCES	158
CHAPTER V	CONSTRUCTION OF A VERSATILE MAGNETIC FIELD GRADIENT CONTROLLER AND STUDY OF SELF-DIFFUSION OF MICELLAR WATER	160
V.1	Introduction	160
V.2	Types of Magnetic Field Gradient Circuits : A Survey	162
V.2.1	Linear Magnetic Field Gradients	162
V.2.2	Switched or Pulsed Linear Magnetic Field Gradients	163
V.2.3	Oscillating or Time-varying Gradients	164
V.3	Construction of a Versatile Magnetic Field Gradient Controller	166
V.3.1	Design Logic	169
V.3.2	Digital Oscillator and DC Reference	169
V.3.3	Computer Interface and Manual Switch to Gradient Controller	178
V.3.4	Circuit Generating Complementary Outputs	180
V.3.5	Switch circuit for Pulsed Linear Magnetic Field Gradient Generation	183
V.3.6	Current Driver Circuit	183
V.3.7	Display Circuit	185
V.3.8	Position of Switches for mode(μ P/Manual) and Sine wave/DC Selection	187
V.4	Details of the Microprocessor and Its Use in Gradient control	187
V.4.1	Description of the Microprocessor	187
V.4.2	Reset and Position/DC-Magnitude Pulses and Gate Control Generation	191

V.4.3	Generation of Switch Control for Pulsed Magnetic field Gradient (PMFG) Spin Echo Experiment	195
V.5	Highlights of our Gradient Controller Circuit	195
V.6	Details of Experimental Setup and Performance Result	199
V.7	Self-Diffusion Coefficient Measurement on the Lecithin Reverse Micellar 'Pool Water'	205
V.7.1	Motivation	205
V.7.2	The Nuclear Spin Echo Method	208
V.7.3	Water Diffusion in Anisotropic Environment	215
V.7.4	Experimental Details	217
V.7.5	Results and Discussion	218
V.8	Conclusions	229
	REFERENCES	230
CHAPTER VI	OVERALL CONCLUSIONS AND FURTHER PROSPECTS	236
APPENDIX		238

LIST OF FIGURES

		Page
Fig.1.1	The Singer and Nicholson 'fluid mosaic' model of a biomembrane.	4
Fig.1.2	General Chemical structure of sphingophospholipids (a) glycerophospholipids (b) main classes of glycerophospholipids with their common names (c).	5
Fig.1.3	The metamorphic mosaic model of biological membranes.	9
Fig.1.4	Approximate frequency ranges of various spectroscopic techniques and molecular motions of lipids.	16
Fig.II.1	Schematic representation of the structure of lecithin/DCC/cyclohexane/ water reverse micelle.	38
Fig.II.2	80 MHz proton NMR spectrum of lecithin and DCC in cyclohexane.	42
Fig.II.3	80 MHz proton NMR spectrum of lecithin/DCC/ cyclohexane/water at R = 5.	43
Fig.II.4	^1H NMR chemical shifts of water protons in lecithin/DCC/cyclohexane/ H_2O as a function of R.	44
Fig.II.5	^1H NMR chemical shifts of $-\text{N}(\text{CH}_3)_3^+$ protons in lecithin/ DCC/ cyclohexane/ H_2O as a function of R.	45
Fig.II.6	^{31}P NMR chemical shifts of the head group phosphate in lecithin/DCC/cyclohexane/ H_2O as a function of R.	47
Fig.II.7	Structure of folded polar head group of Lecithin.	49
Fig.II.8	Interaction of water with the polar head group of Lecithin.	50
Fig.II.9	Variation in T_1 of water protons as a function of R.	53

Fig.II.10	Variation in T_1 of $-\overset{+}{N}(\text{CH}_3)_3$ protons as a function of R.	58
Fig.II.11	Variation in T_2 of water protons as a function of R.	59
Fig.II.12	Variation in ^{31}P NMR linewidth of lecithin head group in the reverse micelle as a function of R.	62
Fig.II.13	Variation in ^{31}P NMR T_1 values of lecithin head group in the reverse micelle as a function of R.	63
Fig.III.1	Energy levels (a) and DMR spectra corresponding to single crystals (b) of a spin $I = 1$ system (and) at two different motional states ((c) and (d))	74
Fig.III.2	Quadrupolar Echo Pulse Sequence	87
Fig.III.3	Two types of water sites in a typical reverse micelle	93
Fig.III.4	^2D -NMR spectra (left) and best-fitting simulations (right) for PC/Cyclohexane/ D_2O at 296 K; (a) $R = 1$ and (b) $R = 3$.	99
Fig.III.5	^2D -NMR spectra (left) and best-fitting simulations (right) for PC/Cyclohexane/ D_2O at 296 K; (a) $R = 5$ and (b) $R = 6$.	100
Fig.III.6	^2D -NMR spectra (left) and best-fitting simulations (right) for PC/Cyclohexane/ D_2O at 296 K; (a) $R = 8$ and (b) $R = 10$.	101
Fig.III.7	^2D -NMR Spectrum (left) and best-fitting simulations (right) for PC/Cyclohexane/ D_2O at 296 K; $R = 12$.	102
Fig.III.8	^2D -NMR spectra (left) and best-fitting simulations (right) for PC/DCC/Cyclohexane/ D_2O at 296 K; (a) $R = 1$ and (b) $R = 3$.	103

Fig.III.9	^2D -NMR spectra (left) and best-fitting simulations (right) for PC/DCC/Cyclohexane/ D_2O at 296 K; (a) $R = 5$ and (b) $R = 6$.	104
Fig.III.10	^2D -NMR spectra (left) and best-fitting simulations (right) for PC/DCC/Cyclohexane/ D_2O at 296 K; (a) $R = 8$ and (b) $R = 12$.	105
Fig. III.11	^2D NMR spectra of (a) Cyclohexane, (b) Lecithin in Cyclohexane solution, (c) D_2O , and (d) distilled water H_2O	107
Fig. III.12	Comparative structures of Phosphatidylcholine and Sphingomyelin	112
Fig.III.13	^2D -NMR spectra (left) and best-fitting simulations (right) for PC/Cyclohexane/ D_2O at 263 K; (a) $R = 1$ and (b) $R = 3$.	113
Fig.III.14	^2D -NMR spectra (left) and best-fitting simulations (right) for PC/Cyclohexane/ D_2O at 263 K; (a) $R = 5$ and (b) $R = 6$.	114
Fig.III.15	^2D -NMR spectra (left) and best-fitting simulations (right) for PC/Cyclohexane/ D_2O at 263 K; (a) $R = 8$ and (b) $R = 10$.	115
Fig.III.16	^2D -NMR spectra (left) and best-fitting simulations (right) for PC/DCC/Cyclohexane/ D_2O at 263 K; (a) $R = 1$ and (b) $R = 3$.	116
Fig.III.17	^2D -NMR spectra (left) and best-fitting simulations (right) for PC/DCC/ Cyclohexane/ D_2O at 263 K; (a) $R = 5$ and (b) $R = 6$.	117
Fig.III.18	^2D -NMR spectrum (left) and best-fitting simulations (right) for PC/DCC/Cyclohexane/ D_2O at 263 K; $R = 8$	118
Fig.III.19	^2D -NMR spectra (left) and best-fitting simulations (right) for PC/DCC/Cyclohexane/ D_2O at 263 K; (a) $R = 10$ and (b) $R = 12$.	119

Fig.IV.1	Longitudinal relaxation process in spin systems through dipolar interaction.	131
(a)	for a single pair of identical spin $-1/2$ (I and J) nuclei ;	
(b)	for a system consisting of three identical spins (I,J and K).	
Fig.IV.2	Energy Level diagram and basis functions for an A_3 spin system in an irreducible basis representation.	135
Fig.IV.3	Pulse sequence used for selective observation of zero- and double quantum filtered spectra.	136
Fig.IV.4	Cone model describing the motion of a methyl group in a spherical micelle	141
Fig.IV.5	Degeneracy present at each M value of the A_9 spin system, under Zeeman Hamiltonian only.	147
Fig.IV.6	(a) Structure of the Deoxycholate(DOC) anion	149
	(b) 400 MHz proton NMR spectrum of DOC reverse micelle at $R = 2.88$. Numbers over the peaks correspond to the numbering of methyl groups given in (a).	
Fig.IV.7	'Inverted cone' model describing motion of methyl group-18 present in DOC molecule in our reverse micelles.	151
Fig.IV.8	400 MHz proton double quantum peak intensities as a function of evolution time for methyl-18, recorded for the $R = 2.88$ DOC reverse micelle; the solid line represents the profile generated theoretically and o's are experimental points.	152
Fig.IV.9	400 MHz proton double quantum peak intensities as a function of evolution time for methyl-18, recorded for the $R = 11.52$ DOC reverse micelle; the solid line represents the profile generated theoretically and o's are experimental points.	153
Fig.IV.10	400 MHz proton zero quantum peak intensities as a function of evolution time for methyl-18, recorded for the $R = 2.88$ DOC reverse micelle; the solid line corresponds to the single exponential fit of experimental data (o's).	155

Fig.IV.11	400 MHz proton zero quantum peak intensities as a function of evolution time for methyl-18, recorded for the R = 11.52 DOC reverse micelle; the solid line corresponds to the single exponential fit of experimental data (o's).	156
Fig.V.1	Types of magnetic field gradient.	161
Fig.V.2	Block diagram of the complete gradient control system used in this work.	168
Fig.V.3	Gradient selection using currents of different amplitudes in a pair of coils, (a)-(d) : Different direct current (DC) amplitudes in left and right coils generate linear magnetic field gradients of different magnitude between the coils as shown (e) Alternating current (AC) amplitude I_0 in the right coil and no AC amplitude in the left coil places the 'selective plane' on the extreme left side. (f) AC amplitude $3I_0/4$ in the right, and complementary AC amplitude $I_0/4$ in the left coil places the 'selective plane' one-fourth the total distance from the left coil.	170
Fig.V.4	Circuit diagram for the digital oscillator.	172
Fig.V.5	Resistive adder network.	176
Fig.V.6	Procedure for shifting out sine wave from digital serial shift registers (74164's).	176
Fig.V.7	Circuit diagram of our computer interface and manual switch to gradient controller.	179
Fig.V.8	Complementary outputs circuits and switch circuit.	181
Fig.V.9	Current driver circuit.	184
Fig.V.10	8-bit binary LED and 3-digit decimal seven segment display circuit.	186
Fig.V.11	Functional block diagram of Intel 8085A based microprocessor kit used in this work.	189
Fig.V.12	Flow chart for the generation of reset and position/DC-magnitude pulse(s) and gate control.	193

Fig.V.13	Flow Chart for the generation of switch control for pulsed magnetic field gradient (PMFG) spin echo experiment.	196
Fig.14	Experimental setup of the current driver, gradient controller, microprocessor kit and RF Probe unit. (Photograph)	200
Fig.V.15	Proton NMR spectra of H ₂ O in the presence of a continuous-linear magnetic field gradient.	202
Fig.V.16	Proton NMR spectra of H ₂ O in (a) absence and (b) presence of a small additional magnetic field in the Y-direction.	203
Fig.V.17	Proton NMR spectra at different orientations of H ₂ O in capillary tubes with respect to the magnetic field gradient direction.	204
Fig.V.18	Proton NMR spectrum of water at the gradient oscillating frequency of 50 Hz. ($V_{p-p} = 6V$; plane number selected = 127; no. of FID's collected = 128. The magnetic field lock was on, and sample tube was not spun.)	206
Fig.V.19	Proton NMR spectrum of water at the gradient oscillating frequency of 25 Hz. ($V_{p-p} = 6V$; plane number selected = 127; no. of FID's collected = 128. The magnetic field lock was on, and sample tube was not spun.)	207
Fig.V.20(i)	Hahn spin echo measurement of T_2 (rotating frame representation).	209
(ii)	Meiboom-Gill pulse sequence for measuring T_2 .	
Fig.V.21	Cumulative phase diagram for spin echo formation in a steady magnetic field gradient.	212
Fig.V.22	Spin echo amplitude versus τ^3 for lecithin/cyclohexane/H ₂ O system.	220
(a)	$G = 3.6 \times 10^{-2} \text{ T/m}$; $D = (-\bullet-\bullet-) = (2.21 \pm 0.01) \times 10^{-9} \text{ m}^2/\text{s}$	
(b)	$G = 3.5 \times 10^{-2} \text{ T/m}$; $D = (-\bullet-\bullet-) = (1.91 \pm 0.01) \times 10^{-9} \text{ m}^2/\text{s}$	

- Fig.V.23 Spin echo amplitude versus τ^3 for lecithin/cyclohexane/H₂O system. 221
- (a) $G = 3.7 \times 10^{-2}$ T/m ; $D = (-\bullet-\bullet-) = (1.61 \pm 0.02) \times 10^{-9}$ m²/s
- (b) The solid line represents the fit of eqn. [V.15] to the experimental data (o).
 $G = 8.9 \times 10^{-2}$ T/m ; $D = (-\bullet-\bullet-) = (1.43 \pm 0.03) \times 10^{-9}$ m²/s
- Fig.V.24 Variation of relative self-diffusion coefficient as a function of added water for lecithin/cyclohexane/ H₂O. 223
- Fig.V.25 Spin echo amplitude versus τ^3 for lecithin/CCl₄/H₂O system. 225
- (a) $G = 3.3 \times 10^{-2}$ T/m ; $D = (-\bullet-\bullet-) = (1.85 \pm 0.04) \times 10^{-9}$ m²/s
- (b) $G = 3.6 \times 10^{-2}$ T/m ; $D = (-\bullet-\bullet-) = (2.01 \pm 0.02) \times 10^{-9}$ m²/s
- Fig.V.26 Spin echo amplitude versus τ^3 for lecithin/CCl₄/H₂O system. 226
- (a) $G = 3.5 \times 10^{-2}$ T/m ; $D = (-\bullet-\bullet-) = (1.97 \pm 0.02) \times 10^{-9}$ m²/s
- (b) $G = 3.7 \times 10^{-2}$ T/m ; $D = (-\bullet-\bullet-) = (1.88 \pm 0.02) \times 10^{-9}$ m²/s
- Fig.V.27 Variation of relative self-diffusion coefficient as a function of added water for lecithin/CCl₄/H₂O 227

LIST OF TABLES

		Page
Table I.1	The most common phases of phospholipids in water.	7
Table I.2	Egg-lecithin based reverse micelles and low molecular weight guest molecules, peptides, enzymes etc. which are solubilized in 'water pool' and bulk organic solvent.	20
Table II.1	Microviscosity of water environment in the Lecithin/DCC/Cyclohexane/H ₂ O reverse micelle.	56
Table II.2	Calculated and Experimental T ₂ values of water protons in Lecithin/DCC/Cyclohexane/H ₂ O reverse micelle.	61
Table III.1	Matrix Representations of I = 1 spin operators.	84
Table III.2	Commutation relation between I = 1 spin Operators and commonly encountered spin-interaction operators.	85
Table III.3	Parameter used in simulating ² D NMR spectra for PC/Cyclohexane/D ₂ O.	109
Table III.4	Parameter used in simulating ² D NMR spectra for PC/DCC/Cyclohexane/D ₂ O.	109
Table III.5	Parameter used in the 'best fit' ² D NMR simulation for the system PC/Cyclohexane/D ₂ O.	111
Table III.6	Parameter used in the 'best fit' ² D NMR simulation for the system PC/DCC/Cyclohexane/D ₂ O.	120
Table IV.1	Phase cycling scheme used in the selection of zero quantum filtered spectra.	137
Table IV.2	Phase cycling scheme used in the selection of double quantum filtered spectra.	137
Table IV.3	Input parameters used for theoretical DQ profile generation.	150
Table V.1	Circulating digital pattern in sine wave generating shift registers.	173

Table V.2	Amplification coefficients for sine wave resistive network.	175
Table V.3	Tabulation of circuit switch positions.	188
Table V.4	A sample program for generating reset and position/DC-magnitude pulses(s) and gate control.	194
Table V.5	A sample program for generating switch control for a typical pulsed magnetic field gradient (PMFG) spin echo experiment.	197
Table V.6	Comparison of T_2 values from experimental linewidth and from CPMG sequence at different R values for the lecithin/cyclohexane/ H_2O system.	218
Table V.7	Variation of Self-diffusion Coefficients of Water as a Function of R for lecithin/cyclohexane/water System.	222
Table V.8	Variation of Self-diffusion Coefficients of Water as a Function of R for lecithin/ CCl_4 /water System.	228

CHAPTER 1

GENERAL INTRODUCTION

I.1 Reverse Micelles

Reverse micelles are the aggregates of amphipathic molecules such as synthetic surfactants and phospholipids in nonpolar media.⁽¹⁻⁴⁾ These aggregates are capable of solubilizing a large amount of water and several other polar solvents, e.g., glycerol and formamide, forming in the case of water, a so-called 'water pool'.⁽⁵⁾ While reverse micelles that possess water cores are water-in-oil (w/o) microemulsions, they are still called reverse micelles in analogy with micelles. In reverse micelles, the polar 'head' groups of surfactant molecules are concentrated in the interior of the aggregate and directed towards the water pool while their hydrophobic 'tail' groups protrude into, and are surrounded by, the bulk nonpolar solvent. The surfactant dissolved in organic phase is found to reduce the interfacial tension between the water and the organic phase, which is the prerequisite for the formation of reverse micelles. These aggregates are thermodynamically stable, homogeneous and optically transparent.

Reverse micelles have been the subject of recent increasing interest not only because of the water core's catalytic effects⁽⁶⁻¹⁶⁾ and their accommodative nature to host proteins and small molecules⁽¹⁶⁻²⁸⁾, but also because these multicomponent structures provide a model for processes in biomembranes⁽⁷⁾ including transbilayer transport⁽²⁹⁾ and fusion.⁽³⁰⁾ While there

is a considerable accumulation of experimental results about these aggregated systems, the information is incomplete. An unambiguous quantitative interpretation of micellar behaviour is still missing. In particular, much work is needed on the dynamic behaviour of reverse micelles, investigating the kinetics of their formation, their catalytic effects, and the solubilization of other molecules by the aggregates. The experimental and theoretical results accumulated on reverse micelles till recently are summarized in published monographs⁽³¹⁻³⁸⁾ and review articles.^(39,40) The references given here are merely meant to be representative, and give by no means a complete view of the many studies which have been published.

In this chapter, we restrict ourselves to reviewing the work pertaining to phospholipid-based reverse micelles only. In the following sections, we shall give a brief summary of the general structure of phospholipids and their different aggregated forms, the possible biological relevance of reverse micelles, their thermodynamics and phase diagrams, and the wide variety of methods (physical and chemical) used to characterize/probe reverse micellar structures. Finally a table containing important phospholipid-based reverse micelles studied till recently is presented.

I.2 Phospholipids : Source and Structure

The biological membranes play a key role in cell biology. They control the cell life by modulating transport and exchange processes between endocellular (inside) and exocellular (outside) compartments and are involved in biosynthesis, energy transduction, information transmission, and cell

recognition.⁽⁴¹⁻⁴⁴⁾ The basic structure of a cell membrane is a bilayer lamellar sheet, approximately 4-5 nm in thickness, comprising polar and neutral lipids and proteins that are embedded in the bilayer (integral) and bound at the surface (peripheral). The Singer and Nicholson⁽⁴⁵⁾ fluid mosaic model of a membrane structure is given in Fig. I.1.

Phospholipids are the primary structural components of all biological membranes. These are polar lipids containing phosphoric acid as mono- or di-ester.⁽⁴⁰⁾ The natural phospholipids are classified into two main groups^(42,46,47), namely

(i) **Sphingophospholipids** : These are derived from sphingosine.

Its general formula is given in Fig. I.2(a), where R represents a hydrophilic group and R' an acyl group. The most common sphingophospholipid is sphingomyelin, where the R group is $-\text{CH}_2\text{CH}_2\overset{+}{\text{N}}(\text{CH}_3)_3$.

(ii) **Glycerophospholipids** : These have glycerol as a backbone with one or two O-acyl or O-alkyl, or O-(1-alkenyl) chains attached at positions one and two and phosphate at position three. Its general chemical structure is given in Fig. I.2(b). The R' and R'' groups are mostly derived from fatty acids, generally unbranched and with an even number of carbon atoms. Fig. I.2(c) shows the main R groups found in natural membranes and their corresponding common names.

Although they are different in terms of structure and function, both are amphipaths. Further details are given below about glycerophospholipids only, since these are the most commonly found membrane lipids⁽⁴⁴⁾ and also since these appear exclusively in phospholipid-based reverse micelles.

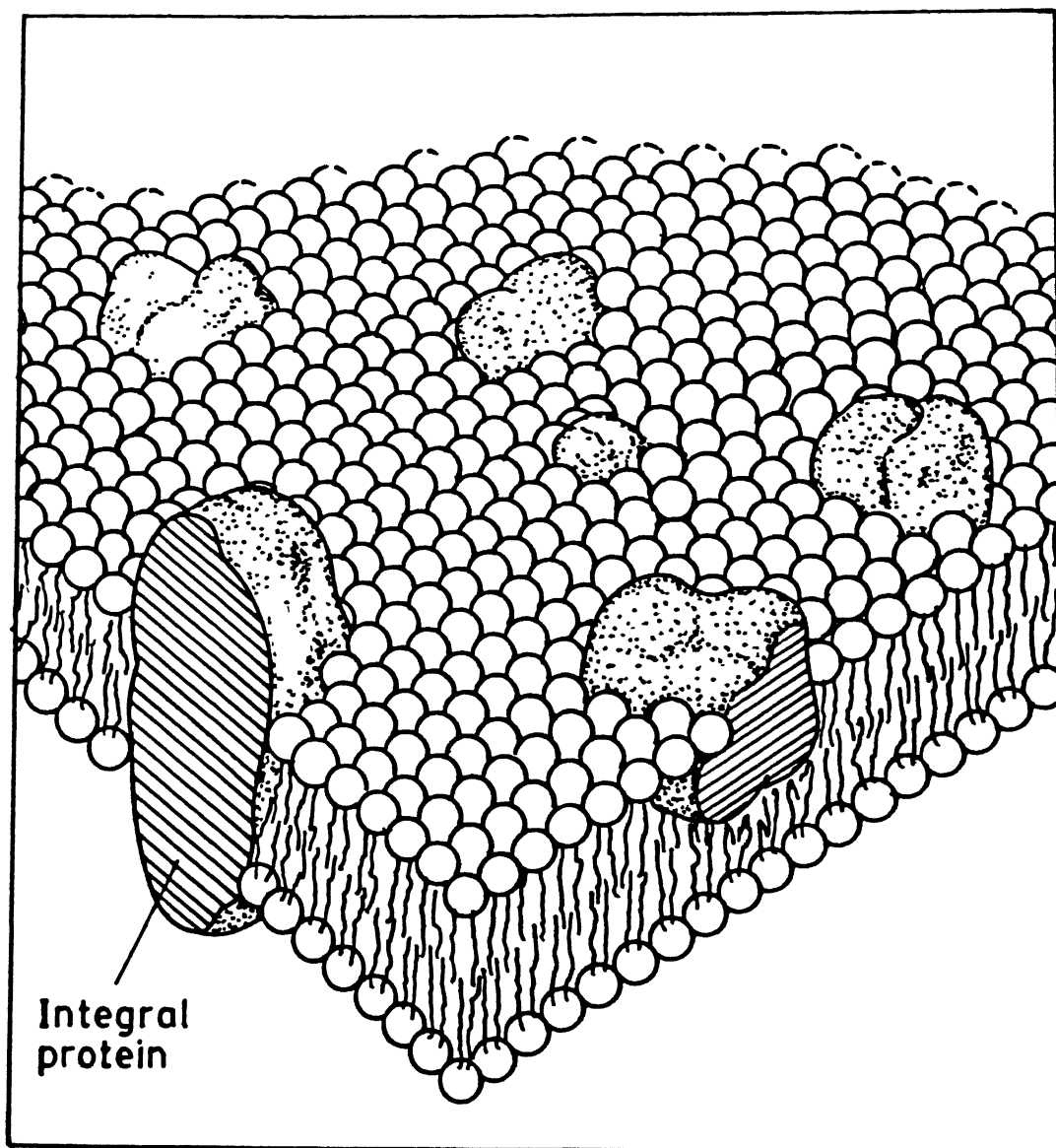


Fig.1.1

The Singer and Nicholson 'fluid mosaic' model of a biomembrane. (adapted from ref. 45).

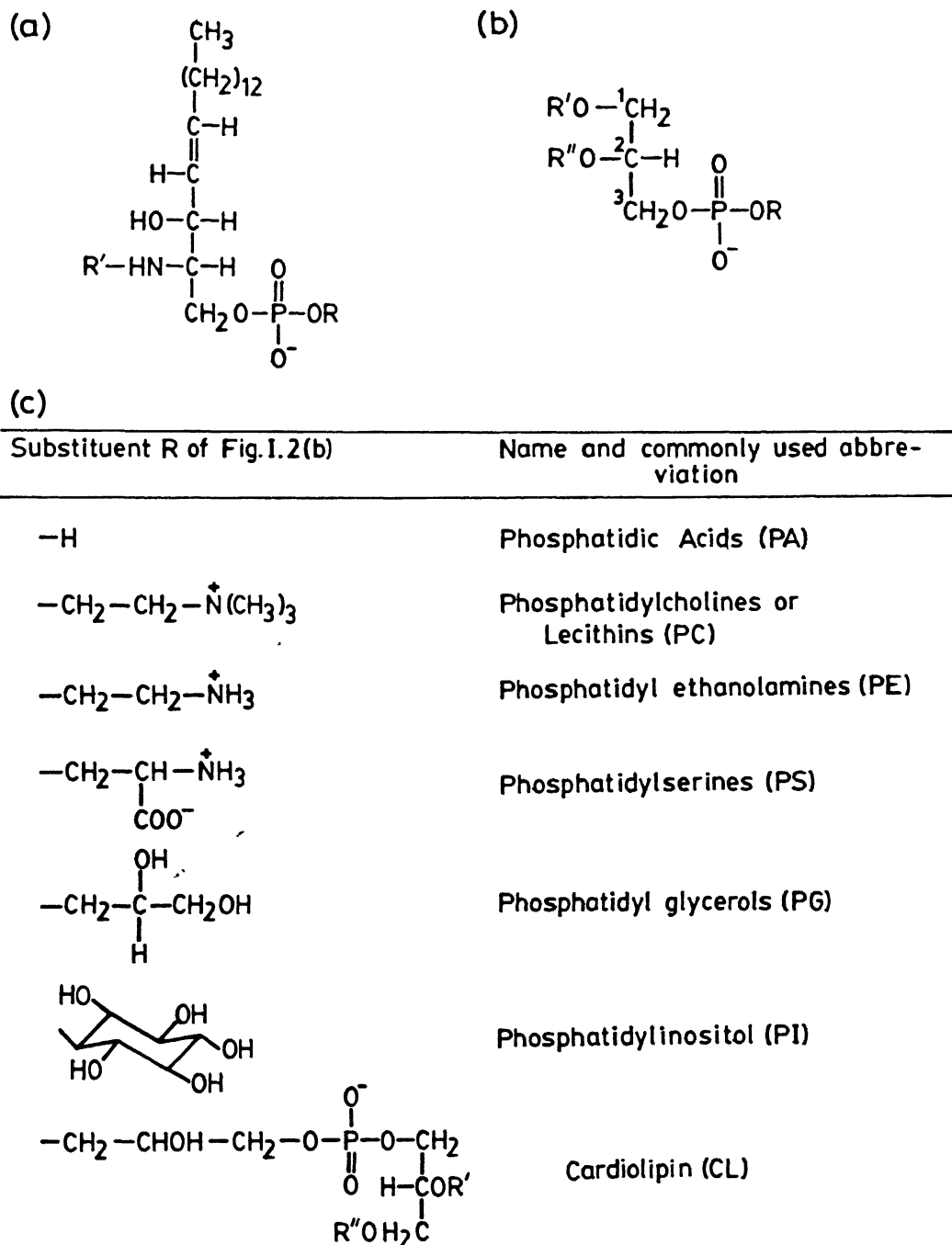


Fig.1.2

General Chemical structure of sphingophospholipids(a) glycerophospholipids(b) & main classes of glycerophospholipids with their common names (c).

I.3 Lipid Polymorphism

Phospholipids are seldom molecularly dispersed in solutions. As amphipathic molecule, phospholipids have a great tendency to aggregate and, like fatty acids, to form more than one structurally different phase in the crystalline (solid) state as well as in aqueous dispersions. This property is referred to as polymorphism.⁽⁴⁸⁾ Various structures have been mainly established by X-ray diffraction^(49,50), electron microscopy⁽⁵¹⁾ and magnetic resonance.^(33,52)

The most common phases of phospholipids in water^(40,49,53) are given in Table I.1. In the Table, L indicates a one-dimensional lamellar lattice, H, P and Q represent a hexagonal two dimensional, rectangular two-dimensional and cubic lattices, respectively. The Greek letters α, β, β' and $\alpha\beta$ indicate the conformation of the hydrocarbon chains.




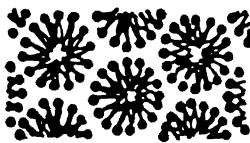

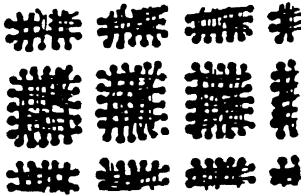

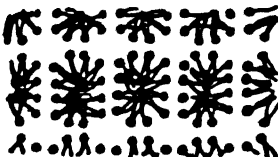




Reverse micelles, the subject of this thesis, belong to $H_{II-\alpha}$ (reversed two-dimensional hexagonal type), $P_{II-\alpha}$ (reversed two-dimensional tetragonal type) and $Q_{II-\alpha}$ (reversed three-dimensional cubic type) containing a water core in an organic environment.

I.4 Existence of Reverse Micellar Structures in Biological Membranes

Although the existence of non-bilayer structures in biological membranes is by no means established conclusively, the existence of reverse micelles of membrane proteins and phospholipids in organic solvents is established.⁽⁵⁴⁾ The possibility of reverse micellar dynamic intermediates⁽⁵⁵⁻⁵⁷⁾

their roles have been analyzed.⁽⁵⁷⁻⁶¹⁾ These and the studies on

Table I.1 The most common phases of phospholipids in water

Type of Packing	Structure [†]		
Coherent double-layers of molecules separated by water; lamellar one-dimensional array	 L	 L _β	 L _β '
Rod-like aggregates with organic core (H _{I-α}) and aqueous core (H _{II-α}); hexagonal two-dimensional array	 H _{I-α}	 H _{II-α}	
Rod-like aggregates with organic core (P _{I-α}) and aqueous core (P _{II-α}); tetragonal two-dimensional array	 P _{I-α}	 P _{II-α}	
Rod-like aggregates with organic core in aqueous environment; rectangular two-dimensional array	 P _{III-α}		
Rippled double layers of molecules separated by water; lamellar two-dimensional array	 P _β '	 P _{αβ}	
Rod-like aggregates with aqueous core (Q _α) and organic core (Q _{I-α}); cubic three-dimensional array	 Q _α	 Q _{I-α}	

[†] adapted from ref. 40, 49a, 53 and 68.

lipid polymorphism led to a new fundamental insight into the physical properties and functional roles of lipids in membranes. A new understanding of biomembranes necessitated a revision of the well-known 'fluid mosaic' model. The new model proposed by Cullis et al.^(62,63), called the 'metamorphic mosaic' model, reproduced in Fig. I.3, includes possible processes which involve reverse micellar structures such as exo- and endocytosis membrane fusion, movement of lipids across the bilayer, transport of ions across the bilayer and perhaps many other processes yet undetected.

I.5 Thermodynamics and Phase Diagrams

Amphipathic or amphiphilic molecules aggregate in nonpolar solvents predominantly due to dipole-dipole and ion pair interactions⁽⁶⁴⁾ and also due to a decrease in the overall free energy of the system. The hydrophobic effect of these molecules provides the driving force for aggregation and the repulsion between head groups limits the size of the aggregated structure. The nature of solvent (its polarity, dielectric constant etc.) also plays a role in the aggregation behaviour of surfactants.

The thermodynamic principles of amphiphatic self-aggregation and the geometric aspects of the phenomenon have been well discussed.^(44,65-68) Israelachvili and Coworkers⁽⁶⁵⁾ discussed these in terms of a parameter called 'critical packing parameter',^(67,68) which is connected with the thermodynamic characteristics of the amphiphile. The enthalpy and entropy changes of aggregation of potassium benzene sulfonate in heptane⁽⁶⁹⁾ (enthalpy (ΔH) = $-79.5 \text{ kJ mol}^{-1}$; entropy (ΔS) = $-62.8 \text{ JK}^{-1} \text{ mol}^{-1}$) suggest that the association energy for reverse micelles to be mainly of enthalpic rather than entropic origin as

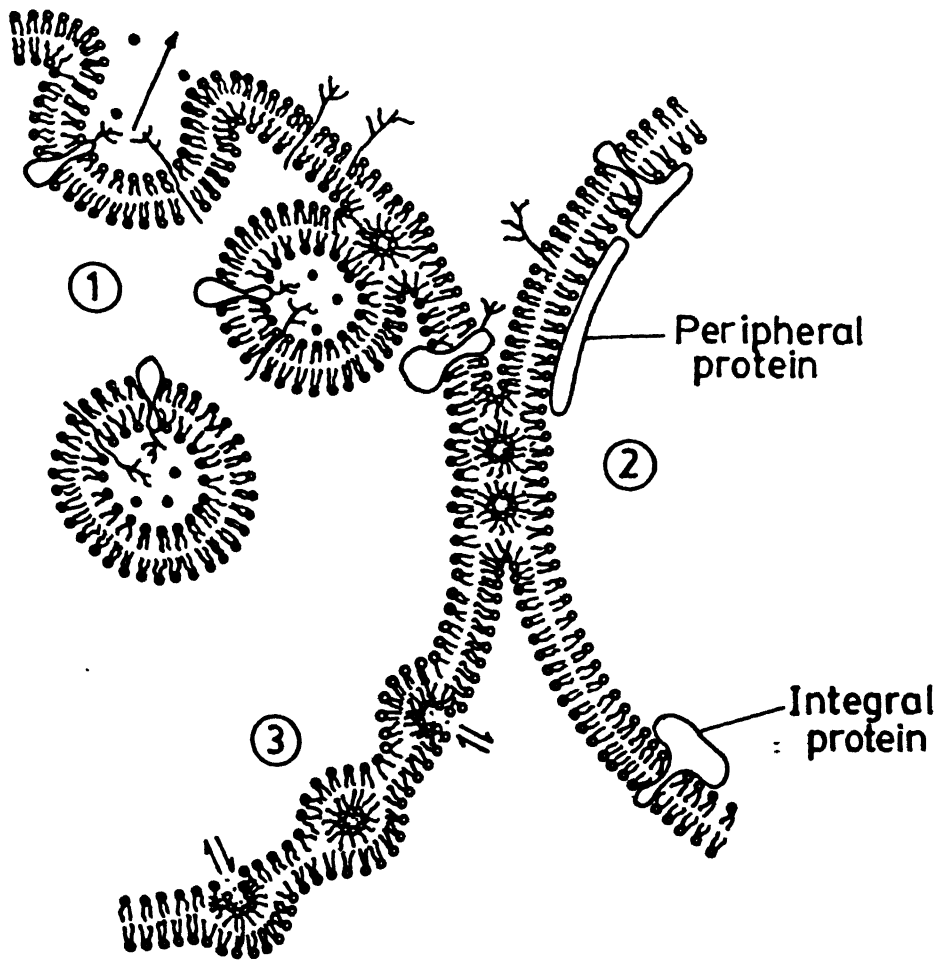


Fig.1.3

The metamorphic mosaic model of biological membranes (taken from ref. (63)). Regions (1) and (3) show the involvement of reverse micellar or reverse cylinder structural intermediate in an exocytotic fusion process and transbilayer molecular -transport process, respectively. Region 2 shows the possible existence of reverse cylinder structure at interbilayer tight junctions.

The thermodynamics of amphiphile aggregation in polar and nonpolar solvents is usually discussed in defining a term called 'critical micellar concentration (CMC)⁽⁴⁾ - a concentration of amphiphile at which aggregation occurs (it is to be noted that the definition of CMC is not unique). Three basic models⁽⁷¹⁻⁷³⁾ have been used for the thermodynamic treatment of micellization. They are : pseudophase, single step equilibrium or mass action law and multistep equilibrium. The first model is frequently used in NMR studies of micelles.⁽⁷³⁾ Giomini et al.⁽⁷⁴⁾ used the mass action law model for finding out the CMC and other thermodynamic parameters of lecithin/benzene/water reverse micelle. Although these theories can in principle be applied to phospholipid aggregates, much progress has not been made due to the following two reasons : (i) The cooperativity of reverse micellar formation is much smaller⁽⁷⁵⁾ compared with that of normal micelles. When the aggregation number is small, the change in physical properties with increasing concentration of the surfactant is gradual and, therefore, a well-defined CMC can seldom be identified.^{(64(b),75)} (ii) Since minute amounts of water are invariably present in the organic solvent, these system should be considered as ternary and the CMC would then lose its significance, as it changes with the amount of water.⁽³⁾

Despite the lack of a clear-cut concept of CMC for reverse micelles as mentioned above, the "CMC" has been determined for many surfactants in nonpolar solvents.^(4,3,74,77,78) Another way of understanding the thermodynamic properties of these systems would be through the construction of ternary phase diagrams. To the best of our knowledge, only two reports have been published on lecithin based

reverse micelles.^(79,118) Shervani et al.⁽¹¹⁸⁾ have studied lecithin-based reverse micelles in benzene, cyclohexane, n-octane and n-dodecane, in the presence and absence of cholesterol.

The role of water in the formation of reverse micelles has also received considerable attention. Previous studies⁽⁸⁰⁻⁸⁵⁾ have concluded in general, that water is a prerequisite to promote the aggregation of amphiphilic surfactants to reverse micelles and that part of the water present serves as 'gluing' agent between the polar head groups of the surfactant monomers in the core of the reverse micellar aggregates. However, Yu et al.⁽⁸⁶⁾ reported recently from their dynamic and static light scattering studies on sodium bis(2-ethylhexyl) phosphate in n-hexane that water is not a prerequisite for reversed micellization, in contrast with earlier reports. Instead, water can function as an antimicellization agent.⁽⁸⁶⁾

I.6 Reverse Micellar 'Water Pool'

A lot of importance attaches to the physico-chemical studies of water in reverse micelles is because of its rather peculiar chemical and physical properties^(4,21,87-90) which differ from those of normal water, especially at low water-to-surfactant ratios. For instance, it has been found by various spectroscopic and other physical methods that these water molecules, exhibit much higher viscosities⁽⁹¹⁻⁹⁴⁾, low mobilities⁽⁹⁴⁻⁹⁶⁾, varied polarity⁽⁹⁷⁻¹¹⁷⁾ and dielectric constant⁽⁹⁸⁾, varied pH⁽⁹⁹⁾ and hydrogen bonding⁽⁸⁸⁾ and low freezing point.^(90,100)

Considerable studies have also been done on the interaction of water with the polar head groups of

phospholipids.^(1,94,102-110) However, the conclusions of some of these studies^(102,103,108,109) are often contradictory or tentative.

Reverse micelles are not rigid but dynamic entities. They can collide freely in the hydrocarbon solution which leads to the exchange of water pools. The dynamics of the exchange of water in reverse micelles and biological systems can be described by qualitative and quantitative models. Qualitative models assume that water molecules exist in two or more environments, with one of these environments being that of pure water. The simplest case would be a two-state model classifying the water molecules as 'bound' and 'bulk'.^(111,112) This was later on extended to a three-state model⁽¹¹³⁻¹¹⁶⁾, the three types of state being :

Type I : "bulk Water" or "Free Water" - the rotational and translational motions of these water molecules are not appreciably altered compared to normal water, with τ_c , the rotational correlation time, being $\sim 10^{-12}$ s.

Type II : "bound water" - the rotational motions, freezing point, etc. of these water molecules are significantly hindered by interactions with the polar head group of surfactants, leading to τ_c values of $\sim 10^{-9}$ s.

Type III : "trapped water" or "irrotationally bound water" (this term, however, does not exclude translational or exchange mechanisms); these water molecules are essentially "trapped" or "site bound" to the surfactant or to the macromolecules, with $\tau_c \sim 10^{-5}$ to 10^{-7} s.

Quantitative estimation of these types of water has also been made. Koenig and Schillinger^{(113(b))} estimated Type III water from the magnitude of NMR spin-lattice relaxation time (T_1)

dispersion. Type II water can be directly estimated from freezing experiments, and the remaining water is to be considered as Type I or bulk water. Although previous studies have led to a reasonably consistent picture of the mobility and organization of water in the 'water pool', there still exists the necessity for obtaining true (or at least reliable) values for the physical properties of the aqueous core of the reverse micelles by using a variety of techniques.

I.7 Experimental Methods Used to Probe Reverse Micelles

Various experimental methods have been used to characterize the reverse micelles. Most of these methods are used to probe the compartmentalized, polar microenvironment, the 'water pool', but some of these are used to get a macroscopic information such as bulk viscosity .

We may broadly categorize the experimental methods into three groups :

- (i) scattering techniques
- (ii) physical methods
- (iii) spectroscopic techniques

(i) Scattering Techniques

Scattering techniques give a macroscopic structural information about reverse micelles. The three most frequently used scattering techniques for studying reverse micelles are : light scattering (LS), small-angle neutron scattering (SANS) and small-angle X-ray scattering (SAXS).

Light scattering techniques essentially probe the Brownian motion of particles. Static and dynamic light scattering⁽¹⁵¹⁾ (also known as quasi-elastic light scattering or

photon correlation spectroscopy) have been used to determine size and translational diffusion coefficients of droplets, to measure intermicellar interactions of reverse micelles and to investigate protein encapsulation in reverse micelles. A good review of these studies is given in Ref. (37).

Light scattering studies of egg lecithin reverse micelles in benzene, carbon tetrachloride (CCl_4) and cyclohexane were reported from our laboratory⁽⁹²⁾. These studies indicate the presence of homodisperse aggregates in benzene and CCl_4 and anisotropic tubular structures in cyclohexane.

The small angle neutron scattering (SANS) technique gives more detailed information on size and size distributions of reverse micelles, due to the fact that the neutron scattering vector has a large range ($0.02\text{--}0.2 \text{ \AA}^{-1}$). This can also be used to study the effect of additives in the reverse micelles.⁽¹⁴⁴⁾ Translational motion of reverse micelles can be monitored by using a quasi-elastic, incoherent neutron scattering method.⁽¹⁴⁵⁾ Several comprehensive reports of SANS studies in micellar and microemulsion systems have been published.^(37,146,151,152)

A SAXS experiment determines the so-called 'radius of gyration', which is related to the polar core radius of reverse micelles. These can be used to probe the change (increase or decrease) in size of the polar core in the presence of additives or solubilized enzymes.⁽¹⁴⁷⁾

(ii) Physical Methods

There are quite few physical methods that have been used to probe reverse micelles. They are :

- (a) Viscosity measurement
- (b) electrical conductivity

(c) electron microscopy

These have been used on egg-lecithin reverse micelles in three different solvents in our laboratory earlier.⁽⁹⁾ The major results of these studies are : the reverse micelles contain dispersed water in small spherical droplets surrounded by a phospholipid layer; the electrolyte (KCl solution) added for measuring specific conductivity is contained in discrete water pools that are formed in the interior of the reverse micelles. The cyclohexane system at water-to-surfactant mole ratio of 5-6 exhibits an elongated tubular structure containing aqueous canals.

(iii) Spectroscopic techniques

A wide variety of spectroscopic techniques may be used to probe the water pool, organic bulk phase and surfactant to get dynamic or motional information of the system.

The selection of a particular technique depends on the type of physical property in which one is interested. A summary of characteristic frequencies of molecular motion of lipids and the approximate frequency ranges over which various spectroscopic techniques are sensitive to molecular motion is given in Fig. I.4. This figure illustrates that the motional frequencies of different parts of the lipids occur in the range of $10^{-6} - 10^{+14} \text{ s}^{-1}$, i.e., spanning a time-scale of 20 orders of magnitude. We note that some techniques yield a static picture since the molecular motions are 'slow' relative to the measurement and some see a time averaged picture of molecules which move between different environments very rapidly relative to the measurement time. Fig.I.4 also indicates that out of all these spectroscopic techniques, NMR can probe the widest range of molecular motions thereby becoming an important tool for motional studies.

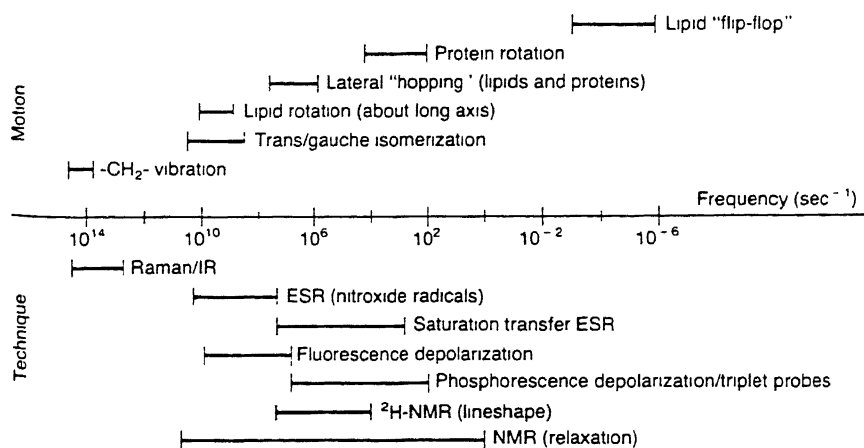


Fig. I.4 Approximate frequency ranges of various spectroscopic techniques and molecular motions of lipids⁽⁴⁴⁾.

The time scale of a particular motion being studied and the time scale of the technique being used for the measurement worth a further emphasis. Consider a general case which could equally apply to an EPR, fluorescence or ²H-NMR measurement of molecule or probe. All three spectroscopic techniques are sensitive to the orientation of the molecules with respect to an axis system defined in the laboratory. For example, in ²H-NMR, the observed spectrum is sensitive to the orientation of C-D, O-D or other bond in relation to the externally applied field. In EPR, the situation is similar, where the spectrum is sensitive to the orientation of the N-O (nitroxide) bond present in most commonly used probes, with respect to the applied magnetic field. In fluorescence spectroscopy, the measured polarization of the emitted light is dependent on the orientation of the molecular transition dipole moment with respect to the direction defined by the polarizer used to make the measurements. Some further elaboration of these techniques is given below :

(a) Optical Spectroscopy (UV-visible, fluorescence, IR, Raman and circular dichroism). (37,39,118,148)

In most of these experiments, some probe molecules are entrapped in either the water pool or the organic phase of micelles, and conclusions are derived from the observed trend of properties such as polarity, hydrogen bonding, mobility, vibrational motion of a bond in a molecule, protein confirmation, activities of solubilized enzymes, etc.

For example using the nitrate ion as a probe and monitoring the $n \rightarrow \pi^*$ band in the UV range, in egg lecithin based reverse micelles in benzene, carbon tetrachloride and cyclohexane⁽⁹⁷⁾ it has been found that the effective polarity of the water pool is lower than that of bulk water. This result is substantiated in the fluorescence emission spectra of the same three systems⁽⁹⁷⁾ by using 8-anilidonaphthalene sulfonic acid (ANSA) as a probe. In the cyclohexane system, this technique indicated a possible presence of liquid crystalline phase when the water to surfactant ratio was six. The near IR spectra of the same systems⁽⁹⁷⁾ give two absorption bands : one at about 1890 nm corresponding to water-dispersed in the organic phase and the other band over a range of 1930-1960 nm corresponds to the water solubilized in the reverse micellar interior. From this study , it is also estimated that only about 0.05% (V/V) of total water is present in the bulk solvent.

The following spectroscopic techniques have also been used, but to a lesser extent, to characterize the water-pools of reverse micelles, namely,

- (a) time-domain dielectric spectroscopy⁽¹⁵³⁾,
- (b) positron annihilation spectroscopy⁽¹⁵⁴⁾,
- (c) photon correlation spectroscopy⁽¹⁵⁵⁾,
- (d) perturbed angular correlation spectroscopy⁽¹⁵⁶⁾.

However, these shall not be further described here.

(b) Magnetic Resonance Techniques

Electron Paramagnetic Resonance (EPR):

Electron paramagnetic resonance (EPR) technique is very sensitive and extremely useful in the study of reverse micelles. It is usually carried out by incorporating either a paramagnetic ion⁽¹⁴⁹⁾ or spin labels or probe⁽¹⁵⁰⁾ in the water pool or organic phase. The properties that can be obtained from EPR are : the aggregation behaviour of different surfactants, microviscosities and local polarities around the probe molecule, the effect of different solubilizates on these properties, and the dynamics of micellization processes.

A wide variety of spin labels have been designed and synthesized to have physico-chemical properties such that they either remain in the water pool (e.g., Fremy's salt ($\text{Na}_2(\text{SO}_3^-)_2\text{NO}$), CuCl_2) or organic phase (e.g., 16-doxyl stearic acid), or they are exclusively present at the water/oil interface (e.g., long chain fatty acid spin label analogs; substituted semiquinones, 5-doxyl stearic acid etc.) or they exchange between different compartments (e.g., 5-doxyl hexylsulfate, sodium salt).

Nuclear Magnetic Resonance (NMR) :

Since all nuclei with nonzero nuclear spin quantum number are NMR 'active', useful information can be obtained from virtually all components of the reverse micelle. This essentially eliminates the need for using a molecule which may be 'invasive'

and change the physico-chemical properties of the system.

The NMR parameters are of two kinds. The first kind consists of steady state parameters (the chemical shift (δ) and scalar (J), dipolar- and quadrupolar coupling constants) which are related to the molecular structure of the system under study; they give information about the chemical environment of the observed nucleus and about its stereochemical relationship with other nuclei in close spatial proximity. The second kind includes dynamic parameters (the longitudinal or spin-lattice relaxation time (T_1) and the transverse or spin-spin relaxation time (T_2)) which are related to the motional characteristics of the nuclear spin system.

The following information can be obtained from NMR studies on reverse micelles^(37,39,40): aggregation numbers and exchange rates of different components of the system, extent of hydration of the polar head group, properties and activities of the solute solubilised in different phases, macroscopic self-diffusion of a molecule and segmental motions, conformations and order parameters of surfactant molecules, etc. Much of the earlier NMR literature on reverse micelles has been somewhat contradictory (see Table I.2). We shall review very briefly the kind of information that has been obtained from NMR studies of egg-lecithin reverse micelles after 1980.

Systematic studies have been carried out in our laboratory on egg-lecithin based reverse micelles^(92,94,97,110) in benzene, CCl_4 and cyclohexane using extensively, ^1H , ^{31}P and ^{13}C NMR and to a limited extent ^2H and water proton diffusion coefficient measurements. Based on these experiments several

1.2 Egg Lecithin based reverse micelles and low molecular weight guest molecules, peptides, enzymes etc. which are solubilised in the 'water pool' and bulk organic solvent (an updated and integrated version of Table III, IV and VI of Ref. 40)

Sol-vent	$R = \frac{[\text{Water}]}{[\text{Egg Lecithin}]}$	Guest molecules, enzymes etc.	Method(s) used	Ref.No.(s)
Benzene	0-45		Light scattering, Osmometry, viscosity, diffusion, electron microscopy, NMR, IR, Fluorescence, electrical conductivity and optical birefringence	1,18,92, 94,97, 101,103, 105,108, 110,119, 120,138, 142,144
	0-16.2	KCL	Electrical conductivity	92
	0-30	NaCl, KCl, MgCl_2 , CaCl_2	NMR and IR	127,141
		Iodine		128
		Dibasic fatty acid	Solublization	129
		m-(p-anilino)-phenylazo- benzene sulfonic acid, potassium and sodium salts	Absorbance studies	119
		8-Anilinonaphthalene sulfonic acid (ANSA)	Fluorescence	97
		Nitrate ions	UV spectroscopy	97
	0-30	4-[(2-hydroxy-1-naphthalenyl)azo]-benzenesulfonic acid monosodium salt (tropacolin 000, Orange II)	Light scattering, Diffusion, Viscosity and solublization	1
		bis(p-chlorophenyl) acetic acid (p,p'-DDA); 1,1 (4-chlorophenyl)-2,2,2-trichloroethanol		130

	Meisenheimer complex; sodium 1,1-dimethoxy-2, 4,6-trinitrocyclohexa- dienylide		131	
0-50	amino acids; di-tri- and penta peptides	IR, NMR	140,18	
18	azobis (2-aminopropane) (ABAP) hydrochloride- an auto-oxidation initiator; antioxidants- 6-hydroxy-2,5,7,8 tetra- methylchromane-2-carboxy- late (Trolox)(water- soluble) and α -Tocopherol (organic solvent-soluble)	^{31}P -NMR, Kinetics	139	
13-14		Proton NMR for CMC determination	74	
	Buffer solution (KH_2PO_4 and Na_2HPO_4)	^{31}P -NMR	143	
0-19	Cholesterol	Temperature- dependent water solubilization and ternary phase- diagram studies.	118	
5-30	Phospholipase A_2 from Vespa Orientalis		132	
Cyclo- hexane	0-15	Optical birefringence, viscosity, light scattering	92	
	0-15	NMR (^{31}P and ^1H)	110,94	
	0-15	ANSA	Fluorescence	97
	0-15	KCl	Electrical conductivity	92
	0-15	Nitrate ions	UV spectroscopy	97

	0-16	Cholesterol	Temperature-dependent water solubilization ³¹ P-NMR, IR, Laser Raman spectroscopy	118
Carbon tetra-chloride	0-15.8		Optical birefringence, viscosity, light scattering	92
	0-15.8		¹ H and ³¹ P-NMR	110, 94
	0-15.8	KCl	Electrical conductivity	92
	0-15.8	Nitrate ions	UV spectroscopy	97
	0-15.8	ANSA	Fluorescence	97
	0-18		² H-and ³¹ P-NMR	109
		Meisenheimer Complex	Absorbance studies	131
	5.5 or 11	Indole ; 1-methylindole; skatole	NMR	133
			NMR	102
n-Octane	3	Chloesterol	Temperature dependent water solubilisation, ternary phase-diagram studies, NMR and IR	118
n-Dodecane	2.5	Cholesterol		
Chloroform			NMR	142
		COCl ₂ ·6H ₂ O	Visible spectroscopy	137
		Meisenheimer complex		131
Chloro-benzene	18	an autoxidation initiator - ABAP; antioxidants-Trolox (water-soluble) and α-Tocopherol (Organic solvent-soluble)	Kinetics	139

O-dichloro benzene	0-10		Ultracentrifugation	109
Heptane		Iodine	Kinetics	128
Toluene	0		Osmometry, light scattering	122
			viscosity, diffusion	123
Butanol	0		Light scattering	124
Ethanol	0		Light scattering	124
Methanol/	10-25	phospholipase A ₂		134
Diethyl ether		from Crotalus adamanteus		
Methanol/ pentanol/ octane	11.1	Acid phosphatase from wheat germ		135
Methanol/ pentanol/ octane	13	Peroxidase from horseradish		136
Hexanol	0		Light scattering	124
Methanol in benzene	0		Light scattering, viscosity and diffusion	125
Diethyl ether	0-46		Ultracentrifugation	106
	0-44	COCl ₂ ·6H ₂ O	visible spectroscopy	107

conclusions have emerged: (i) only one water molecule becomes highly bound to the polar head group ; (ii) the microviscosity of the water environment is very high and falls off rapidly as a function of added water; (iii) the added water is solubilized in the polar core of the reverse micelle; (iv) water addition increases the motion of the polar head group but has no effect on the hydrocarbon chains. Proton T_2 studies on these systems have indicated additional relaxation mechanisms in addition to intramolecular dipole relaxation. Interestingly, the cyclohexane system has shown unusual physical properties in the water-to-surfactant molar ratio range of 5 to 6.

During the same time Boicelli^(18,74,114,127,140-143) have extensively studied the ^1H and ^{31}P NMR of egg-lecithin based micelles in benzene, and have come to conclusions essentially similar to those set forth above. They have also studied the effects of a wide variety of small and medium sized guest molecules^(18,127,140,141) such as NaCl, KCl, MgCl_2 , CaCl_2 , amino acids, peptides etc. (see Table I.2) and have concluded that these guest molecules alter the distribution and organization of water molecules. They have also suggested the possible use of ^{31}P -relaxation parameters for indicating pH of the water pool⁽¹⁴³⁾ using a buffer solution. By measuring proton NMR chemical shift of egg-lecithin in benzene⁽⁷⁴⁾, the same group demonstrated the use of this NMR parameter for measuring the CMC of the reverse micelle.

Most of these studies have been done on the benzene system. Very little attention has been paid to egg-lecithin in cyclohexane reverse micelles. In addition to work from our

laboratory, only one other group⁽¹¹⁸⁾ (see Table I.2) has done some (^{31}P -NMR and water-solubilization) studies recently.

Considering the abovementioned unusual features of the cyclohexane-based lecithin reverse micelles, and also taking into account that relatively little work has been done regarding the effects of water addition in this system, we have taken up this particular solvent for preparing egg-lecithin based reverse micelles. Further, we also been interested to prepare egg-lecithin based reverse micelles with a cosurfactant which may have potential uses in synthesizing biochemically important biomembrane models. We have attempted to characterize such system as far as possible by NMR (^1H , ^2H and ^{31}P) only. Preparation of one such system, and its physical properties, have been presented in Chapters II and III.

Although the main bulk of our experiments has been done on egg-lecithin in cyclohexane, due to reasons spelt out in Chapter IV, we have taken up a deoxycholate reverse micelle for some multiple quantum NMR experiments.

In Chapter V, we describe, in detail, the construction of a versatile magnetic field gradient controller for doing NMR measurements and measurements of self-diffusion coefficients. Measurements of the water ^1H self-diffusion coefficients in lecithin/cyclohexane/ H_2O have been compared with similar measurements in lecithin/ CCl_4 / H_2O system.

REFERENCES

1. P.H. Elworthy and D.S. McIntosh, J. Phys. Chem. 68, 3448 (1964).
2. K. Kon-no and K. Kitahara, J. Colloid Interface Sci. 35, 636 (1971).
3. H.F. Eicke, Top. Curr. Chem. 87, 85 (1980).
4. J.H. Fendler, Membrane Mimetic Chemistry, Wiley & Sons, New York (1982).
5. C.J. O'Connor, E.J. Fendler, and J.H. Fendler, J. Am. Chem. Soc. 96, 370 (1974).
6. J.H. Fendler and E.J. Fendler, Catalysis in Micellar and Macromolecular Systems, Academic Press, New York (1975).
7. J.H. Fendler, Acc. Chem. Res. 9, 153 (1976) and references cited therein.
8. R.T. Medary, O.A. El Seoud, and V.A. Woods, in : Reaction Kinetics in Micelles, E.H. Cordes (ed.), Plenum Press, New York (1973), p. 127.
9. A. Kitahara, Adv. Colloid Interface Sci. 12, 109 (1980).
10. C.J. O'connor, T.D. Lomax, and R.E. Ramage, Adv. Colloid Interface Sci. 20, 21 (1984).
11. M.P. Pileni, Chem. Phys. Lett. 81, 603 (1981).
12. A.J.W.G. Visser and J.H. Fendler, J. Phys. Chem. 86, 947 (1982).
13. J.H. Fendler, Chem. Rev. 87, 877 (1987).
14. E. Ruckenstein and P. Karpe, J. Phys. Chem. 95, 4869 (1991).
15. P.A. Bachmann, P. Walde, P.L. Luisi, and J. Lang, J. Am. Chem. Soc. 112, 8200 (1990); P.A. Bachmann, P.Walde, P.L.Luisi, and J.Lang, J. Am. Chem. Soc. 113, 8204 (1991).
16. K. Martinek, A.V. Levashov, N. Klyachko, Y.L. Khmelnitski, and I.V.Berezin, Eur. J. Biochem. 155, 453 (1986).
17. P.L. Luisi, M. Giomini, M.P. Pileni, and B.H. Robinson, Biochim, Biophys. Acta 947, 209 (1988) and references cited therein.
18. C.A. Boicelli, F. Conti, M. Giomini, and A.M. Giuliani, Chem. Phys. Lett. 89, 490 (1982).
19. E.B. Leodidis and T.A. Hatton, J. Phys. Chem. 94, 6400 (1990); ibid 6411 (1990).

20. M. Waks, *Proteins* 1, 14 (1986).
21. P.L. Luisi, *Angew Chem. (Int. Ed.)* 24, 439 (1985).
22. P.L. Luisi and C. Laane, *Trends Biotech.* 4, 153 (1986).
23. P.L. Luisi and L.J. Magid, *CRC Crit. Rev. Biochem.* 20, 409 (1986).
24. M. Dekker, K. Van't Riet, S.R. Weyers, J.W.A. Baltussen, B. Bijsterbosch, and C. Laane, *Chem. Eng. J.* 33, B27 (1986).
25. C. Nicot, M. Vacher, M. Vincent, J. Gallay, and M. Waks, *Biochemistry* 24, 7024 (1985).
26. R.E. Smith and P.L. Luisi, *Helv. Chim. Acta* 63, 2302 (1980).
27. A.J.W.G. Visser, J.S. Santema, and A. Van Hoek, *Photochem. Photobiol.* 39, 11 (1984).
28. K.F. Thompson and L.M. Gierasch, *J. Am. Chem. Soc.* 106, 3648 (1984).
29. P.R. Cullis and B. Dekruijff, *Biochim. Biophys. Acta* 559, 399 (1979); *ibid* 602, 474 (1980).
30. A. Verklij, C.J.A. Van Echteld, W.J. Gerritsen, P.R. Cullis, and B. Dekruijff, *Biochim. Biophys. Acta* 600, 620 (1980).
31. **Micellization, Solubilization and Microemulsions**, K.L. Mittal (ed.), Plenum Press, New York (1977).
32. C. Tanford, **The Hydrophobic Effect: Formation of Micelles & Biological Membranes**, 2nd edn., John Wiley & Sons, New York (1980).
33. **Reverse Micelles : Biological and Technolgical Relevance of Amphiphilic Structures in Apolar Media**, P.L. Luisi and B.E. Straub (eds.), Plenum Press, New York (1984).
34. **Surfactants in Solution III**, K.L. Mittal and B. Lindman (eds.), Plenum Press, New York (1984).
35. **Physics of Amphiphiles : Micelles, Vesicles and Microemulsions**, V. deGiorgio and M. Cortesi (eds.), North-Holland, Amsterdam (1985).
36. **Microemulsions : Structure and Dynamics**, S.E. Friberg and P. Bothorel (eds.), CRC Press, Florida (1987).
37. **Structure and Reactivity in Reverse Micelles**, M.P. Pileni (ed.), Elsevier, Amsterdam (1989).
38. **Kinetics and catalysis in Microheterogeneous systems**, M. Grätzel and K. Kalyanasundaram (eds.), Marcel Dekker, Inc., New York (1991).
39. K. Vos, C. Laane, and A.J.W.G. Visser, *Photochem. Photobiol.* 45, 863 (1987).

40. P. Walde, A.M. Giuliani, C.A. Boicelli and P.L. Luisi, *Chem. Phys. Lipids* 53, 265 (1990).
41. E.E. Bittar, *Membrane Structure and Function*, Wiley-Interscience, New York (1980).
42. M.K. Jain and R.C. Wagner, *Introduction to Biological Membranes*, Wiley-Interscience, New York (1980).
43. N. Robertson, *The Lively Membranes*, Cambridge University Press, Cambridge (1983).
44. R.B. Gennis, *Biomembranes : Molecular Structure and Function*, Springer-Verlag, New York (1989).
45. S.J. Singer and G.L. Nicholson, *Science* 175, 720 (1972).
46. R. Harrison and G.G. Lunt, *Biological Membranes : Their Structure and Function*, Blackie Editions, Glasgow (1975).
47. J.F. Mead, R.B. Alfin-Slater, D.R. Howton, and G. Popjak, *Lipids : Chemistry, Biochemistry and Nutrition*, Plenum Press, New York (1986).
48. D.M. Small, in : *Handbook of Lipid Research*, D.J. Hanahan (ed.), Plenum Press, New York (1986).
49. (a) V. Luzzati and A. Tardieu, *Ann. Rev. Phys. Chem.* 25, 79 (1974);
(b) V. Luzzati, in *Biological Membranes*, D. Chapman (ed.), Vol. 1, Academic Press, New York (1968).
50. N.P. Franks and Y.K. Levine, in : *Membrane Spectroscopy*, E. Grell (ed.), Springer Verlag, Berlin (1981), Chap. 9 and references cited therein.
51. A.J. Verkleij and J. deGier, in : *Liposomes : From Physical Structure to Therapeutic Applications*, C.G. Knight (ed.), Elsevier - North Holland, Amsterdam (1981), Chap. 4 and references cited therein.
52. S.I. Chan, D.F. Bocian, and N.O. Petersen, in: Ref. 50, Chaps. 1 and 2 and references cited therein.
53. G.H. Brown, J.W. Doane, and V.D. Neff, *Crit. Rev. Solid state Sci.* 1, 303 (1970).
54. M. Montal, in : Ref. 33.
55. P.R. Cullis and B. Dekruiff, *Biochim. Biophys. Acta* 513, 31 (1978).
56. B. Dekruiff, P.R. Cullis, and A.J. Verkleij, *Trends Biochem. Sci.* 5, 79 (1980).
57. A.J. Verkleij, *Biochim, Biophys. Acta* 779, 43 (1984).

58. D.P. Siegel, *Biophys. J.* **49**, 1155 (1986); *ibid* 1171 (1986).
59. P.R. Cullis and B. Dekruijff, *Biochim, Biophys. Acta* **559**, 399 (1979).
60. R.P. Rand and V.A. Parsegian, *Ann. Rev. Physiol.* **48**, 201 (1986).
61. A.J. Verkleij in : **Electron Microscopic Analysis of Subcellular Dynamics**, H. Plattner (ed.) CRC Press Inc., Boca Raton, USA (1989).
62. P.R. Cullis, B. de Kruijff, M.J. Hope, R. Nayar, and S.L. Schmid, *Can J. Biochem.* **58**, 1091 (1980).
63. P.R. Cullis, M.J. Hope, and C.P.S. Tilcock, *Chem. Phys. Lipids* **40** 127 (1986).
64. (a)J.H. Fendler, in : Ref : 33, P. 305;
(b)A.S. Kertes and H. Gutman, in : **Surface and Colloidal Science**, E. Matijevic (ed.), Vol. 8, Wiley, New York (1976);
(c)A.S. Kertes, in : Ref : 31, P. 445.
65. (a)J.N. Israelachvili, in : Ref : 35;
(b)J.N. Israelachvili, and H. Wennerstrom, *J. Phys. Chem.* **96**, 520 (1992).
66. A.C. Balazs, M. Gempe, and J.E. Brady, *J. Chem. Phys.* **92**, 2036 (1990).
67. D.F. Evans, *Langmuir* **4**, 3 (1988).
68. B.L. Silver, *The Physical Chemistry of Membranes*, Allen & Unwin (Boston) and The solomon Press, New York (1985).
69. Y.F.Lo, B.M. Escot, E.J. Fendler, E.T. Adams, R.D. Larsen, and P.W. Smith, *J. Phys. Chem* **79**, 2609 (1975).
70. H.L. Rosano and G.B. Lyons, *J. Phys. Chem* **89**, 363 (1985).
71. B. Lindman and H. Wennerstrom, *Top. Curr. Chem* **87**, 1 (1980).
72. C. Tanford, in : Ref: 31; K.S. Birdi, in : Ref. 31; E. Rucknestein and R. Nagarajan, in : Ref: 31.
73. C. Chachaty, *Prog. NMR Spectrosc.* **19**, 183 (1987) and references cited therein.
74. M. Giomini, A.M. Giuliani, E. Trotta and C.A. Boicelli, *Chem. Phys. Lett.* **158**, 334 (1989).
75. B. Lindman, in : Ref : 35 ; C. Tanford, in : Ref : 31.
76. N. Muller, *J. Phys. Chem.* **79**, 287 (1975).
77. R. Haque, I.J. Tinsley, and D. Schmedding, *J. Biol. Chem.* **247**, 157 (1972).

78. A. Faure, A.M. Tistchenko, T. Zemb and C. Chachaty, *J. Phys. Chem.* **89**, 3373 (1985).
79. S.E. Friberg and M. Podzimek, *Colloid Polym. Sci.* **262**, 252 (1984).
80. G. Zumdell, *Hydration and Intermolecular Interaction*, Academic Press, New York (1969).
81. H.F. Eicke and H. Christen, *Helv. Chim. Acta* **61**, 2258 (1978).
82. M. Zulauf and H.F. Eicke, *J. Phys. Chem.* **83**, 480 (1979).
83. M.J. Rosen, *Surfactants and Interfacial Phenomena*, John Wiley & Sons, New York (1989), p. 150.
84. M. Ueda and Z.A. Schelly, *Langmuir* **4**, 653 (1988).
85. Z.A. Schelly, in : *Aggregation Processes in Solution*, E. Wyn-Jones and J. Gormally (eds.), Elsevier Scientific Press, New York (1983), p. 140.
86. Z.J. Yu, N.F. Zhou, and R.D. Neuman, *Langmuir*, **8**, 1885 (1992).
87. F. Nome, S.A. Chang, and J.H. Fendler, *J. Colloid Interface Sci.* **56**, 146 (1976).
88. M. Wong, J.K. Thomas, and T. Nowak, *J. Am. Chem. Soc.* **99**, 4730 (1977).
89. O.A. El Seound, in : Ref : 33.
90. P. Douzou, *Adv. Enzymology*, **51**, 1 (1980).
91. R.A. Day, B.H. Robinson, J.H.R. Clarke, and J.V. Doherty, *J. Chem. Soc. Faraday Trans. I.* **75**, 132 (1979).
92. V.V. Kumar, C. Kumar, and P. Raghunathan, *J. Colloid Interface Sci.* **99**, 315 (1984).
93. K. Tsujii, J. Sunamoto, and J.H. Fendler, *Bull. Chem. Soc. Jpn.* **56**, 2886 (1983).
94. V.V. Kumar and P. Raghunathan, *Chem. Phys. Lipids* **41**, 159 (1986).
95. H.F. Eicke and P.E. Zinsli, *J. Colloid Interface Sci.* **65**, 131 (1978).
96. E. Keh and B. Valeur, *J. Colloid Interface Sci.* **79**, 465 (1981); C. Bohne, E.B. Abuin, J.C. Scaiano, *Langmuir* **8**, 469 (1992).
97. V.V. Kumar and P. Raghunathan, *Lipids* **21**, 764 (1986).

98. F.M. Menger, G. Saito, G.V. Sanxero, and J.R. Dodd, J. Am. Chem. Soc. **97**, 909 (1975) and references cited therein; R. Schomacker, J. Phys. Chem. **95**, 451 (1991).
99. H. Fujii, T. Kawai, H. Nishikawa, and G. Ebert, Colloid & Polymer Sci. **260**, 697 (1982).
100. C. Balny and P. Douzou, Biochemie **61**, 445 (1979).
101. P.H. Elworthy, J. Chem. Soc. 813 (1959); ibid 1951 (1959).
102. K.P. Henrikson, Biochim, Biophys. Acta **203**, 228 (1970).
103. W.V. Walter and R.G. Hayes, Biochim. Biophys. Acta **249**, 528 (1971).
104. Y-H. Shaw, L-S. Kan, and N.C. Li, J. Magn. Reson. **12**, 209 (1973).
105. G. Klose and F. Stelzner, Biochim. Biophys. Acta **363**, 1 (1974).
106. P.H. Poon and M.A. Wells, Biochemistry **13**, 4928 (1974).
107. M.A. Wells, Biochemistry **13**, 4937 (1974).
108. J.B. Davenport and L.R. Fisher, Chem. Phys. Lipids **14**, 275 (1975).
109. B.M. Fung and J.L. McAdams, Biochim. Biophys. Acta **451**, 313 (1976).
110. V.V. Kumar, P.T. Manoharan and P. Raghunathan, J. Biosci. **4**, 449 (1982).
111. (a) R.C. Cooke and R. Wien, Biophys. J. **11**, 1002 (1971);
(b) L.A. Abetsedarskaya, F.G. Miftakhutdinova, V.D. Fedotov and N.A. Mal'tsev, Mol. Biol. **1**, 451 (1967).
112. P. Grigolini and M. Maestro, Chem. Phys. Lett. **127**, 248 (1986).
113. (a) J.R. Hansen and W. Yellin, in : **Water Structure at the Water-Polymer Interface**, H.H.G. Jellinek (ed.), Plenum Press, New York (1972), p. 19.
(b) S.H. Koenig and W.E. Schillinger, J. Biol. Chem. **244**, 3283 (1969).
(c) A. de Marco, E. Menegatti, P.L. Luisi, J. Biochem. Biophys. Methods **12**, 325 (1986).
(d) H.F. Eicke, in : **Microemulsions**, I.D. Robb (ed.), Plenum Press, New York (1982).
114. C.A. Boicelli, M. Giomini, A.M. Giuliani, Appl. Spectrosc. **38**, 537 (1984).

115. T.K. Jain, M. Varshney and A. Maitra, *J. Phys. Chem.* **93**, 7409 (1989).
116. A. Goto, H. Yoshioka, H. Kishimoto, and T. Fujita, *Langmuir* **8**, 441 (1992).
117. M. Ueda and Z.A. Schelly, *Langmuir* **5**, 1005 (1989); D.M. Zhu and Z.A. Schelly, *Langmuir* **8**, 48 (1992); J. Sunamoto, T. Hamada, T. Seto, and S. Yamamoto, *Bull. Chem. Soc. Jpn.* **53**, 583 (1980).
118. Z. Shervani, A. Maitra, T.K. Jain, and Dinesh, *Colloids and Surfaces*, **60**, 161 (1991); Z. Shervani, T.K. Jain, and A. Maitra, *Colloid & Polymer Sci.* **269**, 720 (1991).
119. I. Blei and R.F. Lee, *J. Phys. Chem.* **67**, 2085 (1963).
120. J.P.M. Janson, M. Kunst, A. Rip and P. Bordewijk, *Chem. Phys. Lipids* **9**, 147 (1972).
121. L.R.C. Barclay, J.M. MacNeil, J.A. van Kessel, B.J. Forrest, N.A. Porter, L.S. Lehman, K.S. Smith and J.C. Ellington Jr., *J. Am. Chem. Soc.* **106**, 6740 (1984).
122. R.J. Braedley, D.H. Grant, V.C. Reinborough and P.A. Ross, *Can. J. Biochem.* **54**, 3070 (1976).
123. P.A. Demchenko, *Colloid J. USSR.* **22**, 309 (1960).
124. P.H. Elworthy and D.S. McIntosh, *J. Pharm. Pharmacol.* **13**, 663 (1961).
125. P.H. Elwothy and D.S. McIntosh, *Kolloid-Z. Zeitschr. Polym.* **195**, 27 (1964).
126. V.R. Ramakrishnan, A. Darszon and M. Montal, *J. Biol. Chem.* **258**, 4857 (1983); M. Montal, in *Ref : 33*, p. 221 and references cited therein.
127. C.A. Boicelli, F. Conti, M. Giomini, and A.M. Giuliani, *Gazz. Chim. Ital.* **113**, 573 (1983).
128. G.L. Jendrasiak, *Chem. Phys. Lipids* **4**, 85 (1970).
129. P.H. Elworthy, *J. Chem. Soc.* **139** (1960).
130. J.D. Mckinney, *Chem. Phys. Lipids* **13**, 249 (1974).
131. J.H. Fendler, E.J. Fendler, and S.A. Chang, *J. Am. Chem. Soc.* **95**, 3273 (1973).
132. M.M. Rakhimov, M.V. Tuichibaev, O.N. Gorbataya, A.V. Kabanov, A.V. Levashov, and K. Martinek, *Biol, Membr.* **3**, 1030 (1986).
133. T.M. Bray, J.A. Magnuson, and J.R. Carlson, *J. Biol. Chem.* **249**, 914 (1974).

134. R.L. Misiorowski and M.A. Wells, *Biochemistry* **13**, 4921 (1974).
135. A.V. Levashov, N.L. Klejachko, A.V. Pshezhetskii, I.V. Berezin, N.G. Kotrikadze, B.A. Lomsedze, and K. Martinek, *Dokl. Akad. Nauk. SSSR* **289**, 1271 (1986).
136. A.V. Kabanov, N.L. Klyachko, A.V. Pshezhetskii, S.N. Namiotkin, K. Martinek, and A.V. Levashov, *Mol. Biol.* **21**, 275 (1987).
137. J. Sunamoto and T. Hamada, *Bull. Chem. Soc. Jpn.* **51**, 3130 (1978).
138. G. Klose, G. Hempel, and T.H.V. Zglinicki, *Chem. Phys. Lipids* **21**, 261 (1978).
139. L.R.C. Barclay, B.J. Balcom, and B.J. Forrest, *J. Am. Chem. Soc.* **108**, 761 (1986).
140. C.A. Boicelli, M. Giomini, and A.M. Giuliani, *Spectrochimica Acta* **37A**, 559 (1981).
141. C.A. Boicelli, M. Giomini, and A.M. Giuliani, in : **Membranes and Membrane Processes**, E. Drioli and M. Nakagaki (eds.), Plenum Press (1986).
142. C.A. Boicelli, F. Conti, M. Giomini, and A.M. Giuliani, in : **Physical Methods on Biological Membranes**, Plenum Press, New York (1985), p. 141.
143. C.A. Boicelli, F. Conti, M. Giomini, and A.M. Giuliani, *Spectrochimica Acta*, **38A**, 299 (1982).
144. A.M. Howe, C. Toprakcioglu, J.C. Dore, and B.H. Robinson, *J. Chem. Soc. Faraday Trans. I* **82**, 2411 (1986).
145. P.D.I. Fletcher, B.H. Robinson, and J. Tabony, *J. Chem. Soc. Faraday Trans. I* **82**, 2311 (1986).
146. S.H. Chen, *Ann. Rev. Phys. Chem.* **37**, 351 (1986).
147. M.P. Pileni, Th. Zemb, and C. Petit, *Chem. Phys. Lett.* **118**, 414 (1985); P.D.I. Fletcher, A.M. Howe, N.M. Perrins, B.H. Robinson, C. Toprakcioglu, and J.C. Dore, in : **Ref : 33**, p. 1745.
148. **Ref: 43**, p. 166.
149. P. Briiggeller, *J. Phys. Chem.* **90**, 1830 (1986); M. Seno, K. Sawada, K. Araki, K. Kise, and K. Iwamoto, *Bull. Chem. Soc. Jpn.* **53**, 2083 (1980); H. Caldararu, A. Caragheorgheopol, M. Dimonie, D. Donescu, I. Dragutan, and N. Marinescu, *J. Phys. Chem.* **96**, 7109 (1992).

150. G. Haering, P.L. Luisi, and H. Hauser, *J. Phys. Chem.* **92**, 3574 (1988); P. Baglioni, H. Nakamura, and L. Kevan, *J. Phys. Chem.* **95**, 3856 (1991); P. Marzola, C. Pinzino, and C.A. Veracini, *Langmuir* **7**, 238 (1991); D. Niethammer, B. Kirste, and Kurreck, *J. Chem. Soc. Faraday Trans.* **86**, 3191 (1990).
151. P. Schurtenberger, L.J. Magid, S.M. King, and P. Linder, *J. Phys. Chem.* **95**, 4173 (1991) and references cited therein.
152. P. Schurtenberger, L.J. Magid, J. Penfold, and R. Heenan, *Langmuir* **6**, 1800 (1990).
153. J. Peyrelasse and C. Boned, *J. Phys. Chem.* **89**, 370 (1985).
154. A. Boussaha and H-J. Ache, *J. Phys. Chem.* **84**, 3249 (1980).
155. M. Zulauf and H-F. Eicke, *J. Phys. Chem.* **83**, 480 (1979); R.A. Day, B.H. Robinson, J.H.R. Clarke, and J.V. Doherty, *J. Chem. Soc. Faraday Trans. I.* **75**, 132 (1979).
156. P. Bode and J.W.J. Van Dorp, *Appl. Radiat. Isot.* **42**, 599 (1991).

CHAPTER II

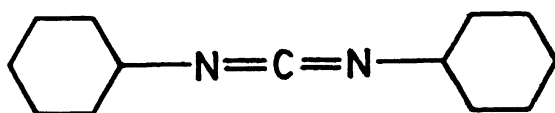
PREPARATION AND ^1H AND ^{31}P NMR STUDIES OF A NEW REVERSE MICELLE,
 LECITHIN/DCC/CYCLOHEXANE/ H_2O

II.1 Introduction

It has been reported recently that peptide bond ($-\text{NH}-\text{CO}-$) formation occurs at the interfacial region of an Aerosol-OT based reverse micellar system⁽¹⁾. This result has been achieved by taking a 'peptide condensing agent',⁽²⁾ as cosurfactant while forming the reverse micelle.

Based on the above, it occurred to us that if we could prepare a phospholipid-based reverse micellar system containing a 'peptide condensing agent' as cosurfactant, it may lead to useful information regarding how the freely diffusing globular proteins are both embedded in the bilayer (integral) and bound at the surface (peripheral) of the biological (or cell) membranes. (see Figs.I.1 and I.3).

We were successful in preparing a lecithin based reverse micelle with the very common 'peptide condensing agent', Dicyclohexyl carbodiimide (DCC)⁽²⁾, as cosurfactant.



Dicyclohexyl carbodiimide (DCC)

Such a reverse micellar system should provide a very appropriate model for cell membranes, as it can also facilitate peptide bond formation and hold peptides and proteins at the

interfacial region. Although we had originally intended to check the formation of peptides inside this reverse micelle, our attention had to be diverted to other important aspect of our further studies.

In this chapter, we report the preparation of the novel reverse micellar system, lecithin/DCC/cyclohexane/H₂O, and the results of our ¹H and ³¹P NMR investigation on this system.

II.2 Experimental Details

II.2.1 Materials Used

The extraction of chromatographically homogeneous egg lecithin was carried out using the method of Singleton et. al.⁽³⁾. The extracted lecithin was stored at -20°C in a 9 : 1 v/v mixture of chloroform and methanol. A single spot on a Silica Gel G (Merck) thin layer chromatogram confirmed the purity of the extracted lipid.

Prior to using the lipid, the solvent was evaporated under vacuum and the residual solid lipid was left in vacuum for about 6 hours. This solid was then dissolved in dry cyclohexane for forming reverse micelles for further characterization. The molecular weight of egg lecithin reported in most studies is in the range of 750-770. We have assumed a value of 760 in our studies.

The cyclohexane used was of AnalaR grade, and this was further dried by distilling and refluxing it in the presence of added sodium wire for about three hours and then redistilling (b.p. 81°C). The dry solvent was stored over sodium in a bottle with a

tight stopper.

The water used for making reverse micelles was deionised and double glass-distilled.

II.2.2 Maximum Water Uptake Measurement

As a first step towards preparing reverse micelles, solutions of 2%, 5%, 8% and 10% w/v lecithin in cyclohexane were prepared. By using 'Sigma Chemical' recalibrated microlitre pipettes, different volumes of water were added to these solutions. Then the samples were shaken thoroughly to ensure homogeneous mixing, allowed to stand for fifteen minutes and centrifuged at 800 rpm in a Clay-Adams table-top centrifuge and then inspected for phase separation. The amount of water added was increased in fixed steps. Based on the results of water uptake studies, the 5% w/v solution of lecithin in cyclohexane was chosen for finding out a suitable (lecithin : DCC) ratio to prepare a lecithin/DCC/Cyclohexane/Water system. On systematically varying (lecithin : DCC) molar ratio in the 5% lecithin solution of cyclohexane and subsequently adding water to form reverse micelles, we have chosen a (lecithin : DCC) molar ratio of 5 : 1 for further investigation. A schematic representation of the structure of this reverse micelle is given in Fig. II.1.

Since our main aim is to study the changes in properties of reverse micelle as a function of added water, we have kept the concentration of lecithin constant at 0.067 M, i.e., an approximately 5% w/v solution of lecithin in cyclohexane. Water

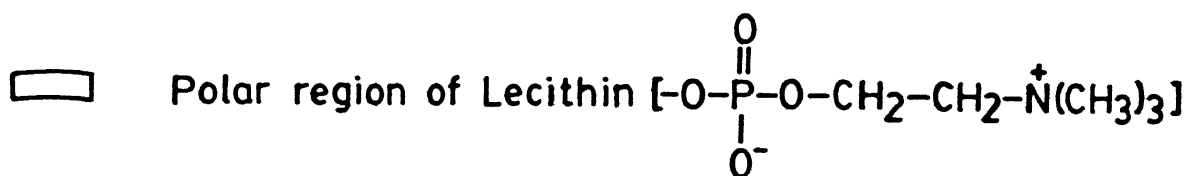
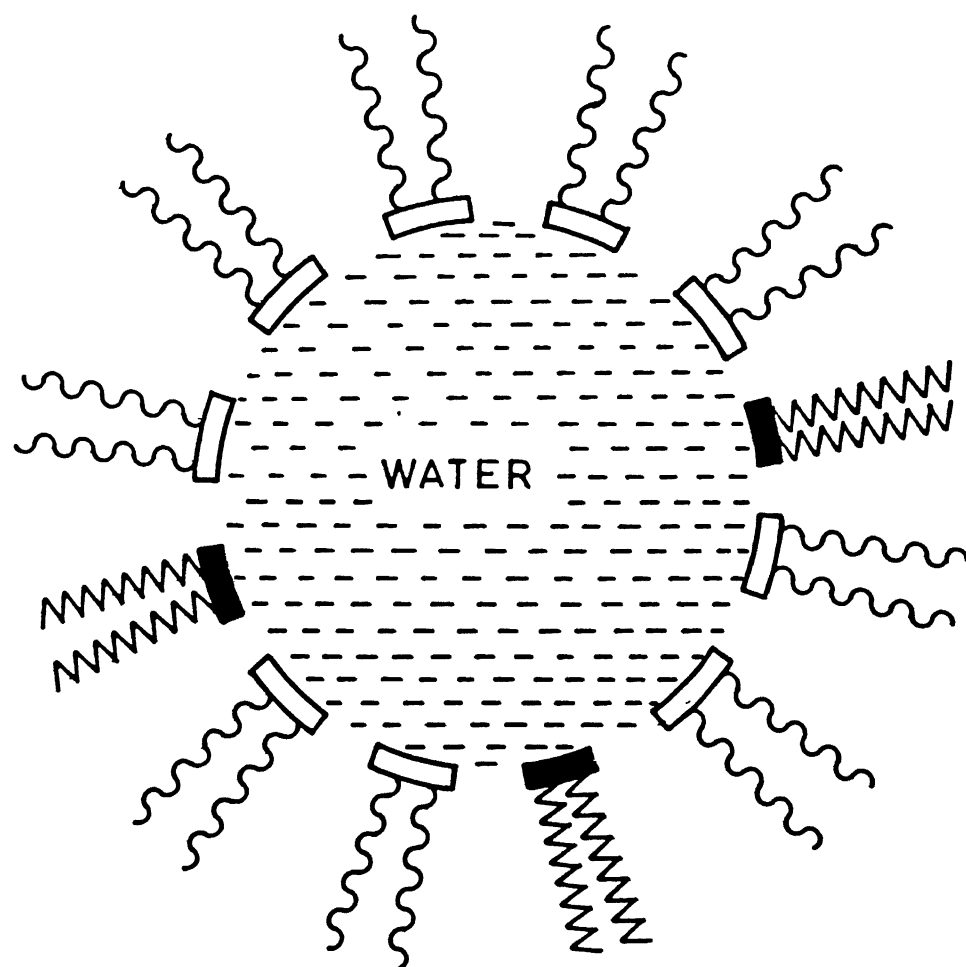


Fig.II.1

Schematic representation of the structure of lecithin/DCC/cyclohexane/ water reverse micelle.

is then added in fixed increments. Here we define a quantity R as the molar concentration ratio of water to lecithin, namely,

$$R = \frac{[\text{water}]}{[\text{lecithin}]} \quad [\text{II.1}]$$

This definition of R shall be maintained throughout this thesis. Further, the terms phosphatidyl choline (PC) and Lecithin shall be used interchangeably.

II.2.3 NMR Studies

(i) Chemical Shift Studies

To probe the electronic environment surrounding the protons of the water molecule and phosphorous of lecithin indirectly, we have measured the ^1H chemical shifts of water and the trimethyl amino group ($-\text{N}^+(\text{CH}_3)_3$) by proton NMR, and the phosphorous present in the phosphatic head group of lecithin by ^{31}P NMR for the reverse micelles at different R values.

(ii) Relaxation Studies

To elucidate further the role of water in this reverse micelle, the ^1H relaxation times of water molecules and those of the head group of lecithin, as well as the ^{31}P relaxation times of the head group, have been measured at various R values.

The longitudinal nuclear relaxation rate ($1/T_1$), also known as spin-lattice relaxation rate, leads us to getting information concerning the motion of molecules in solution⁽⁴⁾. A change in molecular motion usually reflects a change in the structure of the medium and/or the interactions between the

molecules observed and their surroundings.

All the proton NMR spectra were recorded on a BRUKER WP-80 FT NMR spectrometer operating at a ^1H frequency of 80 MHz. As this spectrometer needs a deuterated solvent for establishing magnetic field - to - frequency locking, we inserted a sealed D_2O capillary tube in the 5 mm NMR sample tubes for all our spectral recordings. The common inversion recovery (180° - τ - 90°) pulse sequence was used for spin-lattice relaxation time (T_1) measurements. The 90° pulse width for protons in this spectrometer was 5.2 μs .

All ^{31}P NMR spectra were recorded on a BRUKER WM-400 FT NMR spectrometer operating at a ^{31}P frequency of 161.984 MHz. A capillary tube containing 80% phosphoric acid was used as a reference. T_1 measurements were carried out once again by the inversion recovery method. The 90° pulse width in this case was 44 μs . T_2 values were measured from experimental spectra ($T_2 = \frac{1}{\pi \nu_{1/2}}$, where $\nu_{1/2}$ is the linewidth at half height).

II.3 Results and Discussion

From our water uptake-studies, we could determine that the maximum amount of water that could be solubilized in 5:1 lecithin : DCC in cyclohexane solvent was 0.37 g of water per g of PC, or 15.8 mole of water per mole of PC. This value is only marginally more as compared to the value reported earlier from our laboratory for PC in cyclohexane⁽⁵⁾, which is 0.35 g of water per g of PC or 15.0 mole of water per mole of PC. This indicates that the addition of DCC does not increase the size of the reverse

micelle substantially to accomodate more water in the aqueous core as compared to the non-DCC containing counterpart.

The slightly turbid and viscous solution formed between R values of 5 and 7 in DCC added reverse micellar system, which could be observed visually, were very similar to those observed earlier in our laboratory in PC/cyclohexane/water system. In the latter system, our studies have conclusively proved the viscosity/turbidity changes to be due to the change in the shape of the reverse micelle from spherical to tubular aqueous canals⁽⁵⁾.

Fig. II. 2 shows a proton NMR spectrum of lecithin and DCC in Cyclohexane. The observed peaks are assigned according to their chemical shift (δ) values (relative to TMS). The absence of a peak around 5 ppm in this spectrum clearly shows that there is no water present in the solution before adding water for forming the reverse micelles. Fig. II.3 shows a representative spectrum for the R = 5 reverse micelle.

On systematically increasing the water content of lecithin-DCC solutions from R = 2 to R = 15 for forming the various reverse micelles, and by plotting the observed chemical shift(δ) values for water and $-N(CH_3)_3^+$ protons in each case, one gets the plots of Fig. II.4 and II.5.

From Fig. II.4, the water proton resonance is upfield at lower water content compared to that of normal bulk water ($\delta \sim 5$). This indicates a minimal amount of hydrogen bonding. As the water concentration is increased, there is an upfield shift of the water proton resonance followed by a downfield shift towards the normal

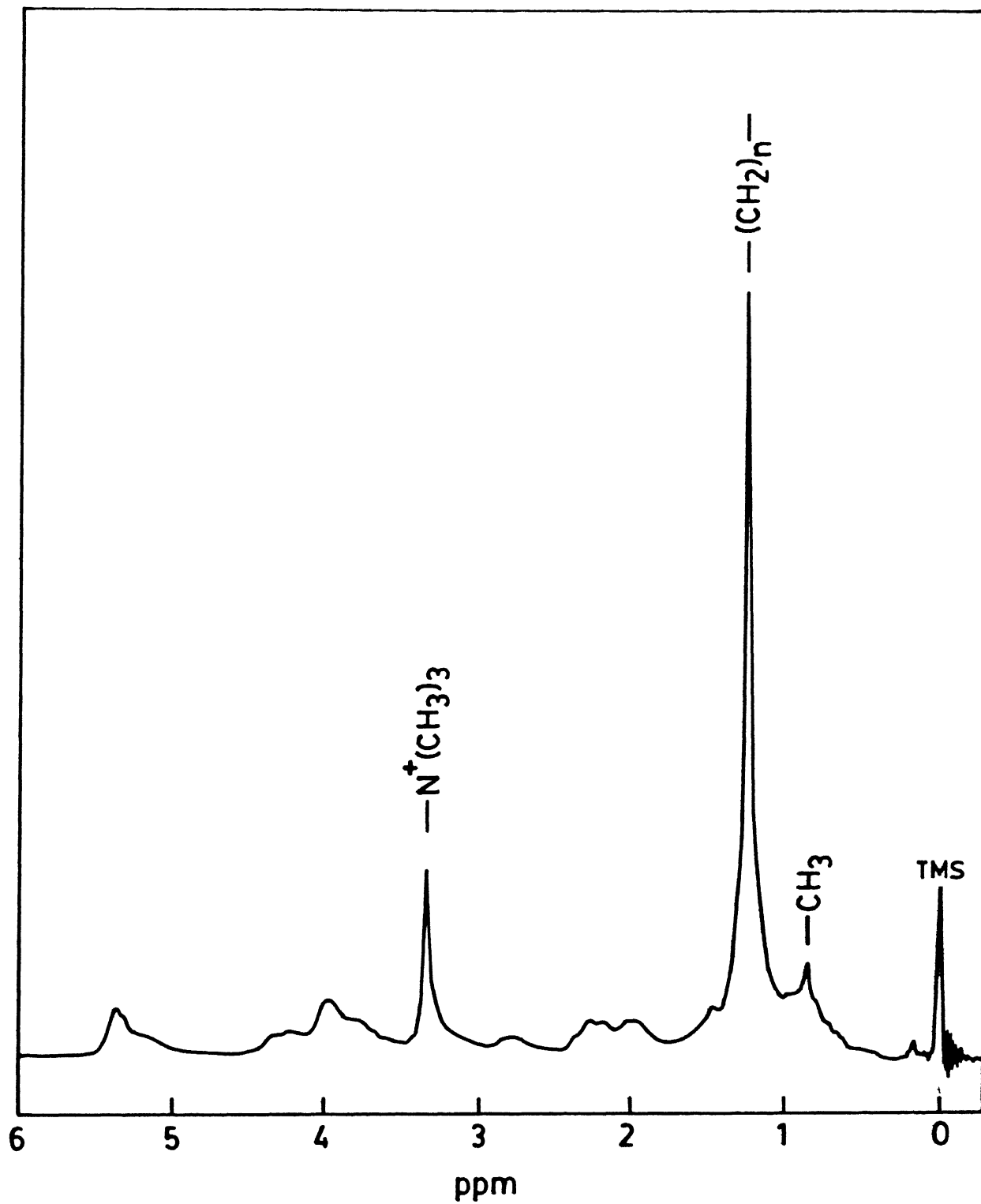


Fig.II.2 80 MHz proton NMR spectrum of lecithin and DCC in cyclohexane.

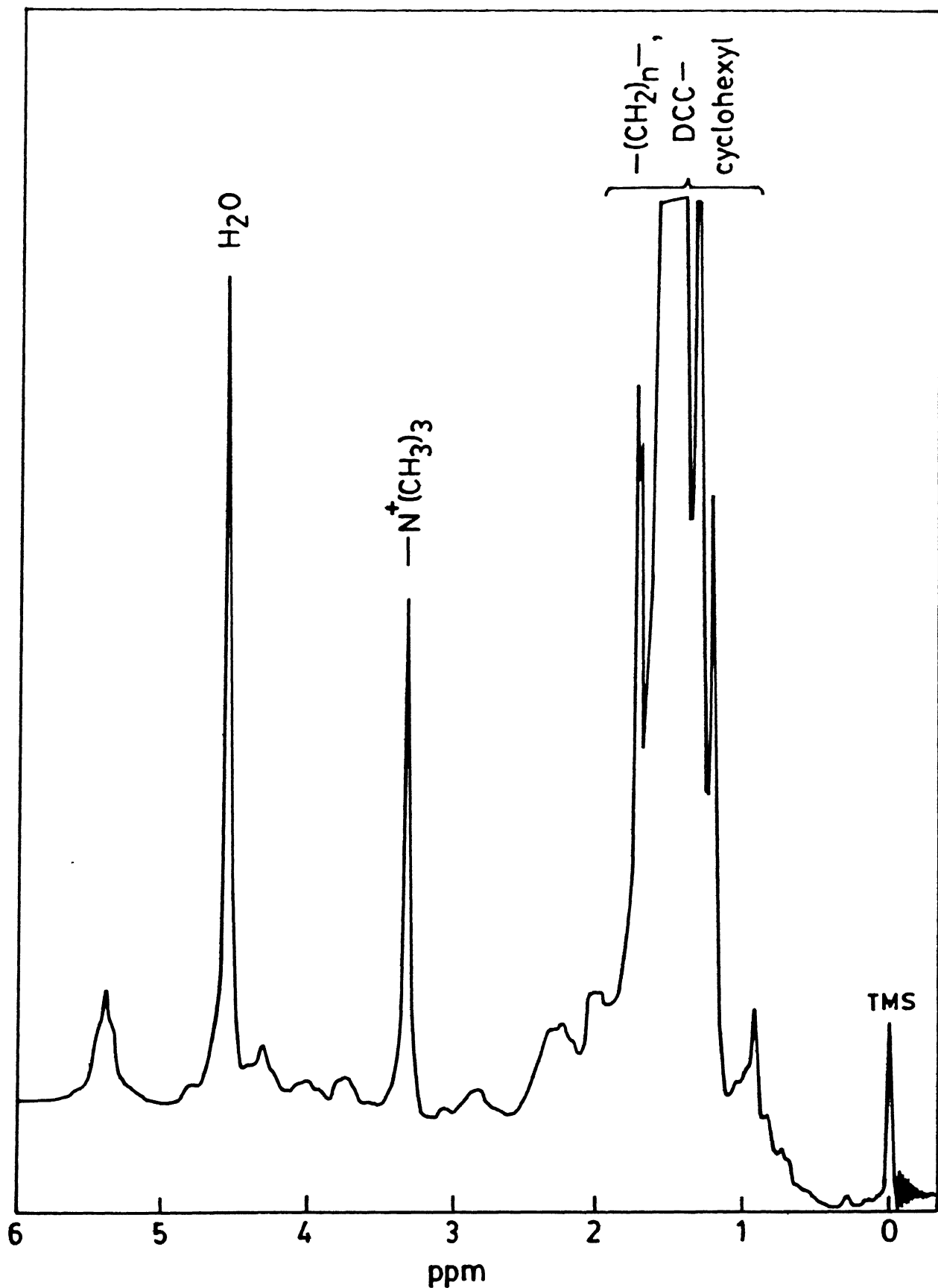


Fig.II.3

80 MHz proton NMR spectrum of lecithin/DCC/cyclohexane/water at R = 5.

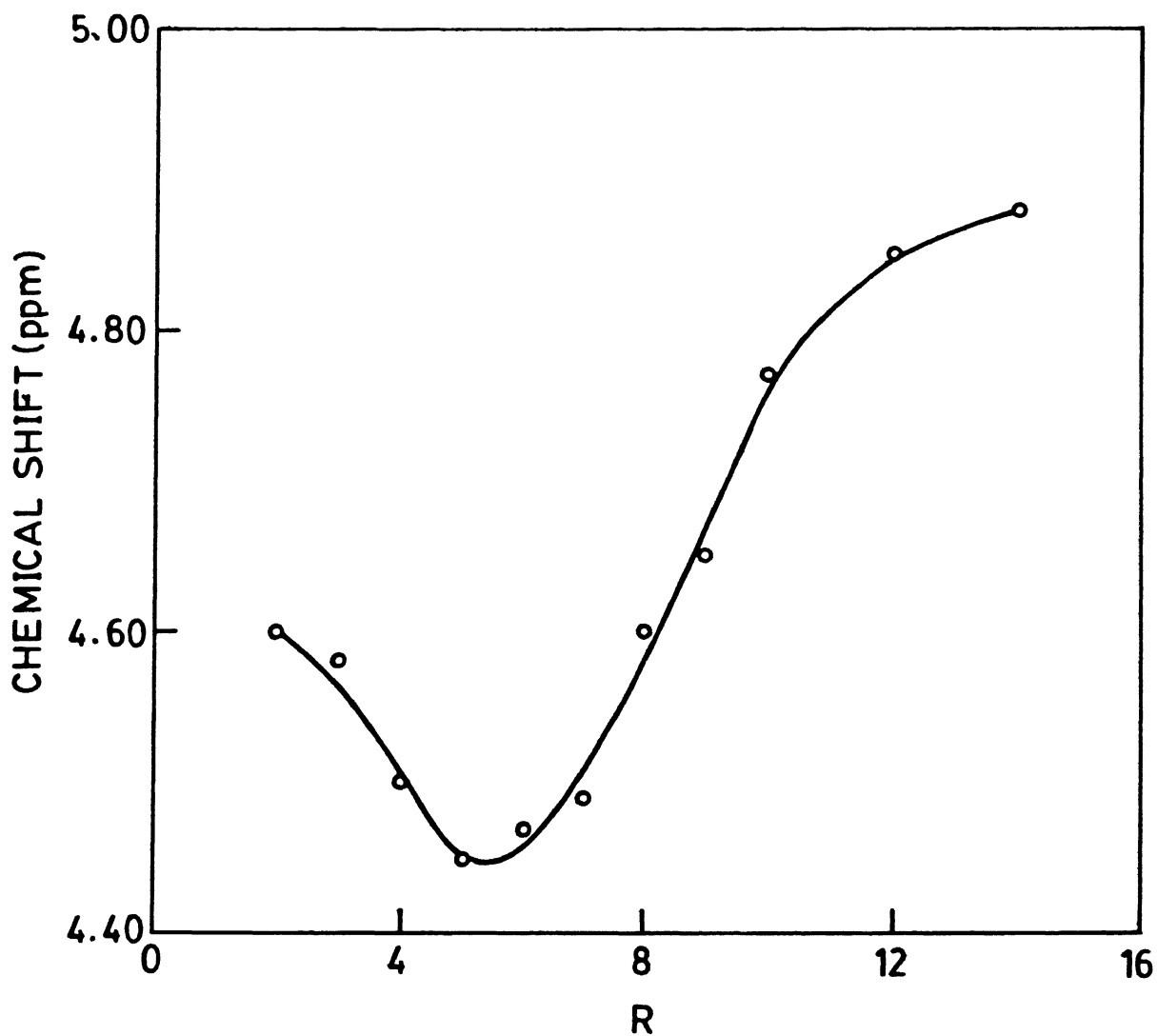


Fig.II.4 ^1H NMR chemical shifts of water protons in lecithin/DCC/cyclohexane/ H_2O as a function of R.

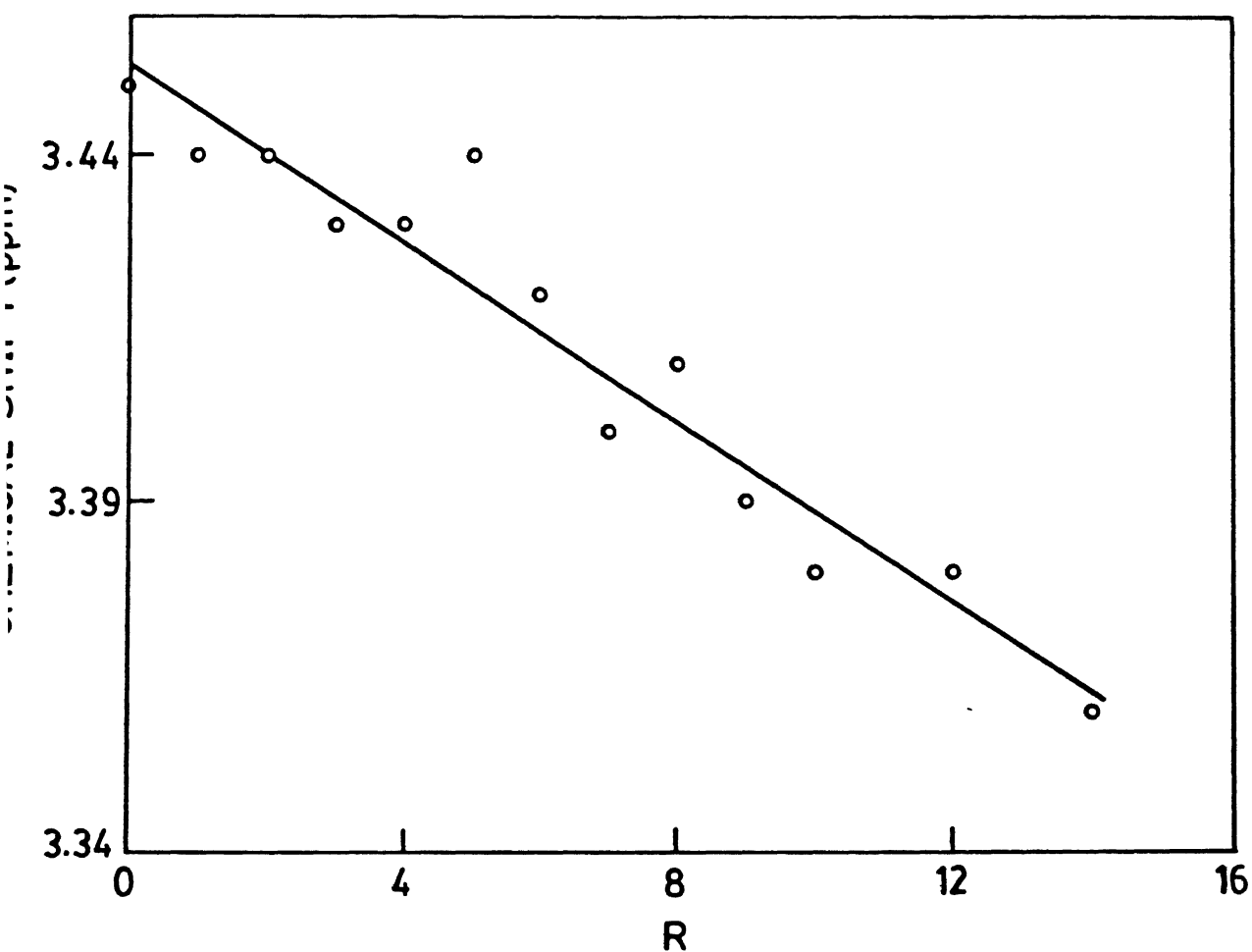


Fig.II.5 ^1H NMR chemical shifts of $-\text{N}^+(\text{CH}_3)_3$ protons in lecithin/DCC/cyclohexane/ H_2O as a function of R.

bulk water δ value of around 5. However, the $-\text{N}^+(\text{CH}_3)_3$ proton resonance moves continuously upfield as the water concentration (R value) increases (see Fig. II.5).

The above trend in the water proton resonance arises because the chemical shifts of the $-\text{OH}$ protons are strongly influenced by the following two factors : (i) changes in the hydrogen-bonded state of water and (ii) changes in the chemical environment of the water molecule, i.e., the ratio of water bound to the lecithin head group to the free, bulk water in the inner 'pool'.

The trend of the water proton chemical shift observed by us at 80MHz is in the same direction as that reported by Shaw et. al.⁽⁶⁾ at 250 MHz for lecithin/ CCl_4 /water system, Klose and Stelzner⁽⁷⁾ at 100MHz for lecithin/benzene/water system, and Kumar and Raghunathan⁽⁸⁾ for lecithin/cyclohexane/water system.

In ^{31}P NMR, a slight increase in δ value is observed upto around $R = 4$, after which there is a jump in δ value at around $R = 6$, the chemical shift further increasing slowly as R is increased (see Fig. II.6).

Given the above trends in the ^1H NMR chemical shifts for water and $-\text{N}^+(\text{CH}_3)_3$, and ^{31}P NMR chemical shifts for the phosphorous present in the lecithin polar head groups, we consider a plausible arrangement of lecithin head group in the reverse micelle. This arrangement derives support from a couple of earlier findings, namely, those of Henderson et. al.⁽⁹⁾ from ^{31}P NMR studies of phospholipids in dry organic solvents and of

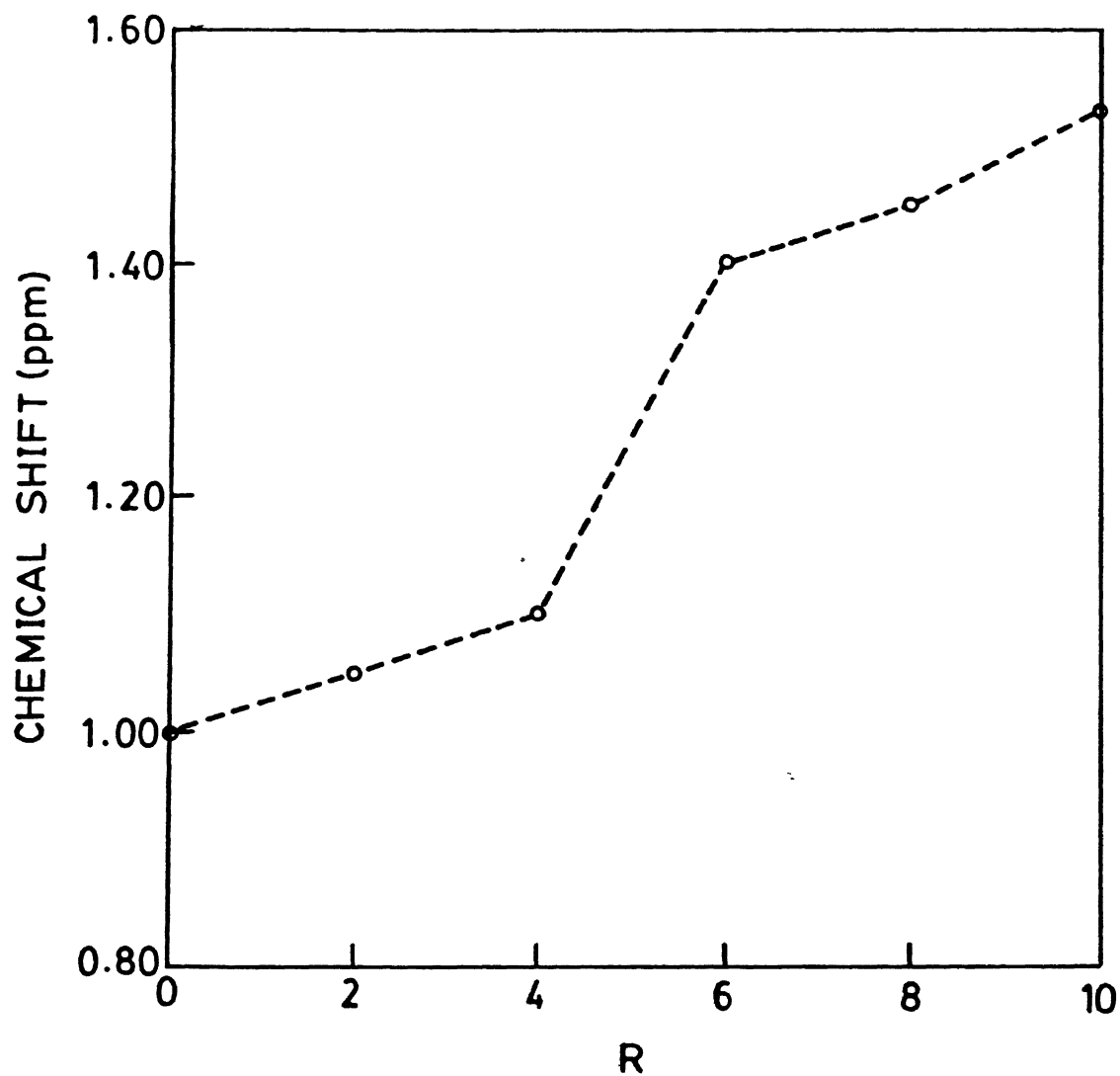


Fig.II.6

^{31}P NMR chemical shifts of the head group phosphate in lecithin/DCC/cyclohexane/ H_2O as a function of R.

Pullman and Berthod⁽¹⁰⁾ from their quantum mechanical studies of energetically preferred conformations of the polar heads of phospholipids. Both the above studies^(9,10) favour the fact that the polar heads of the phospholipids are likely to adopt highly folded structures, as depicted in Fig. II.7.

For a water molecule (or molecules) getting 'bound' to the head group of lecithin, the electrostatic interaction model with positively charged terminal trimethyl-amino group ($-\overset{+}{\text{N}}(\text{CH}_3)_3$) and negatively charged phosphate oxygens suggested by the above studies^(9,10) becomes significant as we shall see presently.

As the water content is increased the most probable effect will be disruption, at least in part, of the folded arrangement of the head group and the production of a more 'swollen' or extended conformation. Indeed, such a phenomenon has been envisaged by Pullman and Berthod⁽¹¹⁾ in connection with the theoretical model of the zwitterionic gamma-aminobutyric acid.

Water addition reduces the electrostatic interaction between the positively charged trimethyl-amino group and the negatively charged phosphate oxygen atoms. Water is more likely to bind to the phosphate portion of the head group. The protons of water will thus form a weak bond with the phosphate group; likewise, the oxygen atoms of water will be in weak electrostatic interaction with $-\overset{+}{\text{N}}(\text{CH}_3)_3$. The suggested interaction of water molecule with the polar head group of lecithin is shown in Fig. II. 8(a).

The possible picture for the electrostatic interaction of water molecule with DCC is given in Fig.II.8(b).

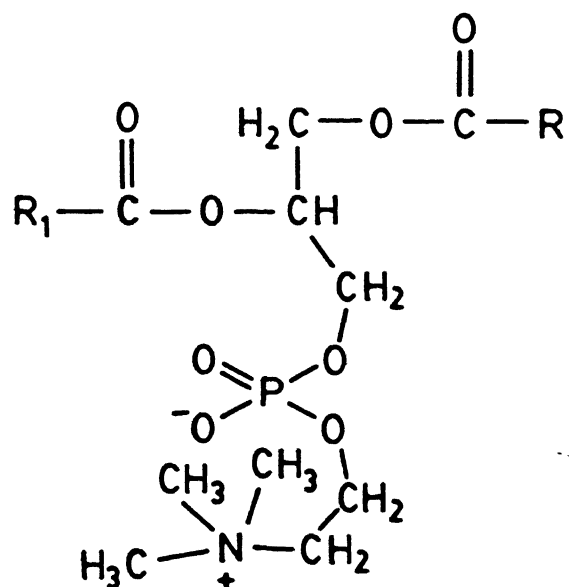
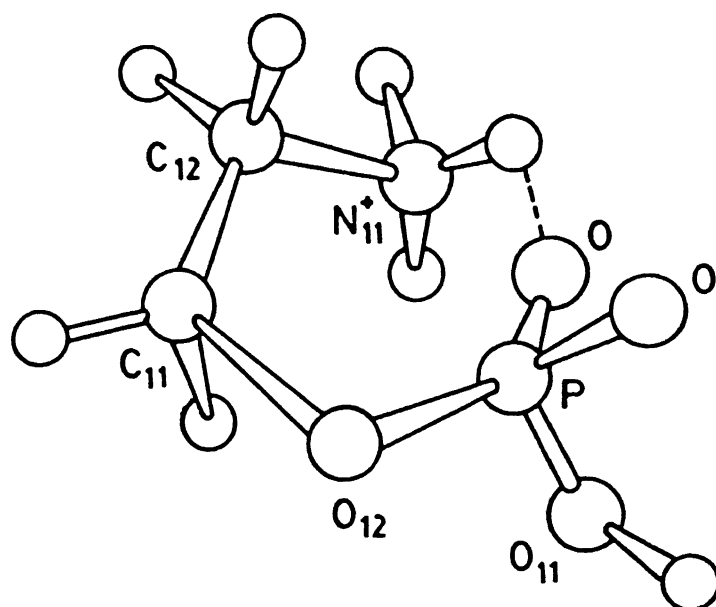


fig.II.7

Structure of folded polar head group of Lecithin.

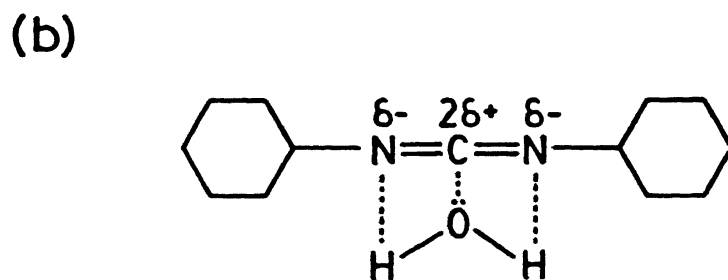
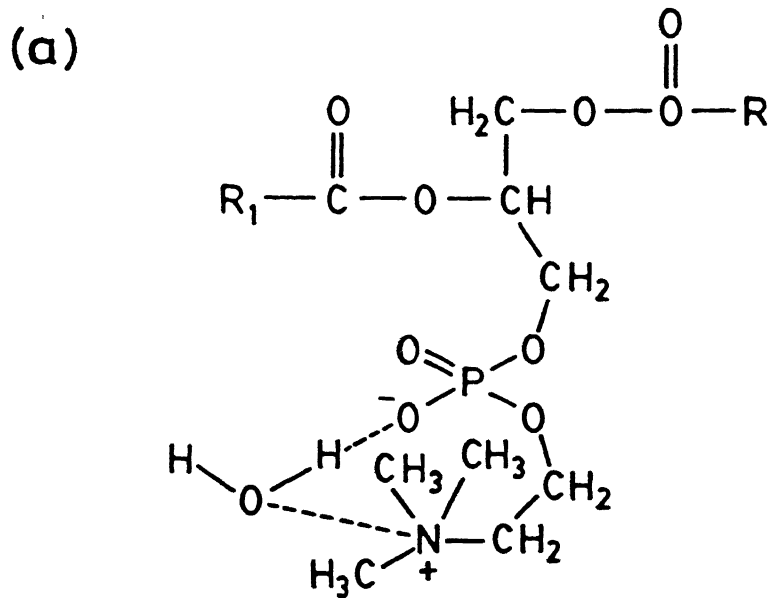


Fig.II.8

Interaction of water with (a) polar head group of Lecithin and (b) DCC.

In addition to the mechanisms suggested above, there also exists the possibility of electrostatic interaction between the polar head groups of lecithin and the polar region ($-N=C=N-$) of DCC. At the moment, however, we do not have experimental evidence to show possible electrostatic interactions of water molecules and lecithin polar heads with DCC. In our suggested model (Fig. II. 8(a)), the water is weakly hydrogen bonded with itself, or equivalently, the oxygen atoms are further removed from the hydrogen atoms⁽¹²⁾. Such a weak hydrogen bonding would, of course, lead to an upfield shift of the $-OH$ protons because it is shielded more thoroughly from the external magnetic field. This explains the initial upfield shift of the $-OH$ proton resonance in Fig. II. 4. In fact, this shift is essentially very similar to that observed whenever structure breakers (i.e., electrolytes) are added to water^(4,13). Furthermore, the above trend in the observed chemical shifts strongly resembles the trend in the PC/cyclohexane/water system studied in our laboratory⁽¹⁴⁾.

At higher values of R , i.e., when the water is in excess, free water pools are formed with an increase in the average level of hydrogen bonding of water due to water-water H-bonds (i.e., self-association), leading to downfield shift in the $-OH$ resonance. This is in accordance with the result of Fig. II.4.

From Fig. II.5, it is evident that $-N(CH_3)_3$ proton resonance continuously moves upfield as a function of added water upto a certain value and then levels off. This, again, is quite expected in view of the added water electrostatically shielding the trimethylamino group.

The arguments given above for rationalising the -OH and ${}^+N(CH_3)_3$ proton chemical shifts are nicely complemented by our ${}^{31}P$ NMR chemical shifts of the lecithin head group presented below.

Fig. II. 6 shows the variation in the ${}^{31}P$ NMR chemical shift as a function of added water. As R increases, the ${}^{31}P$ chemical shifts move downfield and, at R values between 4 and 6, there is a big jump in downfield shifting of chemical shift. As above, the explanation, of course, is that there will be a strong electrostatic interaction between the hydroxyl proton of the added water and the oxygen atoms of phosphate of lecithin. Such an interaction would be expected to deshield phosphorous and hence result in a downfield shift. The jump in chemical shift in the R-value range of 4 and 6 may be due to the onset of a change in structure of the reverse micelle and other physical properties such as viscosity etc. Such changes have been observed in a similar system studied earlier in our laboratory^(5,8,15).

The variation of the spin-lattice relaxation time, T_1 , of the water protons as a function of added water is shown in Fig. II. 9. One notices in this figure that T_1 of the water protons increases roughly linearly from R = 1 to R = 14, except in the range R = 4 and 8, when there is a sharp 'peaking' in T_1 values.

We shall now analyze quantitatively the water proton spin-lattice relaxation times presented above in terms of microviscosity (i.e., viscosity of the reverse micelle at different smaller regions) values. It is well known⁽¹⁶⁾ that the relaxation times are related to molecular motion by the rotational

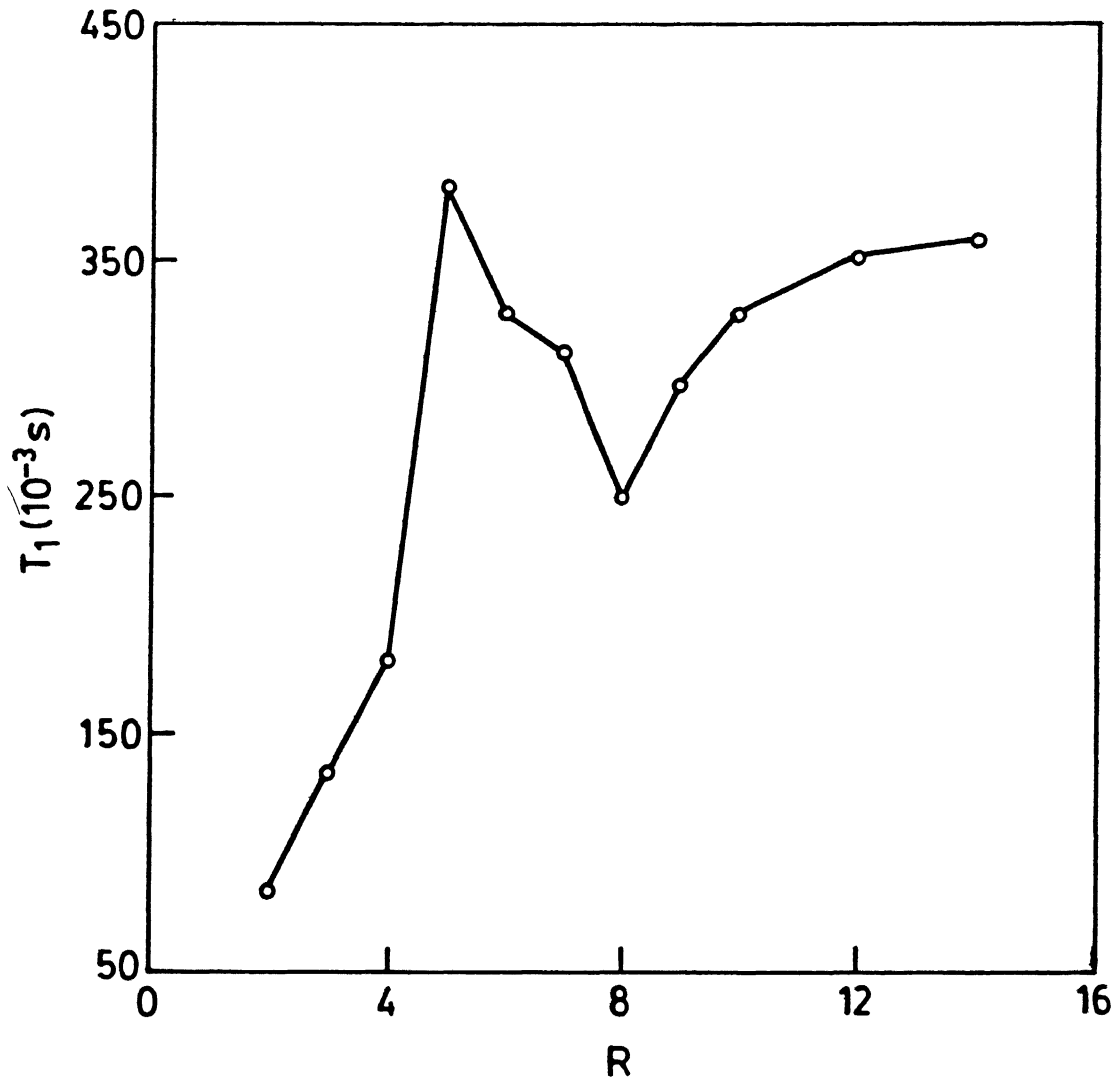


Fig.II.9 Variation in T_1 of water protons as a function of R

correlation time, τ_c , which gives a measure of the mean residence time of the two proton nuclei in a given relative orientation. The correlation time, in turn, depends on the microviscosity. The spin-lattice relaxation time T_1 may be considered to be the result of a combination of intramolecular and intermolecular relaxation effects for any small molecule such as water containing two identical spins. These two relaxation effects can be evaluated theoretically. The relevant equations for intermolecular and intramolecular relaxation effects for the water molecule, as developed in the classic work of Bloembergen et al.⁽¹⁶⁾, are :

$$\frac{1}{T_{1(\text{intra})}} = \frac{2\gamma^4 \hbar^2 I(I+1)}{5r^6} \left[\frac{\tau_c}{1+\omega^2 \tau_c^2} + \frac{4\tau_c}{1+4\omega^2 \tau_c^2} \right] \quad [\text{II.3}]$$

$$\frac{1}{T_{1(\text{inter})}} = \frac{9\pi^2 \gamma^4 \eta \hbar^2 N_0}{5kT} \quad [\text{II.4}]$$

$$\frac{1}{T_1} = \frac{1}{T_{1(\text{intra})}} + \frac{1}{T_{1(\text{inter})}} \quad [\text{II.5}]$$

In eqns. II. 3 to II. 5 $T_{1(\text{intra})}$ and $T_{1(\text{inter})}$ are the intramolecular and intermolecular parts of the dipolar mode of relaxation, γ is the gyromagnetic ratio, r is the proton-proton distance in the water molecule, τ_c is the rotational correlation time, ω is the resonance frequency of the water molecule, η is the microviscosity and N_0 is the volume concentration of spins.

Substituting the value of τ_c obtained from eqn. II. 3 in the well known Debye-Stokes equation

$$\tau_c = \frac{4\pi\eta a^3}{3kT} \quad [\text{II.6}]$$

where a is the radius of the water molecule (approximated to be a sphere), one can get η , the microviscosity of the water molecules whose T_1 is known.

We have analyzed the T_1 data of water protons in two ways : (i) under the simplifying assumption that the intramolecular relaxation mode alone is dominant in equations [II.3] and [II.6] and (ii) under the assumption that both intra- and intermolecular relaxation mechanisms are operative in equations [II.3] - [II.6]. The results of such calculations are presented in Table II.1.

We notice from Table II.1 that the microviscosity (η) of water for this reverse micelle is initially very high and falls off rapidly with the addition of water. The explanation for the downward η trend is that, at lower R values, all water molecules will be bound to the polar head groups and show higher η ; when R increases the amount of free 'pool' water also increases, leading to decreased η values. It reaches a lower limiting value at around $R = 5$. These trends are quite in agreement with the microviscosities of water in other micellar systems. For example, Shinitzky et al⁽¹⁸⁾ reported microviscosities of 17-50 cP for water in cetyltrimethyl ammonium bromide micelles and Pownall and Smith⁽¹⁹⁾ calculated a microviscosity of 151 cP for water in hexadecyl trimethyl ammonium bromide micelles.

Table II.1 Microviscosity of water environment in the Lecithin/DCC/Cyclohexane/H₂O reverse micelle.

R	T ₁ (10 ⁻³ s)	τ_c according to [II.3] and η , [II.6]		τ_c according to [II.5] and η according to [II.6]	
		τ_c (10 ⁻¹⁰ s)	η (cP)	τ_c (10 ⁻¹⁰ s)	η (cP)
2	83	1.787	53.6	1.044	31.3
3	133	1.097	32.9	0.650	19.5
4	181	0.802	24.0	0.477	14.3
5	382	0.378	11.3	0.226	6.8
6	328	0.441	13.2	0.263	7.9
7	312	0.464	13.9	0.276	8.3
8	249	0.582	17.4	0.346	10.4
9	298	0.486	14.6	0.289	8.7
10	328	0.441	13.2	0.263	7.9
12	352	0.411	12.3	0.245	7.3
14	360	0.402	12.0	0.240	7.2

Constants used : $a = 1.50 \times 10^{-12}$ m ; $r = 1.52 \times 10^{-12}$ m ;
 $h = 6.626 \times 10^{-34}$ J s ; $N_O = 6.798 \times 10^{22}$;
 $k = 1.38 \times 10^{-23}$ J/K/molecule ;
 $T = 307$ K

From Table II.1, it is also seen that τ_c of the proton nuclei of water molecules decreases as a function of added water upto an R value of ~6. This shows that the mobility of the water molecules bound to the polar head groups of lecithin and DCC is significantly reduced from that of normal bulk water⁽¹⁷⁾ ($\tau_c = 3 \times 10^{-12}$ s) and hence showing higher τ_c values. There is a

sharp decrease in τ_c around R values 5-6. A similar trend was observed earlier in our laboratory⁽⁸⁾ for lecithin/cyclohexane/water system. Based on our earlier results^(5,8), a plausible reasoning for this sharp reduction in τ_c may be due to the change in shape of the reverse micelle from spherical to tubular aqueous canals. The decrease in τ_c is expected as τ_c depends on the size and shape of the water pool. τ_c decreases as R is increased due to the fact that once the hydration of polar head groups of surfactants by water molecules is complete, the further addition of water results in a free 'pool', which causes τ_c to move gradually towards its normal bulk water value.

The water molecules are only in contact with the polar head groups. Addition of water to the system increases the fluidity of the central aqueous pool and the interfacial region. As a result, the relaxation times of the $-N(CH_3)_3^+$ protons would be expected to increase. This is found to be roughly the case as shown in Fig. II. 10.

Fig. II. 11 shows the trend of spin-spin relaxation times, T_2 , for the water protons as a function of R. T_2 values increase till $R = 6$ and then decrease. This leads us to suggest that some of the molecular organizational rearrangements necessary for the phase transition take place in this region⁽⁸⁾.

The T_1 and T_2 values of water protons roughly follow the same trend, and the noticeable difference is that T_2 values are lower than the T_1 . This difference shows that in addition to intramolecular dipole-dipole mode of relaxation there may be other modes of relaxation available for the water protons. The

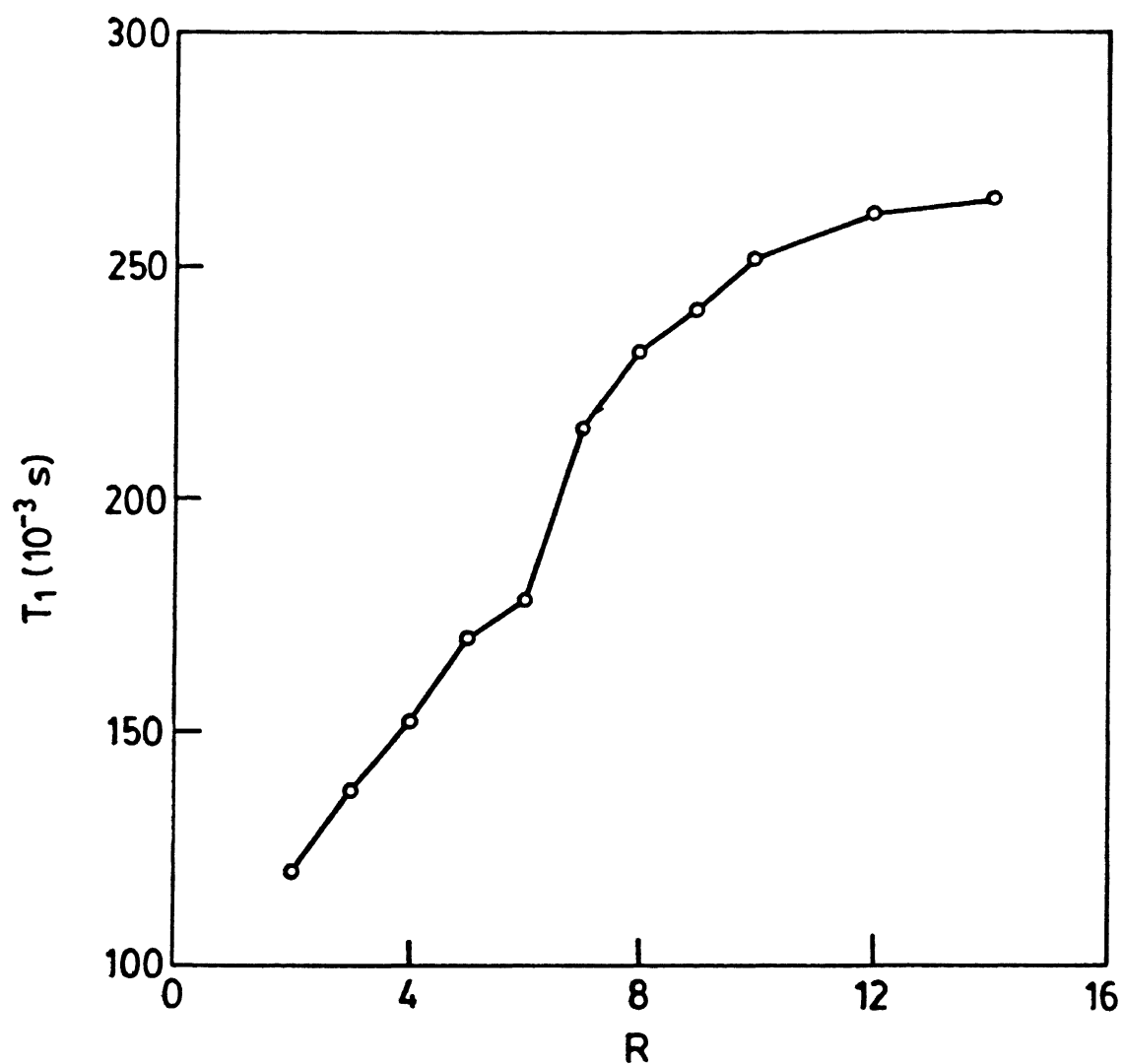


Fig.II.10

Variation in T_1 of $-\text{N}(\text{CH}_3)_3^+$ protons as a function of R .

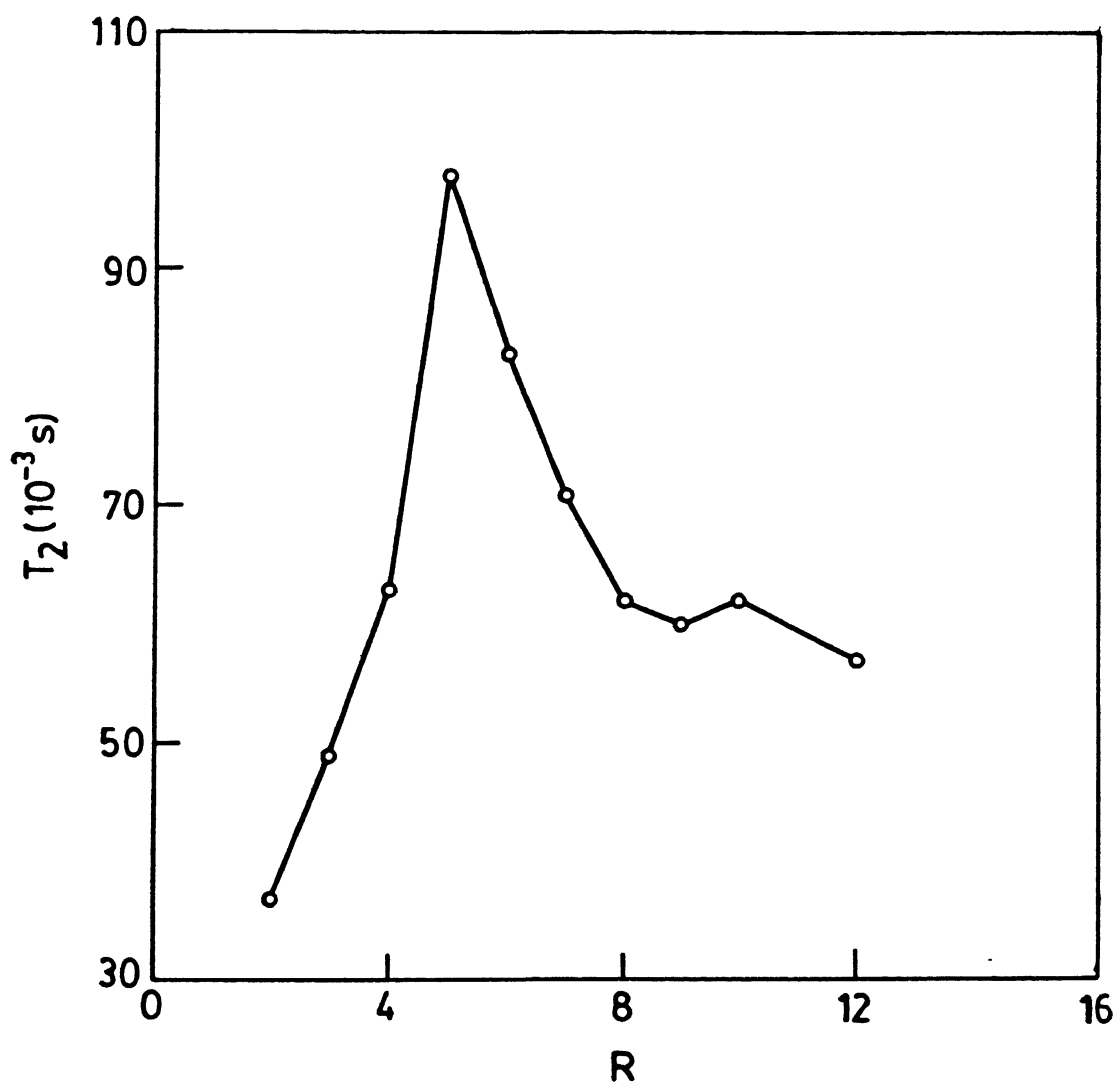


Fig.II.11 Variation in T_2 of water protons as a function of R .

rationalization for this is given below by calculating theoretically the T_2 values assuming that the intramolecular dipole-dipole relaxation mechanism is dominant and that the intermolecular relaxation mechanism can be ignored. The relevant equation is⁽²⁰⁾:

$$\frac{1}{T_{2(\text{intra})}} = \frac{\gamma^4 \hbar^2 I(I+1)}{5r^6} \left[3\tau_c + \frac{5\tau_c}{1+\omega^2\tau_c^2} + \frac{4\tau_c}{1+4\omega^2\tau_c^2} \right] \quad [\text{II.7}]$$

The rotational correlation time, τ_c , obtained from eqn. [II.3] is substituted in equation [II.7] to calculate the T_2 at various water concentrations (i.e., R values). The calculated and experimental T_2 values at different water concentrations are given in Table II.2.

It is seen from the Table II.2 that the experimental T_2 values are consistently much lower than those calculated. Ignoring such unlikely causes as poor magnetic field homogeneity, the results of Table II.2 may be interpreted to mean that other relaxation mechanisms should also be considered for calculating T_2 values, in addition to intramolecular dipole-dipole relaxation. Likely additional relaxation mechanisms are exchange narrowing, spin-rotational interaction and chemical shift anisotropy. We mention here that our experimental T_2 values have been evaluated from the absorption linewidths at half-maximum height. Slight inhomogeneities in the magnetic field would cause additional line broadening and thereby result in a decrease in the apparent relaxation time. However, we are aware of the fact that this can be eliminated by measuring the signal line width at two different

magnetic field strengths, because the field independence of linewidth is a classical test for magnetic field homogeneity⁽²¹⁾.

Table II.2 **Calculated and Experimental T_2 values of water protons in Lecithin/DCC/Cyclohexane/ H_2O reverse micelle.**

R	T_2 calculated from eqn. [II.7], (in seconds)	T_2 obtained from spectra [$T_2 = \frac{1}{\pi \nu_{1/2}}$], (in seconds)
2	0.068	0.037
3	0.110	0.049
4	0.150	0.063
5	0.318	0.098
6	0.273	0.083
7	0.260	0.071
8	0.207	0.062
9	0.248	0.060
10	0.273	0.062
12	0.293	0.057

Fig. II.12 and II.13 show the variation of ^{31}P linewidth and T_1 values, respectively, for the phosphorous in the choline head group of the reverse micellar system.

From Fig. II. 13 it is clear that, when no water is added, lecithin molecules show a high T_1 value of about 1.4 s. This may be ascribed to free-tumbling lecithin molecule which occur in solutions free, non-aggregated monomers. When water is

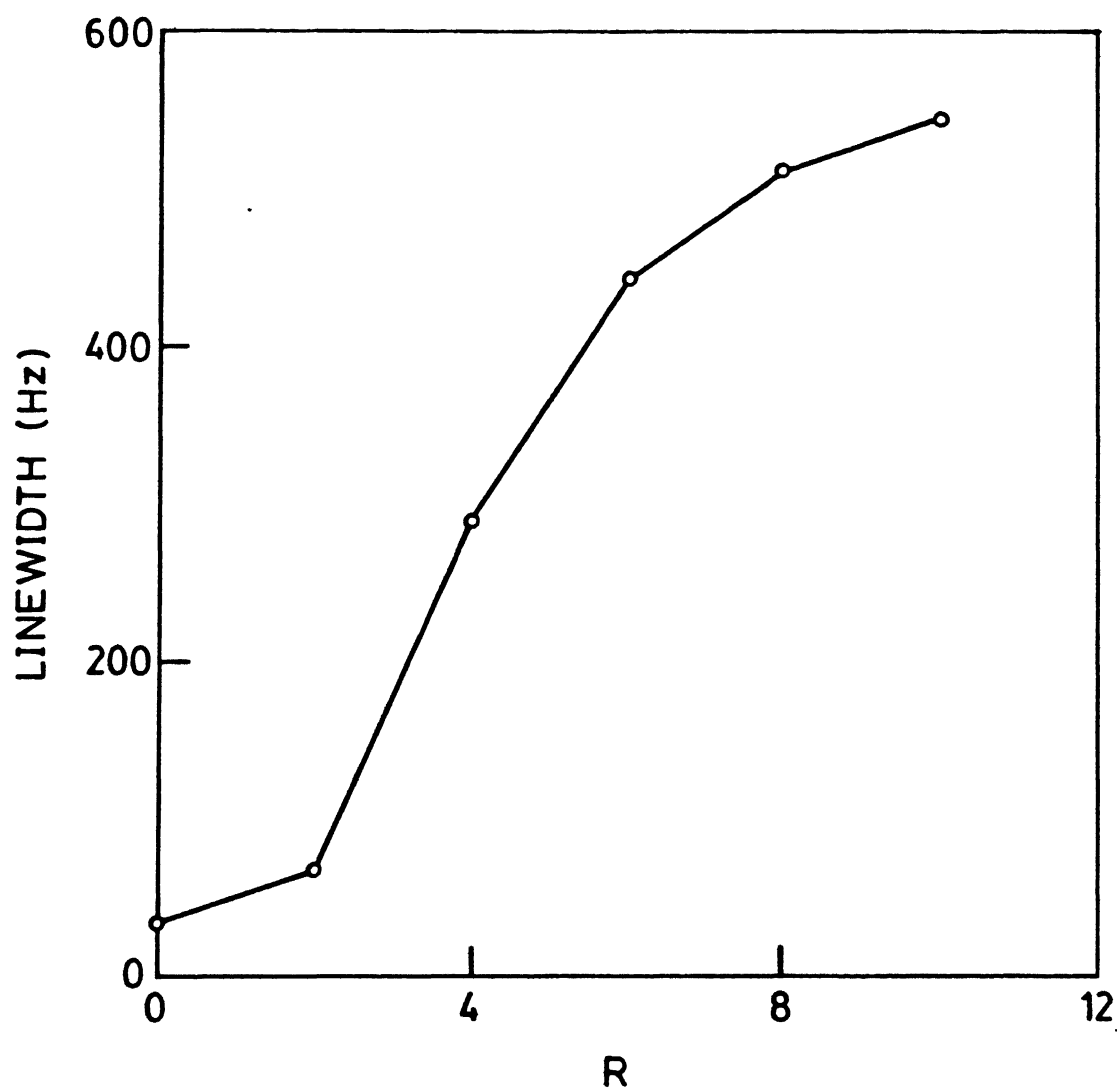


Fig.II.12 Variation in ^{31}P NMR linewidth of lecithin head group in the reverse micelle as a function of R .

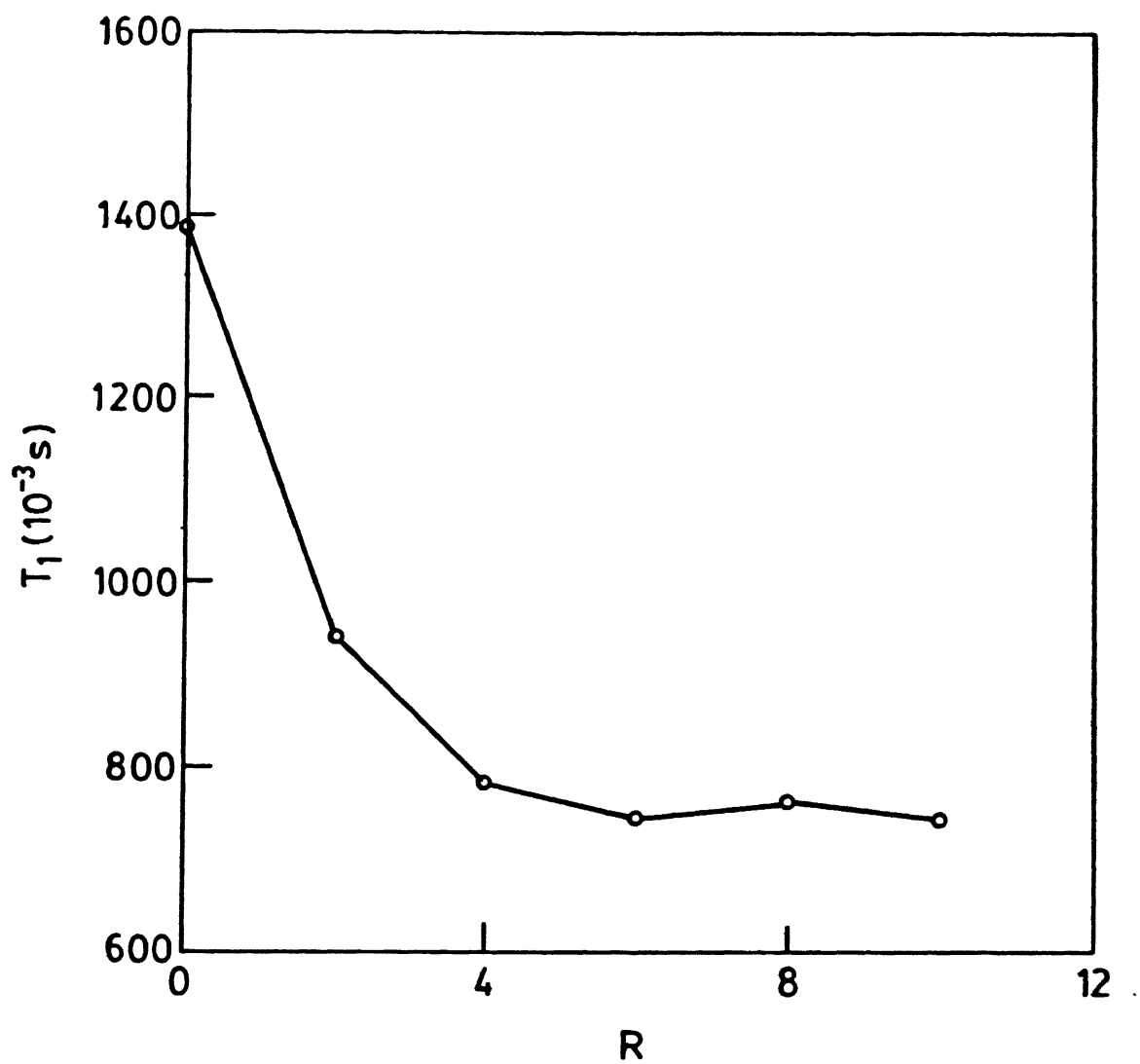


Fig.II.13

Variation in ^{31}P NMR T_1 values of lecithin head group in the reverse micelle as a function of R .

added for forming reverse micelles, ^{31}P T_1 reduces drastically. This is due to the electrostatic interaction between the hydrogen of the water and the oxygen of the phosphate, which restricts the motion of phosphate head groups, thereby leading to a decrease in T_1 . Further addition of water enhances the "structuring" of more water molecules around polar head groups of lecithin, and consequent reduction in the motion of phosphate groups. After all the phosphate groups have been hydrated, further addition of water does not change the T_1 of ^{31}P substantially, as is evident from the final 'plateau' value of ~760 ms (Fig. II.13).

Interestingly, the decreasing trend of the phosphorous ' T_1 vs R' values observed for lecithin/DCC/Cyclohexane/water, which we have justified in terms of an electrostatic model, is quite contrary to the general trend reported for similar lecithin based reverse micelles^(7,22). It is conceivable that the presence of the co-surfactant (DCC) in our system plays a distinct role in altering the head-group dynamics. However, we shall not pursue this point further here.

Fig. II.12 shows a pronounced increase in the ^{31}P linewidth as R increases. This is only to be expected, considering that there is a 'visible' increase in the bulk viscosity of the reverse micelle as R increases, thereby heralding an overall slow-down in micellar motion and/or possible structuring at the micellar interface due to hydration upto R value of ~8.

We have described in this chapter our extensive NMR work

to characterize the novel reverse micelles formed by lecithin/DCC/cyclohexane/water. What is perhaps crucial to a more thorough understanding of the temperature and composition range of the 'reverse micellar phase(s)' of this system is the construction and study of the phase diagram of this multicomponent system. This we have not attempted in our work.

II.4 Conclusions

- (i) The novel reverse micellar system and lecithin/DCC/cyclohexane/water, which may be of much potential use in peptide chemistry, has been prepared and characterized by NMR .
- (ii) A ~5% w/v solution of lecithin in cyclohexane containing DCC in 1:5 mole ratio with lecithin solubilises about 0.37 g of water per 1 g of lecithin. During the course of water addition, a slightly turbid and highly viscous phase is observed visually.
- (iii) Chemical shift values of water protons indicate that the water molecules are weakly hydrogen bonded at lower R values. ^{31}P chemical shifts of phosphate head group show evidence for an electrostatic interaction between water protons and the oxygen of the phosphate head groups of lecithin.
- (vi) The rotational correlation time (τ_c), calculated from proton NMR spin-lattice relaxation time for the reverse micellar water protons, shows that at lower R values it is higher (as compared to normal water) and decreases toward

the normal water value as R is increased.

- (v) The microviscosity of the water environment is very high at low water concentrations, and decreases rapidly as a function of added water.
- (vi) Analysis of proton T_2 values of water suggests contributions from other relaxation processes such as exchange narrowing, spin-rotational and chemical shift anisotropy, in addition to the dominant intramolecular relaxation process.
- (vii) The ^{31}P T_1 values show a decreasing trend as R is increased; this is in contrast to reported trends observed in other lecithin based reverse micelles, and suggests that DCC may be playing a role in altering the head-group dynamics.

REFERENCES

1. D. Ranganathan, G.P. Singh, and S. Ranganathan, *J. Am. Chem. Soc.* **111**, 1144 (1989).
- 2(a) J.C. Sheehan and G.P. Hess, *J. Am. Chem. Soc.* **77**, 1067 (1955); H.G. Khorana, *Chem. & Ind.* 1087 (1955).
- (b) D.H. Rich and J. Singh, *Peptides (N.Y.)* **1**, 241 (1979), a review on the use of carbodiimides for peptide synthesis.
3. W.S. Singleton, M.S. Gray, M.L. Brown, and J.L. White, *J. Am. Oil Chem. Soc.* **42**, 53 (1965).
4. H.H. Hetz, *Prog. NMR Spectrosc.* **3**, 159 (1967).
5. V.V. Kumar, C. Kumar, and P. Raghunathan, *J. Colloid Interface Sci.* **99**, 315 (1984).
6. Y.H. Shaw, L.S. Kan, and N.C. Li, *J. Magn. Reson.* **12**, 209 (1973).
7. G. Klose and F. Stelzner, *Biochim. Biophys. Acta* **363**, 1 (1974).
8. V.V. Kumar and P. Raghunathan, *Chem. Phys. Lipids* **41**, 159 (1986).
9. T.O. Henderson, T. Glonek, and T.C. Myers, *Biochemistry* **13**, 623 (1974).
10. B. Pullman and H. Berthod, *FEBS Lett.* **44**, 266 (1974).
11. B. Pullman and H. Berthod, *C.R. Acad. Sci. Ser. D.* **278**, 1433 (1974).
12. M.A. Wells, *Biochemistry* **13**, 4937 (1974).
13. J.N. Shoolery and B.J. Alder, *J. Chem. Phys.* **23**, 805 (1955).
14. V.V. Kumar, Ph.D. Thesis, Indian Institute of Technology, Kanpur, India (1982).
15. V.V. Kumar and P. Raghunathan, *Lipids* **21**, 764 (1986).
16. N. Bloembergen, E.M. Purcell, and R.V. Pound, *Phys. Rev.* **73**, 679 (1948).
17. R. Cooke and I.P. Kuntz, *Ann. Rev. Biophys. Bioeng.* **4**, 267 (1975).

18. M. Shinitzky, A.C. Dianoux, C. Gilter and G. Weber, *Biochemistry* **10**, 2106 (1971).
19. H.J. Pownall and L.C. Smith, *J. Am. Chem. Soc.* **95**, 3136 (1973).
20. T.L. James, *NMR in Biochemistry*, Academic Press, New York (1975), p. 43.
21. E.R. Andrew, *Nuclear Magnetic Resonance*, Cambridge University Press, New York (1955), p. 109.
22. B.M. Fung and J.L. McAdams, *Biochim. Biophys. Acta* **451**, 313 (1976).

CHAPTER III

DEUTERIUM NMR LINESHAPE ANALYSIS OF REVERSE MICELLAR POOL WATER

III.1 Introduction

In recent years, deuterium magnetic resonance (DMR) spectroscopy has been increasingly widely exploited as a means of investigating molecular dynamics in lipid membranes⁽¹⁻¹⁰⁾ and surfactant aggregates⁽¹¹⁻¹⁷⁾. The great utility of DMR derives from the fact that deuterium lineshapes and relaxation times are determined by a single well-defined interaction, the quadrupole coupling, which permits one to study internal dynamics spanning a wide range of rates between about 10^3 s^{-1} and 10^8 s^{-1} in a relatively direct manner.

With a view to employ DMR for probing the dynamics of reverse micellar 'pool water', we have chosen two systems for our study, namely, (i) Lecithin/Cyclohexane/ D_2O (ii) Lecithin/ Dicyclohexyl Carbodiimide /Cyclohexane / D_2O at two different temperatures. In similar contemporary experiments in aqueous media, DMR studies have been extensive, showing that water near model membranes and biomembranes possesses significantly more structure than, and dynamically very different from, aqueous phase 'bulk'water.

In this chapter, we shall first briefly present the general aspects of DMR spectroscopy. This will be followed by a description of the 'quadrupolar echo' method and the spin system's response to the quadrupolar echo pulse sequence. Our computational method for DMR lineshape simulation, and the interpretation of our experimental results on the two reverse

micellar systems by means of these simulation procedures, shall constitute the rest of this chapter.

III.2 DMR Spectroscopy

2.1 General Theory

In addition to its magnetic dipole moment, a nucleus with $I \geq 1$ possesses an electric quadrupole moment, eQ , which has its origin in a non-spherically symmetric nuclear charge distribution⁽¹⁸⁻²⁰⁾. This moment will interact with eq , the nonuniform electric field gradient (efg), which is produced by the surrounding valence electrons and other nuclei, at each nucleus to give a series of quantized energy levels, even in the absence of an external magnetic field.

Consequently, the total Hamiltonian for the nucleus in the presence of an applied magnetic field is

$$\mathcal{H}_{\text{total}} = \mathcal{H}_Z + \mathcal{H}_Q \quad [\text{III.1}]$$

where \mathcal{H}_Z is the Zeeman Hamiltonian representing the interaction between the applied magnetic field and the nuclear spin (I), and \mathcal{H}_Q the quadrupolar Hamiltonian due to the interactions between quadrupole moment associated with spin I and efg existing at the nuclear site. In eqn. III.1, all other internal Hamiltonians except \mathcal{H}_Q have been momentarily suppressed for simplicity.

The energy levels resulting from a first order perturbation solution^(18,19,21) of the total Hamiltonian, eqn. III.1, are given (in angular frequency units) by

$$E_m = E_m^{(0)} + E_m^{(1)}. \quad [\text{III.2}]$$

Then,

$$E_m = -\omega_o m + \frac{\omega_Q}{3} \left[\frac{3\cos^2\theta - 1}{2} + \frac{\eta_a}{2} \sin^2\theta \cos 2\phi \right] [3m^2 - I(I+1)], [\text{III.3}]$$

where ω_o is the Larmor frequency, m is the magnetic quantum number in a representation where the z -component of I is diagonal, θ and ϕ are the usual polar and azimuthal angles specifying the magnetic field direction in relation to the principal coordinate system of the efg and ω_Q is given by

$$\omega_Q = \frac{3}{8} \frac{e^2 q Q}{\hbar I(2I-1)}. \quad [\text{III.4}]$$

The term η_a in eqn. III.3 is the asymmetry parameter, defined by

$$\eta_a = \left| \frac{V_{xx} - V_{yy}}{V_{zz}} \right|, \quad [\text{III.5}]$$

where V_{ii} are the components of efg tensor defined such that $|V_{zz}| \geq |V_{yy}| \geq |V_{xx}|$. Since the electric field surrounding the nucleus is produced only by charges external to the nucleus, the Laplace equation, given below, holds :

$$V_{xx} + V_{yy} + V_{zz} = 0 \quad [\text{III.6}]$$

Thus η_a ranges from 0 to 1.

The term $\frac{e^2 q Q}{h}$ in eqn. III.4, where $eq = V_{zz} = \frac{\partial^2 V}{\partial z^2}$, is referred to as the nuclear quadrupole coupling constant.

2.2 DMR in D_2O

Since the deuterium nucleus has $I = 1$, m will assume values of 1, 0, and -1. The DMR spectrum arising from a particular deuteron will consist of two sharp peaks centred about ω_0 and separated by

$$\Delta\omega = \omega_Q (3\cos^2\theta - 1) + \eta_a \omega_Q \sin^2\theta \cos 2\phi . \quad [III.7]$$

One notices from eqn. III.7 that, for cases where the efg at a deuteron site has cylindrical symmetry, the asymmetry parameter is practically zero, reducing eqn. III.7 to the simpler form

$$\Delta\omega = \omega_Q (3\cos^2\theta - 1) . \quad [III.8]$$

For water deuterons in our systems, although the major contribution to the efg is from the intramolecular O-D bond, there can be other contributions of intermolecular origin such as the charge distribution in the vicinity of polar head group and other interactions. Furthermore, hydrogen bonding can reduce the contribution of the O-D bond from 312 KHz (as measured in the gas phase) to 213 KHz (22-24). For such reasons ω_Q could be different for different sites. Also, chemical exchange can take place between nuclei in different environments. If the exchange rate is much faster than the quadrupolar splitting ($\Delta\omega$), the observed splitting will be a weighted average over the different sites, given by (25-27)

$$\Delta\omega = \left| \sum_i P_i \omega_Q^i \right|, \quad [\text{III.9}]$$

where P_i is the probability (defined by the fraction of nuclei at site i) of a nucleus at being site i with a characteristic ω_Q^i . The exchange rate will also vary with temperature.

In the extreme limit, if isotropic tumbling motion of the quadrupolar nuclei is fast compared to the static splitting frequency, the angular term in eqn. III.8 is averaged to zero and no splitting is observed. On the other hand, the motion in a lamellar or liquid crystalline phase would in general be expected to be anisotropic, and a splitting of the first order spectrum will usually be observed.

The energy levels and spectra corresponding to single crystals and polycrystalline samples of deuterium are given in Fig. III.1.

In summary, then, $\Delta\omega$ data and exchange of deuterons between different environments can provide useful dynamic information through DMR spectra.

III.2.3 System Response to the Quadrupolar Echo Sequence :

2.3.1 Theoretical Background

In this subsection, we review the general procedure used to follow the time evolution of a spin system.

(i) Density Operator and Time Evolution of the Spin System

The dynamics of coupled spins are often understood elegantly with the help of a quantum mechanical formalism which characterises the state of the system by an operator called the

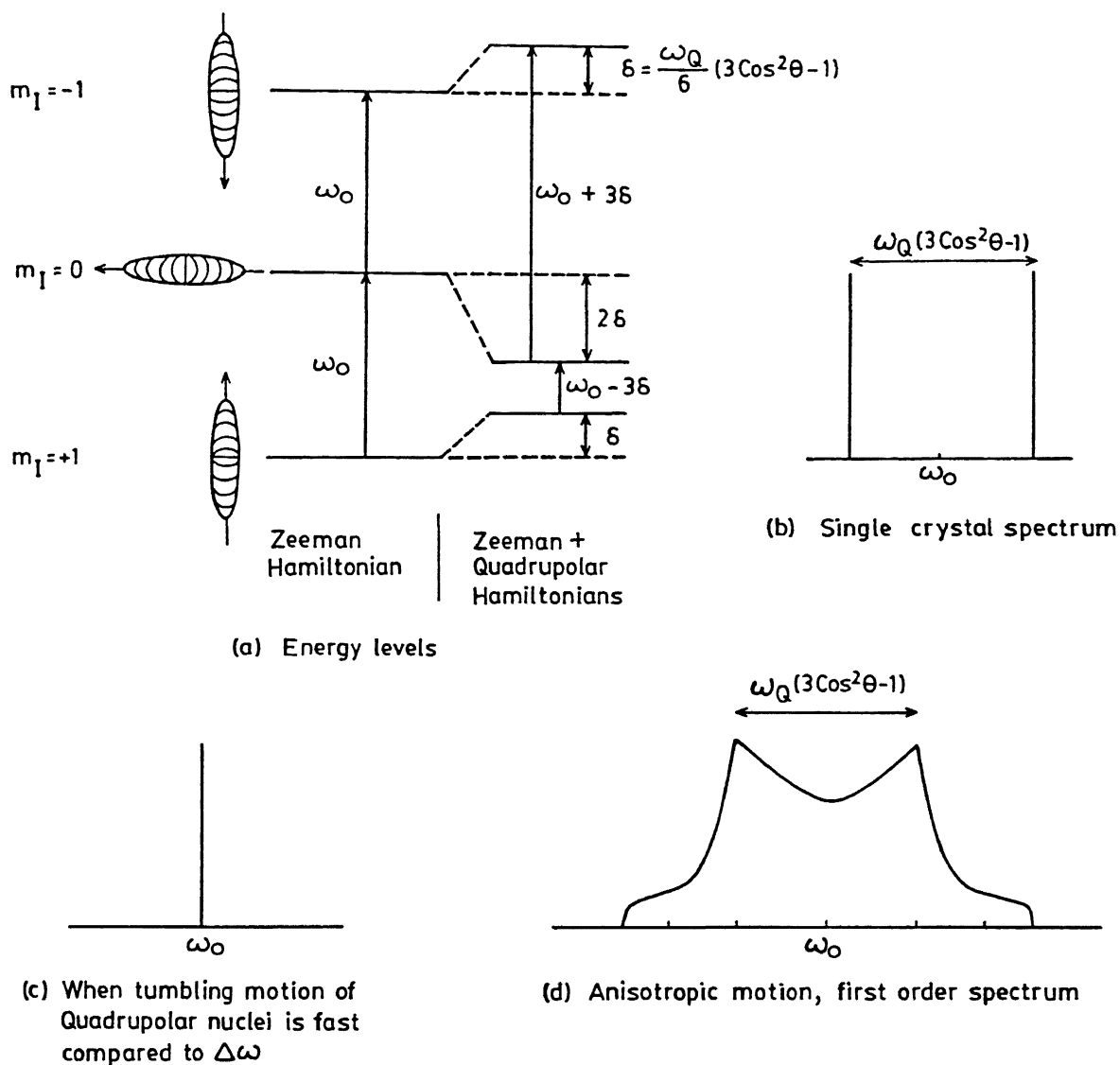


Fig.III.1

Energy levels (a) and DMR spectra corresponding to single crystals (b) of a spin $I = 1$ system (and) at two different motional states ((c) and (d))

density operator, $\rho(t)$ (28,29).

For a multilevel spin system with a complete set of eigenstates $|\phi_k(t)\rangle$, the state of the system can be written as $|\psi(t)\rangle = \sum_k c_k |\phi_k(t)\rangle$. Then, a mixture of independently prepared states $|\psi_n(t)\rangle$ ($n = 1, 2, \dots$) with statistical weights W_n can be completely described by the density operator $\rho(t)$ as

$$\rho(t) = \sum_n W_n |\psi_n(t)\rangle \langle \psi_n(t)| \quad [\text{III.10}]$$

The attributes of this operator and its matrix elements are :

(a) it is Hermitian, that is,

$$\langle \phi_i | \rho(t) | \phi_j \rangle = \langle \phi_j | \rho(t) | \phi_i \rangle^* , \quad [\text{III.11}]$$

(b) the diagonal element $\rho(t)_{ii}$ of the density matrix is equal to the probability of finding the system in the eigenstate $|\phi_i(t)\rangle$,

(c) the off-diagonal element indicates a 'coherence superposition' of eigenstates, simply called 'coherence', and

(d) the expectation value $\langle Q \rangle$ of an arbitrary observable Hermitian operator Q is given by

$$\langle Q \rangle = \text{Tr} \{ Q \rho(t) \} \quad [\text{III.12}]$$

The time development of the spin system under various interactions defined by the Hamiltonian, \mathcal{H} , can then be studied using the equation of motion of the density matrix,

$$\frac{d\rho(t)}{dt} = -i [\mathcal{H}, \rho(t)] \quad [\text{III.13}]$$

This differential equation is familiarly known as the Liouville-von Neumann equation (30), and has the solution

$$\rho(t) = U(t) \rho(0) U(t)^{-1}, \quad [\text{III.14}]$$

$$\text{where } U(t) = T \exp \left\{ -i \int_0^t \mathcal{H}(t') dt' \right\}. \quad [\text{III.15}]$$

$U(t)$ is variously called the 'Liouville operator' and 'Dyson Expression',⁽²⁸⁾ and T is the Dyson time-ordering operator (31) which has the property of ordering the exponential terms appearing in eqn. III.15 with increasing time from right to left.

In magnetic resonance, the time evolution of spin population can be thought of as rotation of spin vectors in a $(2I+1)$ dimensional space. Exponential operators of eqn. III.15 are used to explain such a time evolution. The mathematical physics of exponential operators may be found in standard texts^(19,32).

(ii) Nuclear Spin Interaction Hamiltonians

Various interactions of a nuclear spin system in NMR experiments can be described by a laboratory frame Hamiltonian^(18,19)

$$\mathcal{H}_L = \mathcal{H}_{\text{ext}} + \mathcal{H}_{\text{int}} \quad [\text{III.16}]$$

where \mathcal{H}_{ext} and \mathcal{H}_{int} represent the nuclear spin interactions between external fields (B_0 , B_1) and internal fields,

respectively. H_{ext} consists of two terms, namely,

$$\mathcal{H}_{\text{ext}} = \mathcal{H}_z + \mathcal{H}_{\text{rf}} \quad [\text{III.17}]$$

where $\mathcal{H}_z = -\omega_0 I_z$ [III.18]

$$\mathcal{H}_{\text{rf}} = -2\omega_1(t) I_x \cos(\omega t + \phi) \quad [\text{III.19}]$$

\mathcal{H}_{rf} , the rf Hamiltonian, describes the interaction of the spin system with a linearly oscillating rf field perpendicular to the static field. $\omega_1(t)$ equals $\gamma B_1(t)/2$, where $B_1(t)$ is the rf magnetic field amplitude. ω and ϕ are the frequency and phase of the rf. Typically, the rf field is applied in pulses that are ideally square, so that $\omega_1(t)$ is piecewise-constant, taking on the values 0 and ω_1^0 only. ω_1^0 will be referred to as the nominal rf amplitude. Also, typically, ω is constant and ϕ is piecewise-constant.

In eqn. III.16, \mathcal{H}_{int} describes interactions of the spin system with internal fields, which include dipole-dipole interaction (\mathcal{H}_D), J-coupling interaction (\mathcal{H}_J), spin-rotation interaction (\mathcal{H}_{SR}) and quadrupolar interaction (\mathcal{H}_Q). Since our present focus is only on \mathcal{H}_Q , the secular part of \mathcal{H}_Q (assuming that the field gradients have axial symmetry) may be written as

$$\mathcal{H}_Q = \sum_i \omega_{Qi} \left[I_{zi}^2 - (1/3) I_i^2 \right] \quad [\text{III.20}]$$

and $\omega_{Qi} = \frac{3e^2 qQ}{8\hbar I} (3\cos^2\theta_i - 1)$ [III.21]

where, as defined earlier, eQ and eq are respectively the quadrupole moment and the efg along the unique directions for the

i^{th} spin. θ_i is the angle between the static field direction and the unique field gradient direction.

The dominant term in Eqns. III. 16 and 17 is the interaction with the static field. All the contributions to \mathcal{H}_{int} are usually at least 100 times smaller. Thus, to a good approximation, the eigenstates of \mathcal{H}_L when the rf is turned off are eigenstates of I_z . They occur in Zeeman manifolds characterized by the eigenvalue m of I_z and separated in energy by increments of roughly ω_0 . When the rf field is turned on, it induces a coherent mixing of the eigenstates if ω is about equal to ω_0 .

(iii) Rotating Frame Transformation

The well-characterized, and therefore uninformative, interaction with the static field can be largely removed, the oscillating time dependence of the rf can be made to vanish, and the important parts of \mathcal{H}_{int} can be made apparent by a transformation to a new frame of reference called the 'rotating frame', (18,19,32a,33). This type of transformation from one frame to another commonly known as interaction frame (34,35) in quantum mechanical systems is described very briefly from a general point of view.

A change of reference frame is accomplished by performing a unitary transformation on an equation of motion in a representation, in which time dependence exists in both operators and state vectors, either to remove or to take account of selected portions of the Hamiltonian from the description of motion of the system.

Let us consider a general case with the total Hamiltonian consisting of two terms \mathcal{H}_1 and \mathcal{H}_2 , one or both of which may be time dependent. The equation of motion of the system is

$$\frac{i d|\psi\rangle}{dt} = (\mathcal{H}_1 + \mathcal{H}_2) |\psi\rangle \quad [\text{III.22}]$$

If we perform a unitary transformation, then

$$|\psi(t)\rangle = U_1 |\tilde{\psi}(t)\rangle \quad [\text{III.23}]$$

where $|\psi(t)\rangle$ is the state of the system at time t in the original frame and $|\tilde{\psi}(t)\rangle$ is the same state at time t in the new frame.

Assuming that U_1 is determined by \mathcal{H}_1 via the differential equation

$$\frac{i dU_1}{dt} = \mathcal{H}_1 U_1 \quad [\text{III.24}]$$

with the boundary condition that $U_1(t=0) = U_1^{-1}(t=0) = 1$ eqns.

III. 22-24 give

$$\frac{d|\psi\rangle}{dt} = \frac{\mathcal{H}_1 + \mathcal{H}_2}{i} |\psi\rangle \equiv \frac{(\mathcal{H}_1 + \mathcal{H}_2) U_1 |\tilde{\psi}\rangle}{i} \quad [\text{III.25}]$$

$$\frac{d|\psi\rangle}{dt} = \frac{i dU_1}{dt} |\tilde{\psi}\rangle + \frac{\mathcal{H}_2 U_1 |\tilde{\psi}\rangle}{i} \quad [\text{III.26}]$$

Differentiating eqn. III.23,

$$\frac{d|\psi\rangle}{dt} = \frac{dU_1|\tilde{\omega}\rangle}{dt} + = \frac{dU_1}{dt} |\tilde{\psi}\rangle + U_1 \frac{d|\tilde{\psi}\rangle}{dt} \quad [\text{III.27}]$$

comparing III.26 and III.27

$$U_1 \frac{d|\tilde{\psi}\rangle}{dt} = \frac{\mathcal{H}_2 U_1 |\tilde{\psi}\rangle}{1} \quad [\text{III.28}]$$

Multiplying III.28 on the left by iU_1^{-1} yields the time dependent Schrödinger equation for $\tilde{\psi}$

$$i \frac{d|\tilde{\psi}\rangle}{dt} = U_1^{-1} \mathcal{H}_2 U_1 |\tilde{\psi}\rangle \pm \tilde{\mathcal{H}}_2 |\tilde{\psi}\rangle \quad [\text{III.29}]$$

where $\tilde{\mathcal{H}}_2 = U_1^{-1} \mathcal{H}_2 U_1$

It is seen in eqn. III.29 that $|\tilde{\psi}\rangle$ no longer explicitly depends on \mathcal{H}_1 , the interaction used to perform the transformation. This is a transformation to the 'interaction frame' of \mathcal{H}_1 .

In particular, the type of unitary transformation used to transform the spin system description from laboratory frame to the rotating frame of the Zeeman interaction is

$$U(t)_{\text{rot}} = \exp (-i \mathcal{H}_z t) \quad [\text{III.30}]$$

It is important to note that in this new frame, the Zeeman field is removed from our description of the system, while the rf field becomes stationary.

RF Hamiltonian in the Rotating Frame

The rf Hamiltonian in the laboratory frame is

$$\mathcal{H}_{\text{rf}} = -2\omega_1 I_x \cos(\omega t + \phi) \quad [\text{III.31}]$$

The rotating frame RF Hamiltonian is obtained by performing the unitary transformation defined by eqn. III.30, in which $\mathcal{H}_z = -\gamma\hbar I_z B_0 = -\omega_0 I_z$, because $\omega_0 = \gamma B_0$. Thus, the rotating frame rf Hamiltonian is

$$\tilde{\mathcal{H}}_{\text{rf}} = U_{\text{rot}}^{-1} \mathcal{H}_{\text{rf}} U_{\text{rot}}$$

Using the \mathcal{H}_z value, and neglecting high-frequency terms,

$$\tilde{\mathcal{H}}_{\text{rf}} = -\omega_1 \left[I_x \cos\phi + I_y \sin\phi \right] \quad [\text{III.32}]$$

Quadrupolar Hamiltonian in the Rotating Frame

The quadrupolar Hamiltonian (\mathcal{H}_Q) for the axially symmetric field gradient case is

$$\mathcal{H}_Q = \omega_Q \left[I_z^2 - \frac{I^2}{3} \right]$$

This does not change its form after a unitary transformation to the rotating frame as the operators present in the secular part of \mathcal{H}_Q always commute with \mathcal{H}_z , i.e., $[\mathcal{H}_z, \mathcal{H}_Q] = 0$. Therefore,

$$\tilde{\mathcal{H}}_Q = U_{\text{rot}}^{-1} \mathcal{H}_Q U_{\text{rot}} = \omega_Q \left[I_z^2 - \frac{I^2}{3} \right] \quad [\text{III.33}]$$

(iv) Density Matrix for $I = 1$ case

The evolution of the density matrix in pulse experiments on spin $I = 1$ can be calculated by expressing it in terms of an orthogonal basis set of matrices. Many such orthogonal basis sets are available in the literature⁽³⁶⁻³⁸⁾. We have chosen the orthogonal basis set of matrices proposed by Vega and Luz⁽³⁷⁾, as their method is well-suited to our problem. Their basis set matrices are Hermitian and therefore give a real physical significance to the spin states they represent. Also, these matrices have convenient commutation relations with the operators that occur in the Hamiltonians of our interest.

A system of non interacting $I = 1$ spins in an external magnetic field can be defined by the spin density matrix, ρ , having a dimension of $(2I+1) \times (2I+1)$ and a total number of $(2I+1)^2 - 1$ traceless independent Hermitian operators, A_n ⁽³⁶⁾. This density matrix can be expressed as

$$\rho(t) = \sum_{n=1}^N a_n(t) A_n + a_0 1 \quad [\text{III.34}]$$

where 1 is a unit matrix and $a_n(t)$ time-dependent coefficient. These can be obtained by solving the equation of motion for $\rho(t)$.

For our problem, the set of eight independent traceless operators required are I_x, I_y, I_z for spin $I = 1$ and the following additional operators defined as

$$\left. \begin{aligned} J_x &= I_y I_z + I_z I_y \\ J_y &= I_z I_x + I_x I_z \\ J_z &= I_x I_y + I_y I_x \end{aligned} \right\} \quad [\text{III.35}]$$

$$\left. \begin{aligned} Q_z &= I_z^2 - \frac{I^2}{3} \\ K_z &= I_x^2 - I_y^2 \end{aligned} \right] \quad [\text{III.36}]$$

Alternative linear combinations of Q_z and K_z are :

$$\left. \begin{aligned} Q_x &= I_x^2 - \frac{I^2}{3}, \quad K_x = I_y^2 - I_z^2 \text{ or} \\ Q_y &= I_y^2 - \frac{I^2}{3}, \quad K_y = I_z^2 - I_x^2 \end{aligned} \right] \quad [\text{III.37}]$$

The ninth operator is the 3 X 3 unit matrix, U.

The matrix representation of the operators defined above are given in Table III.1

The transformation relation existing between the three sets of second rank operators (Eqns. III. 36, 37) are

$$\left. \begin{aligned} Q_i &= \frac{1}{2} (-Q_K + K_K) \\ Q_j &= \frac{1}{2} (-Q_K - K_K) \\ K_i &= \frac{1}{2} (-3Q_K - K_K) \\ K_j &= \frac{1}{2} (3Q_K - K_K) \end{aligned} \right] \quad [\text{III.38}]$$

where $i, j, k = x, y, z$ or their cyclic permutation.

Different commutation relations existing between the basis-set operators and the commonly encountered spin-interaction operators are given in Table III. 2.

Table III.1 Matrix representations of $I = 1$ spin operators (from reference 38):

$$I_x = \frac{1}{\sqrt{2}} \begin{pmatrix} 0 & 1 & 0 \\ 1 & 0 & 1 \\ 0 & 1 & 0 \end{pmatrix}$$

$$J_x = \frac{1}{\sqrt{2}} \begin{pmatrix} 0 & -i & 0 \\ i & 0 & i \\ 0 & -i & 0 \end{pmatrix}$$

$$I_y = \frac{1}{\sqrt{2}} \begin{pmatrix} 0 & -i & 0 \\ i & 0 & -i \\ 0 & i & 0 \end{pmatrix}$$

$$J_y = \frac{1}{\sqrt{2}} \begin{pmatrix} 0 & 1 & 0 \\ 1 & 0 & -1 \\ 0 & -1 & 0 \end{pmatrix}$$

$$I_z = \begin{pmatrix} 1 & 0 & 0 \\ 0 & 0 & 0 \\ 0 & 0 & -1 \end{pmatrix}$$

$$J_z = \begin{pmatrix} 0 & 0 & -i \\ 0 & 0 & 0 \\ i & 0 & 0 \end{pmatrix}$$

$$K_z = \begin{pmatrix} 0 & 0 & 1 \\ 0 & 0 & 0 \\ 1 & 0 & 0 \end{pmatrix}$$

Alternative Linear Combinations of Q_z and K_z :

$$Q_x = \frac{1}{6} \begin{pmatrix} -1 & 0 & 3 \\ 0 & 2 & 0 \\ 3 & 0 & -1 \end{pmatrix}$$

$$K_x = \frac{1}{2} \begin{pmatrix} -1 & 0 & -1 \\ 0 & 2 & 0 \\ -1 & 0 & -1 \end{pmatrix}$$

$$Q_y = \frac{1}{6} \begin{pmatrix} -1 & 0 & -3 \\ 0 & 2 & 0 \\ -3 & 0 & -1 \end{pmatrix}$$

$$K_y = \frac{1}{2} \begin{pmatrix} 1 & 0 & -1 \\ 0 & -2 & 0 \\ -1 & 0 & 1 \end{pmatrix}$$

Table III.2 Commutation relation between $I = 1$ spin operators and commonly encountered spin-interaction operators (adopted from ref. 38)

$i[I_Y, I_X] = I_Z$	$i[I_Z, I_X] = -I_Z$
$i[J_Y, I_X] = -J_Z$	$i[J_Z, I_X] = J_Y$
$i[J_X, I_X] = -2K_X$	$i[K_X, I_X] = 2J_X$
$i[I_X, I_X] = 0$	$i[Q_Z, I_X] = 0$
$i[I_X, I_Y] = -I_Z$	$i[I_Z, I_Y] = I_X$
$i[J_X, I_Y] = J_Z$	$i[J_Z, I_Y] = -J_X$
$i[J_Y, I_Y] = -2K_Y$	$i[K_Y, I_Y] = 2J_Y$
$i[I_Y, I_Y] = 0$	$i[Q_Y, I_Y] = 0$
$i[I_X, I_Z] = I_Y$	$i[I_Y, I_Z] = -I_X$
$i[J_X, I_Z] = -J_Y$	$i[J_Y, I_Z] = J_X$
$i[J_Z, I_Z] = -2K_Z$	$i[K_Z, I_Z] = 2J_Z$
$i[I_Z, I_Z] = 0$	$i[Q_Z, I_Z] = 0$
$i[I_X, Q_Z] = J_Z$	$i[J_X, Q_Z] = -I_X$
$i[I_Y, Q_Z] = -J_Y$	$i[J_Y, Q_Z] = I_Y$
$i[I_Z, Q_Z] = 0$	$i[J_Z, Q_Z] = 0$
$i[Q_j, Q_Z] = 0$	$i[K_j, Q_Z] = 0$
	$(j = x, y, z)$

III 3. DMR Measurements

3.1 Solid Echo or Quadrupolar Echo Pulse Sequence :

In conventional FT NMR, spectra are obtained by applying a 90° pulse and then Fourier transforming the free induction decay

(FID). Application of this method to lineshape investigation in deuterated viscous liquids and solids does not give a faithful or true lineshapes as the very early part of the FID, containing the information about broad components of the line, is lost due to 'dead time' effects of the rf receiver and due to pulse length, recovery times, magnetoacoustic ringing, etc. To circumvent dead time problems, Powles and Mansfield⁽³⁹⁾ have proposed a pulse sequence for a pair of spin -1/2 nuclei which has come to be known as the 'solid echo'. The sequence is

$$\left(\pi/2\right)_0 \text{ ---}\tau\text{---} \left(\pi/2\right)_{90^\circ} \text{ ---}\tau\text{---} \text{acquire}$$

where the subscripts denote the phase of the pulse.

Later, Davis et al.⁽⁴⁰⁾ showed that for the deuteron the same sequence gave a perfect refocussing for the quadrupolar Hamiltonian. Hereafter, this sequence will be referred to as quadrupolar echo sequence throughout this thesis.

3.2 Quadrupolar Echo Pulse Sequence and the Spin System's Response :

The quadrupolar echo pulse sequence is illustrated in Fig. III.2.

In this sequence, τ is the variable interval between pulses, the superscripts - and + indicating 'just before' and 'just after' the pulse, respectively. Signal (FID) acquisition

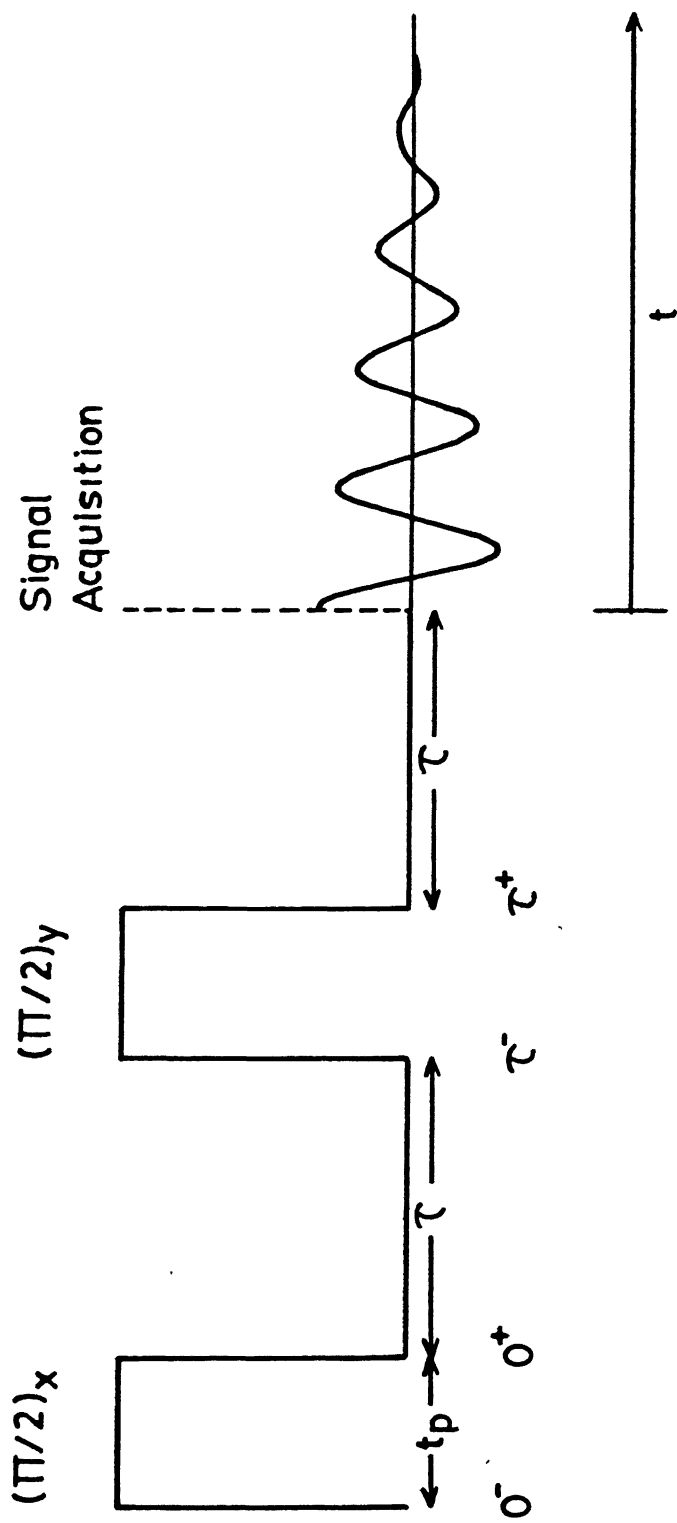


Fig. III.2 Quadrupolar Echo Pulse Sequence

starts from 2τ and recorded for time 't'. The response of the spin system to this sequence is described below.

At thermal equilibrium, when the high-temperature, high-field approximation becomes valid, the density matrix in the laboratory frame can be written as

$$\begin{aligned}\rho_{eq} &= \rho(0) \\ &\approx - \left(\frac{\hbar\omega_0}{KT} \right) I_z \\ \rho_{eq} &= -bI_z\end{aligned}\quad [\text{III.39}]$$

where b is equal to $\left(\frac{\hbar\omega_0}{KT} \right)$ and I_z is the z -component of the total spin operator. This density matrix, on transformation to rotating frame using eqn.III.30, becomes

$$\begin{aligned}\tilde{\rho}(0) &= U_{\text{rot}}^{-1} \rho(0) U_{\text{rot}} \\ \tilde{\rho}(0) &= -bI_z\end{aligned}\quad [\text{III.40}]$$

Eqn.III.40 represents the spin system at time 0^- (see Fig. III.2); thus

$$\tilde{\rho}(0^-) = \tilde{\rho}(0). \quad [\text{III.41}]$$

At the instant 0^- , rf pulse is applied to the spin system for the duration t_p . The resulting rf pulse perturbation can be explained in terms of the unitary operator, U_p , defined as

$$U_p(t_p) = \exp(-i \tilde{H}_{\text{rf}} t_p). \quad [\text{III.42}]$$

Density matrix of the system immediately after $(\pi/2)_x$ pulse (at the instant of 0^+) is

$$\tilde{\rho}(0^+) = U_p \tilde{\rho}(0^-) U_p^{-1}$$

Using Table III.2, and taking the rf phase factor (ϕ) arbitrarily as zero (as it is the first pulse), the above eqn. may be written as

$$\tilde{\rho}(0^+) = b [I_z \cos \omega_1 t_p - I_y \sin \omega_1 t_p] \quad [\text{III.43}]$$

We know that the pulse tip angle, θ , is $\theta = \gamma H_1 t_p = \pi/2$ and substituting $\omega_1 = \gamma H_1$,

$$\theta = \omega_1 t_p = 90^\circ \quad [\text{III.44}]$$

Putting [III.44] in [III.43], we get

$$\tilde{\rho}(0^+) = -b I_y \quad [\text{III.45}]$$

After this pulse, the spin system evolves freely under the influence of \tilde{H}_Q . Neglecting the relaxation effect for the time being and assuming 'on resonance' condition, the density matrix, $\tilde{\rho}(0^+)$, just before the $(\pi/2)_y$ pulse becomes

$$\tilde{\rho}(\tau^-) = e^{-i\tilde{H}_Q \tau} \tilde{\rho}(0^+) e^{i\tilde{H}_Q \tau}$$

Using Table III.2, it can be shown that

$$\tilde{\rho}(\tau^-) = b \left[-I_y \cos \omega_Q \tau + J_y \sin \omega_Q \tau \right] \quad [\text{III.46}]$$

Just after the second pulse, the density matrix is

$$\tilde{\rho}(\tau^+) = \exp(-i\tilde{H}_{rf} t_n) \tilde{\rho}(\tau^-) \exp(+i\tilde{H}_{rf} t_p),$$

$$\tilde{\rho}(\tau^+) = b \left[-I_Y \cos \omega_Q \tau - J_Y \sin \omega_Q \tau \right] \quad [\text{III.47}]$$

Following the $(\pi/2)_Y$ pulse, the density matrix, $\tilde{\rho}(\tau^+)$, evolves under $\tilde{\mathcal{H}}_Q$ again, and spins along Y refocus at time 2τ according to

$$\begin{aligned} \tilde{\rho}(2\tau) &= \exp(-i\tilde{\mathcal{H}}_Q \tau) \tilde{\rho}(\tau^+) \exp(i\tilde{\mathcal{H}}_Q \tau) \\ &= -bI_Y \left[\sin^2 \omega_Q \tau + \cos^2 \omega_Q \tau \right] \end{aligned}$$

$$\tilde{\rho}(2\tau) = -bI_Y \quad [\text{III.48}]$$

We notice the interesting fact that the density matrix at time 2τ is the same as the density matrix immediately after the first pulse, thereby showing that the inherent detector 'dead time' problem is completely removed by employing this pulse sequence for the excitation of the spin system.

3.3 Computational Method for Lineshape Calculation :

The response of the spin system immediately after the pulses, evolution under $\tilde{\mathcal{H}}_Q$ following pulses, and at 2τ , i.e. eqns. III. 45, 46, 47 and 48, prompted Vega and Luz⁽³⁸⁾ to write the evolution of density matrix during the quadrupolar echo experiments in terms of just two components of the basis set as

$$\tilde{\rho}(t) = y(t) I_Y + c(t) J_Y \quad [\text{III.49}]$$

This $\tilde{\rho}(t)$ under $\tilde{\mathcal{H}}_Q$ can be calculated from the usual equation of motion,

$$\frac{d\tilde{\rho}(t)}{dt} = i \left[\tilde{\rho}(t), \tilde{H}_Q \right], \quad [\text{III.50}]$$

that is,

$$\frac{d\tilde{\rho}(t)}{dt} = i \left[y(t) I_Y + c(t) J_Y, \omega_Q Q_Z \right].$$

Using the commutation relations of Table III.2,

$$\frac{d[y(t) I_Y + c(t) J_Y]}{dt} = \omega_Q [-y(t) J_Y + c(t) I_Y]$$

The expectation value of I_Y and J_Y is calculated as

$$\begin{aligned} d \text{Tr} [y(t) I_Y \cdot I_Y + c(t) J_Y \cdot I_Y] = \\ \omega_Q \text{Tr} [-y(t) J_Y \cdot I_Y + c(t) I_Y \cdot I_Y] \end{aligned} \quad [\text{III.51}]$$

$$\begin{aligned} d \text{Tr} [y(t) I_Y \cdot J_Y + c(t) J_Y \cdot J_Y] = \\ \omega_Q \text{Tr} [-y(t) J_Y \cdot J_Y + c(t) I_Y \cdot J_Y] \end{aligned} \quad [\text{III.52}]$$

Using Table III.1, eqns. III. 51 and 52 become

$$\frac{dy(t)}{dt} = \omega_Q c(t) \quad [\text{III.53}]$$

$$\frac{dc(t)}{dt} = -\omega_Q y(t) \quad [\text{III.54}]$$

[III.53] + i [III.54] gives,

$$\frac{d[y(t) + ic(t)]}{dt} = i\omega_Q [y(t) + ic(t)] \quad [\text{III.55}]$$

(38)
Vega and Luz define $y(t) + ic(t)$ as an effective complex magnetization, $G(t)$, namely,

where $y(t)$ is the expectation value of the usual magnetization, M_y along y-axis and $C(t)$ is an NMR unobservable coherence such as J_y etc. The effect of $(\pi/2)_y$ pulse on $G(t)$ is proved to be simply its complex conjugate, i.e.,

$$G(t) \xrightarrow{(\pi/2)_y} G^*(t) \quad [\text{III.57}]$$

Eqn. III.55 may now be written as

$$\frac{dG(t)}{dt} = -i \omega_Q G(t) . \quad [\text{III.58}]$$

It has been shown that $G(t)$ is following a Bloch type of equation under quadrupolar Hamiltonian.

Using the equations described above, a method is derived for simulating deuterium spectra obtained using quadrupolar echo sequence. For this purpose, we assume that there are only two types of sites for D_2O molecules in the reverse micelles; one is D_2O bound to the polar head group in the interfacial region and commonly called as 'bound water', and another is D_2O which are present in the interior of the reverse micelles and called as 'free water' as it is similar to normal bulk water (See Fig. III.3).

As explained in Sect. 2.2, these two types of water will have different ω_Q and T_2 . There is a continuous exchange of water molecules taking place between 'bound water' sites and 'free water' sites and also the two protons of a water molecule flip about its C_2 axis. With this model in mind, we have derived the necessary equations for simulating experimental D_2O spectra

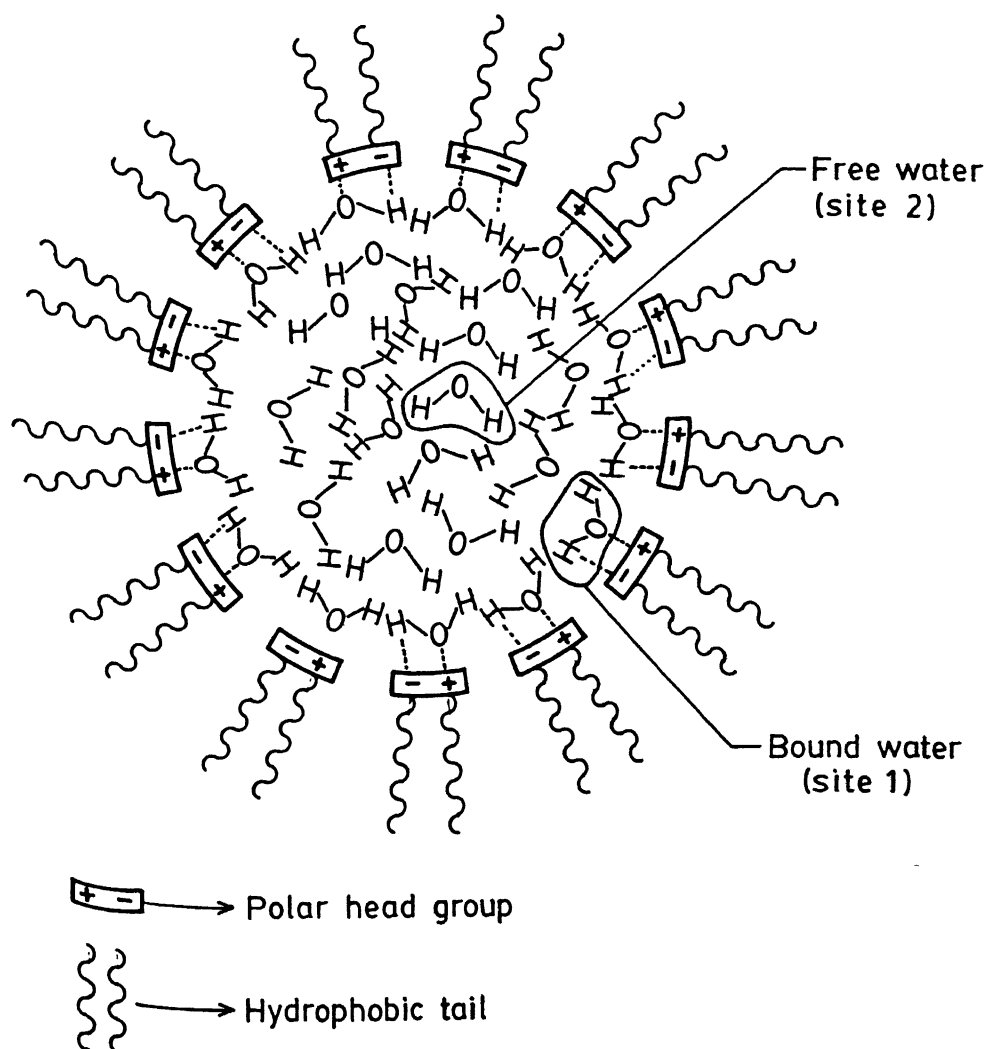


Fig.III.3

Two types of water sites in a typical reverse micelle

water' molecules as site 1 water molecules and 'free water' molecules as site 2 water molecules.

Incorporating exchange and relaxation terms for these two types of water sites, eqn. III. 58 becomes

$$\frac{dG_1(t)}{dt} = - \left[i\omega_{Q1} + K_{21} + \frac{1}{T_2(1)} \right] G_1(t) + K_{12}G_2(t) \quad [\text{III.59}]$$

$$\frac{dG_2(t)}{dt} = - \left[i\omega_{Q2} + K_{12} + \frac{1}{T_2(1)} \right] G_2(t) + K_{21}G_1(t) \quad [\text{III.60}]$$

In the above eqns., $K_{12} = K_{21} = K$, the exchange rate, the subscripts 1 and 2 correspond to site 1 and site 2, respectively, and ω_{Qi} is already defined in eqn. III.21. Eqns. III. 59 and 60 can be combined as below :

$$\frac{dG(t)}{dt} = - RG(t), \quad [\text{III.61}]$$

where $G(t)$ is a column vector having $G_1(t)$ and $G_2(t)$ as its components. R is a matrix whose elements are

$$R_{ii} = i \omega_{Qi} + K + \frac{1}{T_2(i)}$$

$$R_{jj} = -K, \quad i \neq j \text{ and } i = j = 1, 2$$

Immediately after the first $(\pi/2)_x$ pulse in the quadrupolar echo sequence, all magnetizations corresponding to both sites lie along -y direction (ref. eqn. III. 45) with magnitudes proportional to their fractional populations

$$G(0^+) = P, \quad [\text{III.62}]$$

where P is a real column vector defined as

$P \begin{bmatrix} p_1 \\ p_2 \end{bmatrix}$ in which p_i 's are the fractional populations of site i

Following the first pulse, the system evolves according to eqn. III. 61, and just before the second pulse we have

$$\frac{dG(\tau^-)}{dt} = -R G(\tau^-) . \quad [\text{III.63}]$$

$G(\tau^-)$ is obtained by integrating the above equation as shown below :

$$\int_{0^+}^{\tau^-} \frac{dG(\tau^-)}{G(\tau^-)} = - \int_{0^+}^{\tau^-} R dt$$

Then

$$G(\tau^-) = \exp (-R\tau) G(0^+) = \exp (-R\tau) P \quad [\text{III.64}]$$

The spin system just after the $(\pi/2)_y$ pulse, according to eqn. III. 57, is

$$\begin{aligned} G(\tau^+) &= G(\tau^-)^* \\ &= \exp (-R\tau)^* P \end{aligned} \quad [\text{III.65}]$$

Similarly, the complex magnetization at 2τ is

$$G(2\tau) = \exp (-R\tau) G(\tau^+) = \exp (-R\tau) \exp (-R\tau)^* P \quad [\text{III.66}]$$

Here we define J as $J = G(2\tau)$ where J is the column vector having components $j_1 = G_1(2\tau)$ and $j_2 = G_2(2\tau)$.

The total echo amplitude, E , is then calculated by summing j_1 and j_2

$$E = 1. \quad J = 1. \quad \exp(-R\tau) \exp(-R\tau)^* P \quad [\text{III.67}]$$

where 1 is a row vector with its two components equal to unity.

In the actual quadrupolar echo experiment, FID is recorded starting from 2τ and for a time 't'. Therefore,

$$\begin{aligned} \text{FID}(t) &= \text{Re} \left\{ 1.G(2\tau+t) \right\} \\ &= \text{Re} \left\{ 1.\exp(-R\tau).J \right\} \end{aligned} \quad [\text{III.68}]$$

The absorption spectrum is obtained by doing the cosine transformation on $\text{FID}(t)$,

$$I(\omega) = \int_0^{\infty} \text{FID}(t) \cos \omega t \, dt \quad [\text{III.69}]$$

The exponential matrices appearing in the above equations can be very conveniently expressed ⁽⁴¹⁾ for our calculation in terms of a diagonal matrix, Λ , containing complex eigenvalues λ_i of R , and a matrix S of its eigen vectors

$$\left. \begin{aligned} e^{R\tau} &= S e^{\Lambda\tau} S^{-1} \\ e^{-Rt} &= S e^{-\Lambda t} S^{-1} \\ \text{where } S^{-1}RS &= \Lambda \end{aligned} \right\} \quad [\text{III.70}]$$

Substituting [III.70] in [III.68]

$$\begin{aligned} \text{FID}(t) &= \text{Re} \left\{ 1 . S e^{-\Lambda t} S^{-1} . J \right\} \\ &= \text{Re} \left\{ \sum_{ijk} S_{ik} e^{-\lambda_k t} (S^{-1})_{kj} J_j \right\} \end{aligned} \quad [\text{III.71}]$$

and the eqn. III.69 becomes,

$$I(\omega) = \text{Re} \left\{ \sum_{ijk} \frac{S_{ik} \lambda_k (S^{-1})_{kj}}{\omega^2 + \lambda_k^2} J_j \right\} \quad [\text{III.72}]$$

The $I(\omega)$ of Eqn. III.72 is calculated for all possible O-D bond orientations with respect to magnetic field, and the overall spectrum is obtained by summing $I(\omega)$ over all the possible orientations. A fast Monte Carlo algorithm based on systematic sampling^(42,43) has been previously developed in our laboratory^(44,45); this algorithm has been used in the present work for the overall simulation. Eq. III.72 is implemented by means of a programme written in FORTRAN 77 to simulate all our experimental deuterium magnetic resonance spectra. These results will be discussed further in the next section. The programme in its entirety is listed in Appendix I. This programme was executed on the HP 9000 computer system of I.I.T. Kanpur.

III.4 Results and Discussion

All deuterium NMR spectra have been recorded at 61.25 MHz on a JEOL JNM-GSX400 FT NMR spectrometer, by using the quadrupolar echo pulse sequence⁽⁴⁰⁾ with full phase cycling and a pulse sequence recycle delay of 10s. Due to the low rf power transmitter of the spectrometer, 90° pulse width corresponding to deuteron nucleus was 20.2 μ s. The interpulse spacing (τ) chosen was 60 μ s. Depending on signal -to-noise ratio, from 24 to 500 FID's were averaged before doing FT and 32K data memory was used. Also, the 10mm sample tube was not spun and the field frequency lock not established.

The experimental spectra and their simulation shall now be discussed for the following two reverse micellar systems : (i) PC/Cyclohexane/D₂O (ii) PC/DCC/Cyclohexane/D₂O at room temperature (296 K) and at 263 K.

(a) Spectra at 296 K

The spectra for a number of R-values for both the reverse micellar systems are given on the left of Figs. III.4-III.10 and all these spectra show two lines, almost identical for the same R value of both micellar systems, namely, one broad and one sharp line. The sharp line is not shown in some of the experimental spectra as we have expanded the broad peak for obtaining an accurate linewidth measurement.

At first sight at any rate, the appearance of broad and sharp lines leads us to the following tentative interpretation : the broad line may be due to the water molecules which are bound to the polar head groups (see Fig. II.8) present in the interfacial region of reverse micelles and are hence restricted in their translational motion ; slow motion of D₂O molecules does not average out the angular part of the quadrupolar Hamiltonian, and hence the line is broad. The sharp line may then be rationalized on the assumption that, even at low R values the reverse micelles contain some amount of D₂O as 'free water' either dispersed in the organic solvent or present in the inner core of reverse micelles. As this latter type of water is very much similar to normal water whose \mathcal{H}_Q is averaged out to zero due to fast motion, the corresponding line is narrow.

If the above interpretation is correct, then one would expect that the integrated intensity of the sharp line should increase with increasing R value, because free water content

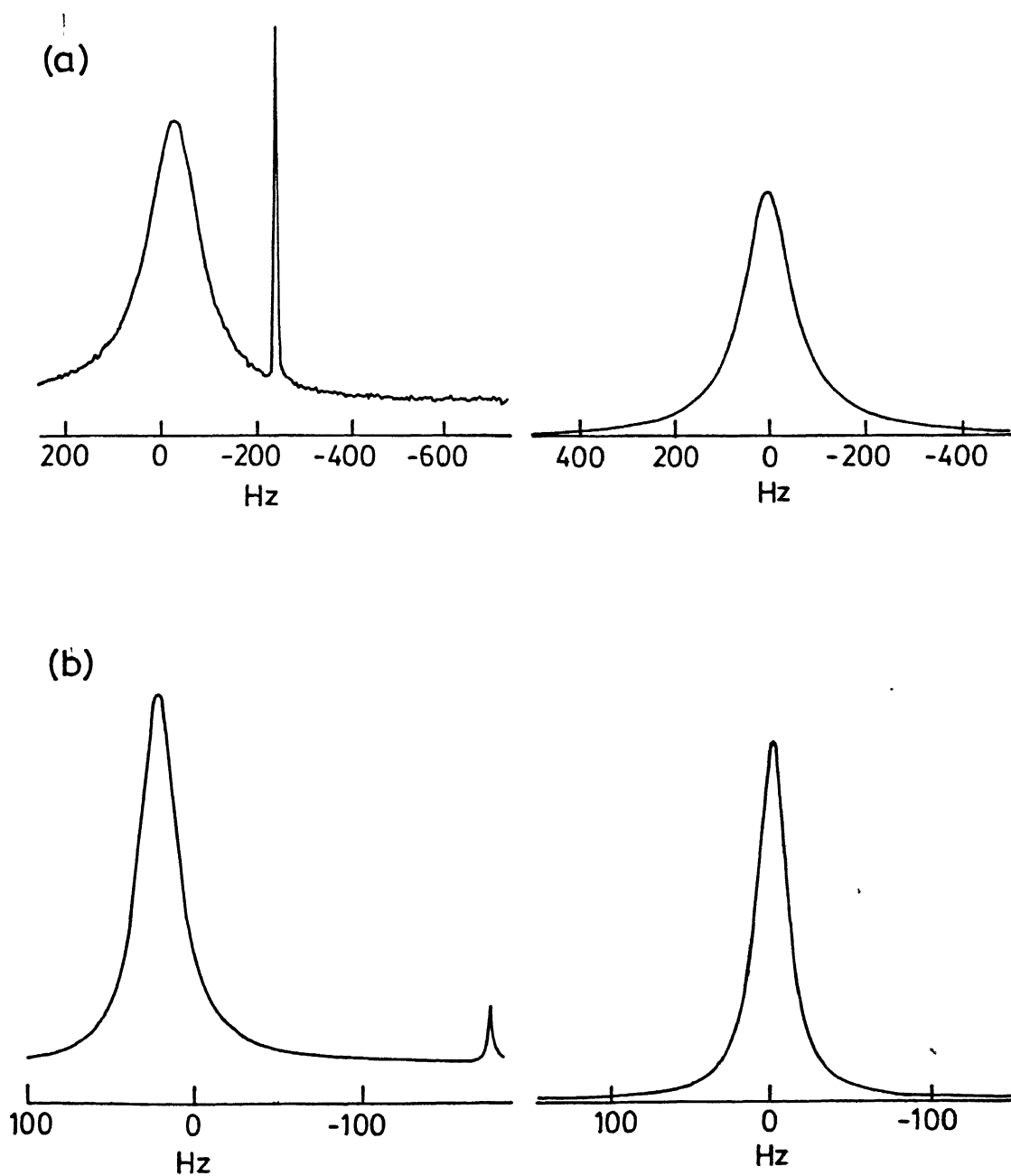


Fig.III.4 ^2D -NMR spectra (left) and best-fitting simulations (right) for PC/Cyclohexane/ D_2O at 296 K; (a) $R = 1$ and (b) $R = 3$.

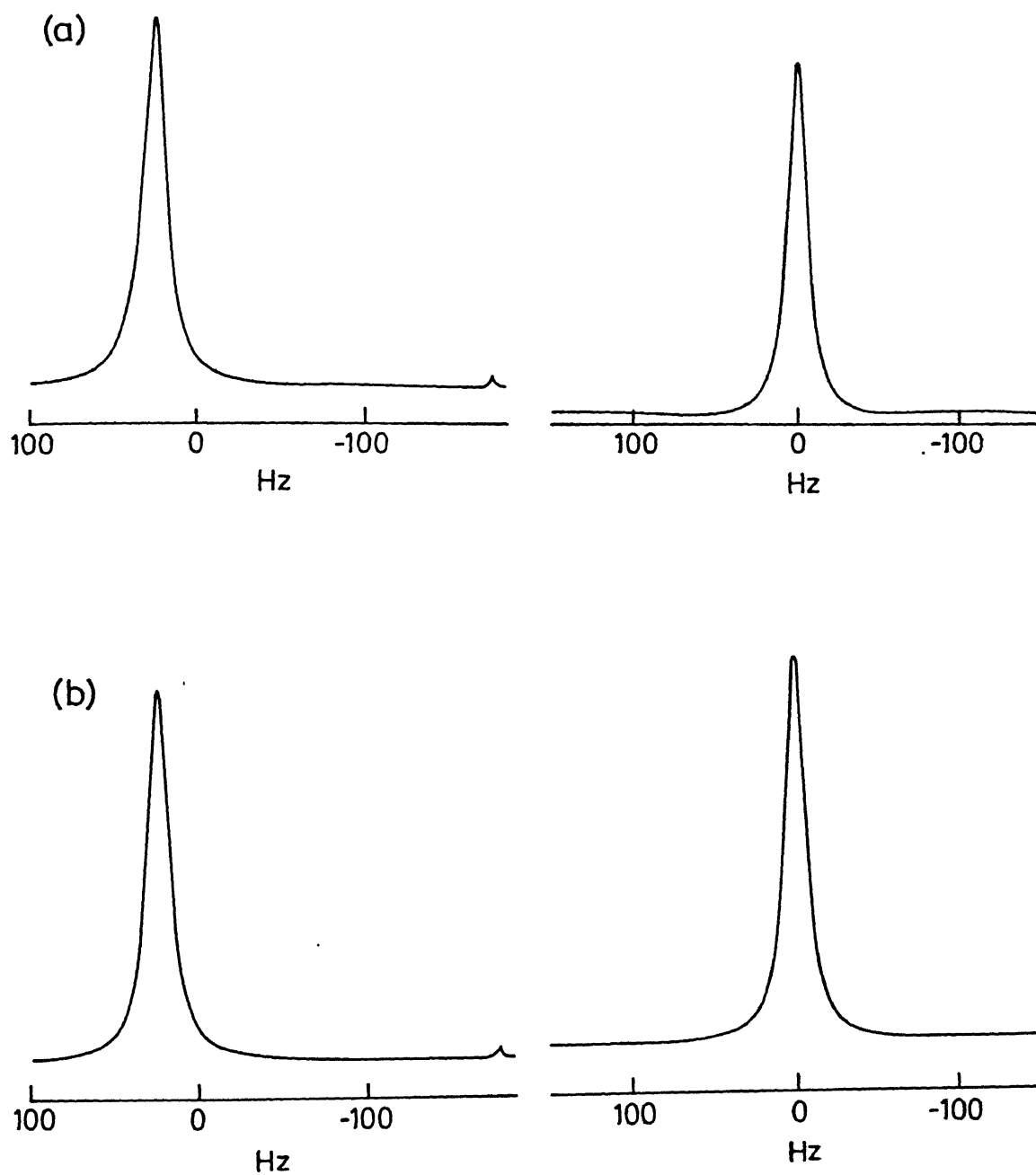


Fig.III.5 ^2D -NMR spectra (left) and best-fitting simulations (right) for PC/Cyclohexane/ D_2O at 296 K; (a) $R = 5$ and (b) $R = 6$.

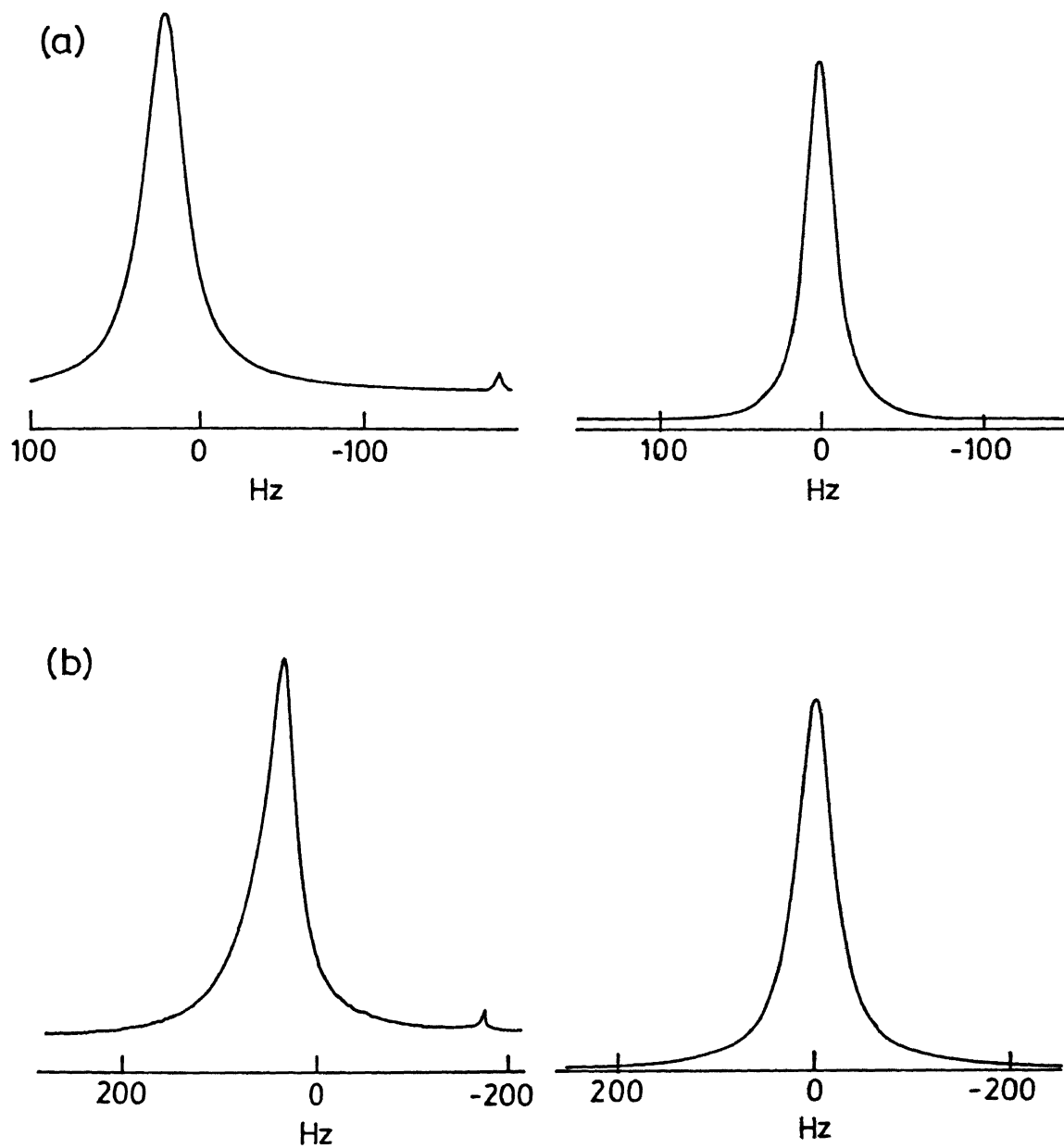


Fig.III.6 ^2D -NMR spectra (left) and best-fitting simulations (right) for PC/Cyclohexane/ D_2O at 296K ; (a) $R = 8$ and (b) $R = 10$.

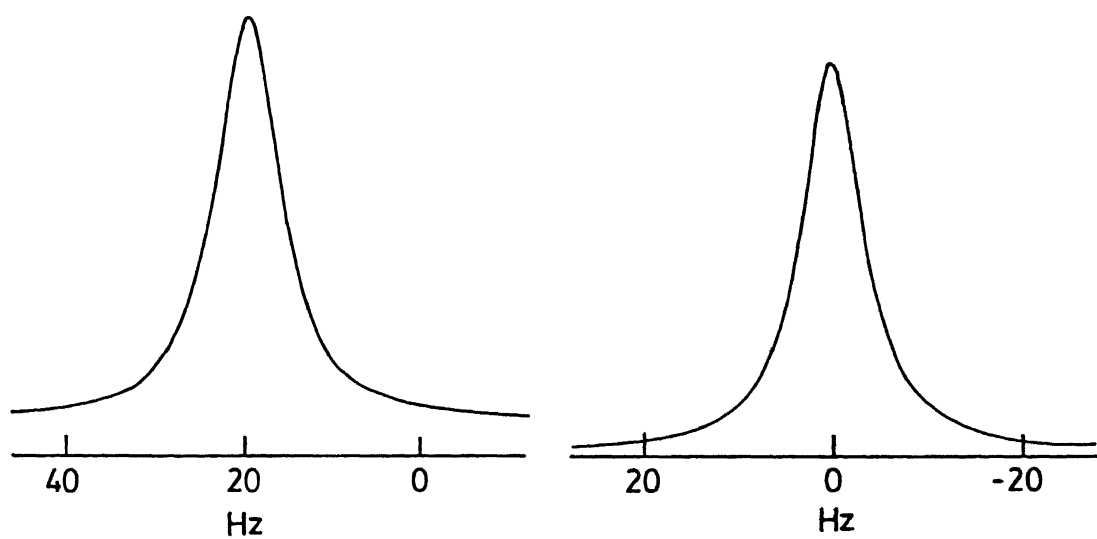


Fig.III.7 ^2D -NMR Spectrum (left) and best-fitting simulations (right) for PC/Cyclohexane/ D_2O at 296 K; $R = 12$.

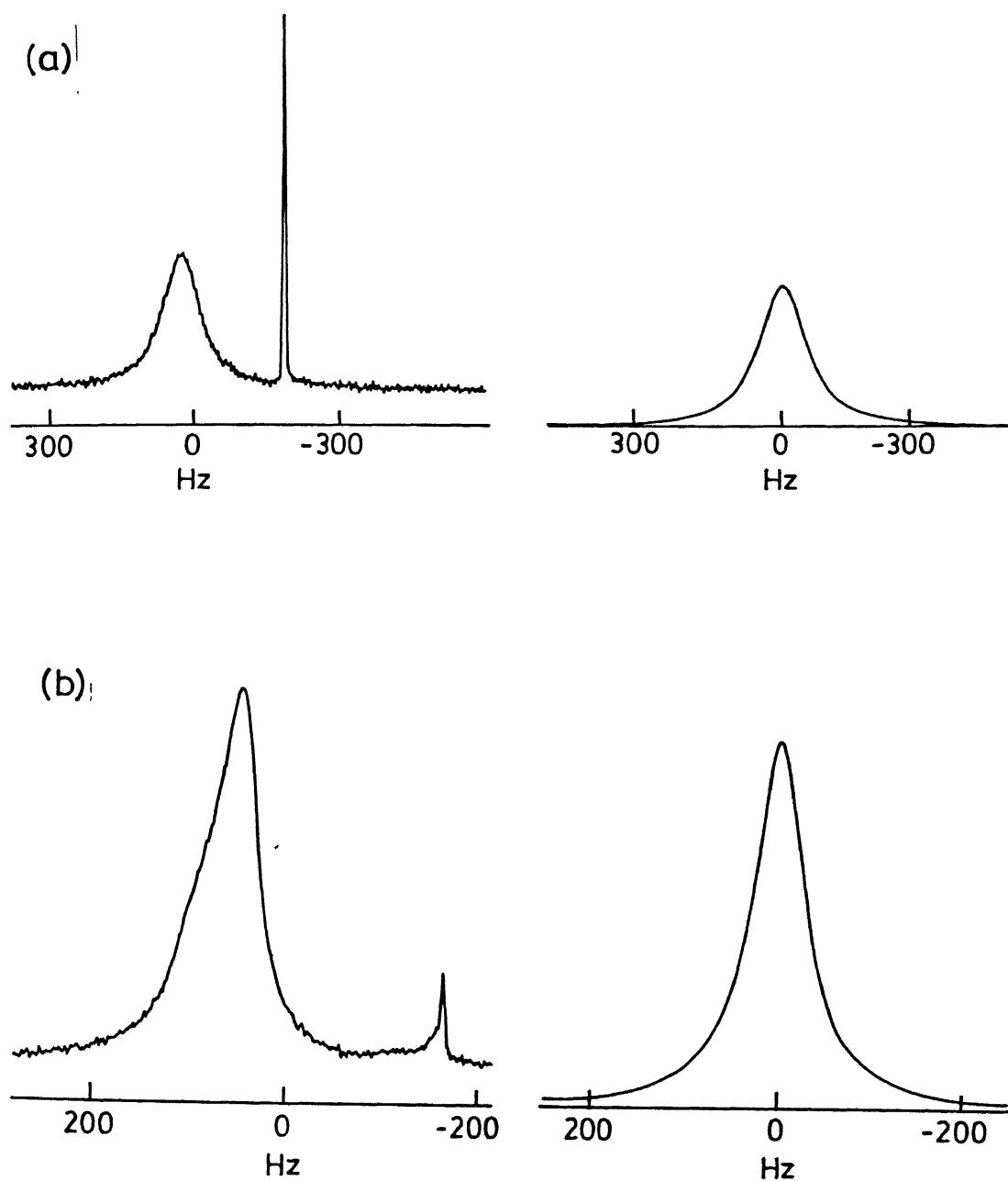


Fig.III.8 ^2D -NMR spectra (left) and best-fitting simulations (right) for PC/DCC/Cyclohexane/ D_2O at 296 K; (a) $R = 1$ and (b) $R = 3$.

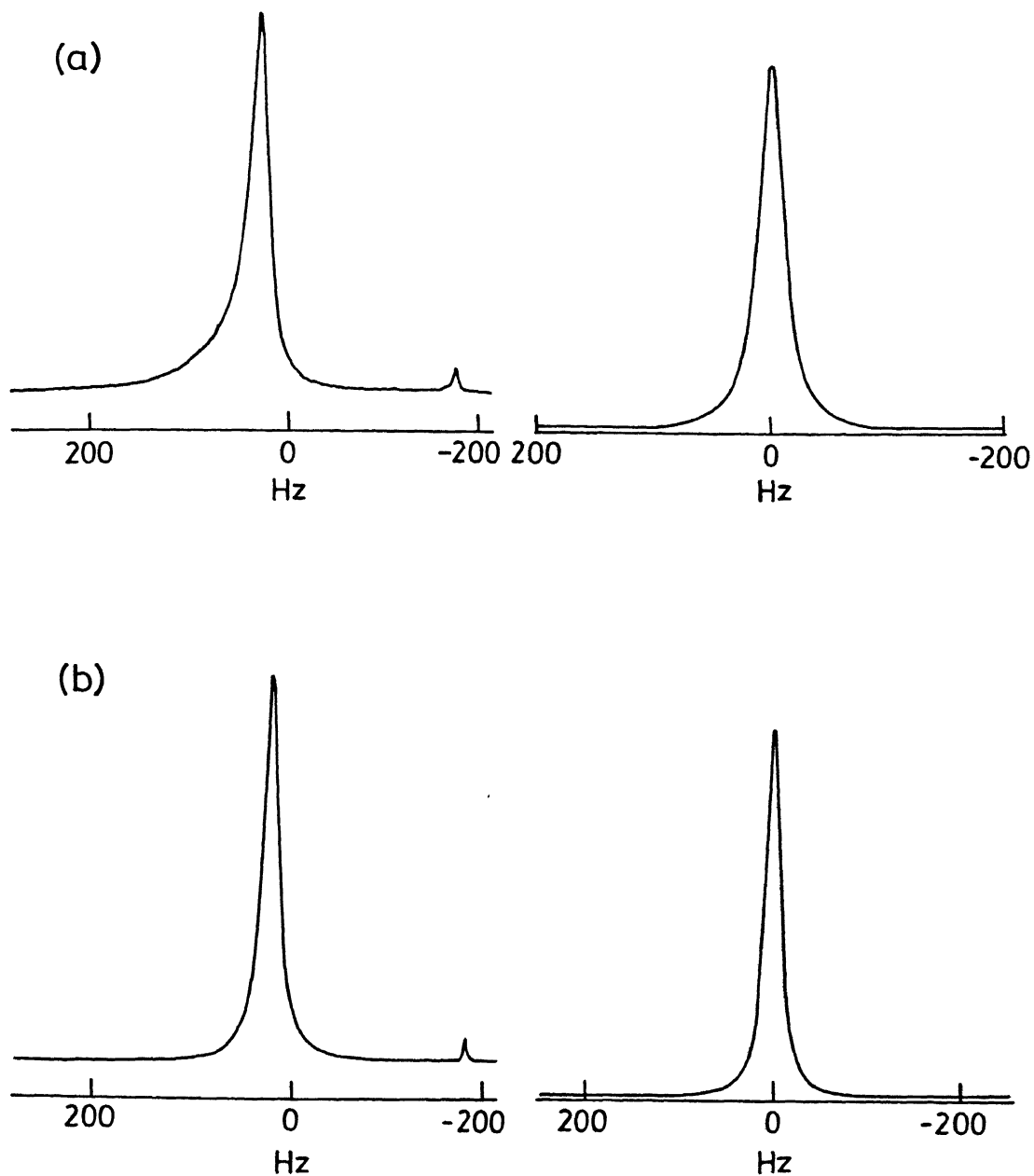


Fig.III.9 ^2D -NMR spectra (left) and best-fitting simulations (right) for PC/DCC/Cyclohexane/ D_2O at 296 K; (a) $R = 5$ and (b) $R = 6$.

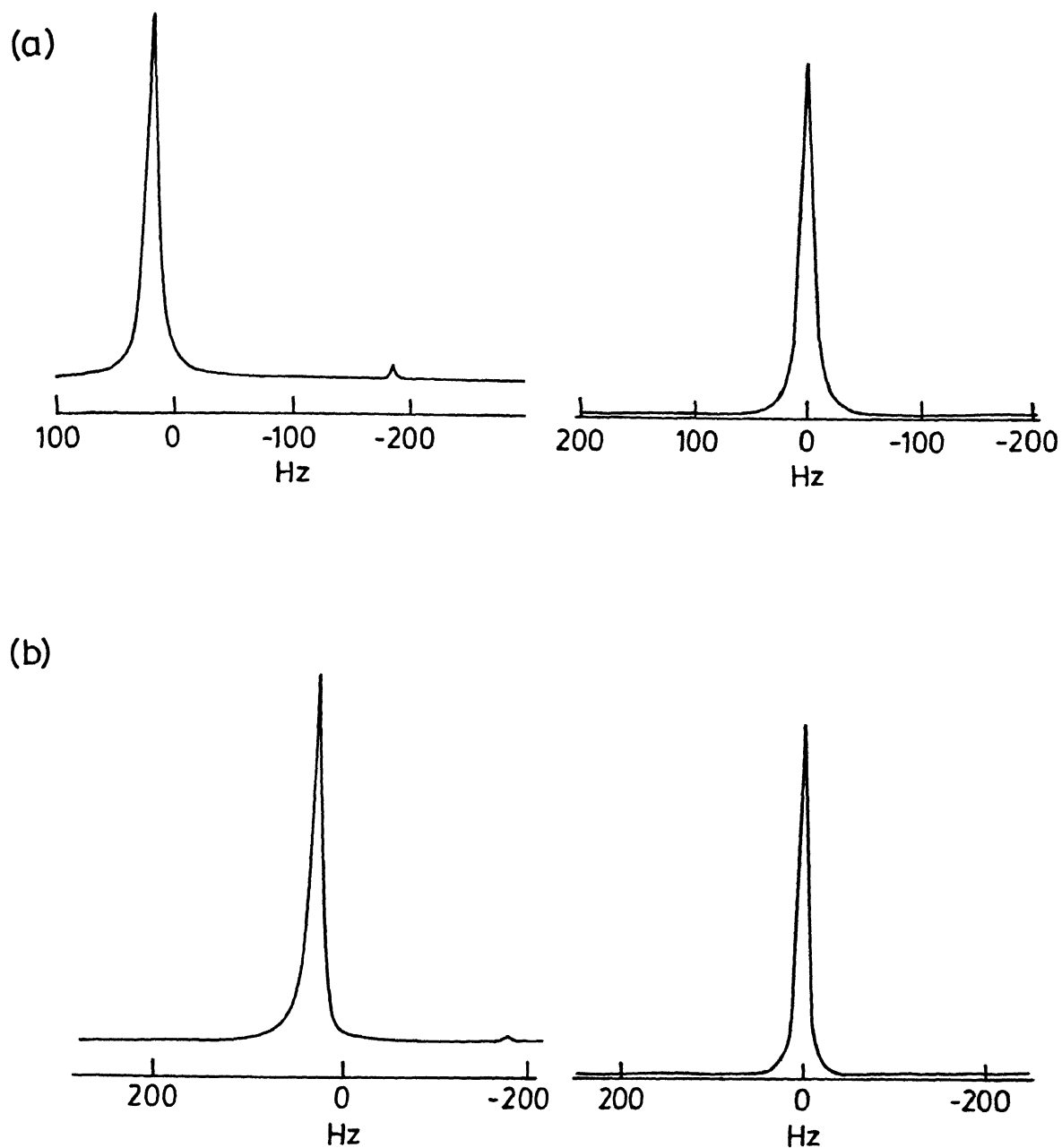


Fig.III.10 ^2D -NMR spectra (left) and best-fitting simulations (right) for PC/DCC/Cyclohexane/ D_2O at 296 K; (a) $R = 8$ and (b) $R = 12$.

should increase as R is increased. Somewhat unexpectedly, however, its intensity starts decreasing as R is increased. Also, the sharp line is appearing in all spectra around 180 Hz instead of around zero Hz (this is due to chemical shift and small variations in the magnetic field which had been left 'unlocked' with respect to deuterium frequency when recording our spectra) as all spectra have been recorded with respect to normal D₂O line (reference) frequency. This forced us to re-examine the origin of this sharp line. When we performed a ²D NMR measurement on (i) cyclohexane and (ii) lecithin dissolved in cyclohexane solution (i.e., a 'blank' run, which should give no ²D spectrum), a sharp line appeared at exactly the same frequency where we observe the 'sharp' component in all our reverse micelles (see Fig. III 11 (a) and (b)). Even the distilled water (H₂O) in just one FID give a strong residual signal in the ²D NMR (see Fig. III. 11(d)). This has been a matter of considerable surprise to us, especially since the natural isotopic abundance of ²D is $1.56 \times 10^{-2}\%$ and the NMR sensitivity at constant field relative to equal number of protons should only be 9.65×10^{-3} .

Having thus identified the origin of the sharp line as being due to naturally abundant ²D, we have simulated the broader component of all our experimental spectra. The input data used for simulations are given in Table III.3 and Table III.4, respectively, for the two reverse micellar systems.

The T₂ values (Tables III.3 and 4) for the 'bound' water are seen to be nearly 100 times less than the corresponding 'free water' values. This leads one to conclude qualitatively that the motion (rotational and translational) of the 'bound' water is

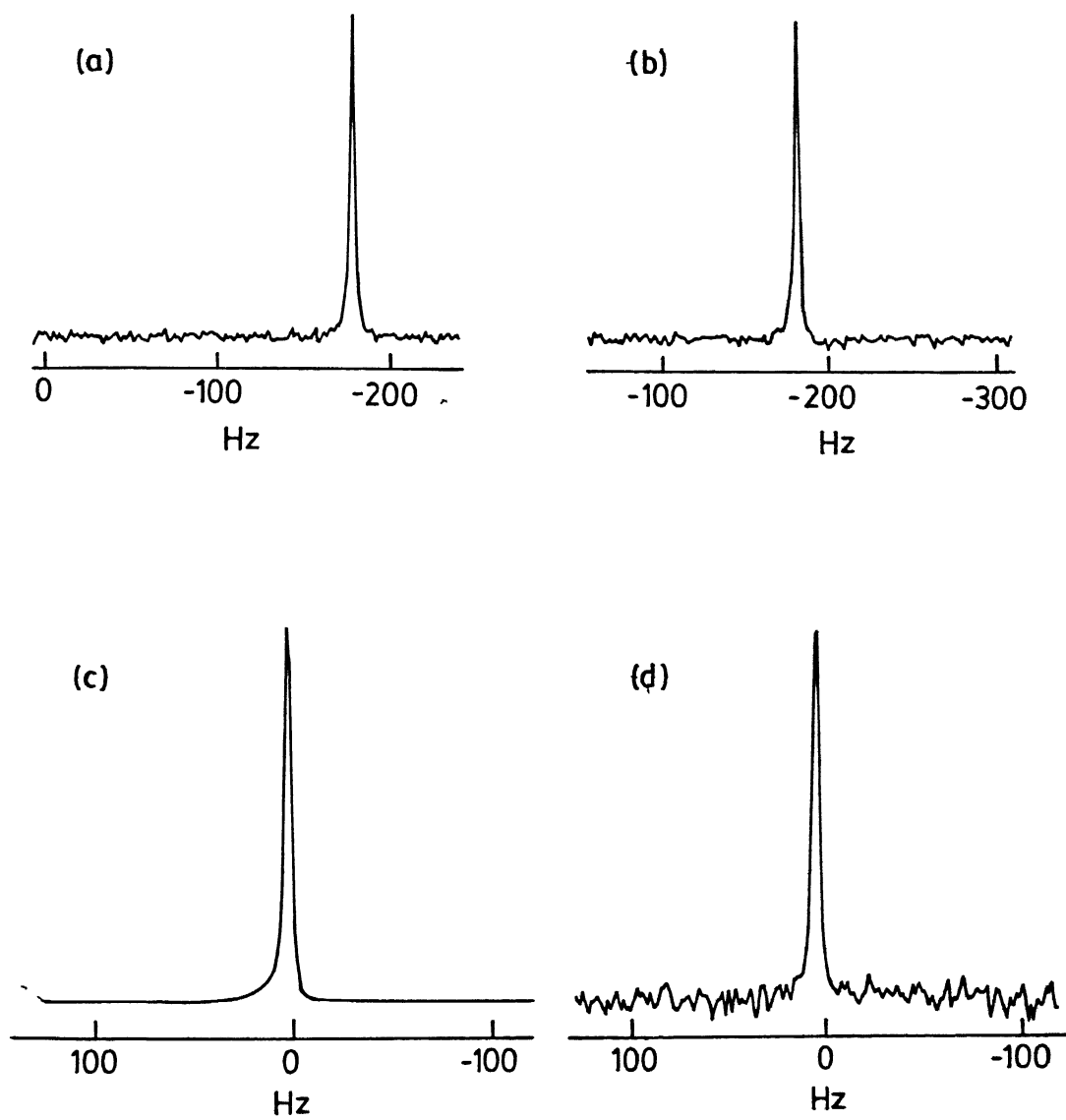


Fig. III.11 ^2D NMR spectra of (a) Cyclohexane, (b) Lecithin in Cyclohexane solution, (c) D_2O , and (d) distilled H_2O

slower than that of the 'free' water or, in other words, the τ_c of the 'bound' water is longer than that of 'free' water. This also substantiates our group's earlier result⁽⁴⁶⁾ and the result presented in Chapter II, by assuming the Stokes-Einstein equation [II.6], that the microviscosity of the water near the interface is higher when compared with 'free' water microviscosity.

As expected from our assumed model, the exchange rates in Table III.3 are seen to increase as R is increased, but the initial rates of increase are rather slow. There is a substantial increase in exchange rate when R is increased above 3. This is in line with our earlier findings that the reverse micellar structure changes from spherical shape to rod-like or tubular channels⁽⁴⁷⁾. In our simulations, the quadrupole coupling constant chosen for the free water is the most commonly used value of 220 KHz (48) while the 'bound' water quadrupole coupling constant has been varied between 150-194 KHz for getting best-fitting simulations in each case. Lower coupling constant was also reported earlier by Quist and Halle (49). These workers have reported 150 KHz for AOT/D₂O/2,2,4- trimethyl pentane system. The plausible reasons for the observations of lower coupling constants for the 'bound water' are :

- (i) change in O-D bond length due to hydrogen bonding^{(48(d))}
 - (ii) electrostatic interaction between the polar head groups and 'bound' water molecules, and
 - (iii) partial averaging of quadrupole coupling due to the libration and single axis rotation (49) as the 'bound' water is loosely held by the polar head groups by electrostatic interaction.
- At least in the case of lecithin/cyclohexane/D₂O, this would be the most reasonable mechanism in view of our earlier

findings^(50,51).

Table III.3 Parameters used in simulating ^2D NMR spectra for PC/Cyclohexane/ D_2O

R	$T_2(1)$ (10^{-5}s)	$T_2(2)$ (10^{-3}s)	Exchange Rate (10^4s^{-1})	Fractional population of		'bound water' quadrupole coupling constant, KHz
				site 1 p(1)	site 2 p(2)	
1	66.3	44.1	62.0	0.99	0.01	190
3	64.6	60.0	64.0	0.85	0.15	175
5	64.3	96.7	69.0	0.70	0.30	170
6	64.3	72.9	70.0	0.63	0.37	180
8	61.8	52.0	71.0	0.55	0.45	165
10	65.2	23.0	66.0	0.35	0.65	160
12	65.2	21.1	67.0	0.15	0.85	150

Table III.4 Parameters used in simulating ^2D NMR spectra for PC/DCC/Cyclohexane/ D_2O

R	$T_2(1)$ (10^{-5}s)	$T_2(2)$ (10^{-3}s)	Exchange Rate (10^4s^{-1})	Fractional population of		'bound water' quadrupole coupling constant, KHz
				site 1 p(1)	site 2 p(2)	
1	67.1	74.1	60.0	0.99	0.01	194
3	67.3	75.3	61.0	0.85	0.15	180
5	62.3	98.6	67.0	0.70	0.30	170
6	61.1	87.2	68.0	0.63	0.37	176
8	60.6	85.5	67.5	0.55	0.45	165
12	61.2	77.0	63.0	0.15	0.85	155

(b) Spectra at 263 K

Most of the earlier studies of water dynamics in reverse micelles have been done at room temperature. In this work, it is of interest to investigate water dynamics at subzero temperature as the anomalous properties of water are known to occur at subzero temperature^(52,53). It is observed that the water present in microemulsion samples does not freeze at the thermodynamic melting point of bulk water. The lowering of temperature in this type of systems initiates crystallization⁽⁵³⁾ (ice formation) through the mechanism of homogeneous nucleation. The temperature of this homogeneous nucleation process decreases as the water droplet size decreases. For example, at atmospheric pressure, for droplet size of a few μm , the homogeneous nucleation temperature is close to -40°C . In the case of our reverse micellar systems, the water pool size is about 350\AA upto an R value of five⁽⁴⁷⁾. Very little information is available about the supercooling of these systems. In aqueous solutions of macromolecules, it has been found that a small amount of unfreezable water remains well below the homogeneous nucleation temperature^(54,55).

Before undertaking the present study, we have not come across any report of 'pool water' freezing point in phospholipid based reverse micelles. Of possible relevance is a very recent report by Wu et al.⁽⁵⁶⁾ on the freezing of interbilayer free water, phosphocholine head group and bound water of fully hydrated egg sphingomyelin bilayers. The freezing points of interbilayer free water, phosphocholine head group and bound water have been reported as -11°C , -34°C and around -70°C , respectively. In the present study, we have recorded all the spectra at -10°C .

since egg sphingomyelin and egg phosphatidylcholine have the same phosphocholine head group structure (see Fig. III.12), we can reasonably assume that, at temperature of our study, only the 'free' water is approaching freezing.

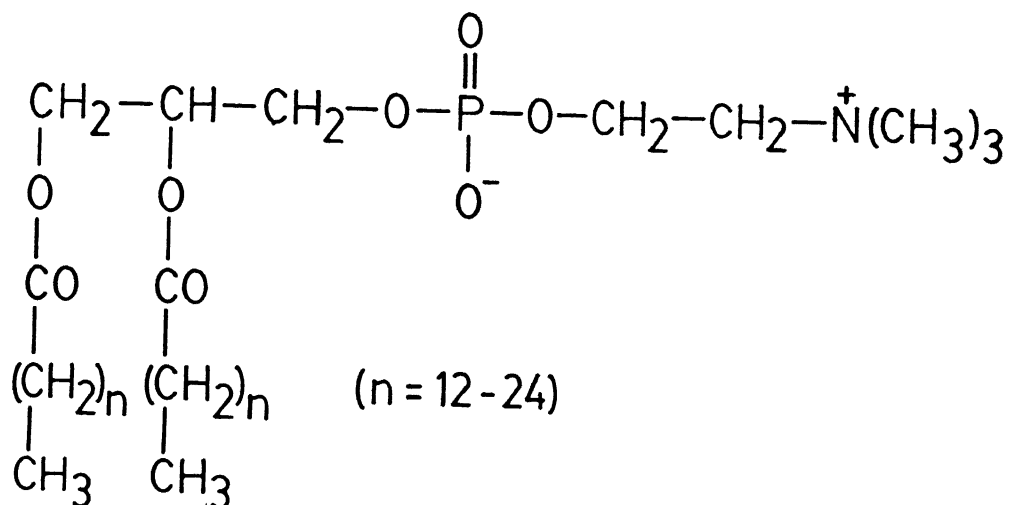
Interpretation of low temperature deuterium NMR spectra becomes difficult due to the fact that the phase behaviour of these reverse micellar systems at subzero temperature has not been characterized to our knowledge. Our interpretation of these spectra is, accordingly, rather tentative.

Spectra of both systems are given in Figs. III.13 to III.19, and the parameters used for simulation are given in Tables III.5 and III.6.

Table III.5 Parameters used in the 'best-fit' ^2D NMR simulation for the system PC/Cyclohexane/ D_2O

R	$T_2(1)$ (10^{-5}s)	$T_2(2)$ (10^{-3}s)	Exchange Rate (10^2s^{-1})	Fractional population of		'bound water' quadrupole coupling constant, KHz
				site 1 p(1)	site 2 p(2)	
1	14.8	3.5	4.23	0.99	0.01	192
3	13.8	1.3	4.40	0.85	0.15	200
5	13.1	1.1	4.70	0.70	0.30	200
6	12.3	1.0	4.90	0.63	0.37	186
8	13.0	0.75	4.80	0.55	0.45	185
10	13.2	1.0	7.0	0.35	0.65	182

(a) Phosphatidylcholine



(b) Sphingomyelin

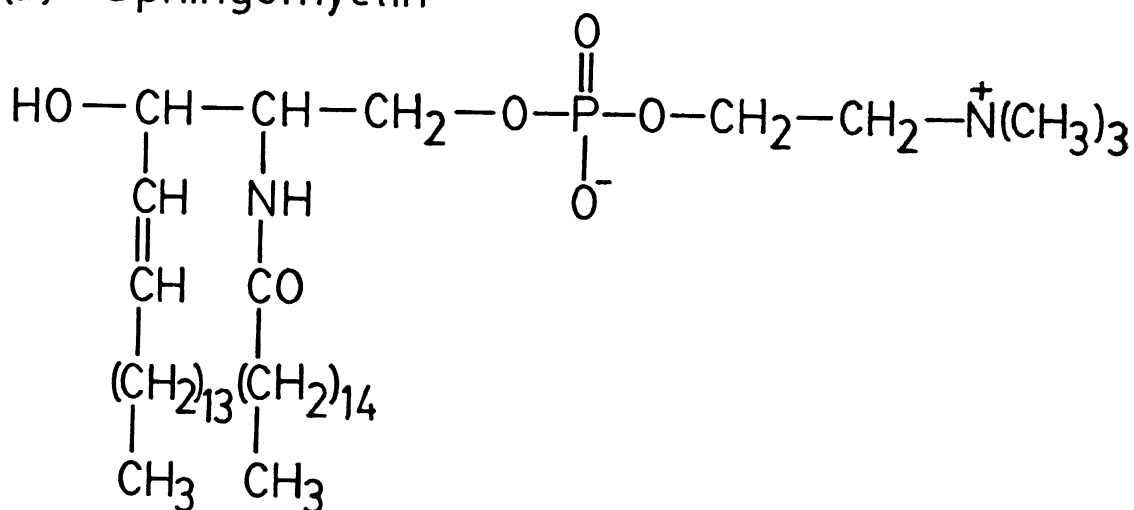


Fig. III.12 Comparative structures of Phosphatidylcholine and Sphingomyelin

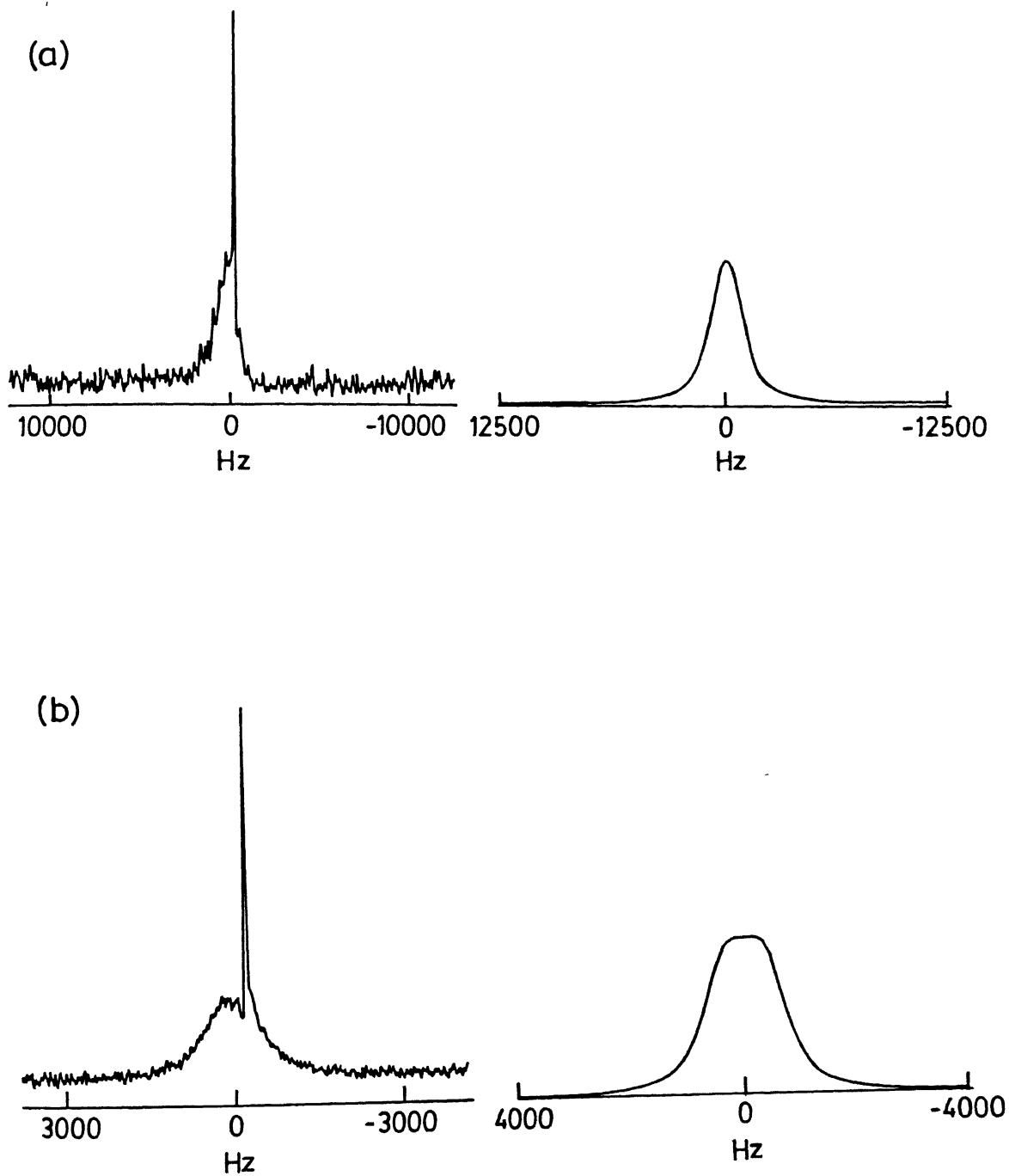


Fig.III.13 ^2D -NMR spectra (left) and best-fitting simulations (right) for PC/Cyclohexane/ D_2O at 263 K; (a) $R = 1$ and (b) $R = 3$.

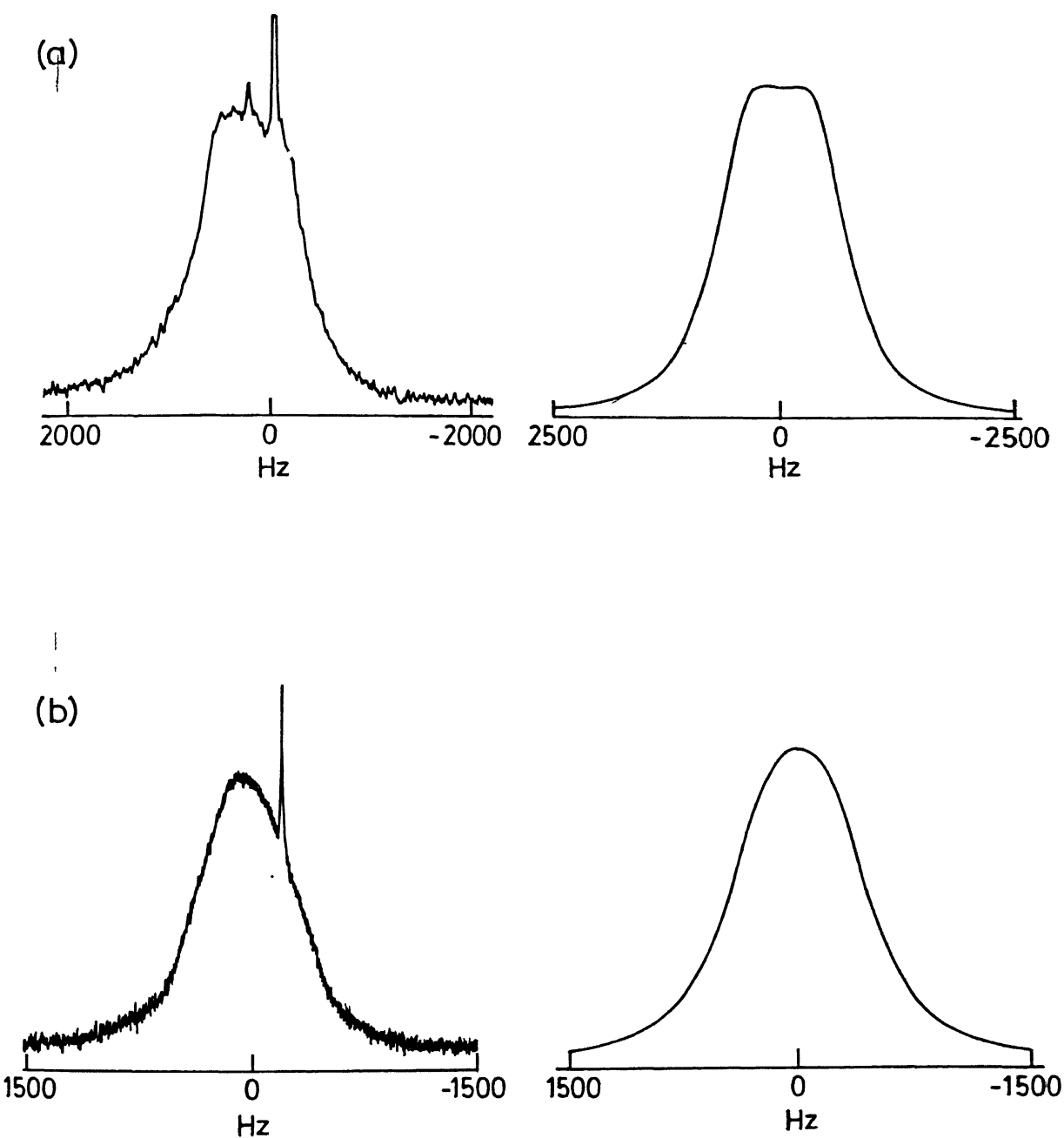


Fig.III.14 ^2D -NMR spectra (left) and best-fitting simulations (right) for PC/ Cyclohexane/ D_2O at 263 K; (a) $R = 5$ and (b) $R = 6$.

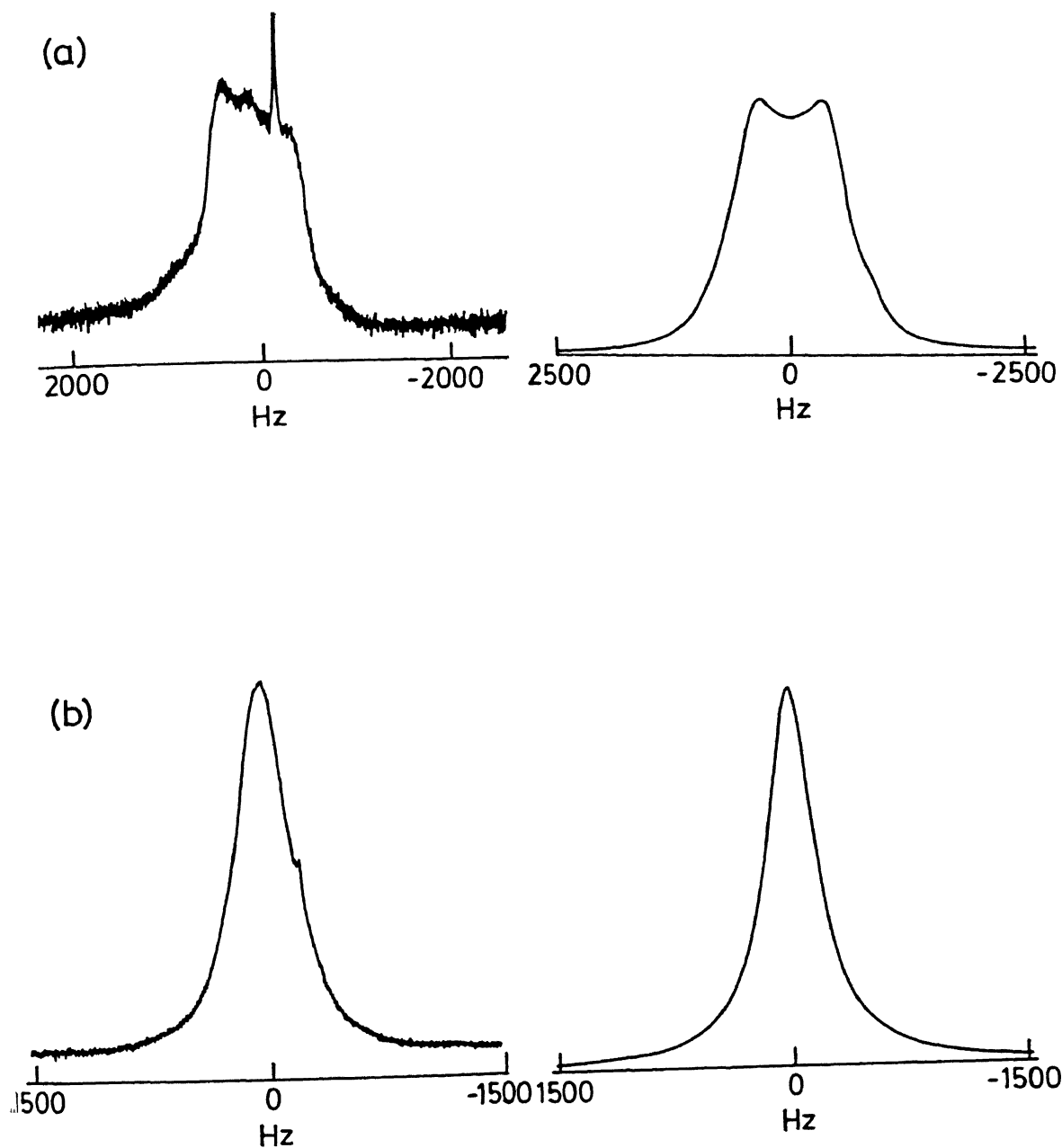


Fig.III.15 ^2D -NMR spectra (left) and best-fitting simulations (right) for PC/ Cyclohexane/ D_2O at 263 K; (a) $R = 8$ and (b) $R = 10$.

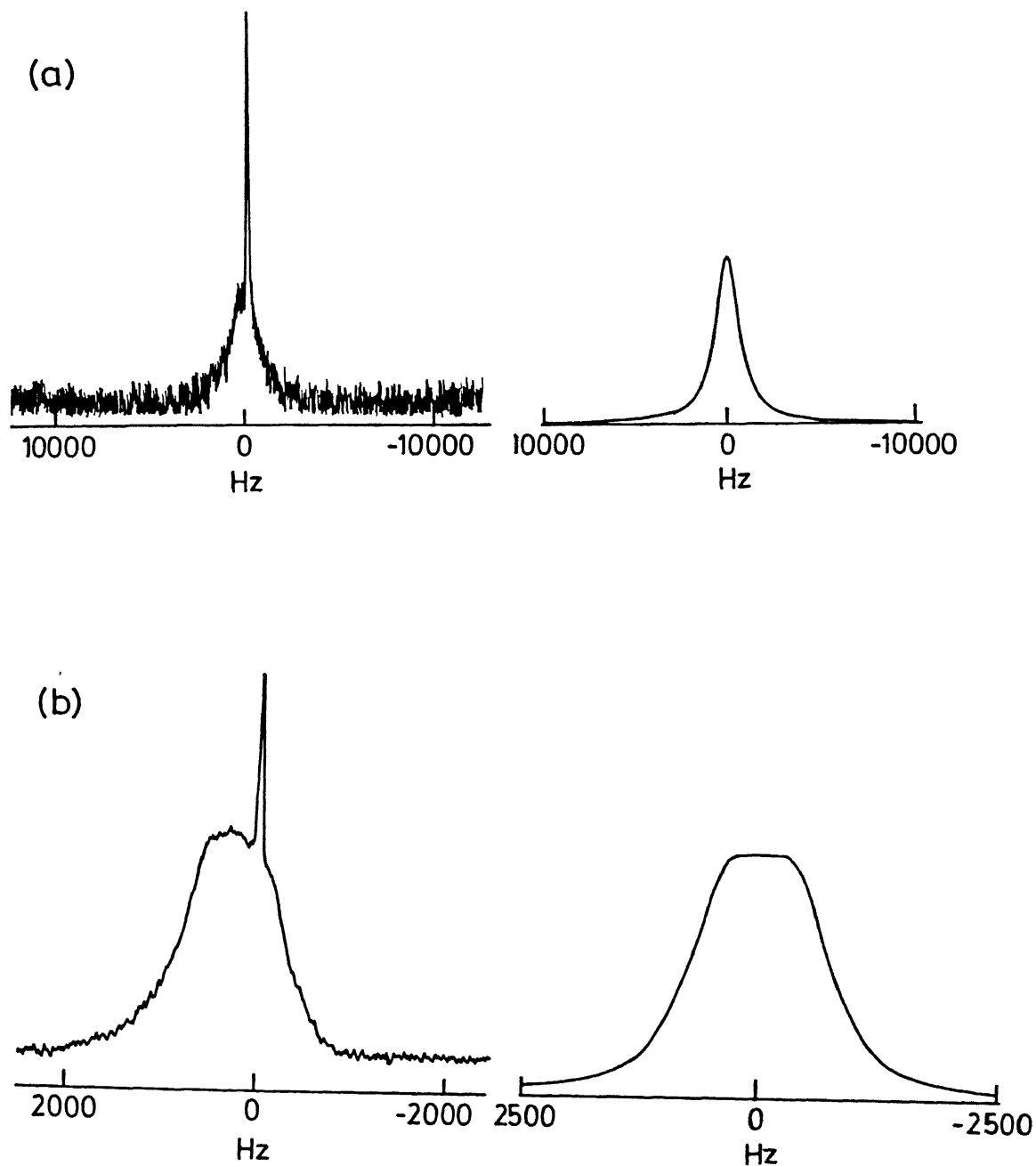


Fig.III.16 ^2D -NMR spectra (left) and best-fitting simulations (right) for PC/DCC/ Cyclohexane/ D_2O at 263 K; (a) $R = 1$ and (b) $R = 3$.

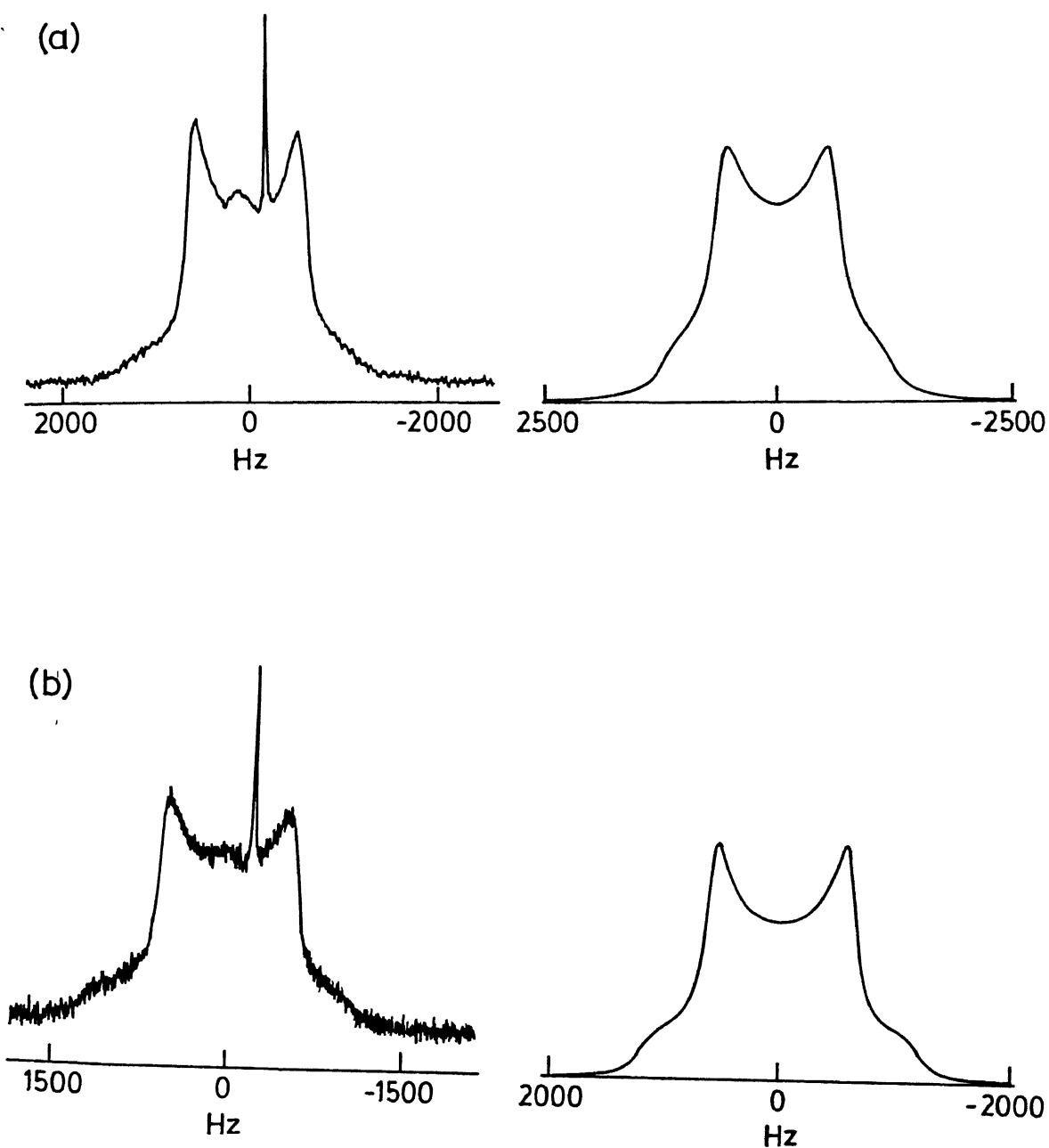


Fig.III.17 ^2D -NMR spectra (left) and best-fitting simulations (right) for PC/DCC/ Cyclohexane/ D_2O at 263 K; (a) $R = 5$ and (b) $R = 6$.

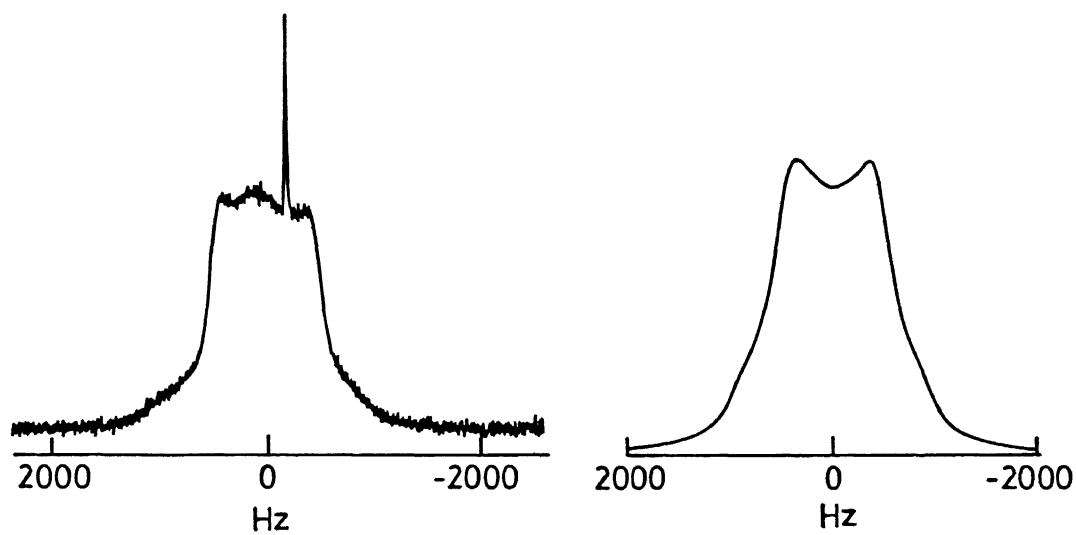


Fig.III.18 ^2D -NMR spectrum (left) and best-fitting simulations (right) for PC/DCC/Cyclohexane/ D_2O at 263 K; $R = 8$

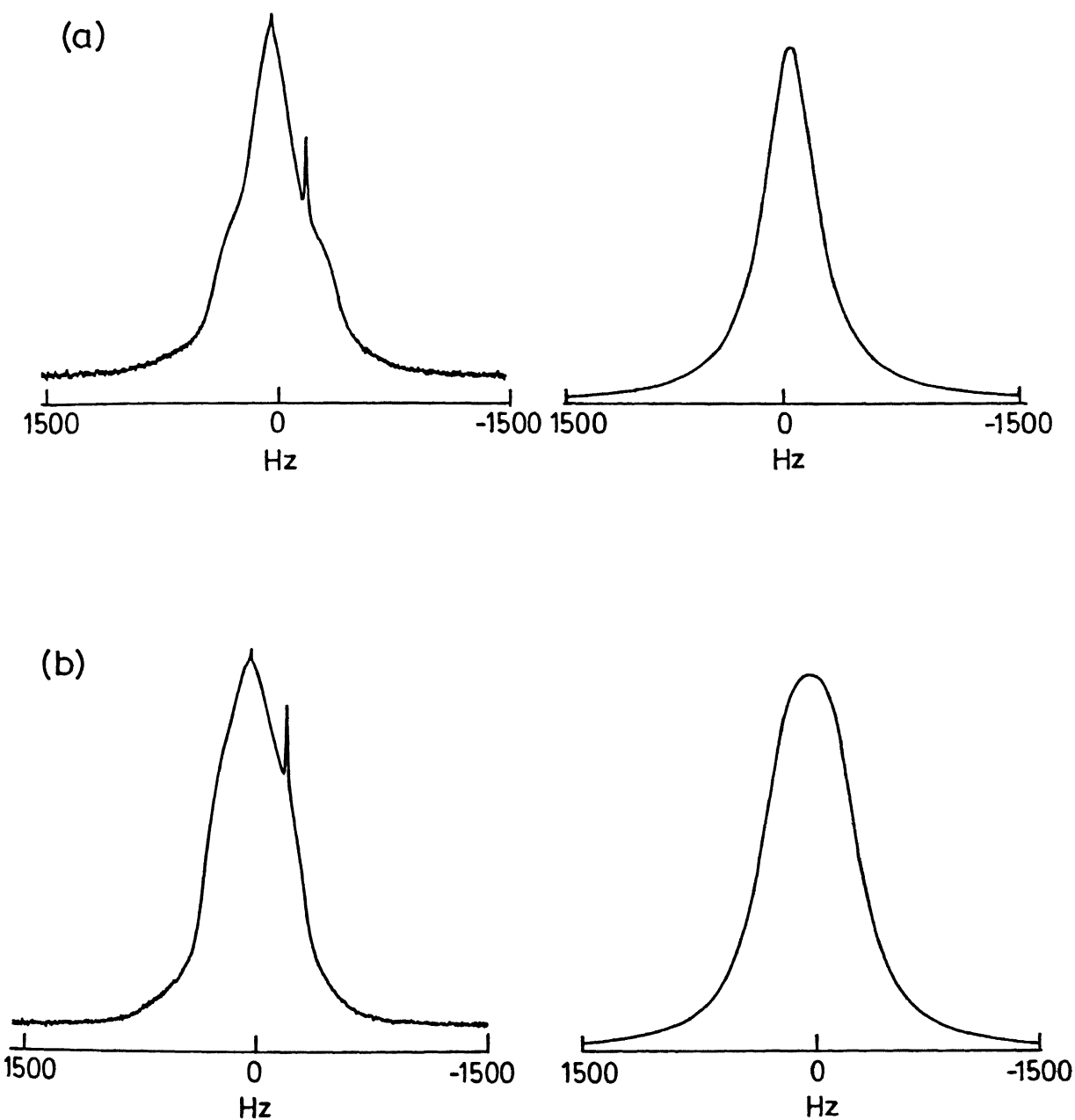


Fig.III.19 ^2D -NMR spectra (left) and best-fitting simulations (right) for PC/DCC/Cyclohexane/ D_2O at 263 K; (a) $R = 10$ and (b) $R = 12$.

Table III.6 Parameters used in the 'best-fit' ^2D NMR simulation for the system PC/DCC/Cyclohexane/ D_2O

R	$T_2(1)$ (10^{-5}s)	$T_2(2)$ (10^{-3}s)	Exchange Rate (10^2s^{-1})	Fractional population of		'bound water' quadrupole coupling constant, KHz
				site 1 p(1)	site 2 p(2)	
1	9.8	3.9	4.31	0.99	0.01	155
3	9.7	1.5	4.52	0.85	0.15	162
5	9.5	0.7	4.40	0.70	0.30	160
6	9.4	0.7	4.60	0.63	0.37	174
8	9.5	0.6	4.50	0.55	0.45	190
10	9.6	1.1	4.90	0.35	0.65	170
12	9.6	0.7	4.85	0.15	0.85	180

From the Tables III.5 and III.6, in each micellar system the T_2 values for both sites are lower, as expected, compared to their corresponding values at 296 K. Exchange rates have also decreased nearly 10^3 times. At this temperature, both the systems give similar types of spectra at all R values, except in the range of $R = 5-8$. This is a strong indication for the fact that the structure or shape of the DCC-containing reverse micelles at $R = 5$ and 6 is aspherical, because the lineshape is a typical powder pattern with $\eta \approx 0$. Although the same trend should also be observable in the DCC-free system, we have not observed it. This may also be due to the difference in the degree of organization of water molecules extending into the cores of these two systems. Measurements of freezing-points of 'bound water' and 'free water' by other specific techniques such as differential scanning

calorimetry (DSC), as well as direct electron microscopic measurements of the aggregation size and geometry of these reverse micelles, are necessary for quantitating our present observations further.

DMR spectra of the $R = 10$ and $R = 12$ cases of DCC-added system clearly show the superposition of a sharp line on a broader line. It is found from the literature that these lineshapes resemble those of lecithin-water system⁽²⁾ with a D_2O : dipalmitoyl lecithin mole ratio of 10.7 at 43°C and of 14.6 at 45.6°C . Such composite lineshapes are characteristic of 'free water' exchanging slowly with the 'bound water'.

The appearance of a small hump in the middle of an otherwise typical powder 2D pattern expected for an asymmetric parameter $\eta \approx 0$ in the $R = 5, 6, 8$ cases of our DCC-added system and in the $R = 8$ case of DCC-free system clearly shows that two physically distinguishable D_2O sites exist in each of these reverse micelles with different T_2 values. The existence of water molecules with distinguishable dynamics in two different binding sites within the same thermodynamically and macroscopically homogeneous system is an interesting result of our studies.

Even though bilayer structures are different from those of reverse micelles, it is at any rate safe to assume that the hydration of phosphocholine head group containing natural surfactants (lipids) by water occurs in an analogous manner in these two structures. One may then conclude with reasonable certainty that, in the reverse micellar systems studied by us at 263 K, only the 'free water' dispersed as small droplets in the cyclohexane and present in the core of the 'water pool' is very close to freezing point, in correspondence with results of the

layer system reported by Wu et al.⁽⁵⁶⁾.

In both the reverse micellar systems studied, some of the experimental spectra observed at 263 K could not be exactly simulated. This is possibly due to (i) the inclusion of only secular terms of \hat{H}_Q in our computations, and (ii) the use of a single Lorentzian lineshape convolution function for the two spectral components; it is expected that the use of two Lorentzian functions, or a Lorentzian shape function for the narrower component and a Gaussian one for the broader component, could improve the simulations further.

II.5 Conclusions

1. The appearance of the sharp 2D line in both reverse micellar systems at all R values is unambiguously assigned as being due to the naturally abundant 2D of cyclohexane and lecithin.
2. Computer simulated spectra at 296 K show that T_2 values for the 'bound water' are nearly 100 times less than corresponding 'free water' values, providing evidence for the higher microviscosity of water near the interface. Substantial increase in exchange rates of water in both systems above $R = 3$ supports our earlier findings that the structure of reverse micelle changes from spherical to a rod-like tubular shape.
3. Computer simulated spectra at 263 K show that the exchange rates of water decrease nearly 10^3 times compared with the same system at 296 K. Resemblance of line shape with typical 2D power patterns for $\eta_a \approx 0$ suggest that the shape of DCC-added reverse micelle between R values of 5 and 8 may be aspherical. Clear indication of exchange of 'free water' with 'bound water' has been

provided from the experimental spectra corresponding to $R=10$ and $R=12$ cases of DCC-added system. The appearance of a small central hump for some of the R values studied shows the existence of water molecules at two different sites with distinct dynamic properties. In comparison with the hydration of similar head group containing lipids, only the 'free water' dispersed in the cyclohexane and present in the core of the 'water pool' is thought to be very close to freezing point at 263 K.

REFERENCES

1. J. Seelig, Q. Rev. Biophys. 10, 353 (1977).
2. J. Ulmius, H. Wennerström, G. Lindblom and G. Arvidson, Biochemistry 16, 5742 (1977).
3. R.G. Griffin, Methods Enzymol. 72, 108 (1981).
4. I.C.P. Smith and H.C. Jarrell, Acc. Chem. Res. 16, 266 (1983).
5. R.L. Smith and E. Oldfield, Science 225, 280 (1984).
6. P. Meier, E. Ohmes, and G. Kothe, J.Chem. Phys. 85, 3598 (1986).
7. A. Blume, W. Hübner, M. Müller, and H.D. Bäuerle, Ber Bunsenges Phys. Chem. 92, 964 (1988) and references cited therein.
8. W. Hübner and A. Blume, J. Phys. Chem. 94, 7726 (1990).
9. B. Halle, J. Phys. Chem. 95, 6724 (1991).
10. J. Stohrer, G. Gröbner, D. Reimer, K. Weisz, C. Mayer and G. Kothe, J. Chem. Phys. 95, 672 (1991).
11. J.R. Hansen, J. Phys. Chem. 78, 256 (1974).
12. B. Lindman, O. Söderman, H. Wennerström, in "Surfactant Solution : New methods of Investigation" R. Zana (ed.) Marcel Dekker, New York (1987), P. 295.
13. A. Faure, T. Ahlnäs, A.M. Tistchenko and C. Chachaty, J. Phys. Chem. 91, 1827 (1987).
14. U. Olsson, M. Jonströmen, K. Nagai, O. Söderman, H. Wennerström, and G. Klose, Progr. Colloid Polym. Sci. 76, 75 (1988).
15. G. Carlström and B. Halle, Langmuir 4, 1346 (1988).
16. G. Carlström and B. Halle, J. Phys. Chem. 93, 3287 (1989).
17. M. Sjöberg, U. Henriksson, and T. Wärnheim, Langmuir 6, 1205 (1990).
18. A. Abragam, 'Principles of Nuclear Magnetism' Oxford University Press, London, (1961).
19. C.P. Slichter 'Principles of Magnetic Resonance', Third Enlarged and Updated Edn., Springer Verlag, New York (1990).
20. T.L. James, 'NMR in Biochemistry', Academic Press, New York (1975).

21. M.H. Cohen and F. Reif, Solid State Physics 5, 321 (1957).
22. P. Waldstein, S.W. Rabideau and J.A. Jackson, J. Chem. Phys. 41, 3407 (1964).
23. S.W. Rabideau and J.A. Jackson, J. Chem. Phys. 41, 4008 (1964).
24. T. Chiba, J. Chem. Phys. 41, 1352 (1964).
25. H. Wennerström, G. Lindblom and B. Lindman, Chemica Scripta 6, 97 (1974).
26. H. Wennerström, Mol. Phys. 24, 69 (1972).
27. E.G. Finer, J. Chem. Soc. Faraday Trans. II 69, 1590 (1973).
28. K. Blum, Density Matrix Theory and Applications, Plenum Press, New York (1937).
29. U. Fano, Rev. Mod. Phys. 29, 74 (1957).
30. J. Jeener, Adv. Magn. Reson. 10, 1 (1982).
31. F. Dyson, Phys. Rev. 75, 486 (1949); *ibid* 1736 (1949).
32. (a) B.C. Gerstein and C.R. Dybowski, Transient Techniques in NMR of Solids, Academic Press, Florida (1985).
(b) P.L. Corio, Structure of High-Resolution NMR Spectra, Academic Press, New York (1966), Appendix II.
33. I.I. Rabi, N.F. Ramsey, and J. Schwinger, Rev. Mod. Phys. 26, 169 (1954).
34. J.C. Pratt, P. Raghunathan, and C.A. McDowell, J. Chem. Phys. 61, 1016 (1974).
35. J.C. Pratt, P. Raghunathan, and C.A. McDowell, J. Magn. Reson. 20, 313 (1975).
36. S. Vega and A. Pines, J. Chem. Phys. 66, 5624 (1977).
37. (a) A. Wokaun and R.R. Ernst, J. Chem. Phys. 67, 1752 (1977);
(b) H.W. Spiess, J. Chem. Phys. 72, 6755 (1980);
(c) A.J. Vega, Polym. Prepr. Am. Chem. Soc. Div. Polym. Chem., 22, 282 (1981);
(d) B.C. Sanctuary, T.K. Halstead, and P.A. Osmet, Mol. Phys. 49, 753 (1983);
(e) G.J. Bowden and W.D. Huchison, J. Magn. Reson. 67, 403 (1986);
(f) T.M. Barbara, J. Magn. Reson. 67, 491 (1986).

38. A.J. Vega and Z. Luz, J. Chem. Phys. **86**, 1803 (1987).
39. J.G. Powles and P. Mansfield, Phys. Lett. **2**, 58 (1962).
40. J.H. Davis, K.R. Jeffrey, M. Bloom, M.I. Valic, and T.P. Higgs, Chem. Phys. Lett. **42**, 390 (1976).
41. (a) R.G. Gordon and T. Messenger, in : **Electron Spin Relaxation in Liquids**, L.T. Muus and P.W. Atkins (eds.), Plenum Press, New York (1972);
 (b) R. Bellman, **Introduction to Matrix Analysis**, 2nd edn., McGraw-Hill Inc., New York (1970).
42. A. Papalis, **Probability, Random Variables and Stochastic Processes**, McGraw-Hill Inc., New York (1965).
43. H. Kahn, in : **Symposium on Monte Carlo Methods**, H.A. Meyer (ed.), John Wiley & Sons, New York (1956).
44. P. Raghunathan and S.C. Sivasubramanian, Proc. Indian Acad. Sci. (Chem. Sci.) **96**, 565 (1986).
45. S.C. Sivasubramanian, Ph.D. Thesis, Indian Institute of Technology, Kanpur, India (1989).
46. V.V. Kumar and P. Raghunathan, Chem. Phys. Lipids **41**, 159 (1986).
47. V.V. Kumar, C. Kumar, and P. Raghunathan, J. Colloid Interface Sci. **99**, 315 (1984).
48. (a) E. Long and H.D. Lüdemann, Ber. Bunsenges, Phys. Chem. **84**, 462 (1980);
 (b) B. Halle and H. Wennerström, J. Chem. Phys. **75**, 1928 (1981);
 (c) D.T. Edmonds and A.L. Mackay, J. Magn. Reson. **20**, 515 (1975);
 (d) P.L. Cummins, G.B. Bacskay, N.S. Hush, B. Halle and S. Engström, J. Chem. Phys. **82**, 2002 (1985).
49. P.O. Quist and B. Halle, J. Chem. Soc. Faraday Trans. **1**, **84**, 1033 (1988).
50. V.V. Kumar, P.T. Manoharan, and P. Raghunathan, J. Biosci, **4**, 449 (1982).
51. V.V. Kumar and P. Raghunathan, **The Nineth International Symposium on Nuclear Quadrupole Resonance**, Kanpur, India (1988), Abstract P. 80.
52. E. Lang and H.D. Lüdemann, Angew, Chem., Int. Ed. Engl. **21**, 315 (1982).
53. C.A. Angell, Ann. Rev. Phys. Chem. **34**, 593 (1983).
54. I.D. Kuntz, Adv. Chem. Ser. **180**, 27 (1979).

55. F. Franks, in : **Water - A Comprehensive Treatise**, F. Franks (ed.), Plenum Press, New York (1982), Vol. 7, Chap. 3.
56. W.G. Wu, L.M. Chi, T.S. Yang, and S.Y. Fang, J. Biol. Chem. **266**, 13602 (1992).

CHAPTER IV

PROTON MULTIPLE QUANTUM RELAXATION OF A DEOXYCHOLATE METHYL GROUP IN REVERSE MICELLE

IV.1. Introduction

It is now well established that the structure and dynamics of macromolecules and molecular aggregates can be obtained by extracting cross-relaxation times of coupled nuclear spins through two dimensional NMR methods^(1,2). However, interpretation of the resulting data from the molecular aggregates is rendered difficult due to the modulating effects of motions of a group in a molecule, or of the molecule itself, or even of the aggregate as a whole, these various motions often occurring at different time scales. For example, the methyl group of a surfactant in a reverse micelle may be complicated by the following motions :

- (i) motion of a methyl group about its C_3 axis,
- (ii) motion of the whole molecule in which the methyl group is present and
- (iii) motion of the reverse micelle as a whole.

Additionally, for systems such as reverse micelles consisting of heterogeneous molecules, the inter- and intra- molecular interactions can also affect interactions among spins thereby adding to the complexity of our interpretation.

These difficulties were overcome by Kay and Prestegard⁽³⁾, Wong et al.⁽⁴⁾ and Wang and Hwang⁽⁵⁾ by using the results of an one-dimensional analog of n-quantum filtered 2D experiment ($n=0,2,3$) combined with transverse^(3,4) and longitudinal⁽⁵⁾ relaxations.

In an effort to study the dynamics of polar head groups of surfactants in a reverse micelle and to get dynamic information at the interface as well as the interaction of reverse micellar 'pool water' with the polar head groups, we first attempted to study the $-N^+(CH_3)_3$ of lecithin theoretically by calculating the response of this A_9 proton-spin system to rf pulses. However, the mathematical complexity of handling this A_9 case was soon realised and we then took up the well studied sodium deoxycholate as the surfactant for forming reverse micelles.

This chapter contains (i) a brief introduction to cross-relaxation effects in coupled nuclear spin systems and the consequent appearance of forbidden peaks in multiple quantum filtered NMR, (ii) our theoretical calculations for an A_9 spin system (formed by the nine protons of $-N^+(CH_3)_3$), and (iii) experimental results of zero- and double- quantum filtered 1D analog of 2D experiments on deoxycholate reverse micelles. Motional parameters have been extracted by way of matching the experimental data profile to the theoretical one assuming an appropriate model for the reverse micelle, and certain overall conclusions have been made based on our results.

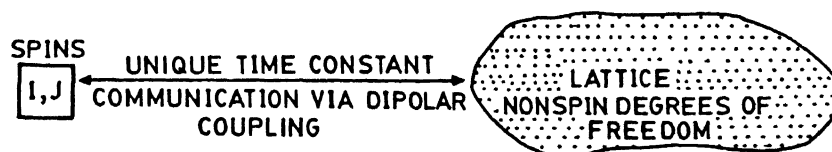
IV.2. Cross-relaxation Times

The fast molecular motions of macromolecules and molecular aggregates can be probed by ^{13}C spin-lattice relaxation time (T_1) and nuclear Overhauser effect (nOe) measurements performed at different magnetic field strengths. The spectral densities of fast molecular motions fall in the frequency range of $10^8 - 10^9 \text{ s}^{-1}$. But the information about slow motions or

processes such as diffusion, chemical exchange etc. (correlation time (τ_0) $> 10^{-8}$ s) which have negligible spectral density⁽⁶⁾ near or above the Larmor frequency are obtained by spin echo measurement of spin-spin relaxation time (T_2). The rates for these processes are obtained from the pulse spacing dependent dephasing rates in 2-pulse or multiple-pulse experiments. However, it was believed earlier that the relaxation rate dependence on pulse spacing is due to the existence of low frequency components of molecular motions, whereas on the contrary it is due to the existence of cross-relaxation between components of transverse magnetization of spin coupled multiplets. This is explained below.

Two important relaxation mechanisms for spin-1/2 nuclei in liquids in the absence of inhomogeneous magnetic field and chemical exchange are : inter- and intramolecular dipole-dipole and spin-rotation interactions. Much of the earlier NMR literature has dealt with intramolecular dipole-dipole interaction of two coupled spins only. For the case of three or more coupled spins, assuming that the motion of any two nuclei is uncorrelated with that of a third (ie., the case where cross-correlation functions go to zero), it can be readily shown that the total relaxation rate is just the sum of all individual pairwise dipole-dipole interactions. In reality, however, for a methyl group the motion of the third proton is clearly determined by the motions of the other two. An elegant pictorial explanation of this has been provided by Werbelow and Grant⁽⁷⁾, and this figure is reproduced in Fig. IV.1

(a) SINGLE PAIR OF TWO IDENTICAL SPINS



(b) CHAIN OF COMMUNICATION IN A SYSTEM OF THREE IDENTICAL SPINS

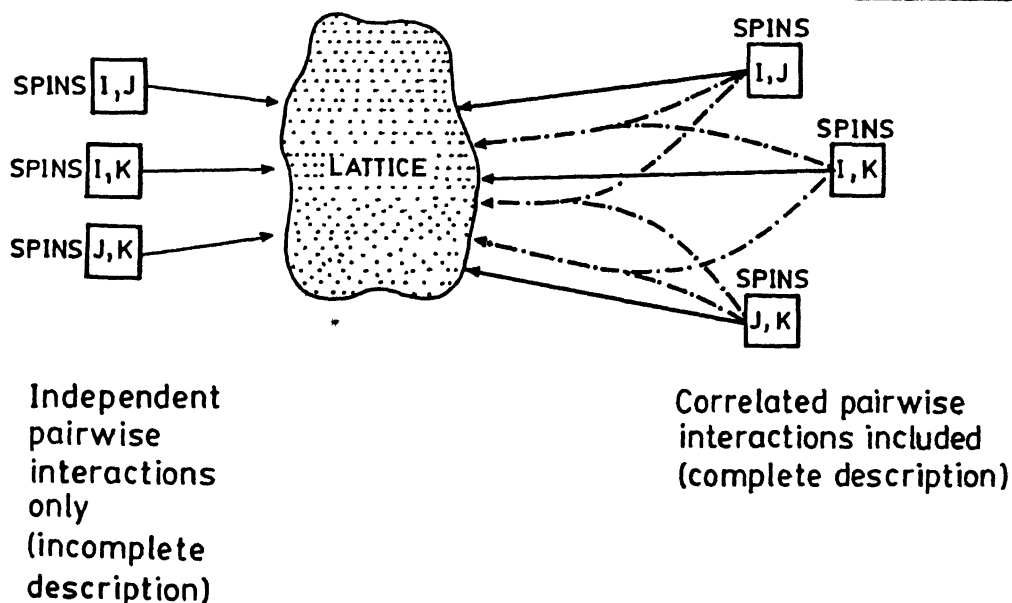


Fig.IV.1 Longitudinal relaxation process in spin systems through dipolar interaction (adapted from ref. (7))

- (a) for a single pair of identical spin $-1/2$ (I and J) nuclei ;
- (b) for a system consisting of three identical spins (I, J and K).

For a system of two identical coupled spin $-1/2$ nuclei, I and J (see Fig. IV. 1(a)), the longitudinal relaxation processes are characterized completely by one unique time constant. When we consider spin systems consisting of three identical spins and assume that the system has only three independent pairwise interactions, we may, again, always propose that a unique time constant exists for this system. Strictly, however, it is realised from Fig. IV 1(b) that these three pairwise interactions are interlinked and any resultant change at any one nucleus due to a coupling with the other two must be correlated. Therefore, the correct relaxation equation should contain terms corresponding to these correlation processes. The correlation processes are of two types :

- (i) auto-correlation, when the orientation of I-J dipole-dipole vector at time t is related to the orientation of the same vector at time $t+\tau$;
- (ii) cross-correlation, when the orientation of I-J dipole-dipole vector at time t is related to the orientation of J-K dipolar vector at time $t+\tau$.

Vold and coworkers^(6,8) and Grant and coworkers⁽⁷⁾ have calculated these cross-correlation spectral density terms by fitting T_1 and T_2 relaxation data; they have shown the usefulness of these terms for studying the motional properties of spin systems. Later on two other methods for extracting these terms have been reported, namely, the use of polarization transfer pulse sequence (DEPT and INEPT)⁽⁹⁾ and of the heteronuclear multi-pulse schemes⁽¹⁰⁾.

The spin systems considered till to-date are mostly AX_2 or AX_3 having ^{13}C or ^{19}F and ^1H . However, the above methods invariably require isotopic enrichment, which is difficult in the case of biomolecules. To overcome this and other problems related to the extraction of cross-correlation terms from T_1 and T_2 data, Kay and Prestegard⁽³⁾ have proposed an interesting 1D analogue of double quantum 2D experiment. Their method is explained in detail in the next section.

IV.3 Extraction of Cross-correlation Spectral Density Terms Using Multiple Quantum NMR

In 1985, Muller et al.⁽¹¹⁾ reported the appearance of forbidden cross-peaks, in violation of coherence-transfer selection rules^(12,13) derived neglecting transverse relaxation, in proton multiple quantum filtered correlation spectroscopy and multiple quantum NMR. The selection rules⁽¹²⁾ governing multiple quantum filtered 2D correlated spectroscopy of weakly coupled spin systems are:

- (i) The 'diagonal' peaks, representing inequivalent nuclear sites, in n-quantum filtered spectra imply that the spin in question has resolved scalar couplings to at least (n-1) equivalent or nonequivalent spins.
- (ii) The 'cross' peak, representing J-coupling between two spins in an n-quantum filtered spectrum indicates that, in addition to their direct coupling, there are nonvanishing couplings to a common set of at least (n-1) additional spins.

For a macromolecule having a methyl group attached to a tertiary carbon, for instance, these rules predict that a single

resonance line corresponding to this methyl should not appear in two-or higher quantum filtered correlation spectroscopy. However, contrary to this prediction, MQ peaks do arise in similar degenerate spin systems^(11,14) due to multiexponential (or cross-relaxation between pairs of spins) 'transverse relaxation. Although the appearance of such forbidden cross-peaks can lead to wrong resonance assignments in 2D NMR, these peaks can nevertheless give useful motional as well as structural parameters for a macromolecule⁽³⁾. A brief summary of equations derived for A_3 spin system for zero- and double quantum filtered 1D analogue of 2D NMR experiments by Kay and Prestegard⁽³⁾ and Wong et al.⁽⁴⁾ is given below, since we have used their derivations as such for our work on deoxycholate reverse micelles.

The energy level diagram and basis functions for an A_3 spin systems, typified by the methyl ($-\text{CH}_3$) group, are given in Fig. IV. 2. The pulse sequence⁽³⁾, and the schemes used for transmitter and receiver phase cycling^(3,4) in order to observe the zero- and double quantum filtered forbidden peaks selectively, are given in Fig. IV.3 and Tables IV.1 and 2, respectively.

The first two $\pi/2$ pulses in the sequence (Fig. IV.3) generate different orders of multiple quantum coherence, and the π pulse refocuses the precessional loss due to chemical shift offset during the period 2τ . Therefore, only transverse relaxation effects are present at the end of 2τ in the case of unresolved scalar coupled spin systems. It is also assumed that the relaxation effects originate from proton dipolar interaction only⁽¹⁵⁾. The spin-lattice interaction Hamiltonian of this system is written as

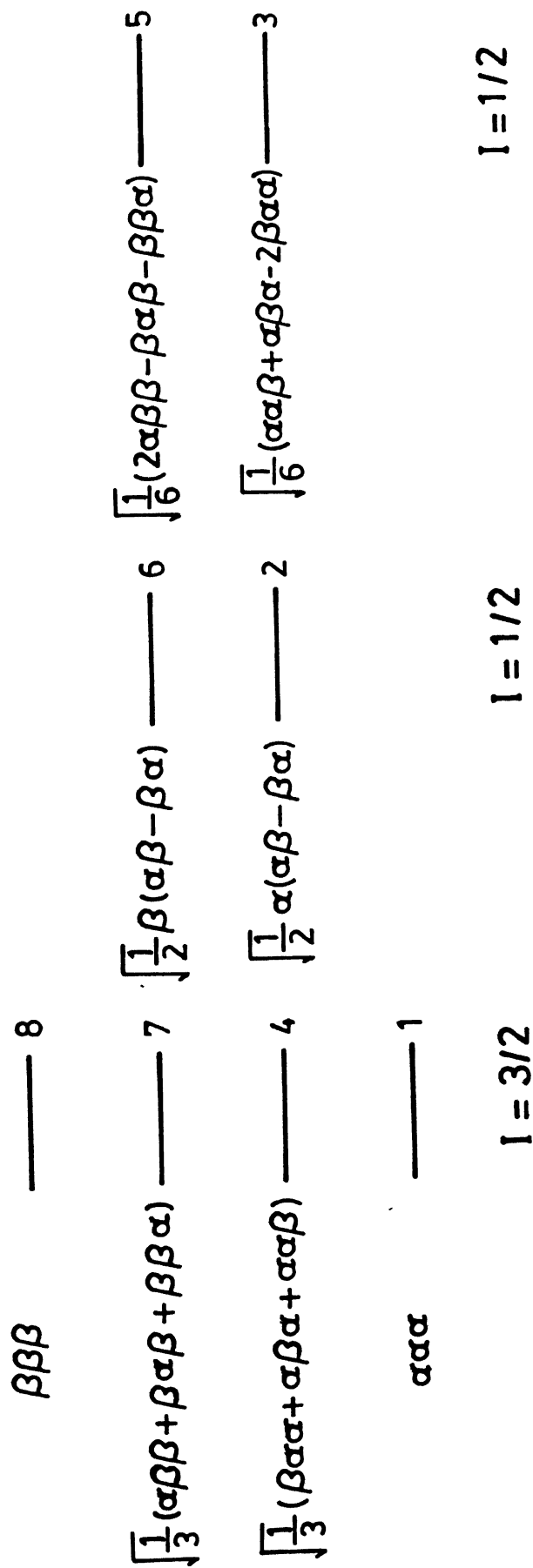


Fig.IV.2 Energy Level diagram and basis functions for an A_3 spin system in an irreducible basis representation.

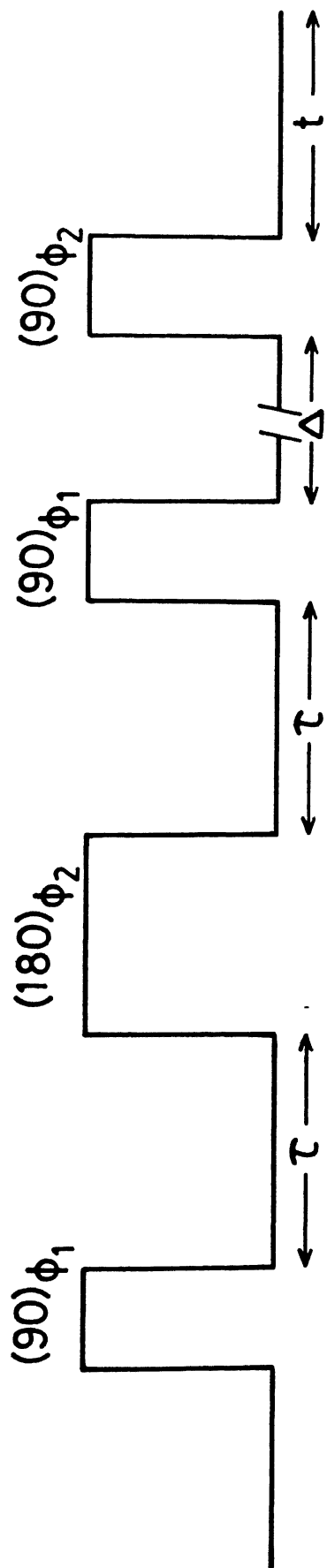


Fig.IV.3 Pulse sequence used for selective observation of zero- and double quantum filtered spectra.

Table IV.1

Phase cycling scheme used in the selection of zero quantum filtered spectra (adapted from ref. (4)).

ϕ_1^a	ϕ_2^b	receiver phase	ϕ_1^a	ϕ_2^b	receiver phase
x	x	x	-x	-x	-x
y	x	x	-y	-x	-x
-x	x	x	x	-x	-x
-y	x	x	y	-x	-x
y	y	y	-y	-y	-y
-x	y	y	x	-y	-y
-y	y	y	y	-y	-y
x	y	y	-x	-y	-y

Table IV.2

Phase cycling scheme used in the selection of double quantum filtered spectra (adapted from ref. (3)).

ϕ_1^a	ϕ_2^b	receiver phase	ϕ_1^a	ϕ_2^b	receiver phase
x	x	x	x	-x	-x
y	x	-x	y	-x	x
-x	x	x	-x	-x	-x
-y	x	-x	-y	-x	x
x	y	-y	x	-y	y
y	y	y	y	-y	-y
-x	y	-y	-x	-y	y
-y	y	y	-y	-y	-y

^a phase of excitation pulses. ^b phase of observation pulses.

$$\mathcal{H}(t) = \sum_{i < j} \epsilon_{ij} \sum_m (-1)^m T_2^m(i, j) Y_2^{-m}(\phi_{ij}) + \sum_i \gamma_i \sum_m (-1)^m T_1^m(i) B_1^{-m}(i, t) \quad [\text{IV.1}]$$

In the above equation,

$$\epsilon_{ij} = \left[(6\pi)^{1/2} / 5 \right] \gamma_i \gamma_j \hbar / r_{ij}^3,$$

$T_2^m(i, j)$ = the dipolar spin tensor operator of rank 2 connecting spins i and j .

$Y_2^{-m}(\phi_{ij})$ = the spherical harmonic of rank 2 whose value depends on the orientation of the i - j dipolar vector relative to the external field,

T_1^m = spin tensor of rank 1,

γ_i = magnetogyric ratio of the methyl proton i ,

r_{ij} = distance between protons i and j in the methyl group, and

$B_1^{-m}(i, t)$ = the lattice random field interaction operator.

The first term in eqn. [IV.1] is due to the intramolecular dipolar interactions among the three protons of the methyl group and the second term takes into account all other interactions. The second term is approximated to be isotropic⁽⁷⁾, i.e.,

$$|B_1^0(i, t)|^2 = |B_1^{+1}(i, t)|^2 = |B_1^{-1}(i, t)|^2.$$

The relaxation processes for the methyl group are described, by using Redfield theory^(7,15), in terms of evolution of the density matrix (ρ) according to the equation of motion given below :

$$\frac{d\rho}{dt} = R\rho \quad [\text{IV.2}]$$

where R is the Redfield relaxation matrix and

$$\rho = \begin{bmatrix} \rho_{14} \\ \rho_{26} \\ \rho_{35} \\ \rho_{47} \\ \rho_{78} \end{bmatrix} \quad [\text{IV.3}]$$

The subscripted numbers represent the spin energy levels shown in Fig. IV.1. The dipolar part of the relaxation matrix is given by⁽⁷⁾

$$\begin{aligned} R_{\alpha\nu\epsilon}^{ijkl} &= \sum_{m,n} \left\{ 2J_{ijkl}^{mn}(\omega_{\alpha\nu}) \langle \alpha | T_2^m(i,j) | \nu \rangle \right. \\ &\quad \langle \epsilon | T_2^n(k,l) | \sigma \rangle - \delta_{\alpha\nu} \sum_{\beta} J_{ijkl}^{mn}(\omega_{\epsilon\beta}) \langle \epsilon | T_2^m(i,j) | \beta \rangle \\ &\quad \langle \beta | T_2^n(k,l) | \sigma \rangle - \delta_{\sigma\epsilon} \sum_{\beta} J_{ijkl}^{mn}(\omega_{\nu\beta}) \langle \alpha | T_2^m(i,j) | \beta \rangle \\ &\quad \left. \langle \beta | T_2^n(k,l) | \nu \rangle \right\} \quad (\text{IV.4}) \end{aligned}$$

where $J_{ijkl}^{mn}(\omega)$ is a typical spectral density function defined by

$$J_{ijkl}^{mn}(\omega) = \epsilon_{ij} \epsilon_{kl} \int_0^{\infty} \langle Y_2^m(\phi_{ij}(t)) Y_2^n(\phi_{kl}(t+\tau)) \rangle \cos \omega \tau d\tau \quad (\text{IV.5})$$

The spectral density functions given above are calculated under two situations, namely, spin being (i) autocorrelated and (ii) cross correlated. These terms have been explained already in section IV.2. A complete listing of all the elements of R in terms of auto- and cross-spectral densities can be found in ref. (3). The spectral density function corresponding to the second term of eqn. [IV.1] is given by⁽⁴⁾

$$j(n\omega) = (-1)^n \gamma^2 \delta_{ij} \int_0^{\infty} \langle B_1^{+n}(i,0) B_1^{-n}(j,t) \rangle \cos(n\omega t) dt. \quad [\text{IV.6}]$$

For the specific case of a methyl group in a macromolecule, the above spectral densities are evaluated by using an appropriately modified "cone model" of Brainard and Szabo⁽¹⁶⁾. Fig. IV.4 thus describes the dynamics of the methyl groups in a spherical micelle. Using the motional parameters defined in Fig. IV.4, eqn. [IV.5] is written as

$$J_{ijkl}^{mn}(\omega) = \delta_{m-n} \frac{(-1)^n 3\gamma^4 \hbar^2}{10r^6} \left\{ \frac{1}{4} S^2 \frac{6D}{(6D)^2 + \omega^2} + \right. \\ \frac{1}{4} \frac{(1-S^2) [6D + 6D_w / (1-S^2)]}{[6D + 6D_w / (1-S^2)]^2 + \omega^2} + \\ \frac{3}{4} \cos(\Omega_{ijkl}) \frac{S^2 (6D + 4D_i)}{(6D + 4D_i)^2 + \omega^2} + \\ \left. \frac{3}{4} \cos(\Omega_{ijkl}) \frac{(1-S^2) [6D + 4D_i + 2D_w / (1-S^2)]}{[6D + 4D + 2D / (1-S^2)]^2 + \omega^2} \right\} \quad [\text{IV.7}]$$

In our model (depicted in Fig. IV.4), the overall reorientational motion of the micelle is characterized by a correlation time $\tau_0 \equiv \frac{1}{6D}$, the internal rotation of the methyl group about its C_∞ axis

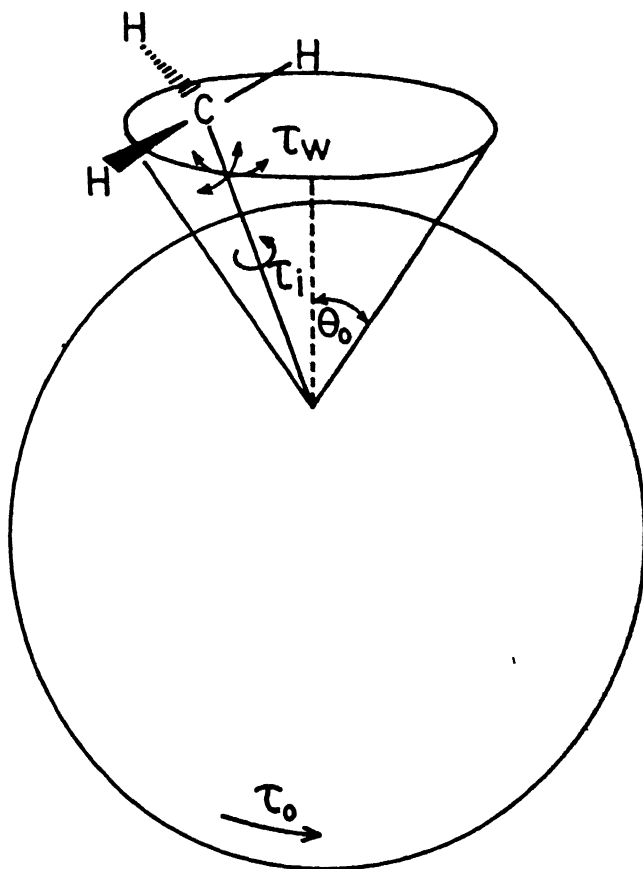


Fig.IV.4

Cone model describing the motion of a methyl group in a spherical micelle (adapted from ref.(3)).

has a correlation time $\tau_i \equiv \frac{1}{4D_i}$, and the correlation time corresponding to the wobbling motion of the methyl C_3 axis is $\tau_w \equiv \frac{1}{6D_w}$. The C_3 or C_∞ axis of methyl group is assumed to be wobbling within a cone of angle θ with a frequency of $6D_w$ and an order parameter of S . S is related to θ as⁽¹⁶⁾

$$S_{\text{cone}} = \left(\frac{1}{2}\right) \cos\theta (1+\cos\theta) . \quad [\text{IV.8}]$$

In equation [IV.7], Ω_{ijkl} is the angle between $i-j$ and $k-l$ $^1\text{H}-^1\text{H}$ vectors. The value of this angle for auto-correlated relaxation process is $\Omega_{ijkl} = 0$, with $ij = kl$ whereas it will be $\Omega_{ijkl} = 60^\circ$, for cross-correlated relaxation $ij \neq kl$, as the three protons of a methyl group occupy the vertices of an equilateral triangle.

Using standard techniques of matrix algebra⁽⁷⁾, one can solve eqn. [IV.2] to get the relevant density matrix elements for the zero-and double quantum coherences after the second $(90)_Y$ pulse. These elements are

(i) for zero-quantum coherence :

$$\left. \begin{aligned} \rho_{11}(2\tau^+) &= \frac{-\sqrt{3}}{4} \left[\rho_{14}(2\tau^-) + \sqrt{3} \rho_{47}(2\tau^-) + \rho_{78}(2\tau^-) \right] \\ \rho_{11}(2\tau^+) &= -\rho_{88}(2\tau^+) \\ \rho_{44}(2\tau^+) &= -\frac{1}{4} \left[\sqrt{3}\rho_{14}(2\tau^-) - \rho_{47}(2\tau^-) + \sqrt{3} \rho_{78}(2\tau^-) \right] \\ \rho_{44}(2\tau^+) &= -\rho_{77}(2\tau^+) \end{aligned} \right\} [\text{IV.9}]$$

(ii) for double-quantum coherence :

$$\left. \begin{aligned} \rho_{17}(2\tau^+) &= -\frac{1}{4} \left[\rho_{14}(2\tau^-) - \sqrt{3} \rho_{47}(2\tau^-) + \rho_{78}(2\tau^-) \right] \\ \rho_{48}(2\tau^+) &= \frac{1}{4} \left[\rho_{14}(2\tau^-) - \sqrt{3} \rho_{47}(2\tau^-) + \rho_{78}(2\tau^-) \right] \end{aligned} \right\} \text{ [IV.10]}$$

In the above equations [IV.9] and [IV.10], and in the following ones, the + and - superscript signs represent the density matrix just after and before, respectively. The multiple quantum coherences due to nonuniform relaxation of the transverse elements ρ_{14} , ρ_{47} , and ρ_{78} of A_3 spin system, created by the second $\pi/2$ pulse, evolve during the time Δ . These nonobservable coherences are converted into detectable single-quantum coherence by applying the last $(\pi/2)$ pulse. The zero- and double-quantum coherences are selectively observed⁽¹⁷⁾ by employing the respective phase-cycling schemes given in Tables IV.1 and IV.2. The elements (ρ_{14} , ρ_{47} , and ρ_{78}) of the density matrix for zero-quantum selective excitation are :

$$\left. \begin{aligned} \rho_{14}(2\tau+\Delta^+) &= \frac{\sqrt{3}}{8} \left[\rho_{11}(2\tau+\Delta^-) + \rho_{44}(2\tau+\Delta^-) + \rho_{77}(2\tau+\Delta^-) \right. \\ &\quad \left. + \rho_{88}(2\tau+\Delta^-) \right] \\ \rho_{47}(2\tau+\Delta^+) &= \frac{1}{8} \left[3\rho_{11}(2\tau+\Delta^-) - \rho_{44}(2\tau+\Delta^-) + \rho_{11}(2\tau+\Delta^-) \right. \\ &\quad \left. - 3\rho_{44}(2\tau+\Delta^-) \right] \\ \rho_{78}(2\tau+\Delta^+) &= \frac{\sqrt{3}}{8} \left[\rho_{11}(2\tau+\Delta^-) + \rho_{44}(2\tau+\Delta^-) + \rho_{77}(2\tau+\Delta^-) \right. \\ &\quad \left. + \rho_{88}(2\tau+\Delta^-) \right] \end{aligned} \right\} \text{ [IV.11]}$$

The corresponding elements for double-quantum selective excitation are

$$\left. \begin{aligned} \rho_{14}(2\tau+\Delta^+) &= \frac{1}{8} \left[-\rho_{17}(2\tau+\Delta^-) - 3\rho_{48}(2\tau+\Delta^-) + 3\rho_{71}(2\tau+\Delta^-) \right. \\ &\quad \left. + \rho_{84}(2\tau+\Delta^-) \right] \\ \rho_{47}(2\tau+\Delta^+) &= \frac{\sqrt{3}}{8} \left[-\rho_{17}(2\tau+\Delta^-) + \rho_{48}(2\tau+\Delta^-) - \rho_{71}(2\tau+\Delta^-) \right. \\ &\quad \left. + \rho_{84}(2\tau+\Delta^-) \right] \\ \rho_{78}(2\tau+\Delta^+) &= \frac{1}{8} \left[3\rho_{17}(2\tau+\Delta^-) + \rho_{48}(2\tau+\Delta^-) - \rho_{71}(2\tau+\Delta^-) \right. \\ &\quad \left. - 3\rho_{84}(2\tau+\Delta^-) \right] \end{aligned} \right\} \text{ [IV.12]}$$

The observed magnetization M_x or "signal" during the period $t > 2\tau + \Delta$ is given by

$$\begin{aligned} M_x &= \gamma \hbar \text{Tr}(\rho I_x) \\ &\propto (\sqrt{3} \rho_{14} + 2\rho_{47} + \sqrt{3} \rho_{78} + \sqrt{3} \rho_{14}^* + 2\rho_{47}^* + \sqrt{3} \rho_{78}^*) \end{aligned} \quad \text{[IV.13]}$$

Kay and Prestegard⁽³⁾ and Wong et al.⁽⁴⁾ have shown that, in essence, one can calculate theoretically the MQ filtered forbidden peak intensity profile as a function of MQ evolution time by using eqns. IV.11 or IV.12 and IV.13. They have also demonstrated that these profiles can be matched with those of the experimental data, whereby useful motional parameters for the spin system could be derived.

IV.4. The A_9 Spin System (e.g : the $-\overset{+}{N}(CH_3)_3$ head group):
 Derivation of Pure State Basis Functions and
 Demonstration of Difficulties in Mathematical
 Tractability

A system of nine coupled 'like-spin 1/2' nuclei will have a total number of $2^9 = 512$ eigenstates or basis functions. A convenient spin basis is necessary to formulate these many states for further calculations. The most convenient basis in which to represent these many states is the one adopted by Bersohn and Gutowsky⁽¹⁸⁾, Lalowicz et al.⁽¹⁹⁾ and Raghunathan and Ray⁽²⁰⁾ based on coupling of angular momenta^(21,22), for coupled spin systems. The representation is given in $|IM\rangle$ basis where

$$A = I_1 + I_2$$

$$B = I_3 + I_4$$

$$C = I_5 + I_6$$

$$D = I_7 + I_8$$

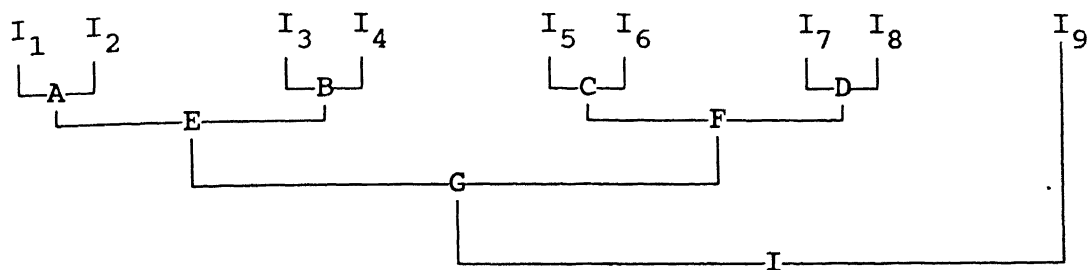
$$E = A + B$$

$$F = C + D$$

$$G = E + F$$

$$I = G + I_9$$

and M is the z -component of I , the total angular momentum quantum number, projected along the direction of B_0 such that $-I < M < +I$. The abovementioned coupling pattern is given below in a simpler form :



The complete basis set for representing the A_9 case will therefore become $|ABCDEFGIM\rangle$. Under the operation of the Zeeman Hamiltonian, these 512 pure states can be arranged according to their energy. The energy levels, and degeneracy (no. of states), are given in Fig. IV.5.

While considering these many pure states, and giving a true representation to each state by taking a linear combination among these and going further to give a matrix representation for the whole system for calculating its evolution under an rf excitation, one soon realises that the problem is not easily tractable mathematically. Further theoretical work on the A_9 system was therefore abandoned, and an easier micellar model was pursued instead, choosing the well-studied sodium deoxycholate as the surfactant. The structure of the deoxycholate anion is given in Fig. IV.6. We recall here that sodium deoxycholate is the well-known 'bile-salt' which is useful for forming large and well-defined micellar structure models.

IV.5 Studies on the Deoxycholate (DOC) Reverse Micelles

IV.5.1 Experimental Details

The reverse micellar system chosen for our study is sodium deoxycholate/benzyl alcohol/ H_2O , as similar types of soap/alcohol/water systems form reverse micellar solutions^(23,24).

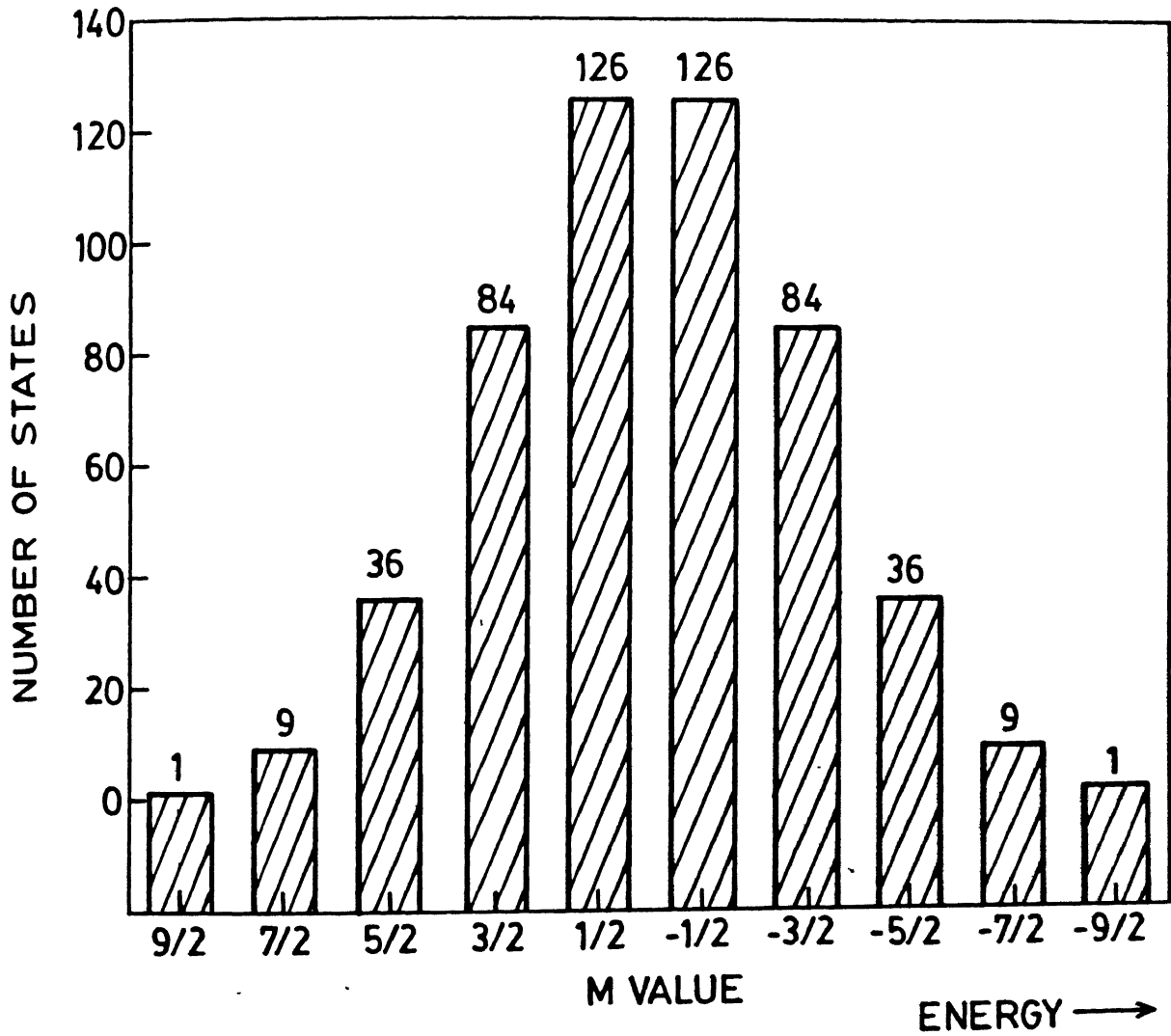


Fig.IV.5 Degeneracy present at each M value of the A_9 spin system, under Zeeman Hamiltonian only.

sodium deoxycholate used was procured from S.D. Fine-chem, India, and was further purified by dissolving it in ethanol/acetone mixture and recrystallizing the salt after filtering the hot solution through a charcoal bed. Benzyl alcohol (Fisher) was distilled once before use, and the water used was double-distilled and deionised.

Proton zero-and double-quantum filtered 1D analog's of the 2D experiment were done at 297 K on a Bruker WM400 FT NMR spectrometer operating at the proton frequency of 400 MHz. The pulse sequence and phase cycling schemes used are given in Fig. IV.3 and Tables IV.1 and IV.2, respectively. The 90° pulse width corresponding to protons in this spectrometer was $16 \mu\text{s}$. All spectra were recorded with the following conditions : 192 scans, sweep width of 3496 Hz, relaxation delay of $5T_1$ and 8 K data points. All spectra were zero-filled to 16 K before Fourier transforming, and recorded in magnitude corrected mode, $\sqrt{\text{Re}(\omega)^2 + \text{Im}(\omega)^2}$, where $\text{Re}(\omega)$ and $\text{Im}(\omega)$ are data from real and imaginary channels, respectively. The data were not apodized. The multiple quantum evolution time (Δ) used was $5 \mu\text{s}$.

IV.5.2 Results and Discussion

In the structure of DOC (Fig. IV.6(a)), there are three methyl groups, labelled as 18, 19, and 21. The proton 1D NMR spectrum of our DOC reverse micelles is given in Fig. IV.6(b). The peak selected for multiple quantum NMR study is that of methyl group-18, as it is well-resolved and can be considered as an isolated A_3 spin system⁽³⁾. Theoretical data were generated by using a program developed by Hwang (Dept. of Chemistry, National

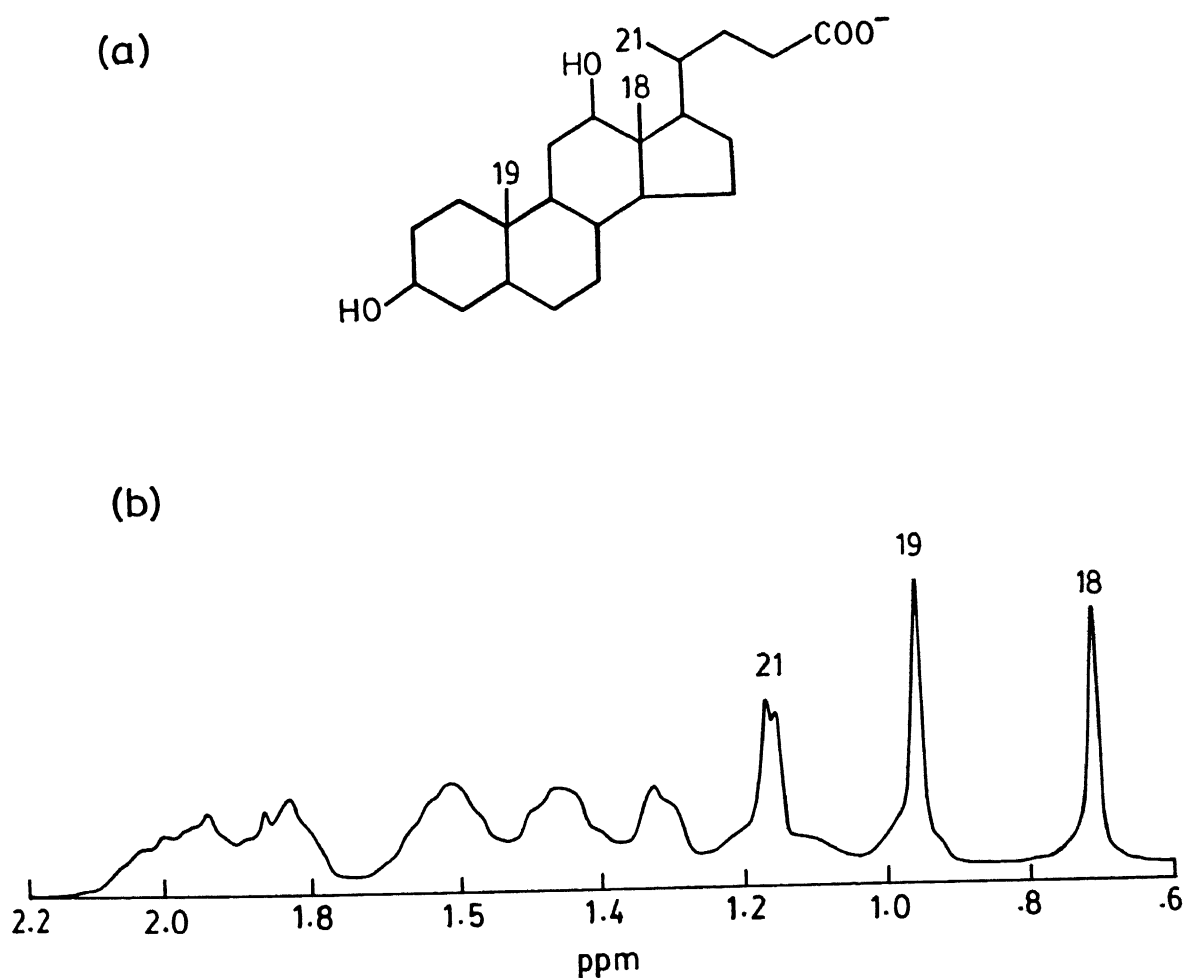


Fig.IV.6 (a) Structure of the Deoxycholate(DOC) anion
 (b) 400 MHz proton NMR spectrum of DOC reverse micelles at $R = 2.88$. Numbers over the peaks correspond to the numbering of methyl groups given in (a).

Taiwan University, and Institute of Atomic and Molecular Science, Academia Sinica, Taipei, Taiwan, Republic of China).

We note that our model for the reverse micelle is simply the reverse of the one given by Kay and Prestegard⁽³⁾ (for the micelle), and is illustrated in Fig. IV.7. The symbols used in this figure are defined in a manner similar to the ones given for Fig. IV.4. The input data used for getting double-quantum filtered forbidden peak intensity profile theoretically for $R = 2.88$ and $R = 11.52$ are given in Table IV.3. The theoretically calculated as well as experimentally determined DQ-profiles corresponding to both R values are given in Figs. IV.8 and IV.9.

Table IV.3 Input parameters used for theoretical DQ profile generation

R	S	$\tau_o(10^{-9}s)$	$\tau_i(10^{-12}s)$	$\tau_w(10^{-12}s)$	$j(o)$	$j(\omega)$
2.88	0.87	3.1	4.6	46.0	15.4	-0.75
11.52	0.78	3.7	3.9	31.5	8.6	-0.55

Table IV.3 shows that the isotropoic rotational correlation time (τ_o) of the reverse micelle increases as R increases, which indicates that, as expected, the size of the aggregate increases at higher R values thereby showing increase in τ_o . However, τ_w decreases as R increases. This may be due to a less-compact structure at $R = 11.52$ as compared to that at $R = 2.88$ and/or due to an increase in the overall micellar size which generates more space for methyl-18 'wobbling' motion. The order

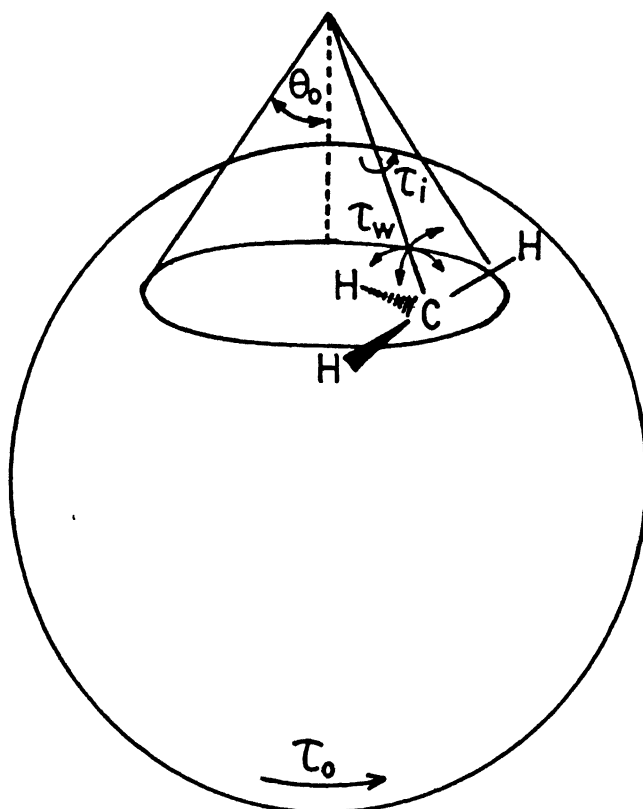


Fig.IV.7

'Inverted cone' model describing motion of methyl group-18 present in DOC molecule in our reverse micelles.

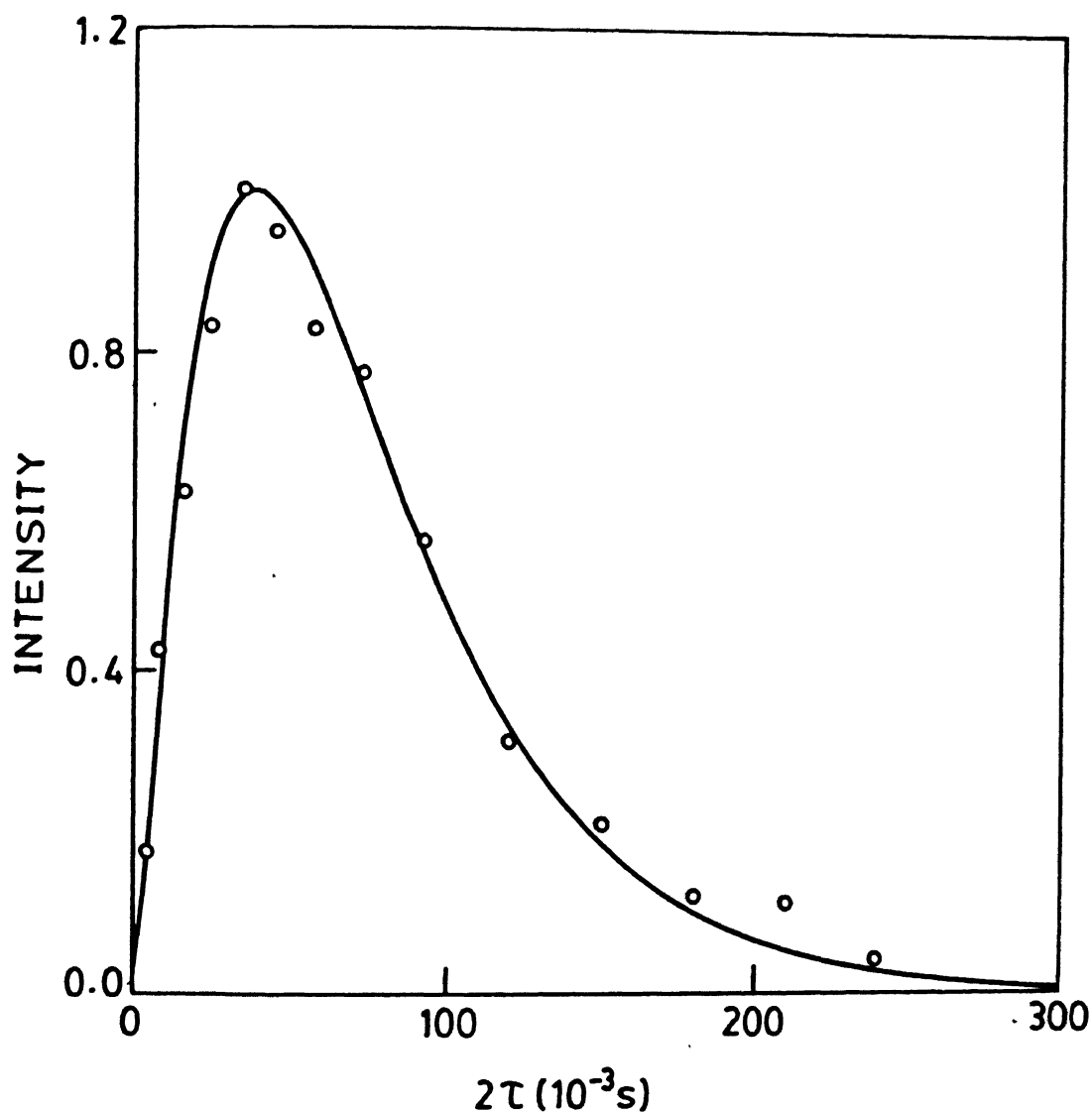


Fig.IV.8

400 MHz proton double quantum peak intensities as a function of evolution time for methyl-18, recorded for the $R = 2.88$ DOC reverse micelles; the solid line represents the profile generated theoretically and o's are experimental points.

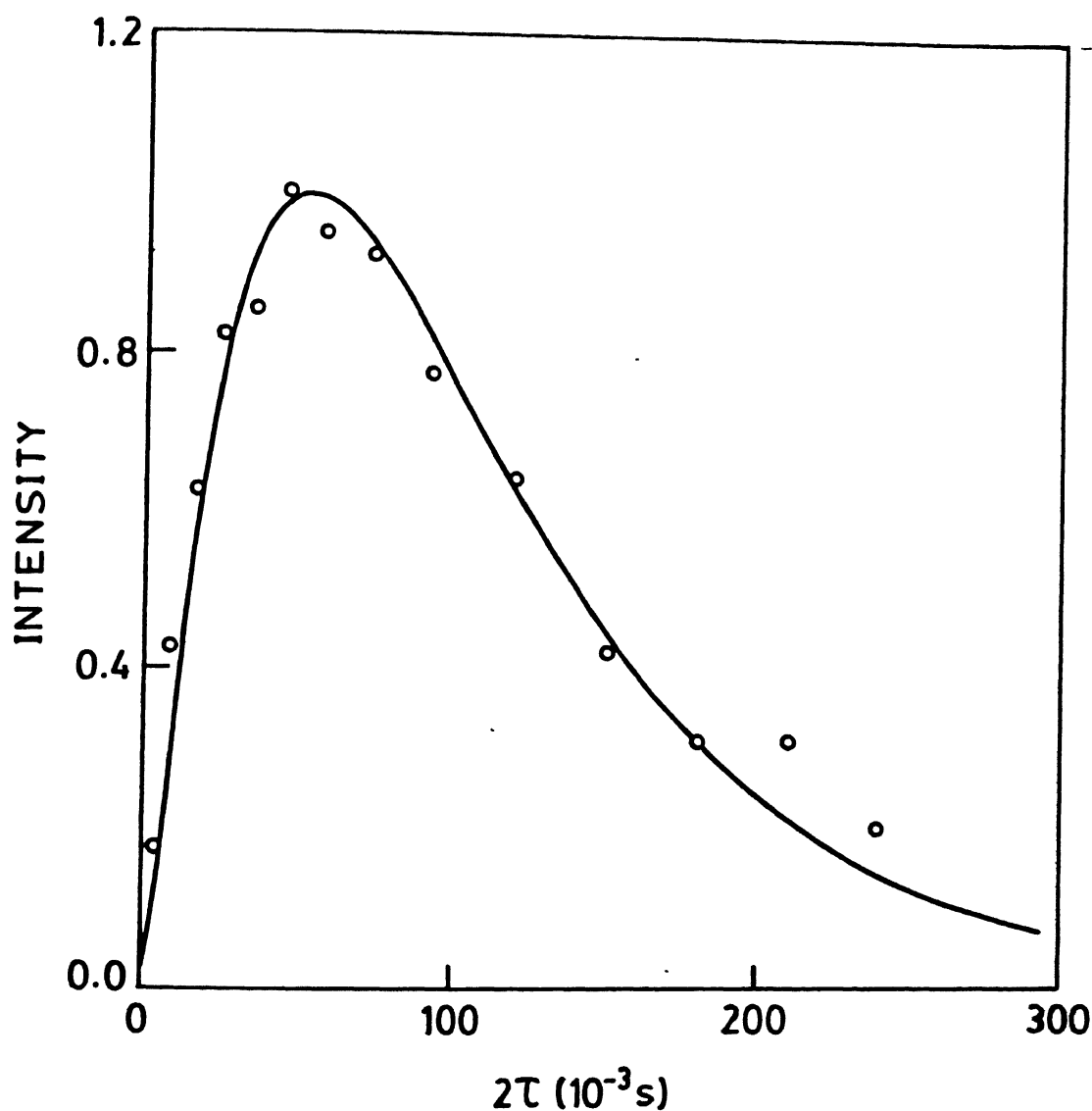


Fig.IV.9

400 MHz proton double quantum peak intensities as a function of evolution time for methyl-18, recorded for the $R = 11.52$ DOC reverse micelles; the solid line represents the profile generated theoretically and o's are experimental points.

parameter (i.e., ordering of methyl group-18) shows a marginal decrease with increase in R values indicating that as aggregate size increases the relative ordering of methyl group-18 is less, and τ_w decreases as well. The theoretical profile generation is very sensitive to the input variables S, τ_o , $j(o)$, and $j(w)$. An almost similar theoretical profile can be obtained by using more than one data set^(3,4), as there are six input variables for its generation. The parameters given in Table IV.3 is one such input variable set. Realistically, these parameters may have to be optimized further either by giving more limiting conditions or from results of other independent (e.g. light scattering, ^{13}C T_1 , nOe at several magnetic fields and using the recently reported differential line broadening(DLB)⁽²⁵⁾ effects in degenerate spin systems) experiments at each R value.

Experimental zero-quantum filtered forbidden peak intensity profiles as a function of the excitation time are given for $R = 2.88$ and $R = 11.52$ in Figs. IV.10 and IV.11, respectively. Unfortunately, the data appear very scattered for $R = 11.52$ system. Due to this, and due to the nonavailability of T_2 data for both R values, we have fitted the experimental zero quantum peak intensities to a simple single exponential function only and we have not undertaken any theoretical intensity profile generation for getting other meaningful information. The solid line (exponential fit-line) in Figs. IV.10 and IV.11 shows clearly the need for multiexponential function fit and also indicates the existence of cross-relaxation among spins.

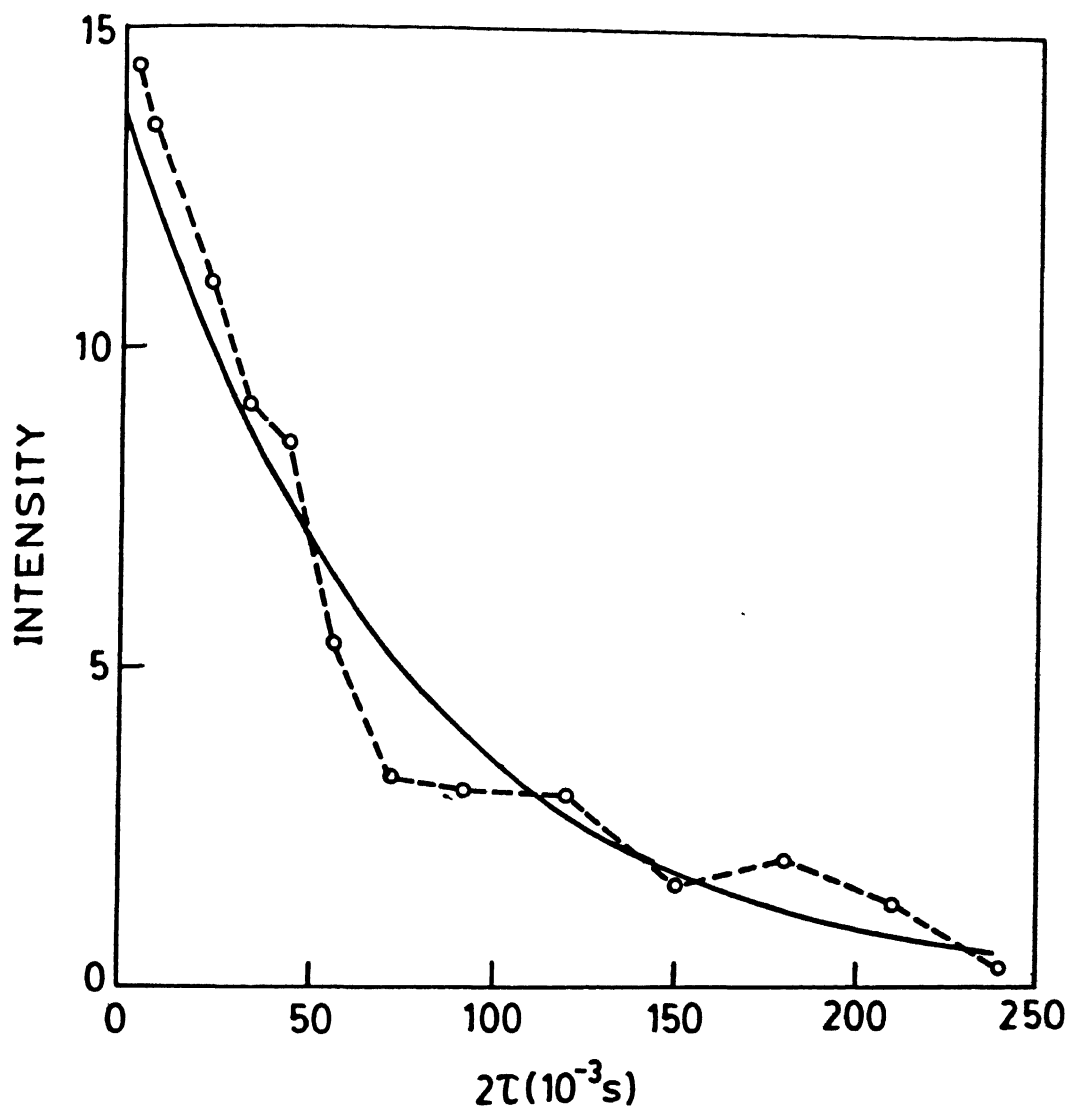


Fig.IV.10 400 MHz proton zero quantum peak intensities as a function of evolution time for methyl-18, recorded for the $R = 2.88$ DOC reverse micelles; the solid line corresponds to the single exponential fit of experimental data (o's).

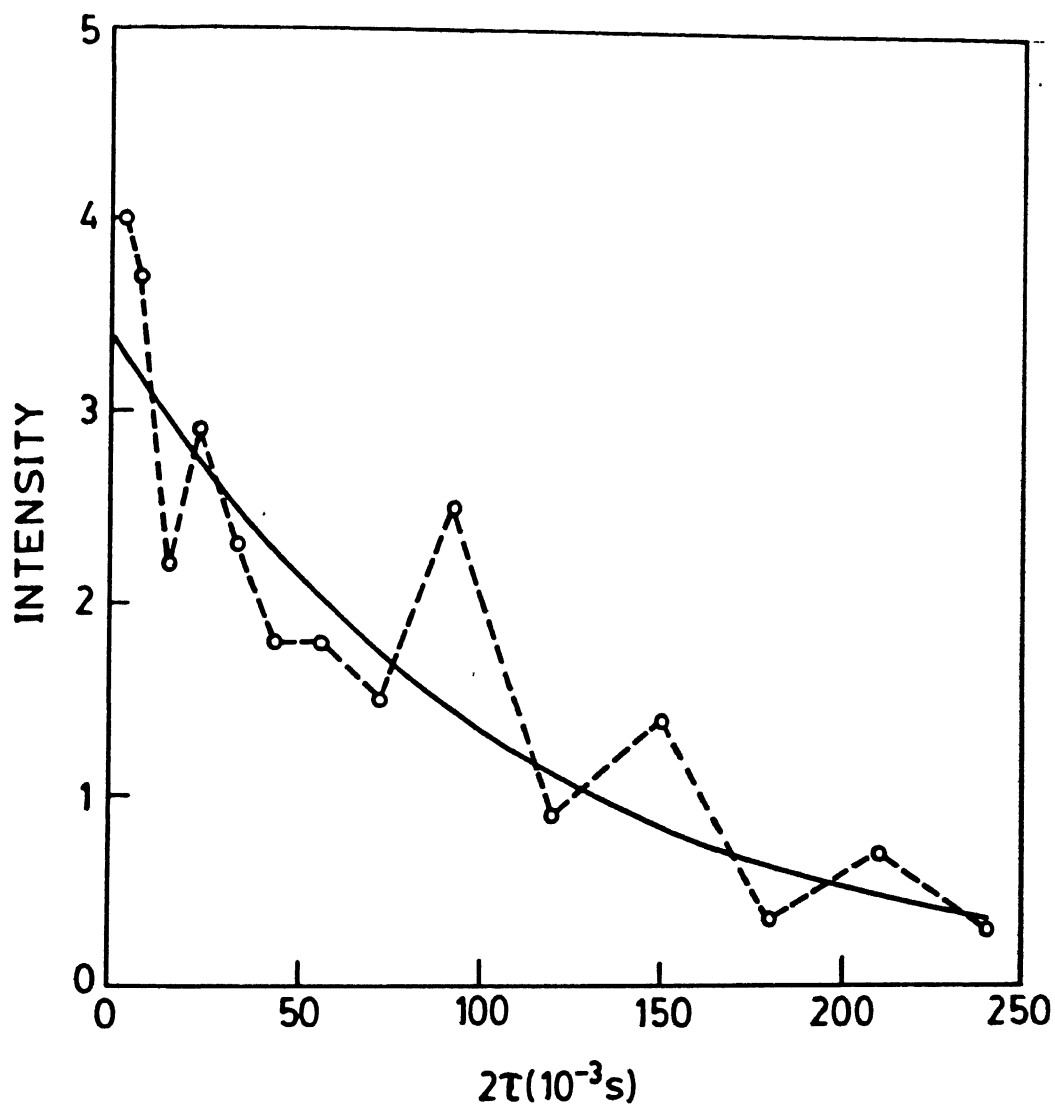


Fig.IV.11

400 MHz proton zero quantum peak intensities as a function of evolution time for methyl-18, recorded for the $R = 11.52$ DOC reverse micelles; the solid line corresponds to the single exponential fit of experimental data (o's).

IV.6 Conclusions

Using recently reported techniques, multiple quantum filtered 1D analog of 2D experiments has been performed on DOC/benzyl alcohol / H_2O reverse micelles. For the DOC reverse micelles, the input data list used to generate a theoretical double quantum peak intensity profile which provides the 'best-fit' to the experimental profile leads us to infer that the size and motional parameters offer good support to a general, intuitive model of spherical-structure expansion as a function of water addition. The nonuniqueness of the input data required to generate a particular profile may be eliminated by using information/data from additional NMR experiments. Although the input data list is in agreement with that of micelles reported earlier, we cannot comment further about it because its uniqueness has not been verified by us. As expected, the zero quantum peak intensities as a function of evolution time does show multiexponential functional form.

We have also shown the mathematical difficulty in treating A_9 spin systems (e.g., $-N(CH_3)_3$). If one overcomes this, an easy access would be available for probing the polar head group of lecithin-based reverse micelles.

To a reasonable extent, we can conclude that meaningful motional and structural parameters can be obtained for a methyl group present on the surfactant molecule and aggregate as a whole by extracting the cross-relaxation effects through proton multiple quantum NMR and analysing them in combination with conventional NMR measurements.

REFERENCES

1. T.A. Holak and J.H. Prestegard, *Biochemistry* **25**, 5766 (1986).
2. H.P. Williamson, T.F. Havel, and K. Wuthrich, *J. Mol. Biol.* **182**, 295 (1985).
3. L.E. Kay and J.H. Prestegard, *J. Am. Chem. Soc.* **109**, 3829 (1987) and references cited therein.
4. T.C. Wong, P.L. Wang, D.M. Duh, and L.P. Hwang, *J. Phys. Chem.* **93**, 1295 (1989).
5. P.L. Wang and L.P. Hwang, *J. Magn. Reson.* **84**, 351 (1989).
6. R.R. Vold and R.L. Vold, *J. Chem. Phys.* **64**, 320 (1976).
7. L.G. Werbelow and D.M. Grant, *Adv. Magn. Reson.* **9**, 189 (1977) and references cited therein.
8. R.L. Vold and R.R. Vold, *Prog. NMR Spectrosc.* **12**, 79 (1978).
9. M.R. Bendall and D.T. Pegg, *J. Magn. Reson.* **53**, 40 (1983).
10. J. Brondeau, D. Canet, C. Millot, H. Nevy, and L. Werbelow, *J. Chem. Phys.* **82**, 2212 (1985).
11. N. Muller, G. Bodenhausen, K. Wuthrich, and R.R. Ernst, *J. Magn. Reson.* **65**, 531 (1985).
12. U. Piantini, O.W. Sorensen, and R.R. Ernst, *J. Am. Chem. Soc.* **104**, 6800 (1982).
13. L. Braunschweiler, G. Bodenhausen and R.R. Ernst, *Mol. Phys.* **48**, 535 (1983).
- 14(a) M. Rance and P.E. Wright, *Chem. Phys. Lett.* **124**, 572 (1986).
 (b) N. Muller, R.R. Ernst and K. Wuthrich, *J. Am. Chem. Soc.* **108**, 6482 (1986).
15. L.G. Werbelow and A.G. Marshall, *J. Magn. Reson.* **11**, 299 (1973).
16. J.R. Brainard and A. Szabo, *Biochemistry* **20**, 4618 (1981).
17. A. Wokaun and R.R. Ernst, *Chem. Phys. Lett.* **52**, 407 (1977).
18. R. Bersohn and H.S. Gutowsky, *J. Chem. Phys.* **22**, 651 (1954).
19. Z.T. Lalowicz, C.A. McDowell, and P. Raghunathan, *J. Chem. Phys.* **70**, 4819 (1979).

20. P. Raghunathan and S.S. Ray, Proc. Indian Acad. Sci. (Chem. Sci.) **102**, 769 (1990).
21. M.E. Rose, Elementary Theory of Angular Momentum, John Wiley and Sons, U.S.A. (1957).
22. A.R. Edmonds, Angular Momentum in Quantum Mechanics, Princeton University Press, New Jersey (1957).
23. P. Ekwall, Advances in Liquid Crystals, G.H. Brown (ed.), Vol.1, Academic Press, New York (1975), p.1.
24. S. Lindenbaum and M., Vadhere, in Reverse Micelles : Biological and Technological Relevance of Amphiphilic Structures in Apolar Media, P.L. Luisi and B.E. Straub (eds.), Plenum Press, New York (1984), p. 239.
25. L.P.Hwang, P.L.Wang, and T.C.Wong, J.Phys.Chem. **92**, 4753 (1988); T.C.Farrar, B.R.Adams, G.C.Grey, R.A.Quinter Arcaya, and Q.Zuo, J.Am.Chem.Soc. **108**, 8190 (1986); T.C.Farrar and R.A.Quinter Arcaya, J.Phys.Chem. **91**, 3224 (1987) and references cited therein.

CHAPTER V

CONSTRUCTION OF A VERSATILE MAGNETIC FIELD GRADIENT CONTROLLER AND
STUDY OF SELF-DIFFUSION OF MICELLAR WATER

V.1 Introduction

A magnetic field gradient may be described, in general, by a second rank tensor $\mathcal{G}^{(1)}$. It is written in Cartesian coordinates as a dyadic⁽²⁾,

$$\mathcal{G} = \begin{bmatrix} ii \frac{\partial B_x}{\partial x} & ij \frac{\partial B_x}{\partial y} & ik \frac{\partial B_x}{\partial z} \\ ji \frac{\partial B_y}{\partial x} & jj \frac{\partial B_y}{\partial y} & jk \frac{\partial B_y}{\partial z} \\ ki \frac{\partial B_z}{\partial x} & kj \frac{\partial B_z}{\partial y} & kk \frac{\partial B_z}{\partial z} \end{bmatrix} \quad [V.1]$$

However, for a small gradient imposed on a high static magnetic field (B_0), i.e., $B_0 \gg |\Delta B|$, where B_0 defines the z-axis of the system, the components ΔB_x and ΔB_y can be discarded. The field gradient is then equivalent to retaining only the last row of \mathcal{G} in eqn. [V.1], whereby the vector G results, with components

$$G_x = \frac{\partial B_z}{\partial x} \quad [V.2a]$$

$$G_y = \frac{\partial B_z}{\partial y} \quad [V.2b]$$

$$G_z = \frac{\partial B_z}{\partial z} \quad [V.2c]$$

As shown in Fig. V.1, three types of magnetic field gradient have been employed in NMR, namely,

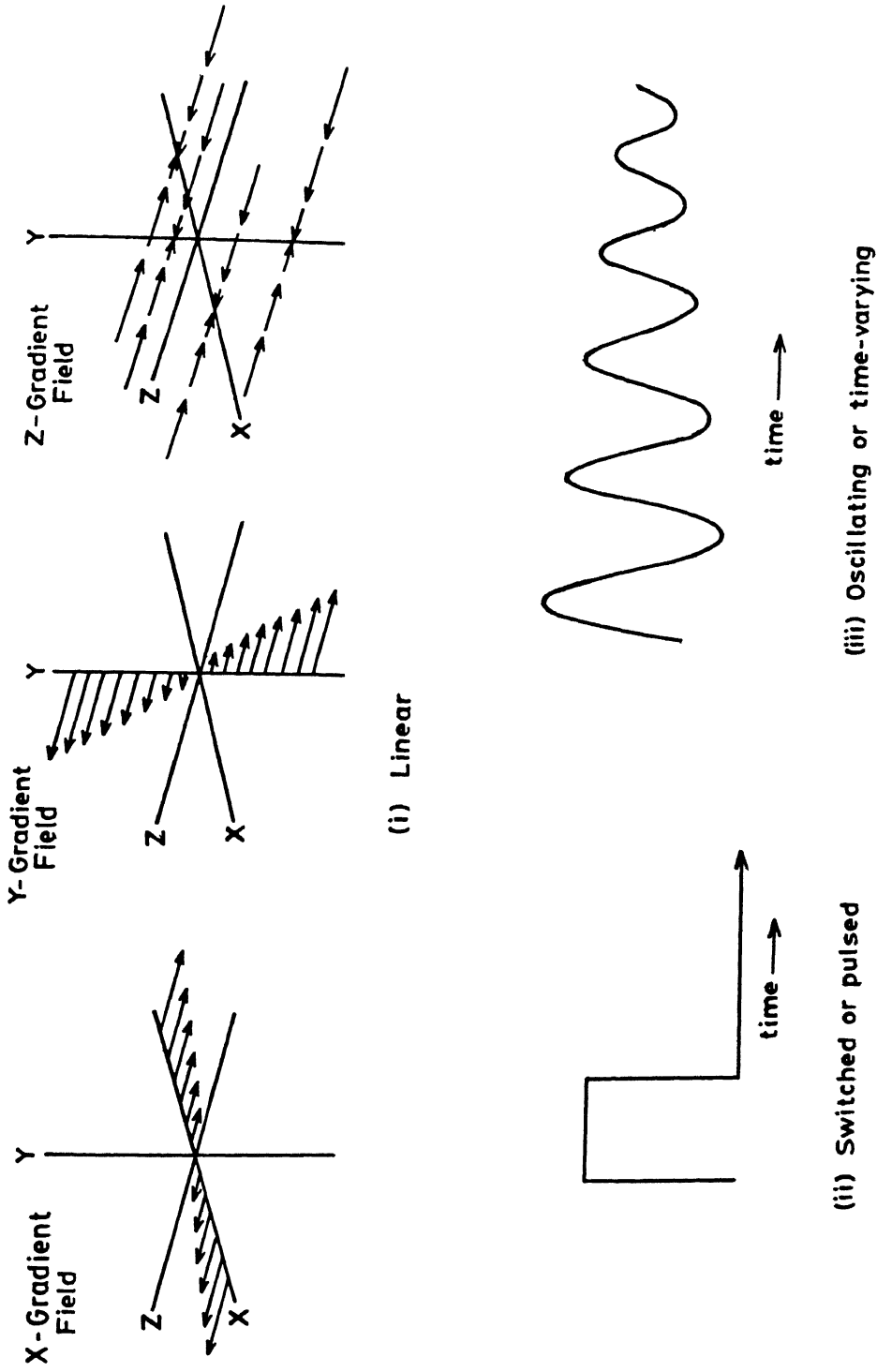


Fig.V.1 Types of magnetic field gradient.

- (i) linear,
- (ii) switched or pulsed linear,
- (iii) oscillating or time-varying.

The choice of a particular type of gradient is often dictated by the type of NMR parameter to be measured. For example, diffusion and flow measurements would require one of the first two types of gradient, whereas NMR 'imaging' variously employs all three types.

In the next (second) section of this chapter, we review the methods available in the literature for generating the three types of gradients. In section three, detailed discussion is made of a particular circuit design for generating all the three types of gradients, including our own modifications for constructing a versatile magnetic field gradient controller. Performance test results of this novel circuit, and measurement of self-diffusion coefficient of H_2O in Lecithin-based reverse micelles, are given in the subsequent two sections. The last section incorporates the overall conclusions of this chapter.

V.2 Types of Magnetic Field Gradient Circuits : A Survey

A literature survey of how magnetic field gradients have been generated and used in NMR applications is given in the following three subsections.

V.2.1 Linear Magnetic Field Gradients :

The idea of using linear^{*} magnetic field gradients in NMR is almost as old as NMR itself⁽³⁻⁶⁾. The early workers⁽³⁻⁵⁾

*It would perhaps be more correct to say 'gradients constant in space'

realized that gradients or inhomogeneities in B_0 were often the limitation in obtaining narrow NMR absorption lines in liquids.

A linear gradient is employed in self diffusion coefficient measurements and more recently, in the important area of NMR imaging. Since linear magnetic field gradient along any direction can be easily generated with a pair of current-carrying coils, numerous methods are available in the literature. As a brief sampling, a number of methods published within the last decade⁽⁷⁻¹¹⁾ may be cited.

V.2.2 Switched or Pulsed Linear Magnetic Field Gradients

The homogeneous (uniform) magnetic field pulsing techniques were pioneered by Kapitza⁽¹²⁾, who produced a 50 T field by a battery discharge through a small low resistance coil. Since Kapitza's work, a number of workers have achieved pulsed high and very high magnetic fields⁽¹³⁾.

In 1955, Anderson et al.⁽¹⁴⁾ demonstrated how nuclear spin echoes in the presence of pulsed field gradient may be used for the purpose of information storage. Although they noted the effect of diffusion on their experiment, they did not further develop the idea for the measurement of self-diffusion coefficients. McCall et al.⁽¹⁵⁾ realised the experimental potential of this technique for measuring self-diffusion coefficients, but did not undertake a mathematical analysis or experimental test of the method.

Following McCall et al.⁽¹⁵⁾, Stejskal and Tanner presented the methodology, first experiments with the pulsed gradient and a detailed analysis⁽¹⁶⁾. Tanner's⁽¹⁷⁾ pulsed field

gradient circuit has two principal parts (i) the coils for producing linear magnetic field gradient (ii) transistor switches for gating the current through these coils. The transistor switch consisted of a 2N1480 and a 2N174 connected together in a Darlington (series) mode, with some minor modifications of the circuit elements to improve switching characteristics⁽¹⁶⁾. This transistor switch was later further refined by Tanner himself⁽¹⁷⁾.

Many circuit designs have been published since. Different schemes for producing pulsed linear field gradient have been discussed in detail by Gross et al.⁽¹⁸⁾, Karlicek and Lowe⁽¹⁹⁾, Hrovat et al.⁽²⁰⁾, and Callaghan et al.⁽²¹⁾.

With the advent and rapid progress of NMR imaging, the need for realising fast switched or pulsed linear magnetic field gradient has increased further. In 1975, Kumar et al.⁽²²⁾ have produced pulsed magnetic fields by means of a fast solid state DIP relays for use in NMR Zeugmatography. Hutchison et al.⁽²³⁾ provide perhaps the most detailed design for generating pulsed magnetic fields by using SCR's to charge capacitors which are then discharged into gradient coils. More recent technical advances for generating pulsed linear magnetic field gradient have been published^(7,9,24).

V.2.3 Oscillating or Time-varying Gradients

Oscillating or time-varying gradients are presently used extensively only in NMR imaging. Since the early experiments of NMR imaging using gradient fields for spatial selectivity^(25,26) a wide variety of novel imaging approaches has

been used.

Imaging experiment with oscillating gradients was first proposed by Hinshaw^(27,28), who applied sinusoidally oscillating field in X, Y and Z directions in such a manner that only one point - the sensitive point - of the sample experienced a time - independent field. This sensitive point is the only element whose NMR signal is not modulated by the alternating gradients, and therefore it alone passes through a low-pass filter. This technique is simple and direct, and requires no calculations or computer for producing the image; it did in fact produce the first 3D NMR images⁽²⁹⁾. The mathematical solution of the NMR signal produced by a series of pulses in the presence of time-dependent gradient has also been published⁽³⁰⁾.

Since the oscillating gradient method requires a longer signal acquisition time, it is not competitive with other imaging modalities. In addition, the impulse response or localization function is relatively inflexible, and results in poor localization⁽³¹⁾.

Time-dependent gradients have subsequently been employed by Mansfield⁽³²⁾ and Mansfield and Pykett⁽³³⁾ in their "Echo-Planar Imaging (EPI)" method. Following these workers, a modified EPI method has been proposed by Ljunggren⁽³⁴⁾. In the original experiment, only an alternating gradient with a rectangular waveform was applied, but the use of cosinusoidal gradient waveforms have also been theoretically analysed by Feiner and Locher⁽³⁵⁾ and by Tropper⁽³⁶⁾. Experimental results in the presence of sinusoidal or cosinusoidal time-varying gradients have been given by Frahm and Hänicke⁽³⁷⁾.

Following up on the proposal of Tropper⁽³⁶⁾, Macovski et al.^(31,38) have introduced newer techniques in MRI using time-varying gradients, the basic innovative feature consisting of post processing the FID recorded in the presence of time-varying gradients. It is shown by Macovski et al. that (i) it is possible to achieve very good ("narrow") localization functions for the imaging process and the processed images have a significant insensitivity to inhomogeneity and chemical shift⁽³¹⁾ and (ii) images are possible even in the presence of B_0 inhomogeneities, and one can simultaneously acquire data from more than one dimension⁽³⁹⁾.

Norton⁽⁴⁰⁾ proposed a new imaging scheme employing a time-varying gradient that simultaneously oscillates and rotates. This method offers the potential of great imaging speed, with the advantages of reducing or eliminating switching transistors, reducing the system bandwidth, enhancing frequency selectivity and reducing power dissipation by utilizing resonant circuits. Finally, oscillating gradient methods, compared to methods employing stationary gradients, are found to be inherently less sensitive to field inhomogeneities when $\gamma\Delta B < \omega_m$ where ΔB is the maximum field inhomogeneity and ω_m is the modulation frequency.

Further novel approaches to magnetic resonance imaging using time-varying gradients have been published recently⁽⁴¹⁾.

V.3 Construction of a Versatile Magnetic Field Gradient Controller

In our laboratory, the need for a versatile magnetic field gradient controller arose not only for studying/measuring

the translational self-diffusion coefficient of 'pool water' protons in reverse micelles but also because of our continuing interest in NMR imaging studies of biosystems⁽⁴²⁾.

The first circuit for the generation of linear and oscillating gradients, published in 1979 by Lauterbur et al.⁽⁴³⁾, was based on the principle that linear field gradients corresponded to vectors, and could therefore be generated from their orthogonal components. Their microprocessor based controller was used in two-dimensional reconstruction experiments⁽⁴⁴⁾ and for sensitive point scanning^(27,29). The same idea was later adapted to construct a device for three dimensional imaging purposes⁽⁴⁵⁾.

In 1982, Fitzsimmons⁽⁴⁶⁾ described a simple design for generating an oscillatory gradient and suggested methods for generating linear and pulsed linear magnetic field gradients from the same circuit with a little modification/addition of components.

Based on the work of Fitzsimmons⁽⁴⁶⁾, we have designed and constructed a field gradient controller for generating all the three types of gradients by simply making modifications in order to increase the resolution of the oscillatory gradient. In our circuit, certain complexities of the original design⁽⁴⁶⁾ have been simplified.

The block diagram of the complete gradient control system used in this work is given in Fig. V. 2.

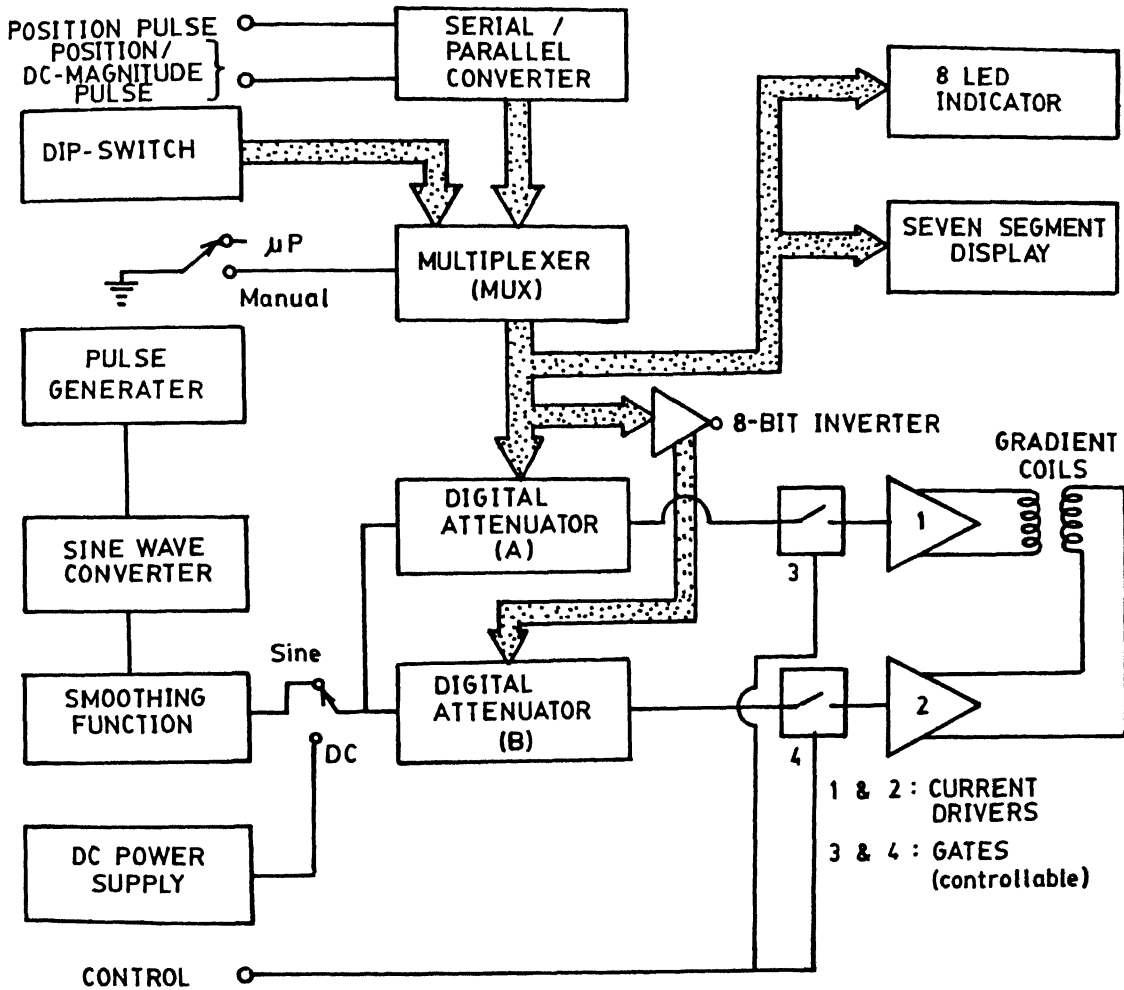


Fig.V.2

Block diagram of the complete gradient control system used in this work.

The hardware may be divided into five subsections :

- (i) digital oscillator and DC reference power supply,
- (ii) computer interface and manual switch for gradient controller,
- (iii) circuit for generating complementary outputs,
- (iv) current driver circuit, and
- (v) display circuit.

The design logic and detailed circuitry for generating all the three types of gradients are described in detail below.

V.3.1 Design Logic

The generation of linear and oscillating field gradients is explained pictorially in Fig. V.3. The different configurations of Fig. V.3 lead to the simple idea that with a pair of field gradient coils, and by controlling the relative amplitude of the direct/alternating current for each coil, one can generate easily the linear/oscillating magnetic field gradient. Following this basic idea, we have designed and constructed a versatile gradient controller. The necessary circuits are described one by one below.

V.3.2 Digital Oscillator and DC Reference

As shown in the previous subsections, the required alternating (sine/cosine) current amplitude waveform for oscillatory gradient is generated by digital oscillator, and DC reference for linear magnetic field gradient is derived from DC power supply.

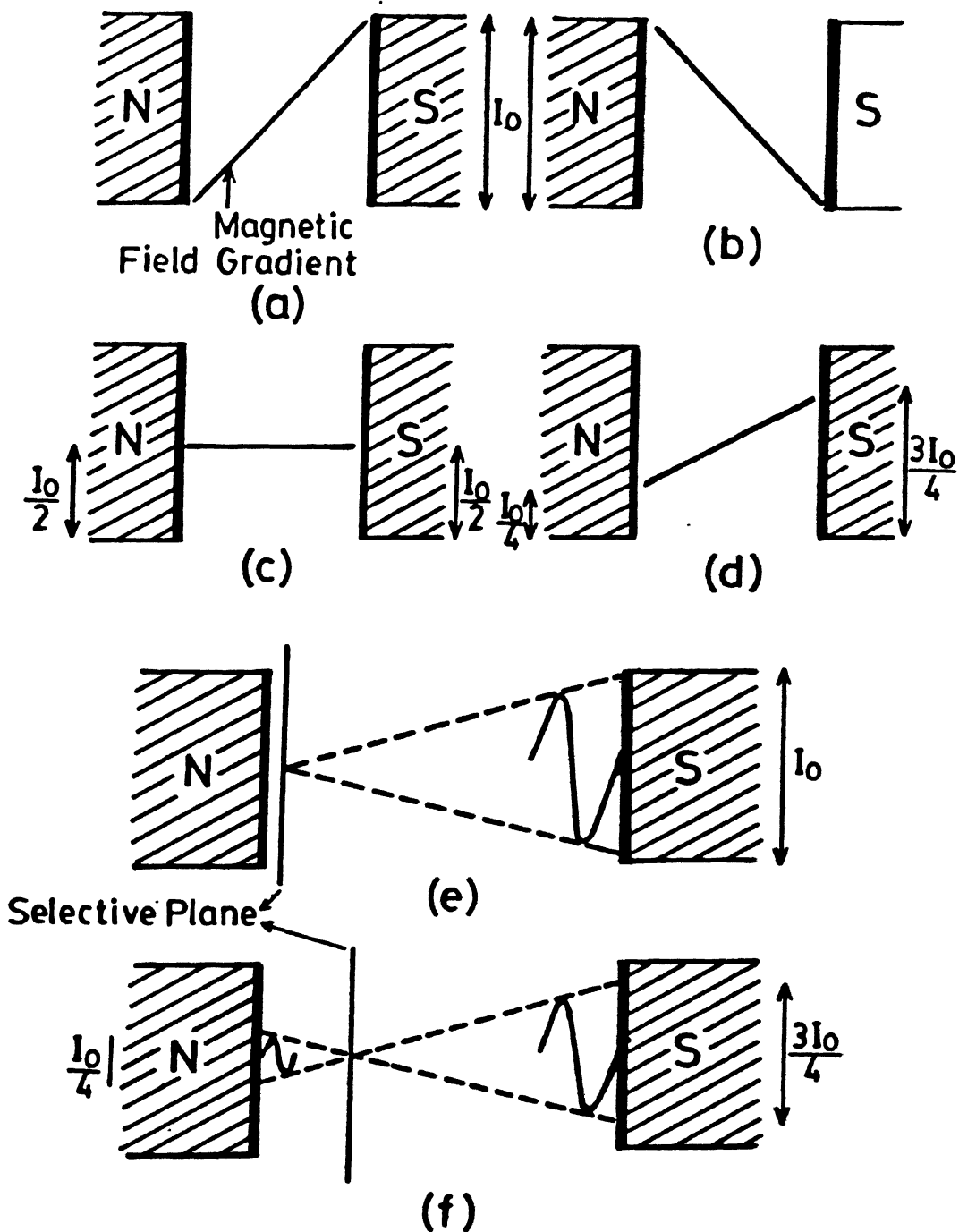


Fig.V.3

Gradient selection using currents of different amplitudes in a pair of coils, (a)-(d) : Different direct current (DC) amplitudes in left and right coils generate linear magnetic field gradients of different magnitude between the coils as shown (e) Alternating current (AC) amplitude I_0 in the right coil and no AC amplitude in the left coil places the 'selective plane' on the extreme left side. (f) AC amplitude $3I_0/4$ in the right, and complementary AC amplitude $I_0/4$ in the left coil places the 'selective plane' one-fourth the total distance from the left coil.

The oscillator consists essentially of a digital square-wave multivibrator, digital serial shift registers with inverter in feedback and a resistive network to approximate the sine and cosine (sine wave phase shifted by $\pi/2$) wave forms. This staircase approximation is smoothed using a voltage controlled voltage source (VCVS) and a low-pass filter to obtain sine/cosine waveforms.

The detailed circuit, along with actual component values and the function of important components, is described below sequentially. As seen from Fig. V.4, a 555 timer chip is used to generate the basic clock waveform. This waveform is, however, rectangular in shape (i.e., duty cycle is not 50%). In order to get a 50% duty cycle waveform (square wave) the rectangular waveform is divided by two using a JK flip-flop (7476). The square wave thus obtained has half the oscillating frequency of the 555 timer. This square wave is used to clock two pairs of digital serial shift-register IC's (74164). Sixteen registers of one pair of shift-register along with an inverter feed back IC (7404) shift out a sine wave, and sixteen registers of the other pair shift out a cosine wave.

The digital pattern that circulates in the sine generating shift registers is set forth in Table V.1. This pattern must be converted by a resistive addition network to a staircase approximation sine wave. The values of resistors used by Fitzsimmons⁽⁴⁶⁾ cannot be used here because the length of our shift register sequence is sixteen (compared to his twelve). As the sine wave is odd symmetric, we therefore have to obtain only 8 values of resistances (also known as amplification

Table V.1 Circulating digital pattern in sine wave generating shift registers.

in binary				in Hex
0000	0000	0000	0001	0001
0000	0000	0000	0011	0003
0000	0000	0000	0111	0007
0000	0000	0000	1111	000F
0000	0000	0001	1111	001F
0000	0000	0011	1111	003F
0000	0000	0111	1111	007F
0000	0000	1111	1111	00FF
0000	0001	1111	1111	01FF
0000	0011	1111	1111	03FF
0000	0111	1111	1111	07FF
0000	1111	1111	1111	0FFF
0001	1111	1111	1111	1FFF
0011	1111	1111	1111	3FFF
0111	1111	1111	1111	7FFF
1111	1111	1111	1111	FFFF→max
1111	1111	1111	1110	FFFE
1111	1111	1111	1100	FFFC
1111	1111	1111	1000	FFF8
1111	1111	1111	0000	FFFO
1111	1111	1110	0000	FFEO
1111	1111	1100	0000	FFCO
1111	1111	1000	0000	FF80
1111	1111	0000	0000	FF00
1111	1110	0000	0000	FE00
1111	1100	0000	0000	FC00
1111	1000	0000	0000	F800
1111	0000	0000	0000	F000
1110	0000	0000	0000	E000
1100	0000	0000	0000	C000
1000	0000	0000	0000	8000
0000	0000	0000	0000	0000→min

coefficients) associated with each bit.

By solving the following equation for the n th clock pulse (n increases modulo 16),

$$a_1(x_n)_1 + a_2(x_n)_2 + \dots + a_{16}(x_n)_{16} = 1 + \sin \left(\frac{n\pi}{16} - \frac{\pi}{2} \right) \quad [V.3]$$

where a_i is the amplification coefficient corresponding to i th number of output signal of IC's 74164 and i varies from 1 to 16, with the additional constraints that

$$\left. \begin{aligned} (x_n)_i &\forall 1 \leq i \leq 16 \\ (x_n)_i &= 1 \text{ if } i \leq n \\ &= 0 \text{ if } i > n \end{aligned} \right\} \quad [V.4]$$

$$\text{and } a_i = a_{17-i} \forall 1 \leq i \leq 16, \quad [V.5]$$

we have the following set of simultaneous equations :

$$a_1 = 1 + \sin \left(\frac{\pi}{16} - \frac{\pi}{2} \right)$$

$$a_1 + a_2 = 1 + \sin \left(\frac{2\pi}{16} - \frac{\pi}{2} \right)$$

$$a_1 + a_2 + a_3 = 1 + \sin \left(\frac{3\pi}{16} - \frac{\pi}{2} \right),$$

or, in general,

$$\sum_{i=1}^n a_i = 1 + \sin \left(\frac{n\pi}{16} - \frac{\pi}{2} \right) \text{ for } 1 \leq n \leq 16. \quad [V.6]$$

Using eqn. [V.5] in [V.6],

$$\sum_{i=1}^n a_i = 1 + \sin \left(\frac{n\pi}{16} - \frac{\pi}{2} \right) \text{ for } 1 \leq n \leq 8 \quad [V.7]$$

Eqn. [V.7] yields a set of eight equations, which are sufficient to determine uniquely the values a_1 to a_8 . These can be suitably multiplied by a factor (we simply used a factor of 2) to obtain the required sine wave amplification value. We must keep one important point in mind while selecting the multiplication factor, that is, that the peak-to-peak voltage output of the waveform should not exceed +10V, at which voltage the output of a 741 Op. Amp. with $V_{SS} = +12V$ normally saturates.

The a_i 's obtained from eqn. [V.7] are given below in Table V.2.

Table V.2 Amplification Coefficients for sine-wave Resistive Network

Coefficients of Eqn.V.7	$\frac{100a_1}{a_i}$
$a_1 = 0.0192$	100
$a_2 = 0.0569$	33.8
$a_3 = 0.0924$	20.8
$a_4 = 0.1244$	15.4
$a_5 = 0.1515$	12.7
$a_6 = 0.1729$	11.1
$a_7 = 0.1876$	10.2
$a_8 = 0.1951$	09.8

The numbers listed in the second column of Table V.2 are the resistance values in $K\Omega$ to be used for getting a staircase approximated sine wave; the resistance values chosen for our circuit are the corresponding rounded-off values. Our resistive adder network is given in Fig. V.5. The sine wave shiftout procedure from the digital serial shift registers (74164) followed by the above resistive network is given in Fig. V.6. A

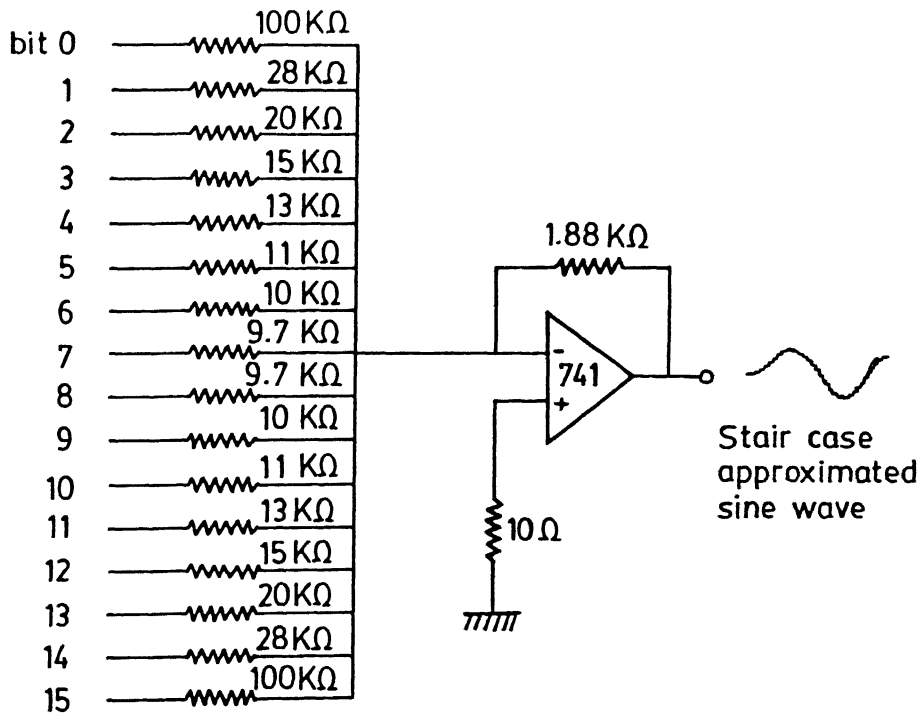


Fig.V.5 Resistive adder network.

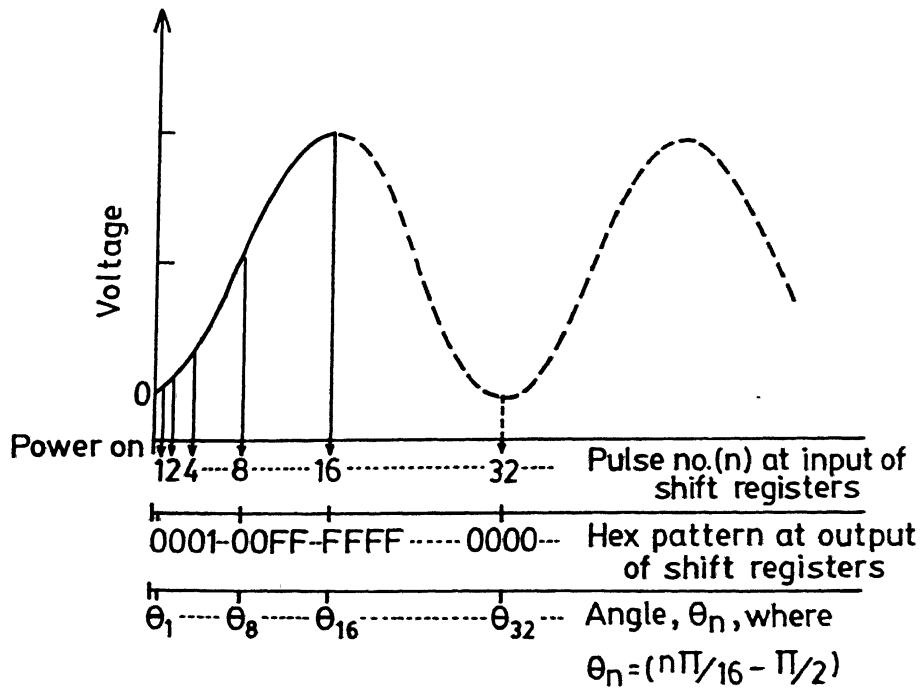


Fig.V.6 Procedure for shifting out sine wave from digital serial shift registers (74164's).

little tuning is required for the resistive network to account for any round off errors in various steps of the calculation. The Op. Amp. 741 (in Fig. V.5) sums up the 16 bit resistive network outputs and produces a staircase approximated sine wave as its output. There should not be a clipping at either extremity of the waveform, with a maximum peak-to-peak excursion of about 9V. In case clipping is observed, the feedback resistor (1.88 K Ω) in the summing operational amplifier may be further reduced till the peak-to-peak excursion reduces sufficiently to become distortionless.

At higher frequencies, the waveform may be distorted; in that case all the resistors in the network should be increased by a factor of 5 to 6 or even more in order to realise undistorted waveforms.

The next stage is a low-pass filter (Fig. V.4) which removes the high frequency component of the staircase sine wave and gives smoothed sine wave at its output. In order to carry this to the other parts of the controller, it is current-buffered by a 741 Op. Amp. in 'voltage-follower' configuration because of its superb buffering qualities, extremely high input impedance, low output impedance and unity voltage gain.

Cosine wave is generated by coupling its shift register to the shift register of sine wave appropriately. Sine and cosine outputs are digitally phase locked regardless of the frequency of operation. The sine and cosine outputs allow gradients to be controlled in quadrature when this is needed.

The frequency of the sine/cosine wave can be varied easily by varying the 100 K Ω potentiometer connected to the 555

timer (see Fig. V.4) within a fixed range depending on the value of the capacitor marked with asterisk in Fig. V.4. The frequency range can be increased further by simply replacing it with a suitable capacitor; in our circuit, the range is 1-25 Hz with 0.1 μF and 12-300 Hz with 100 nF.

V.3.3 Computer Interface and Manual Switch to Gradient Controller

We have a twofold objective for designing a computer interface and manual switch for gradient controller, namely :

- (i) to select at least 256 (numbered between 0 and 255) 'selective planes', as shown in design logic subsection, for imaging purposes;
- (ii) to vary the magnitude (in T/m) of the continuous/pulsed linear magnetic field gradient.

To achieve these objectives via microprocessor (μP) control, we used two 4-bit binary counters (7493) cascaded to form an 8-bit serial to parallel converter shown in Fig. V.7. As argued by Fitzsimmons⁽⁴⁶⁾, this requires only two pulse lines (one for reset and another for outputting plane position number of pulses) from microprocessor, whereas a parallel design would require as many as eight pulse lines from the microprocessor.

The number of pulses which is equal to the number of planes to be selected, or the magnitude of the required linear magnetic field gradient serially coming from the microprocessor, are converted into a binary form by this 8-bit binary counter (serial - to - parallel conversion). A reset pulse is required to initialize the counter.

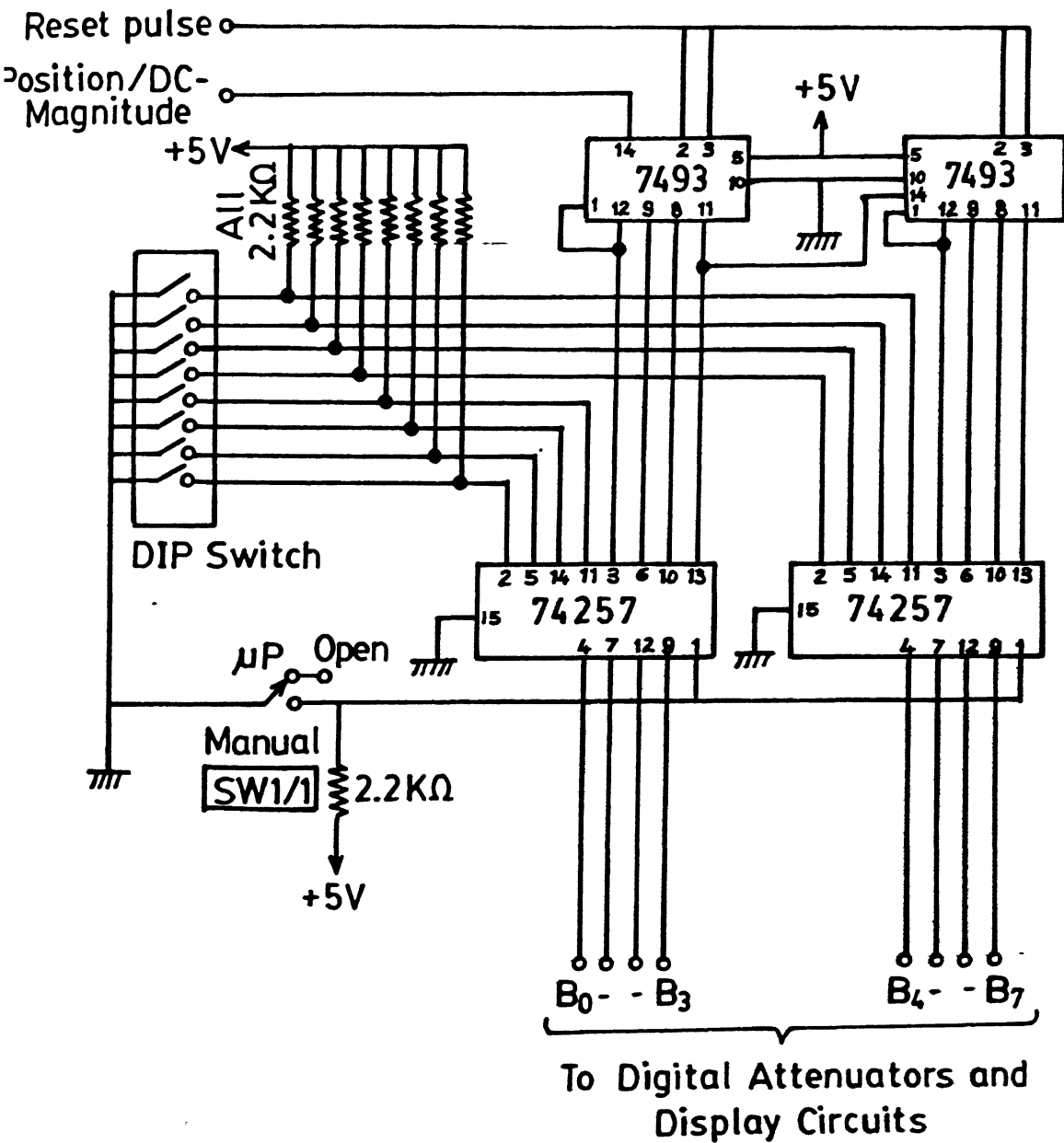


fig.v.7 Circuit diagram of our computer interface and manual switch to gradient controller.

The same objectives are also achieved in manual mode by setting an 8-bit DIP switch in either on or off position to select the required binary number which is displayed in decimal form.

The selection of computer or manual control of gradients is done by a set of multiplexers (74257) which takes either computer outputs or manual switch outputs as its input depending upon the position of the toggling switch (SW1/1).

V.3.4 Circuit Generating Complementary Outputs

The purpose of this circuit is to generate two DC/AC (sine or cosine) signals needed for a pair of gradient coils with the condition that the current amplitude of these two signals should complement each other. Our circuit generates a total of 256 complementary outputs between 0 and 255. The resulting outputs, which have the following relationship (see Fig. V.3),

$$|I_{\text{coil } 1}| + |I_{\text{coil } 2}| = |I_0| \quad [\text{V.8}]$$

are fed to the gradient coils. The corresponding circuit, represented in Fig. V.8, consists of a set of Digital-to-Analog converters (DAC) and four 741 Op. Amp's. The inputs to the DAC's are :

- (i) 8-bit binary data from the multiplexer (see Fig. V.7),
- (ii) sine wave from the digital oscillator or -12V DC from power supply, as its negative reference, $V_{\text{ref}}(-)$.

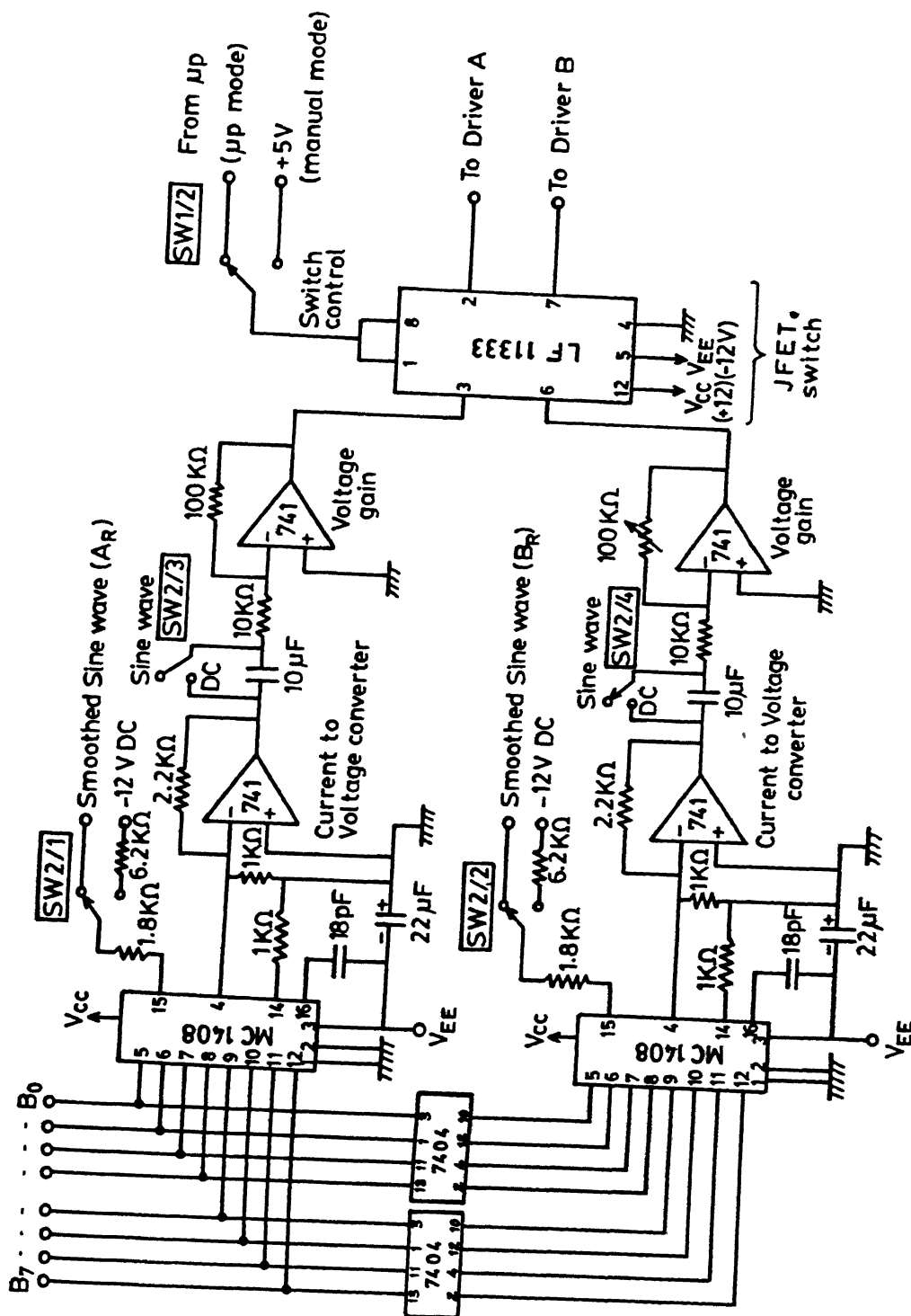


Fig. V.8
Complementary outputs circuits and switch circuit.

The output of DAC's is the same as their input with only the amplitudes dependent upon the binary input data (also called as attenuation factor). One DAC receives the 8-bit binary data from the multiplexer (Fig. V.7) directly and another receives the inverted multiplexer-output so that the attenuation factor of the DAC's will have a complementary relationship.

Output current (I_{analog}) of the DAC is given by

$$I_{\text{analog}} = \frac{V_{\text{ref}}(-)}{R_{15}} \left\{ \frac{A_1}{2} + \frac{A_2}{4} + \frac{A_3}{8} + \dots + \frac{A_8}{256} \right\} \quad [\text{V.9}]$$

where binary data, $A_n = 1$ (A_n at high level),

and $A_n = 0$ (A_n at low level),

$V_{\text{ref}}(-)$ = negative reference voltage (sinewave or -12V DC)

R_{15} = resistance at pin no. 15 of DAC IC MC1408.

The negative V_{ref} is selected here because the digital oscillator circuit output is negative due to the current sinking property of transistor-transistor-logic (TTL) shift register (74164).

Since the output of the DAC is in current mode, it is converted into voltage mode by a 741 OP.Amp. In the case of sine wave, the output of Op. Amp. is DC-blocked by using a 10 μF capacitor and then fed to the voltage gain amplifier (741 Op. Amp.), but in the case of DC output it is directly applied to the voltage gain amplifier.

V.3.5 Switch Circuit for Pulsed Linear Magnetic Field Gradient Generation

The linear magnetic field gradient is achieved by simply replacing the sine wave reference given to the DAC (pin number 15 of MC1408 in Fig. V.8) with a -12V DC. The magnitude of the gradient can be varied by varying the 8-bit data input to DAC's. It can also be made to rotate by applying 'reset' and 'position' pulses continuously from the microprocessor.

The linear magnetic field gradient thus generated should be gated at a suitable point before feeding it to the gradient coils in order to achieve a pulsed linear magnetic field gradient. We place a simple JFET switch (LF11333) at the output of the 741 Op. Amp. in voltage gain configuration (see Fig. V.8). This switch can be either microprocessor-controlled, or set manually by applying +5V DC. The outputs of this IC are fed to current drivers, described below.

V.3.6 Current Driver Circuit

We have used a fairly conventional design with a single Op. Amp. (741) providing the input to the driver and complementary pair of power transistors. The complete circuit diagram is shown in Fig. V.9, and consists of a 741 in negative feedback mode, transistors (2N 3055, ECP 055) and two diodes (1N914). The negative feedback path has a push-pull amplifier comprising a 2N 3055, ECP 055 and one 2N 1183. The 1Ω feedback resistor (marked with * in the circuit) in the circuit provides a suitable point for measuring the current being delivered to the gradient coils since it is in series with them. The gain can be

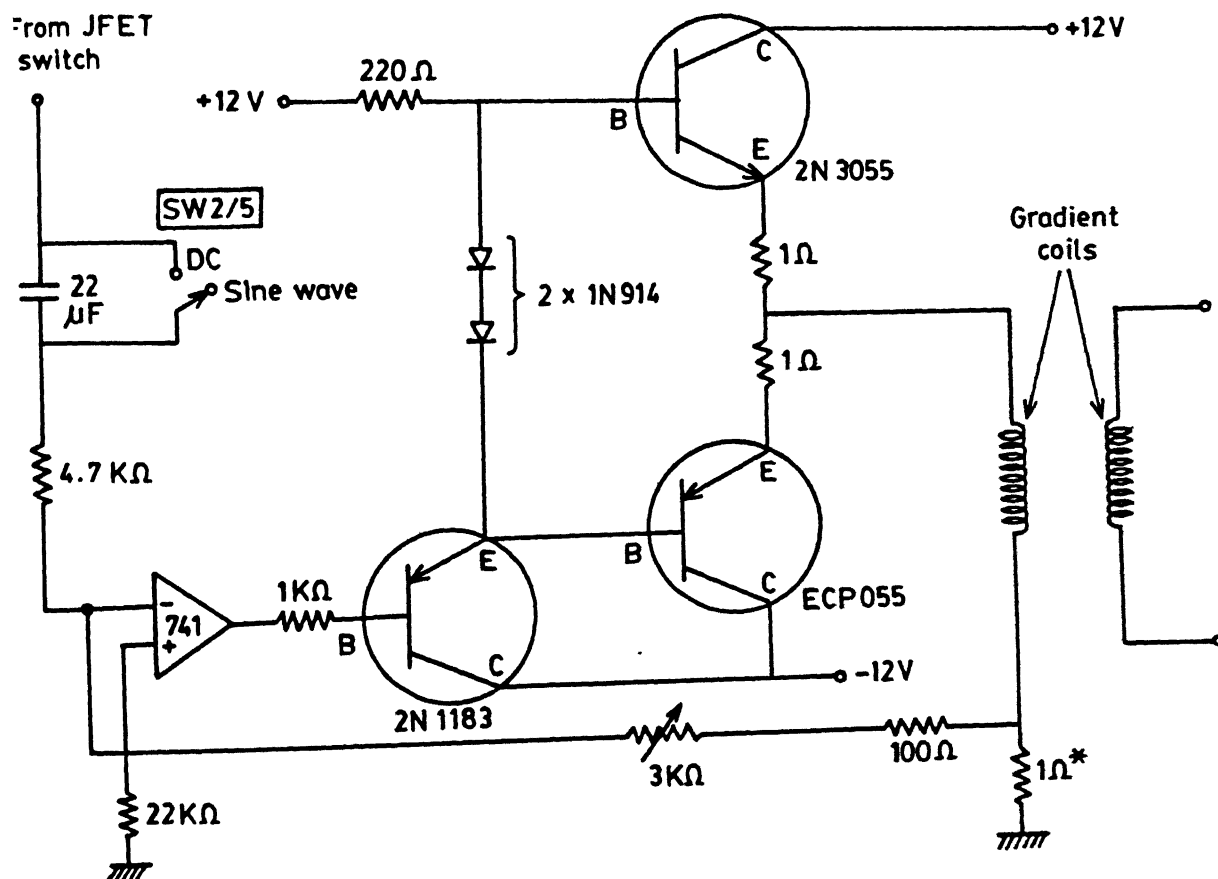


Fig.V.9

Current driver circuit.

varied with the help of the $3K\Omega$ potentiometer in the feedback path.

V.3.7 Display Circuit

The binary number selected for generating complementary outputs can be displayed conveniently in two ways, namely, (i) in a binary form and (ii) in a decimal form.

(i) Binary Display

This is done by simply connecting eight Light Emitting Diodes (LED's), one for each bit, in the 8-bit data output of the multiplexer (see Fig. V. 10). The common anode of all LED's is given +5V DC, which enables them to display the complement of the binary number selected, in spite of the fact that the LED's are not present in the inverted multiplexer-output line.

(ii) Decimal Display

Since it was inconvenient to see the selected number in an 8-bit binary form, we decided to display the same in a decimal form.

To accomplish this, the 8-bit binary data from the multiplexer is first converted into three nibbles (nibble = a group of four bits) of Binary Coded Decimal (BCD) by a set of three binary-to-BCD converters (74185), shown in Fig. V.10. Each of the resulting BCD nibbles is given to a BCD-to-7 segment decoder (7448), which is an active 'high' requiring pull-up resistors for converting the BCD to a decimal number. The seven output lines of 7448 are connected to a common cathode seven-segment display (LTS543R).

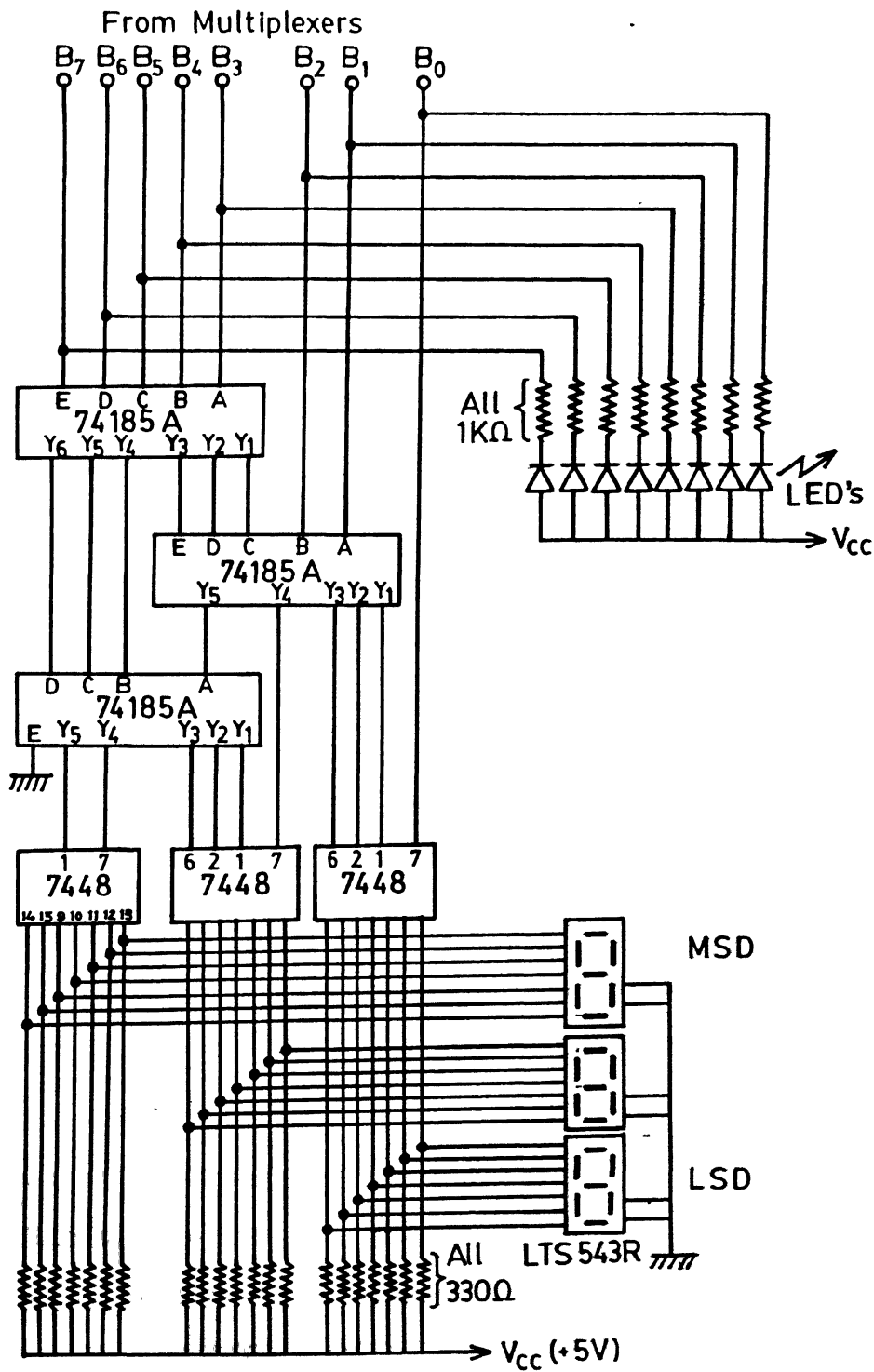


Fig.V.10

8-bit binary LED and 3-digit decimal seven segment display circuit.

V.3.8 Position of Switches for Mode (μ P/manual) and Sine Wave/DC Selection

There are a total of seven switches in the circuits which are to be put in appropriate position to select mode (μ P/manual) and reference signal (sine wave/DC) to DAC. These are grouped into two and given in Table V.3 for easy visualization and generation of linear/oscillating magnetic field gradient.

V.4 Details of the Microprocessor and Its Use in Gradient Control

V.4.1 Description of the Microprocessor

The microprocessor used in our work is a low cost Intel 8085 A based 8-bit system (Microfriend-I, Dynalog Microsystems (DMS), Bombay, India). Its functional block diagram is shown in Fig. V.11.

The 8085 A processor chip contains six general purpose 8-bit registers B,C,D,E,H and L for both data transfer and data storage, and an 8-bit accumulator (register A) for both arithmetical and logical operations. With 6.144 MHz crystal, the CPU operates at 3.072 MHz i.e., 1.3 μ s instruction cycle.

The microprocessor (μ P) has a powerful system monitor in 2732 Erasable Programmable Read Only Memory (EPROM) of 4K bytes. The on-board 24 pin zero insertion force (ZIF) EPROM Programmer is driven by a Programmable Peripheral Interface (PPI) 8255A to burn the developed software program into either 2716 or 2732 EPROM from Random Access Memory (RAM). The powerful on-board system monitor program enables us to load any software program into on-board RAM through a 21-key keyboard or through an audio

Selection for	Fig.No.	Switch No.	Switch
Mode (μp / manual)	V.7	SW1/1	
	V.8	SW1/2	
Sine wave / DC	V.8	SW2/1 SW2/2	
	V.8	SW2/3 SW2/4	
	V.9	SW2/5	

Table V.3

Tabulation of circuit switch positions.

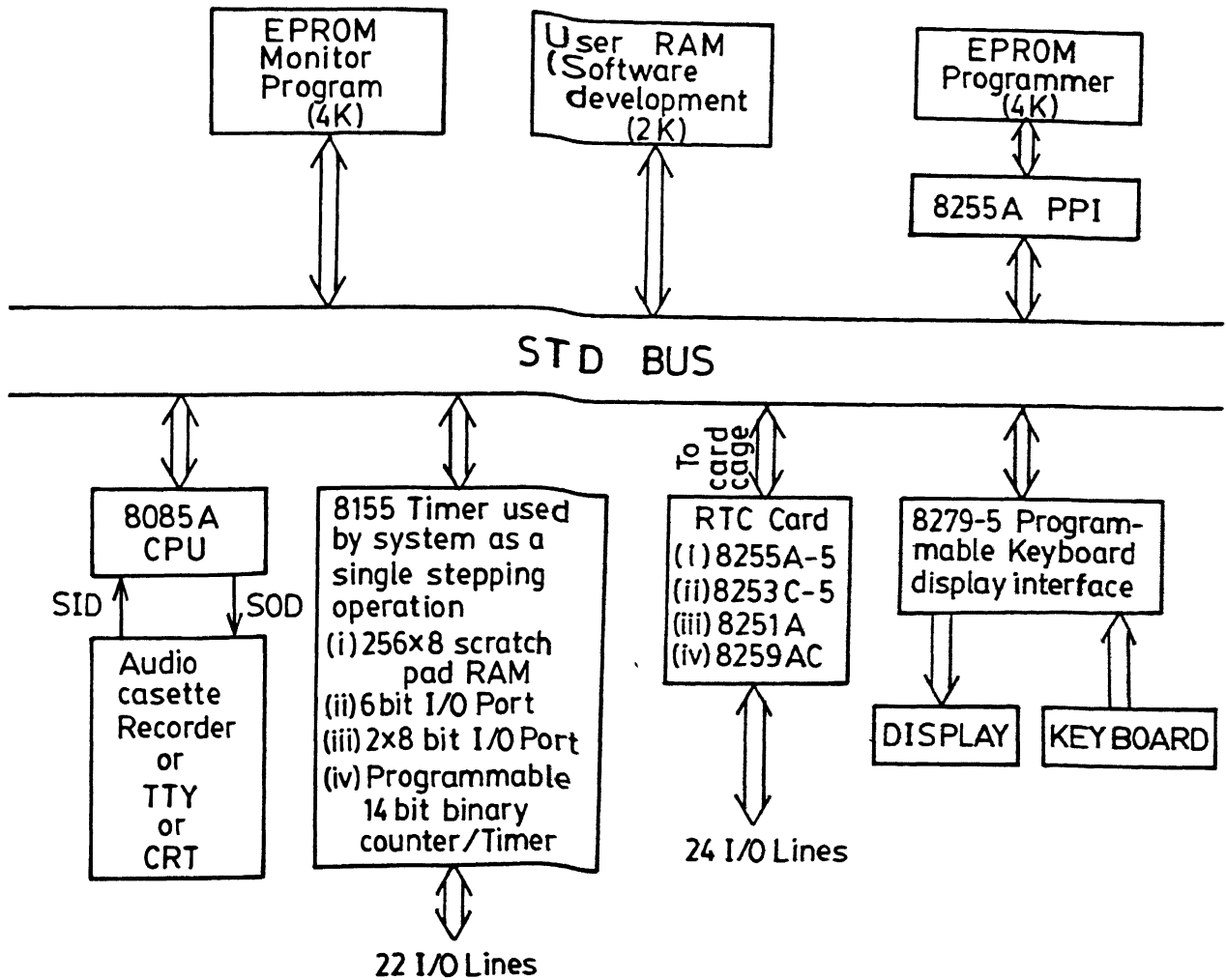


Fig.V.11

Functional block diagram of Intel 8085A based microprocessor kit used in this work.

cassette interface or from ZIF EPROM. An on-board 2K RAM (6116) user memory is suitable for developing and executing software programs. Intel 8279-5 is a programmable keyboard display interface IC which is used for a 21-key keyboard and 7-segment display. The display consists of a four byte memory address and a two byte data.

The IC 8155 comprises a 256x8 bit static MOS RAM with I/O ports and timer. The system monitor uses up about 100 bytes of static RAM as CPU scratch pad and stack area. The remaining 156 bytes are available for the user. The timer is used by the system for single stepping operations which are useful for debugging the developed machine code program.

The address, data and control buses fully buffered (by IC's 8212, 74LS244 and 74LS245) are available as an STD bus, which is a 56 pin double-sided edge connector provided for expansion of the system. Through this STD bus is hooked up a Real Time Controller (RTC) card mounted in card cage.

The RTC card consists of a 8255A-5 PPI, 8253C-5 programmable interval timer, 8251A Universal Synchronous Asynchronous Receiver and Transmitter (USART) and 8259AC Programmable Interrupt Controller (PIC).

The PPI 8255 A-5 has three 8-bit I/O ports, port A, Port B and Port C. Each Port and control register have distinct addresses to set control word in control register and to communicate with different devices through each port. This 8255 A-5 PPI can be set in various modes by writing suitable codes in the control register. The available modes are : Bit Set Reset (BSR) mode, simple I/O mode, handshake mode and bidirectional

mode. We use the 8255 A-5 in a simple output mode to output reset and position/DC-magnitude pulses and gate-control through BNC connectors to gradient controller box for selecting the plane or increasing DC magnitude and gate the output.

V.4.2 Reset and Position/DC-Magnitude Pulses and Gate Control Generation

V.4.2.1 Initialization

All the PPI ports are set in output mode by writing the appropriate word in control register. The number (N) corresponding to the first plane/DC-magnitude to be selected is stored at memory location M(X1). Next, a reset pulse is sent at BNC-1, which sets gradient controller at zeroth plane/DC-magnitude for a short computer time. Bringing the contents of memory location M(X1) in E-register is the next step. Here E-register is used as a 'scratch memory' for count down.

V.4.2.2 Software Counter

As explained above, one pulse is sent at BNC-2 and the BNC-3 level is set high for gating. The number of pulses is brought out from E-register for countdown and the decremented number is restored back in the E-register. If countdown is not over, the program loops back to pulse generation at BNC-2 stage. During each loop a pulse is sent through BNC-2 to gradient controller which in turn increments the plane/DC-magnitude by one. After the set number of pulses at M(X1) have been sent, the countdown ends; the desired plane/DC-magnitude is selected, and the program jumps to the system monitor program.

V.4.2.3 Pulse Output Method

There is one-to-one correspondence between the eight accumulator bits and 8-bits of each port. We set a particular bit of accumulator high (and other bits low) corresponding to a bit of a port from where the pulse output is taken. The content of the accumulator is output to PPI port, say port A. This makes the selected pin of port A high. Next, accumulator is immediately reset to zero and the content is output in the same port. This brings the selected pin of port A level low. This method generates about $5\mu\text{s}$ pulse at selected pin of port A. In the case of gating, level is left high for turning on the JFET switch.

V.4.2.4 Successive Increment of Plane/DC-magnitude

Our μP system has a user key U1 which, when tapped, takes the program from system monitor to scratch pad memory location 209C. At this memory location we write a jump instruction to jump into our program area. Here we have a program to read a number of pulses from $M(X1)$ and then increment it by a fixed number (N_0) and store the result again at $M(X1)$. After this, the program enters the initialization part of the main program. Every time the U1 key is pressed it selects/increases a plane/DC-magnitude higher by the fixed number (N_0). In this incrementation process, the 'carry' is discarded (i.e., the number rotates between 0 and 255).

The pulse generation details described above are given below in the form of a flow chart, Fig. V.12; a sample program for generating reset and position/DC-magnitude pulses and gate control is given in Table V.4.

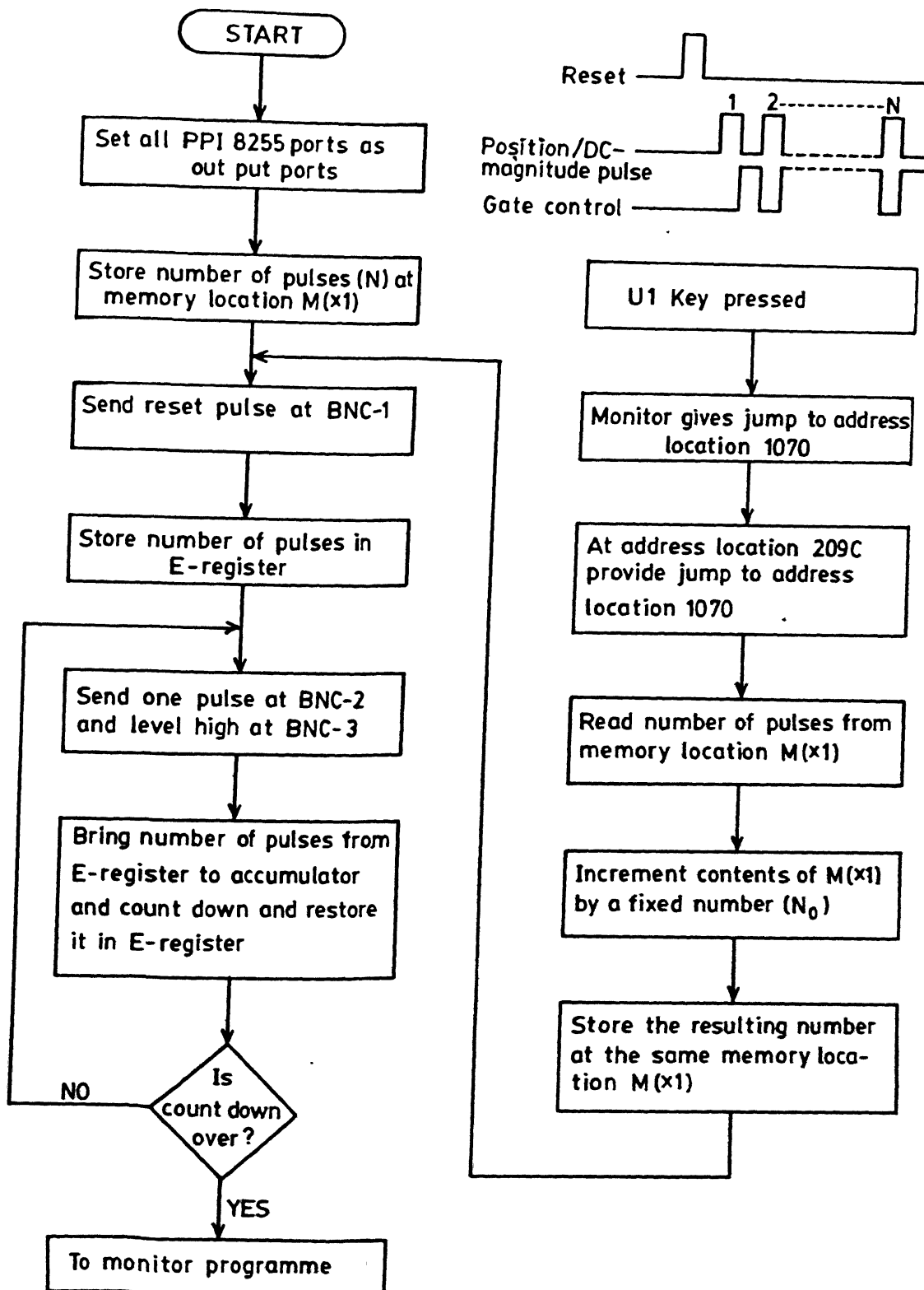


Fig.V.12

Flow chart for the generation of reset and position/DC-magnitude pulse(s) and gate control.

Table V. 4 A sample program for generating reset and position/DC-magnitude pulse(s) and Gate Control

Address	Mnemonic	Machine Code	Comment/Remark
1000	MOVI A, 80 OUT 2F	3E 80 D3 2F	} PPI in output mode
1004	MOVI A, 01 STA 1012	3E <u>01</u> 32 12 10	
1009	MOVI A, 80 OUT 2C MOVI A, 00 OUT 2C	3E 80 D3 2C 3E 00 D3 2C	} A reset pulse is sent at BNC-1 (bit 8 of port A is used)
1011	MOVI E, 01	1E 01	
1013	MOVI A, 20 OUT 2C MOVI A, 10 OUT 2C	3E 20 D3 2C 3E 10 D3 2C	} For sending position/DC-magnitude pulses at BNC-2 (bit 6 of port A is used) and Gate control at BNC-3 (bit 5 of port A is used)
101B	MOV A, E SUI 01 MOV E, A	7B D6 01 5F	
101F	JNZ 1013	C2 13 10}	Loop back if count down is not over
1022	RST 0	<u>C7</u> }	For monitor, ready for U1 key
1022	JMP 1009	<u>C3</u> 09 10}	} These instructions are for displaying reset and position/DC-magnitude pulses and gate control on oscilloscope, with scope triggered by reset pulse
209C	JMP 1070	C3 70 10}	
1070	LDA 1012 ADI 10 STA 1012	3A 12 10} C6 <u>01</u> 32 12 10}	} Read number of position/DC-Magnitude pulses from 1012 (i.e. M(X1), increment it by a fixed number (N) stored at 1074 and store back
1078	JMP 1009	C3 09 10}	

Note : Underlined numbers can be changed as required

V.4.3 Generation of Switch Control for Pulsed Magnetic Field Gradient (PMFG) Spin Echo Experiment

All PPI ports are set in output mode by writing the appropriate word in control register. Various delay counts (DC1, DC2 and P1) are stored in memory locations M(X1), M(X2) and M(X3).

The pulse output method here is the same as described in section V.4.2.3. However, delays are introduced to lengthen pulse width (P1) and to introduce intervals between pulses.

For short pulse width, 8-bit number is brought into the accumulator and counted down. Thereafter, the level at BNC-3 is changed. This generates pulse widths dependent upon an 8-bit number.

For large pulse interval delays, two 8-bit numbers are used. For each decrement of the second 8-bit number, the first 8-bit number goes to complete count down. By this method we get delays dependent upon multiplication of two 8-bit numbers.

The details described above are given below in the form of a flow chart, Fig. V. 13, followed by a sample program in Table V. 5

V.5 Highlights of Our Gradient Controller Circuit

In this section we summarise the technical features of our improved gradient controller circuit; improvements over the earlier design of Fitzsimmons⁽⁴⁶⁾ are also pointed out.

(1) In digital oscillator circuit (Fig. V.4),

(i) after the 555 timer, a JK flip-flop is added to get a square waveform with 50% duty cycle.

Table V.5 A sample program for generating switch control for a typical pulsed magnetic field gradient (PMFG) spin echo experiment

Address	Mnemonic	Machine Code	Comment/Remark
1030	MOVI A, 80 OUT 2F	3E 80 D3 2F	} All PPI ports in output mode
1034	MOVI A, 02 STA 1091	3E <u>02</u> 32 91 10	
1039	MOVI A, 04 STA 1092	3E <u>04</u> 32 92 10	} Delay count DC1 stored at memory location 1091
103E	MOVI A, 04 STA 1093	3E <u>04</u> 32 92 10	
1043	MOVI A, 10 OUT 2C	3E 10 D3 2C	} Delay count DC2 stored at memory location 1092
1047	LDA 1093 SUI 01 JNZ 104A	3A 93 10 D6 01 C2 4A 10	
104F	MOVI A, 00 OUT 2C	3E 00 D3 2C	} Delay count P1 stored at memory location 1093
1053	MOVI A, 0F SUI 01 JNZ 1055 LDA 1091 SUI 01 STA 1091 JNZ 1053	3E <u>0F</u> D6 01 C2 55 10 3A 91 10 D6 01 32 91 10 C2 53 10	
1065	MOVI A, 10 OUT 2C	3E 10 D3 2C	} Level high to turn on JFET switch (bit 5 of port A)
1069	LDA 9310 SUI 01 JNZ 106C	3A 10 93 D6 01 C2 6C 10	
1071	MOVI A, 00 OUT 2C	3E 00 D3 2C	} Count down P1
1075	MOVI A, 0F SUI 01 JNZ 1077 LDA 1092 SUI 01 STA 1092 JNZ 1075	3F <u>0F</u> D6 01 C2 77 10 3A 92 10 D6 01 32 92 10 C2 75 10	
1087	JMP 1034	C3 34 10	Count down T1 where $T1 = 0F \times [DC1]$
			Level low to turn off JFET switch
			Count down P1
			Level low to turn off JFET switch
			Count down T2 where $T2 = 0F \times [DC2]$
			Jump back to reinitialize delay count and give waveform

Note : Underlined numbers can be changed as required

- (ii) Four TTL 8-bit parallel out serial shift registers (74164's) have been used instead of three CMOS dual four stage registers (4015's) to shift out sine and cosine waves.
 - (iii) The sine/cosine wave resolution in our circuit is (32 x input period to 74164), as contrasted from Fitzsimmons (24 x input period to 4015).
 - (iv) To get a smoothed sine/cosine wave, we have used a very simple single pole low-pass filter instead of using an MC 1408 current sync. IC.
- (2) In the computer interface and manual switch circuit (Fig. V.7), we have used two 74257 (quad 2 input multiplexer tristate) instead of two 74367 (tristate hex buffer) which makes DIP switch connections easier, and operation in both modes simpler.
- (3) In the complementary outputs generating and switching circuit (Fig. V.8),
- (i) We feed the smoothed sine-wave/DC to negative reference of DAC's;
 - (ii) A JFET switch LF 11333 is used in the input to the current driver circuit Op. Amp. (Fig. V. 9) instead of the CMOS transmission gates suggested by Fitzsimmons⁽⁴⁶⁾.
- (4) We have used 2N 1183, 2N 3055 and ECP 055 transistors instead of ECG 185, MJE 3055 T and MJE 2955 T in the current driver circuit (Fig. V. 9).
- (5) We have added a decimal seven segment LED display for showing the selected plane/DC-magnitude level (Fig. V. 10).

In the photograph, Fig. V. 14, we show the experimental setup of our current driver, gradient controller, microprocessor and RF probe units.

V.6 Details of Experimental Setup and Performance Result

The versatile magnetic field gradient controller described above has been constructed with the idea of dedicating it to our microprocessor-controlled low frequency (15 MHz) home made NMR spectrometer⁽⁴⁷⁾. Unfortunately, during the last stages of our work, our electromagnet and its power supply became non-functional.

As a result, a commercial spectrometer (BRUKER WP-80) had to be used to complete our experiments. Even here, we were constrained by the fact that the usual T_2 experiments could not be done without modifying the existing hardware of the WP-80, which thus ruled out the possibility of doing diffusion measurements on the WP-80. With these restrictions, we limited ourselves to checking the performance of our versatile magnetic field gradient controller.

Details of the gradient coils used, and of experimental set up, are given below :

Spectrometer	:	BRUKER WP-80, with BNC-28 Computer
Probe used	:	WP-80- $^{13}\text{C}/^1\text{H} - ^1\text{H} - ^2\text{H}$, 5mm
Gradient Coil } specification }	:	OHFC Copper wire thickness : 0.6 mm
		Coil outer diameter : 13.8 mm
		Number of turns : 10
		Coil used : Miniductor coil No. 3004
		(From Barker & Williamson, Bristol, Pa., U.S.A.)

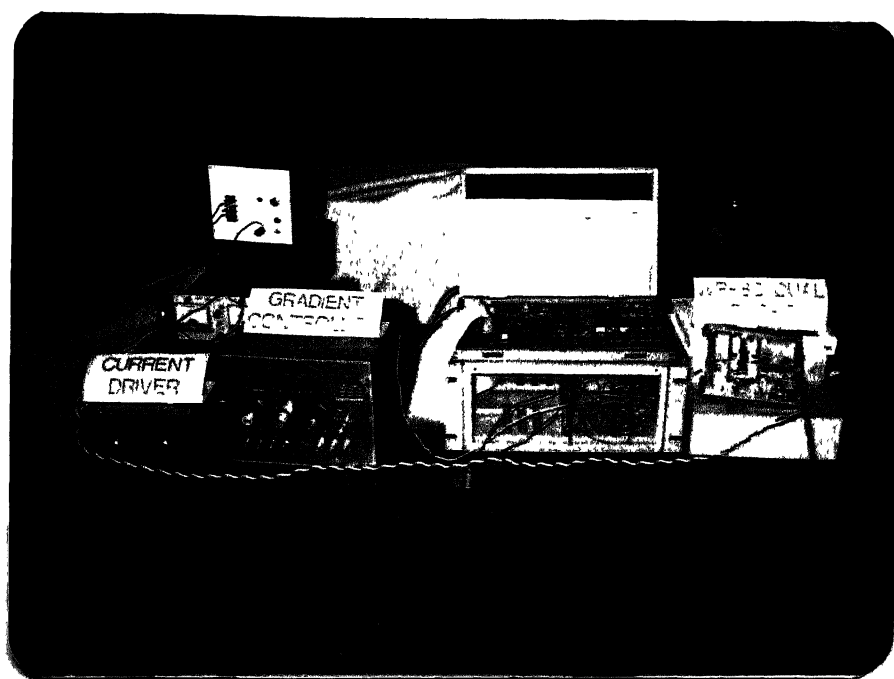


Fig.14

Experimental setup of the current driver, gradient controller, microprocessor kit and RF Probe unit.
(Photograph)

The gradient coils were fixed rigidly by supporting them with batts of thermocol (styrofoam) in the empty space on each side of the sample coil (along y-direction) in such a configuration that it generated y-gradient. The y-gradient was chosen because there was no empty space in the probe box for fixing coils to generate a z-gradient.

(i) **Linear Magnetic Field Gradient :**

For checking this, we have selected a 5mm NMR tube containing D_2O (this is for field-to-frequency locking), into which two H_2O capillaries of different diameter were inserted.

The experimental spectra corresponding to four different conditions are given in Fig. V. 15 and Fig. V.16. Due to small voltage offset difference between the Op. Amp.'s of the current driver circuit, the spectra shown in Fig. V.15(a) and (b) are not exactly symmetric. Spectrum in Fig. V. 16 (b) shows that when the DC-magnitude 127 is selected, both the coils receive the same amount of voltage and this imposes a small additional magnetic field in the y-direction, as compared to the situation in Fig. V. 16(a) where no current is passed through the coils. The broadening in Fig. V. 16(b) may be explained due to the field inhomogeneity generated by the current flowing through the gradient coil pair.

Fig. V. 17 shows spectra at different orientation of the capillary tubes with respect to the magnetic field gradient direction.

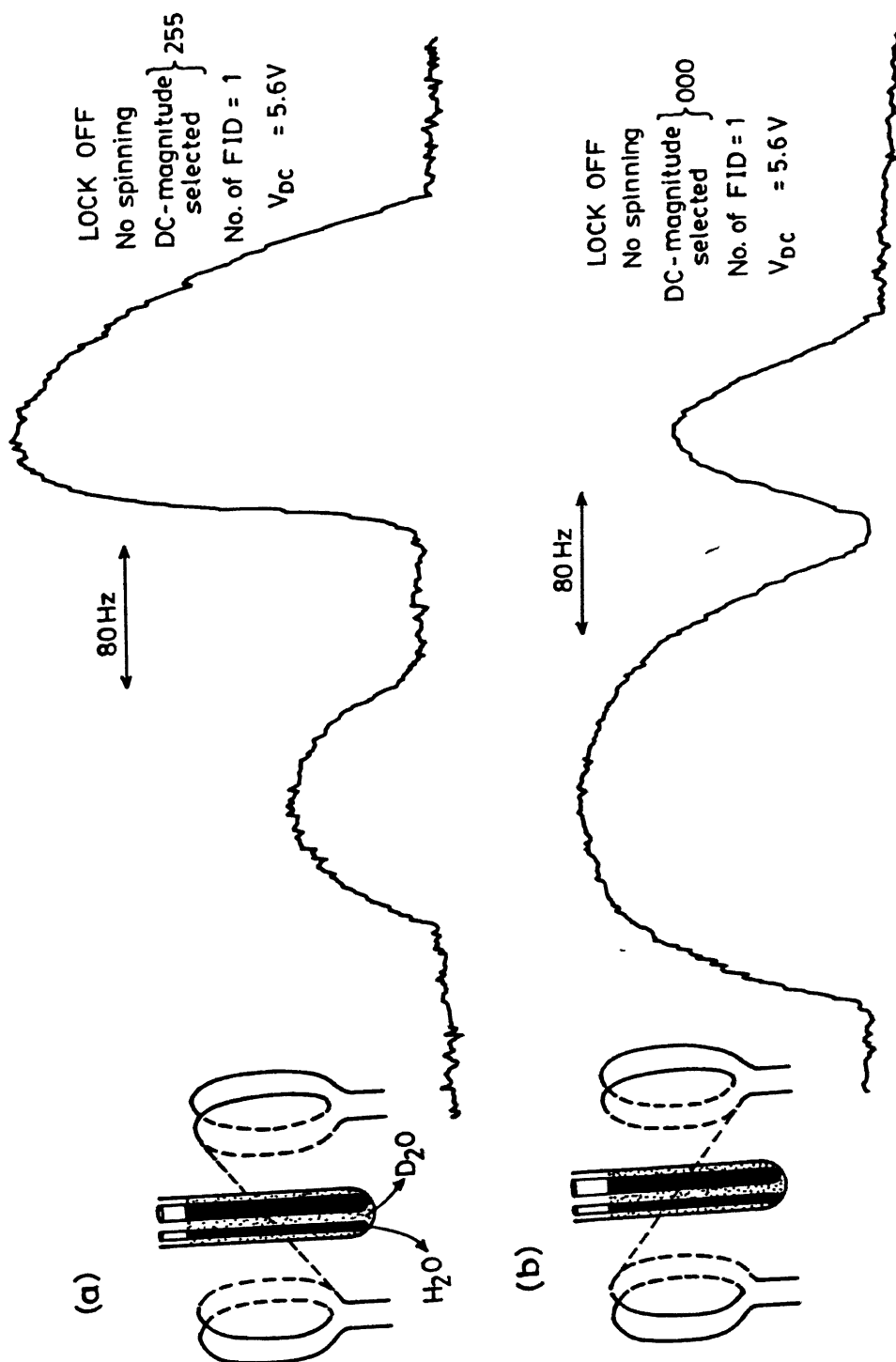


Fig.V.15 Proton NMR spectra of H_2O in the presence of a continuous-linear magnetic field gradient.

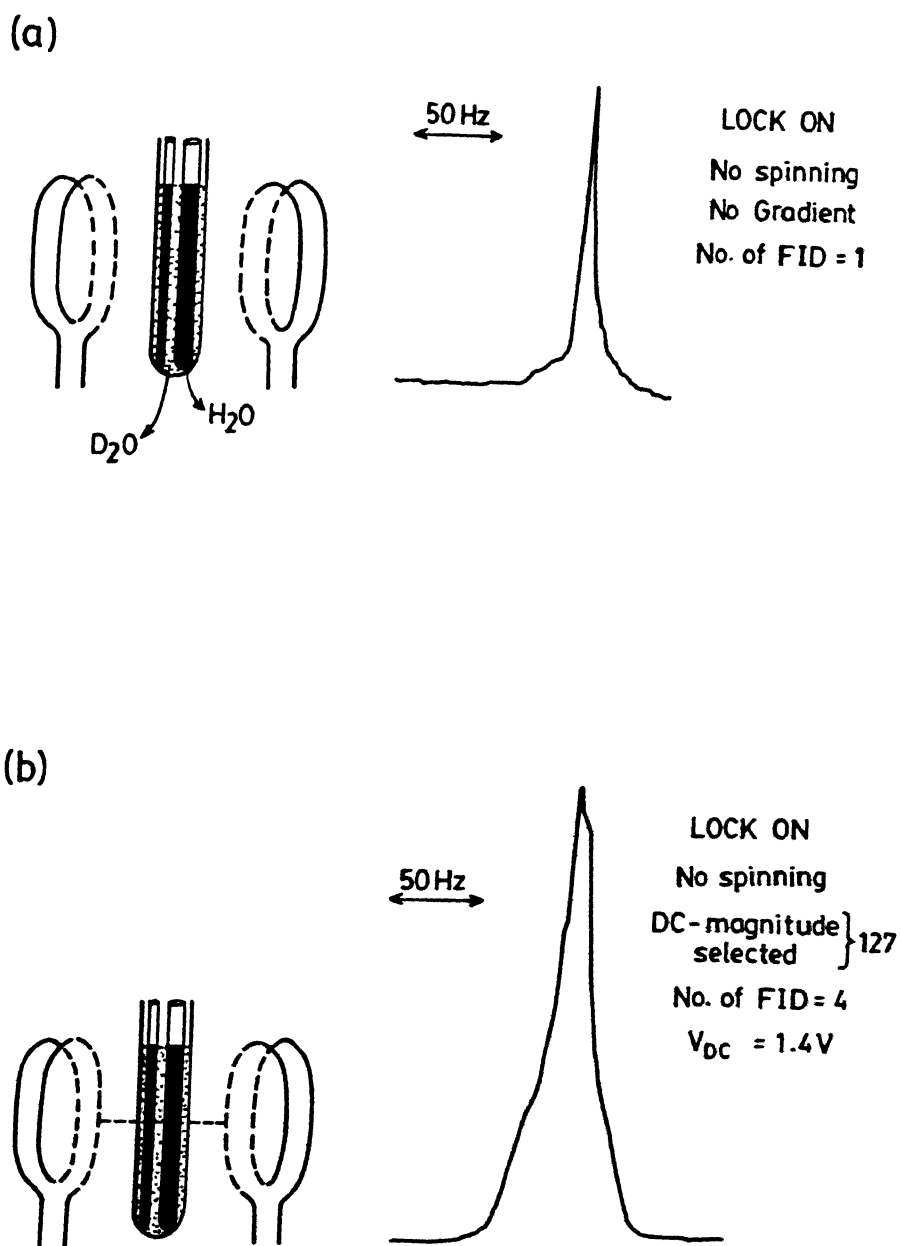


Fig.V.16

Proton NMR spectra of H_2O in (a) absence and (b) presence of a small additional magnetic field in the Y-direction.

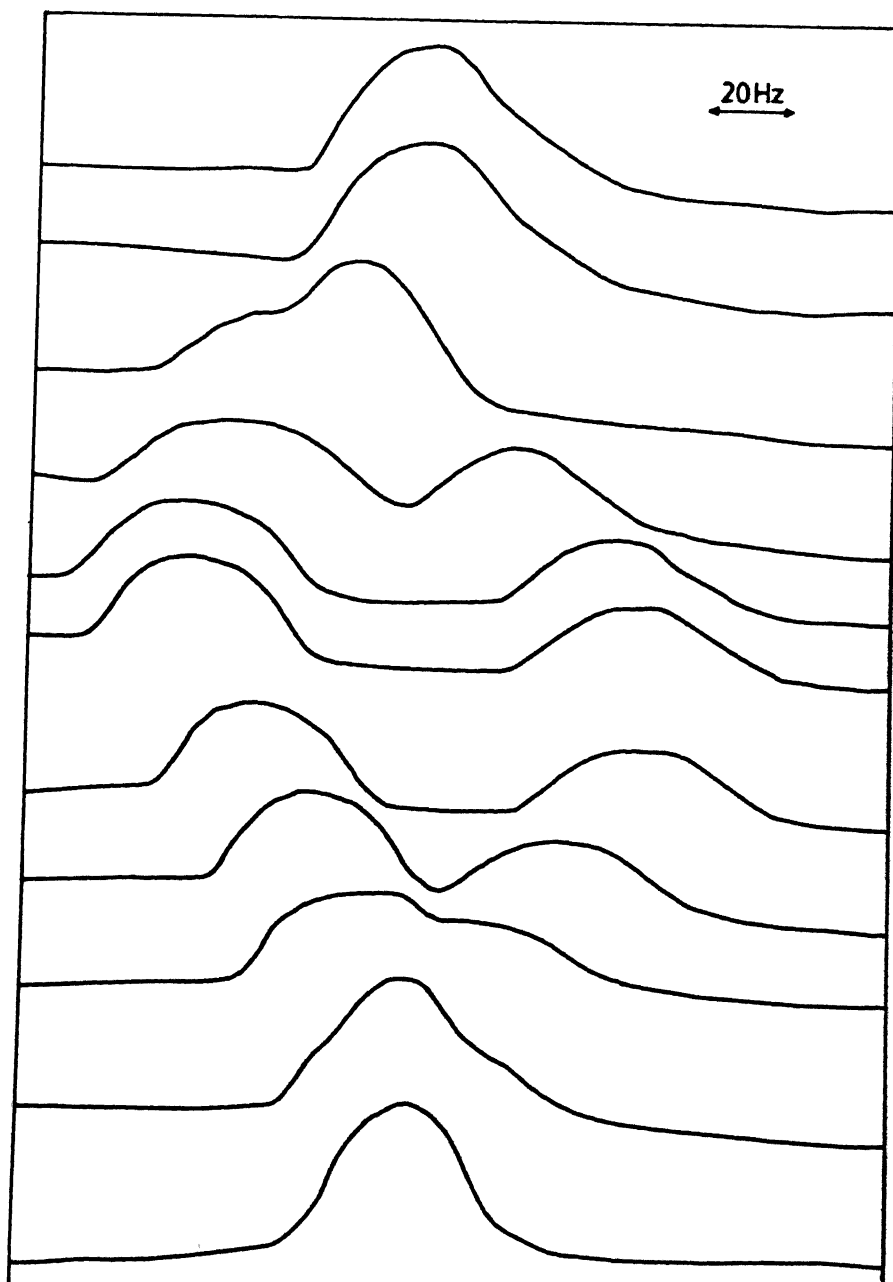


Fig.V.17

Proton NMR spectra at different orientations of H₂O capillary tubes with respect to the magnetic field gradient direction.

(ii) Oscillating Field Gradient

For checking this, we have used a sealed D_2O tube, a small amount of H_2O present there being sufficient to give a strong NMR line. Figs. V.18 and 19 have been recorded at two different oscillating frequencies. As expected, multiple lines are observed in each spectrum due to magnetic field modulation at the oscillating frequency.

V.7 Self-Diffusion Coefficient Measurements on the Lecithin Reverse Micellar 'Pool Water'

V.7.1 Motivation

Self-diffusion is the net result of thermally induced random-walk process experienced by molecules in solution, and self-diffusion coefficients provide important information on aggregate structure and association behaviour because association of molecules in solution greatly affects the translational motion of the molecules. Indeed, it has been well established that self-diffusion coefficients provide a direct approach for elucidating the structural organization in aggregated systems⁽⁴⁸⁻⁵⁶⁾. Typical self-diffusion coefficients in liquid systems at room temperature range from about $10^{-9} \text{ m}^2\text{s}^{-1}$ to $10^{-12} \text{ m}^2\text{s}^{-1}$. Elsewhere in the literature, measurements of the diffusion coefficient of cell water in biological systems have disclosed reductions of as much as 50% in the diffusion coefficient of this state of water compared to that of free water⁽⁵⁷⁾; likewise, in other 'structured' phases such as water containing microemulsions⁽⁵⁸⁾, the diffusion coefficient of water has been found to be less than 10% of that of free water.

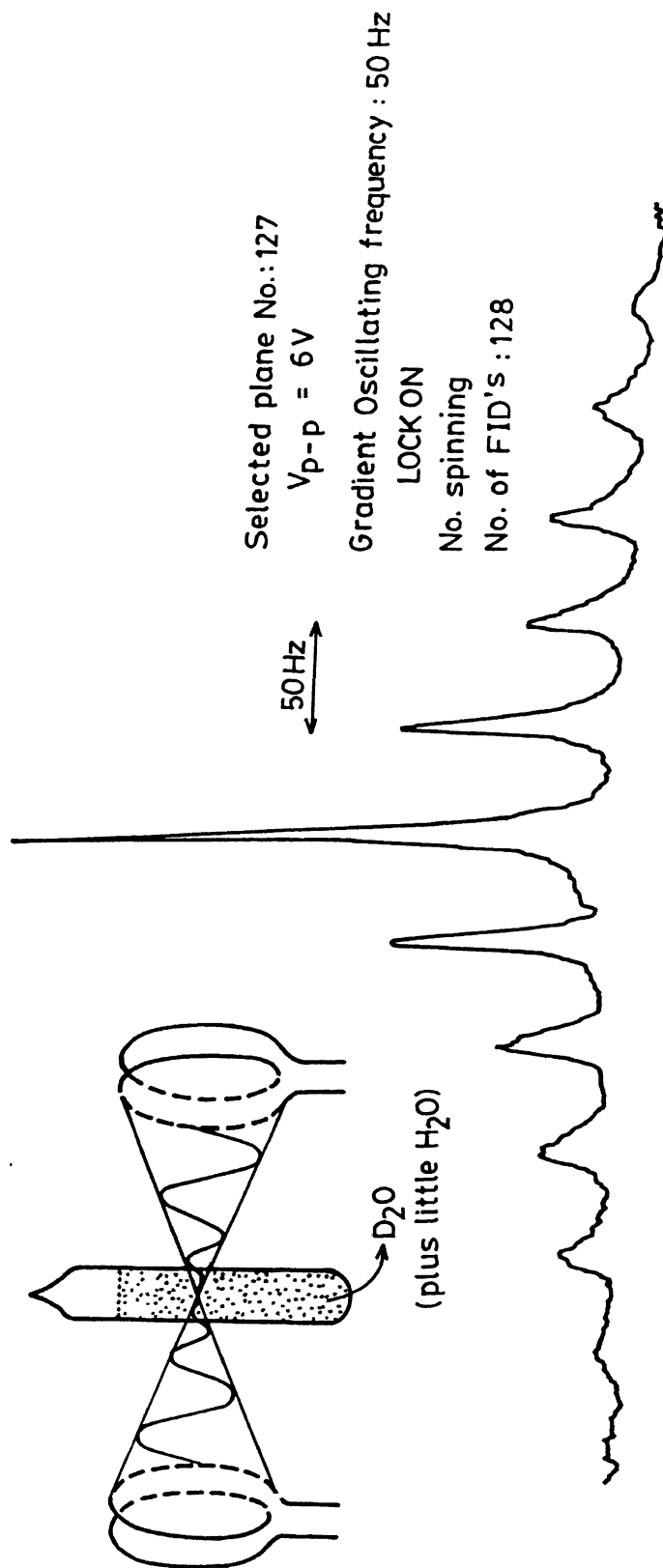


Fig.V.18

Proton NMR spectrum of water at the gradient oscillating frequency of 50Hz. ($V_{p-p} = 6\text{V}$; plane number selected = 127; no. of FID's collected = 128. The magnetic field lock was on, and sample tube was not spun.)

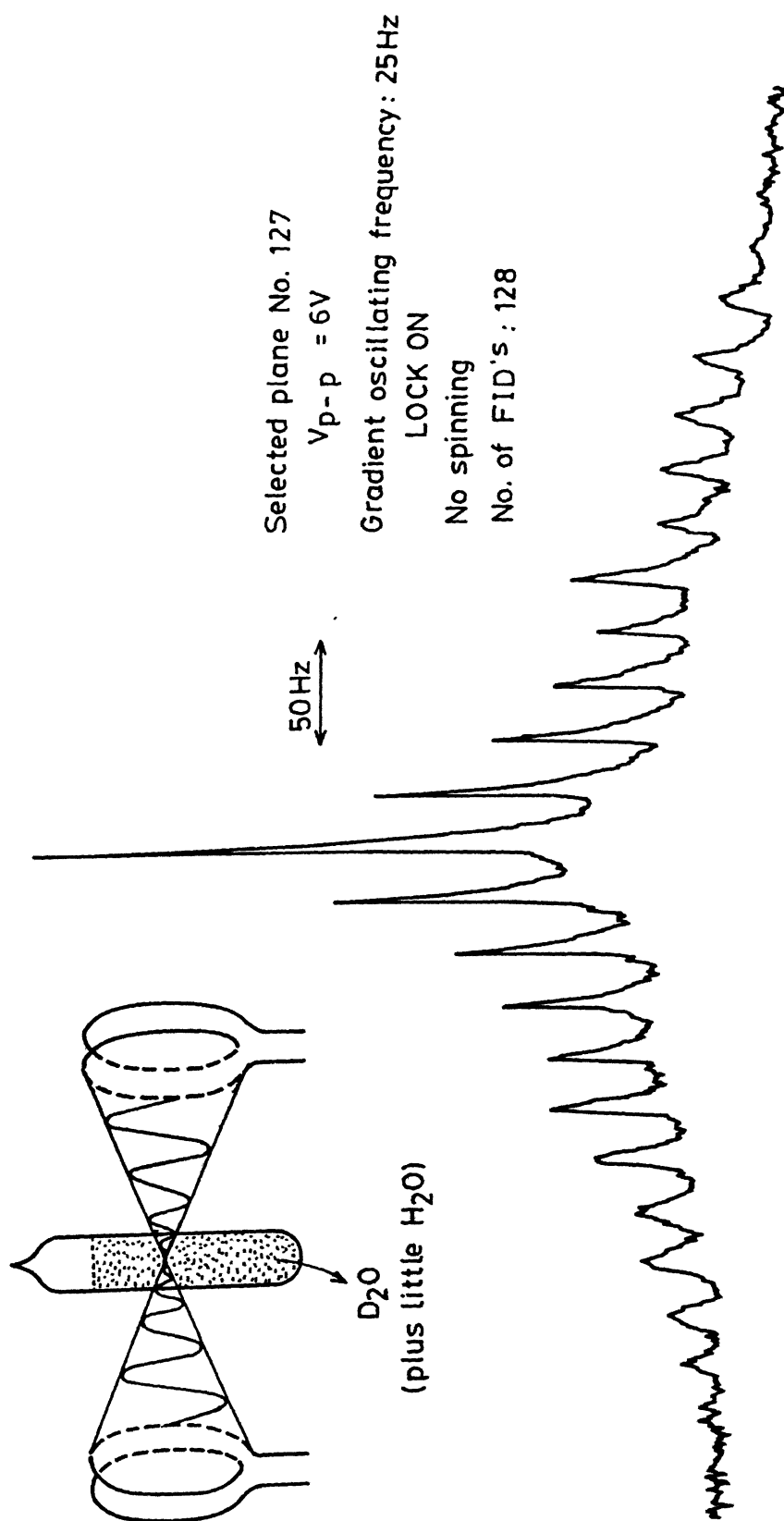


Fig.V.19 Proton NMR spectrum of water at the gradient oscillating frequency of 25 Hz. ($V_{p-p} = 6V$; plane number selected = 127; no. of FID's collected = 128. The magnetic field lock was on, and sample tube was not spun.)

Self-diffusion coefficient can be measured by using the following techniques :

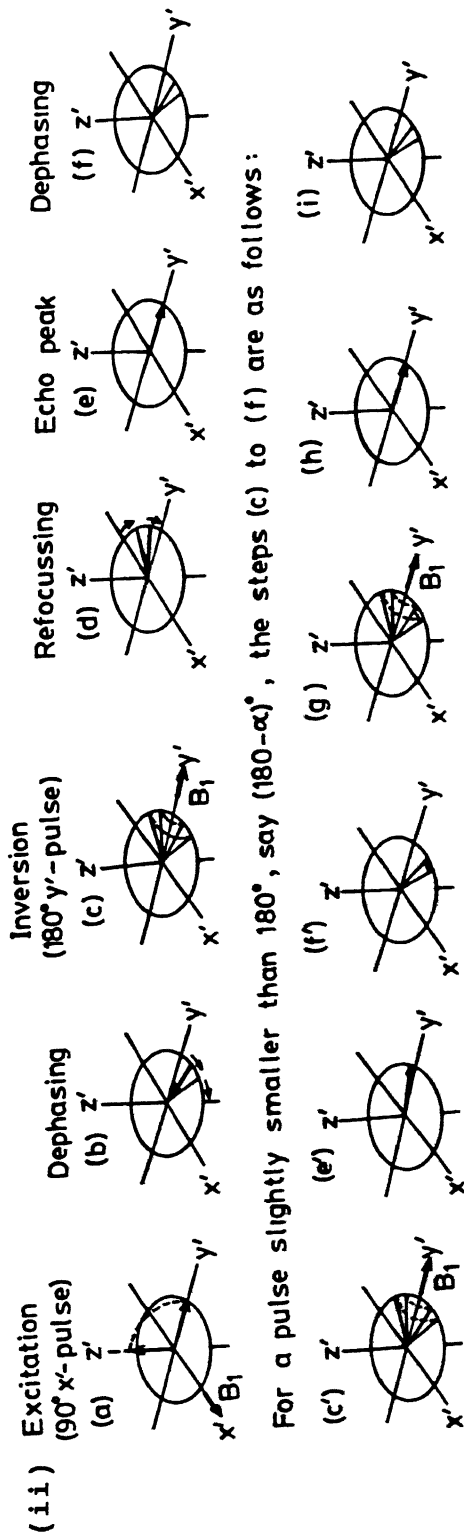
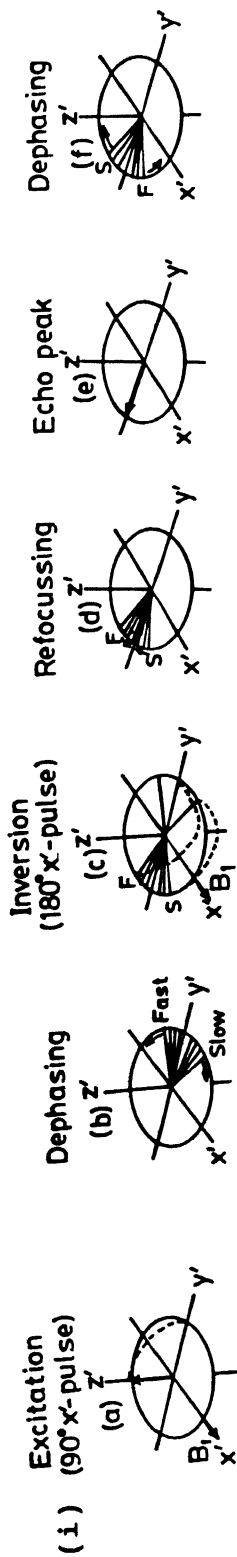
- (i) Tracer techniques^(59,60)
- (ii) Nuclear spin echo method⁽⁶¹⁾,
- (iii) Transient optical grating methods⁽⁶²⁻⁶⁴⁾,
- (iv) Neutron spin echo method⁽⁶⁵⁾,
- (v) Gouy interferometric techniques⁽⁶⁶⁾.

Our interest is to measure self-diffusion coefficients by the nuclear spin echo method, which is therefore described in further detail below.

V.7.2 The Nuclear Spin Echo Method

Translational self-diffusion coefficients (D) in single as well as multiphase systems are measured by observing the loss of phase coherence of a set of precessing nuclear spins due to their random motion over a gradient in the magnetic field. This method is the basis of the measurements presented in the present section, and a brief review of the principle of the method shall be presented first.

As is well known^(67,68), a general method for measuring transverse relaxation times T_2 is by studying the decay of the transverse component of magnetization, i.e., the component in the XY-plane when the Zeeman field is along the Z-direction. Hahn⁽⁶¹⁾, in a classic early paper, has pioneered the use of the 90° - τ - 180° RF pulse sequence for measuring T_2 . Fig. V. 20(i) illustrates the vector model which is usually employed to describe the process.



For a pulse slightly smaller than 180°, say $(180-\alpha)^\circ$, the steps (c) to (f) are as follows:

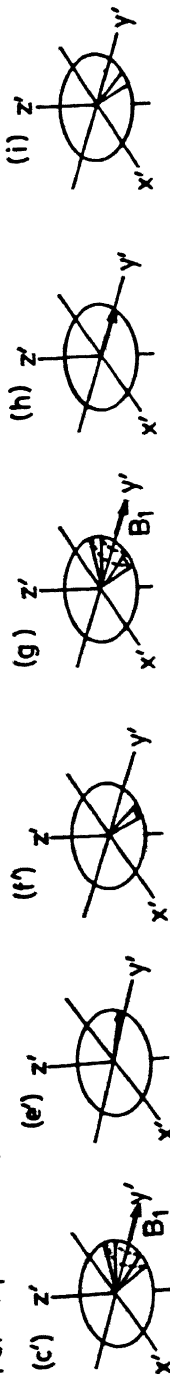


Fig.V.20(i) Hahn spin echo measurement of T_2 (rotating frame representation, from ref. (86)).

(ii) Meiboom-Gill pulse sequence⁽⁷⁰⁾ for measuring T_2 .

A 90° pulse causes the macroscopic magnetization, M , to tip to the y' axis. This magnetization loses phase coherence as there is a spread of frequencies in the sample owing to the spin-spin relaxation process (time constant T_2) and inhomogeneities of the magnetic field, some nuclear moments precessing more quickly than average, some more slowly. The signal detected along the y' axis by a coil set in the xy -plane, the free induction decay (FID), therefore decreases in magnitude. A 180° pulse applied at a short time, τ , after the initial pulse reverses the moments by rotation about the x' -axis. Phase coherence is first regained, and subsequently lost. Thus the signal appears as a reversed FID followed by a second pulse to give the echo. The echo height is less than that of the FID, and the echo is slightly asymmetric, owing to the spin-spin relaxation and diffusion during the time interval of the experiment, 2τ , but the additional loss of phase due to the imperfect field, which would otherwise have occurred, is eliminated by this Hahn pulse sequence. Therefore, measurements of spin echo amplitude for different values of τ provides a means for determining T_2 .

In Hahn's method, after each point is recorded it is necessary to wait for the magnetization to return to equilibrium (say $\geq 5 T_1$) before the next pair of pulses is triggered.

A variation of Hahn's spin echo method has been developed by Carr and Purcell⁽⁶⁹⁾; in their method, a 90° pulse is followed by a train of 180° pulses at times τ , 3τ , 5τ , etc. The major drawback of this sequence is that the cumulative effect of the out-of-plane refocussing due to imperfect 180° pulses can be serious.

To overcome this difficulty, Meiboom and Gill⁽⁷⁰⁾ further modified the Carr-Purcell sequence. Here, the 180° pulses are not applied in phase with the 90° pulses, but rather with a phase shift of 90° (Fig. V. 20(ii)). This modification of a 90° phase shift after the first 90° pulse renders the precise setting of the 180° pulse width less critical. The phase shift also eliminates the effects caused by inhomogeneities in the RF field. At present, the common pulsed NMR method for T_2 measurements, and perhaps the most accurate, is the one utilizing the Carr-Purcell-Meiboom-Gill (CPMG) pulse sequence.

The same spin echo experiment, done in an inhomogeneous magnetic field (generally linearly inhomogeneous in one direction only), provides the basis for NMR self-diffusion experiments. The 90° - τ - 180° spin echo experiment refocusses spins of any precession frequency, but only if the precession frequency is constant during the experiment. Therefore, if the nuclei move in an inhomogeneous magnetic field, their frequencies vary as well. For coherent motion in the direction of the gradient, the spins just refocus completely in another direction. But for the incoherent random motions such as self-diffusion, a random phase shift of individual spin vectors occurs, resulting in incomplete refocussing at the time of the echo. This is best demonstrated pictorially by Callaghan⁽⁷¹⁾, as in Fig. V.21.

In the figure, the positive and negative sign in the triangle indicate the successive, random jump (translational motion) of molecules with respect to the gradient direction. The horizontal sum of these elements gives the phase shift which occurs in the mean time between jumps (τ_s) while the spin is at

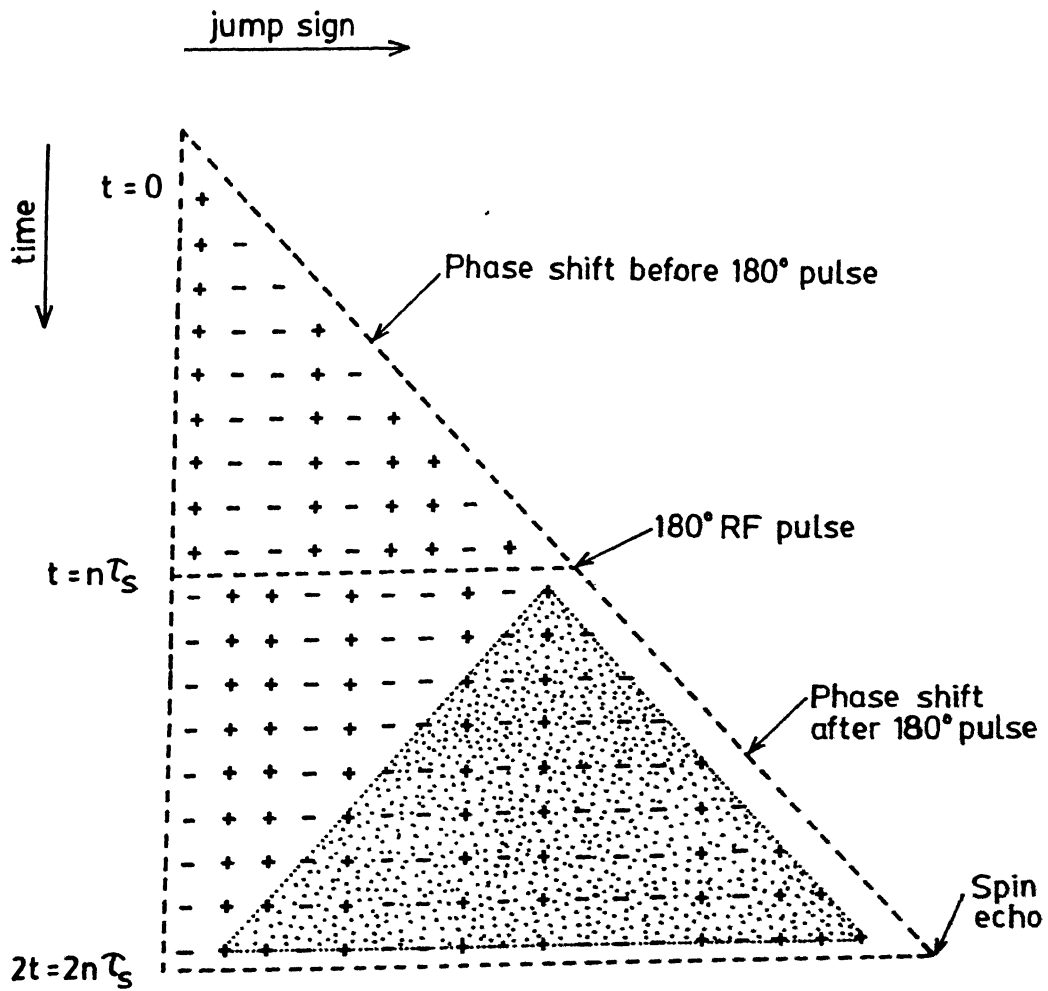


Fig.V.21

Cumulative phase diagram for spin echo formation in a steady magnetic field gradient⁽⁷¹⁾.

current location. The net phase shift is the sum of those occurring before and after the 180° RF pulse, and corresponds to the dotted region.

The self-diffusion coefficient of the molecule in which the nuclei are situated is calculated quantitatively from the echo attenuation effect, according to the equation

$$M(2\tau) = M(0) \left[\exp \left(-2\tau/T_2 - \frac{2}{3} \gamma^2 D G^2 \tau^3 \right) \right] \quad [V.10]$$

where γ represents the gyromagnetic ratio of the nuclei, G the strength of the linear magnetic field gradient in T/m, and D is the diffusion coefficient in m^2/s and τ the interval between the 90° and 180° pulses. T_2 is the (natural) transverse spin relaxation time of the nuclei. Since T_2 can be measured rather precisely by using CPMG sequence, and since G is known (by calibration), D can be determined directly from a plot of $\log [M(2\tau) + 2\tau/T_2]$ versus τ^3 .

Use of large currents in the gradient coils for producing linear magnetic field gradient has the following problems: (i) heating of gradient coils and (ii) NMR linewidth increases with corresponding decrease in the width of the FID and echo. Therefore, the detector bandwidth must be increased, thereby decreasing the signal-to-noise ratio. This linear magnetic field gradient technique has a diffusion coefficient limit of about $10^{-11} m^2 s^{-1}$, which is set by the maximum field gradient that can be used.

To overcome this limitation, Stejskal and Tanner⁽⁷²⁾ have proposed the pulsed gradient spin echo method (PGSE) which

involves transient field gradient pulses of a few milliseconds. The amplitude of these pulses must be of the order of a T/m in the case of the small diffusion coefficients encountered in the 10^{-12} - $10^{-10} \text{ m}^2 \text{ s}^{-1}$ range.

The amplitude of the echo signal detected is given by

$$M(2\tau) = M(0) \left[\exp \left(-2\tau/T_2 - (\gamma\delta G)^2 D(\Delta - \frac{\delta}{3}) \right) \right] \quad [\text{V.11}]$$

where δ is the duration of the gradient pulse and Δ is the delay between two gradient pulses.

By Fourier transforming the second half of the echo signal^(73,74) the pulsed field gradient spin echo method can be adapted to high resolution experiments, thus allowing the measurement of the diffusion coefficients of different components in a solution^(75,76).

Interest in self-diffusion coefficient measurements has grown rapidly during the last fifteen years. The information that can be obtained from the self-diffusion behaviour of surfactant systems may be classified into :

- (i) surfactant micellization⁽⁷⁷⁾
- (ii) solubilization equilibria⁽⁷⁸⁾
- (iii) micellar breakdown by solubilizates⁽⁷⁹⁾
- (iv) relations between diffusional rates and phase structure⁽⁸⁰⁾
- (v) micelle size, shape, hydration, and intermicellar interactions⁽⁸¹⁾.

Excellent reviews by Stilbs on the FT PGSE studies of molecular diffusion⁽⁸²⁾, mesophase structure of membrane lipids by Lindblom⁽⁸³⁾, micellar solutions by Chachaty⁽⁸⁴⁾, reversed micelle by Vos et al.⁽⁸⁵⁾, and microemulsions by Lindman and

Stilbs⁽⁸⁶⁾ have been published.

From the results of previous studies in this laboratory⁽⁸⁷⁻⁸⁹⁾ there is strong empirical evidence to suggest that, in the lecithin/cyclohexane/H₂O reverse micelle, at R values in excess of 6, a marked change occurs in the arrangement of the phospholipid head groups as well as in the dynamic state of water trapped in the core structure of the micelle. These changes have been rationalised as being due to the possible onset of a non-isotropic phase⁽⁸⁷⁻⁸⁹⁾.

In the following subsections, the above mentioned structural transition in the lecithin/cyclohexane/H₂O is further probed and compared with lecithin/CCl₄/H₂O by measuring the self-diffusion coefficient of water over a range of R values.

V.7.3 Water Diffusion in Anisotropic Environment

For water diffusion in an anisotropic environment, Eqn. V.10 has to be modified⁽⁹⁰⁾. In the specific instance of a liquid crystalline or two dimensional phase, the diffusion of trapped water will be mainly parallel to the long axis. An angular dependence is then imparted into the diffusion tensor (which will now be cylindrically symmetric) according to the formula

$$D_{\text{aniso}} = \langle D_{\perp} \rangle + \left(\langle D_{\parallel} \rangle - \langle D_{\perp} \rangle \right) \sin^2 \theta \quad [\text{V.12}]$$

where $\langle D_{\parallel} \rangle$ and $\langle D_{\perp} \rangle$ are the components of the average diffusion tensor parallel and perpendicular to the long axis of the anisotropic phase, and θ is the angle between the field gradient direction and the normal to the preferred axis for diffusion⁽⁹⁰⁾.

Since, for our assumed model, $\langle D_{\parallel} \rangle \gg \langle D_{\perp} \rangle$ which has also been generally referred to as the 'capillary' model in the literature⁽⁹¹⁾, the latter may be neglected and Eqn. V.12 may then be rewritten as

$$D_{\text{aniso}} = \langle D_{\parallel} \rangle \sin^2 \theta = D \left(1 - \mu^2 \right) \quad [\text{V.13}]$$

where $D = D_{\parallel}$ and $\mu = \cos \theta$

With the above redefinition, the echo amplitude, Eqn. V. 10, may be modified to

$$M(2\tau) = M(0) \exp \left[\frac{(-2\tau)}{T_2} - \frac{2}{3} \gamma^2 G^2 D (1 - \mu^2) \tau^3 \right] \quad [\text{V.14}]$$

In our model, all values of $\mu = \cos \theta$ are equally probable, and therefore we have to perform an integration over the angular variable, namely,

$$M(2\tau) = M(0) \exp (-2\tau/T_2) \int_0^1 \exp \left(-\frac{2}{3} \gamma^2 G^2 D (1 - \mu^2) \tau^3 \right) d\mu$$

$$M(2\tau) = M(0) \exp (-2\tau/T_2) \exp \left(-\frac{2}{3} \gamma^2 G^2 D \tau^3 f(y) \right) \quad [\text{V.15}]$$

where $y = \left(\frac{2}{3} \gamma^2 G^2 D \tau^3 \right)^{1/2}$ and $f(y) = \frac{1}{y} \int_0^1 \exp (-\mu^2) d\mu$

It is thus seen that the term $f(y)$ supplies the requisite correction to eqn. V.10 for our case of anisotropic diffusion in the randomly oriented long tubular (or capillary) structure.

V.7.4 Experimental Details

Using a BRUKER B-KR 322s NMR spectrometer and a precalibrated BRUKER B-KR 300z 18 magnetic field gradient unit, the rate of decay of spin echo signals has been measured in the presence of known magnetic field gradients to estimate the self-diffusion coefficient of the 'pool water' of the two reverse micellar systems : (i) lecithin/cyclohexane/H₂O and (ii) lecithin/CCl₄/H₂O. Echoes of the water proton signal have been observed at time 2τ of a $90^\circ - \tau - 180^\circ_{(90^\circ)}$ NMR pulse train, where the subscript (90°) indicates that the phase of the RF carrier of the second pulse is shifted by 90° relative to the first. T_2 has been evaluated to an estimated accuracy of $\pm 5\%$ using the Carr-Purcell-Meiboom-Gill pulse train⁽⁷⁰⁾ corrected for baseline drift by the procedure of Hughes⁽⁹¹⁾.

All signal amplitude measurements have been either read out directly from a Tektronix storage oscilloscope or (for weaker signals) recorded by an electronic digital read out at the output of a high speed signal averager.

In our diffusion coefficient measurements, it was important that during each experiment the NMR probe was thermostated to within ± 0.5 K. Depending on the choice of field gradient strengths, probe temperatures ranged from 296 K to 298 K. Larmor frequencies also had to be readjusted slightly from experiment to experiment around a central value of 30 MHz. The repetition time of the pulse trains was always greater than six times the T_1 of the sample.

To minimize errors due to the probe temperature and other variations to which absolute value of D may be sensitive,

all results have been converted to the dimensionless ratios D/D_0 , the diffusion coefficient of the 'pool water' relative to that of triply distilled water; here the sample size and diameters of the tubes (5 mm OD) have been chosen to be identical.

V.7.5 Results and Discussion

We shall first present the value of T_2 obtained by CPMG method and the T_2 value calculated from the experimental spectrum $\left(T_2 = \frac{1}{\pi \Delta\nu_{1/2}}\right)$, at different R values of lecithin/cyclohexane/ H_2O system (Table V.6).

Table V.6 Comparison of T_2 values from experimental linewidth and from CPMG sequence at different R values for the lecithin/cyclohexane/ H_2O system

R (nearest integer values)	T_2 from linewidth $\left(T_2 = \frac{1}{\pi \Delta\nu_{1/2}}\right)$, in seconds ^{1/2}	R	T_2 from CPMG sequence, in seconds
1	--	1.0	0.045
2	0.040	2.0	0.066
4	0.071	4.3	0.080
6	0.091	6.0	0.112
8	0.053	8.6	0.063
10	0.043	10.8	0.045
		13.0	0.041

Figs. V.22 and 23 show the linear least square fit plots of $\ln \left[M(2\tau) + \frac{2\tau}{T_2} \right]$ versus τ^3 through the set of experimental data points at different field gradients for samples with different R values. We have used T_2 values from our (more accurate) CPMG experiments, col. 4 of Table V.6, in our calculations.

From the slopes of Figs. V.22 and V.23 the diffusion coefficient, D, of water in the reverse micelle is calculated using

$$\text{slope} = \frac{2}{3} \gamma^2 G^2 D.$$

The standard-errors in the D value measurements range between $\pm 0.02 \times 10^{-9}$ and $\pm 0.04 \times 10^{-9} \text{ m}^2/\text{s}$.

Samples with R values > 10 became markedly more viscous⁽⁸⁷⁻⁸⁹⁾, and examination under crossed polarisers revealed that the system was optically anisotropic. The non-linear trend seen in Fig. V. 23(b) clearly corresponds to diffusion in the anisotropic phase. To calculate D from this curve, Eqn. V.15 was fitted to the data points by a two-parameter (D, τ) non-linear least squares fit where the integral was numerically evaluated by a "Simpson's $\frac{1}{3}$ -rule" subroutine⁽⁹²⁾. Fig. V. 23(b) shows the experimental points and the 'best fit' line through them. The ratio of this D to the D_0 value obtained for triple-distilled water under identical experimental conditions turns out to be 0.60, as shown in Table V.7. The D_0 value, $2.35 \times 10^{-9} \text{ m}^2\text{s}^{-1}$, used throughout in our calculations is an average value of many experiments.

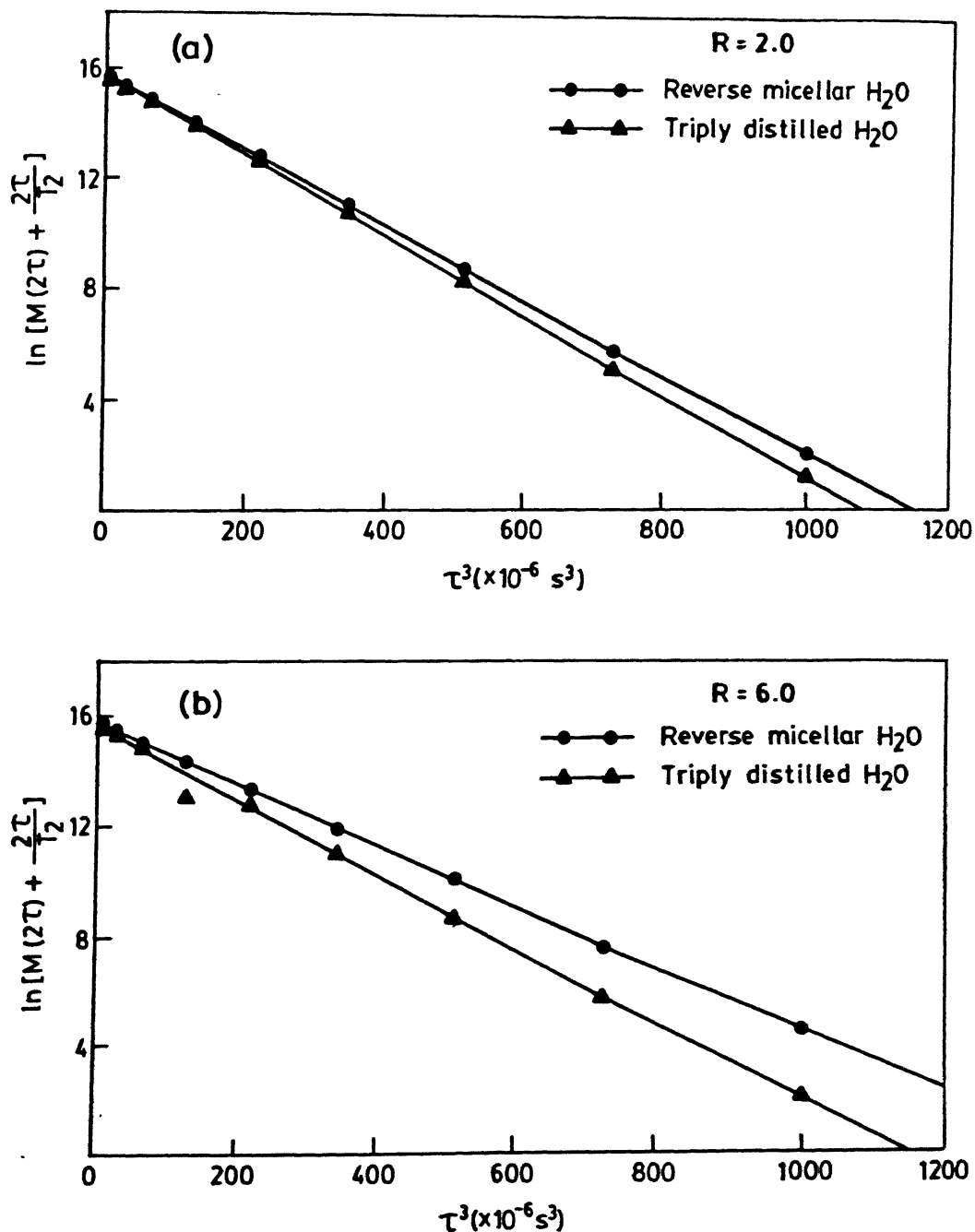


Fig.V.22 Spin echo amplitude versus τ^3 for lecithin/cyclohexane/ H_2O system.

- (a) $G = 3.6 \times 10^{-2} \text{ T/m}$; $D = (-\bullet-\bullet-) = (2.21 \pm 0.01) \times 10^{-9} \text{ m}^2/\text{s}$
- (b) $G = 3.5 \times 10^{-2} \text{ T/m}$; $D = (-\bullet-\bullet-) = (1.91 \pm 0.01) \times 10^{-9} \text{ m}^2/\text{s}$

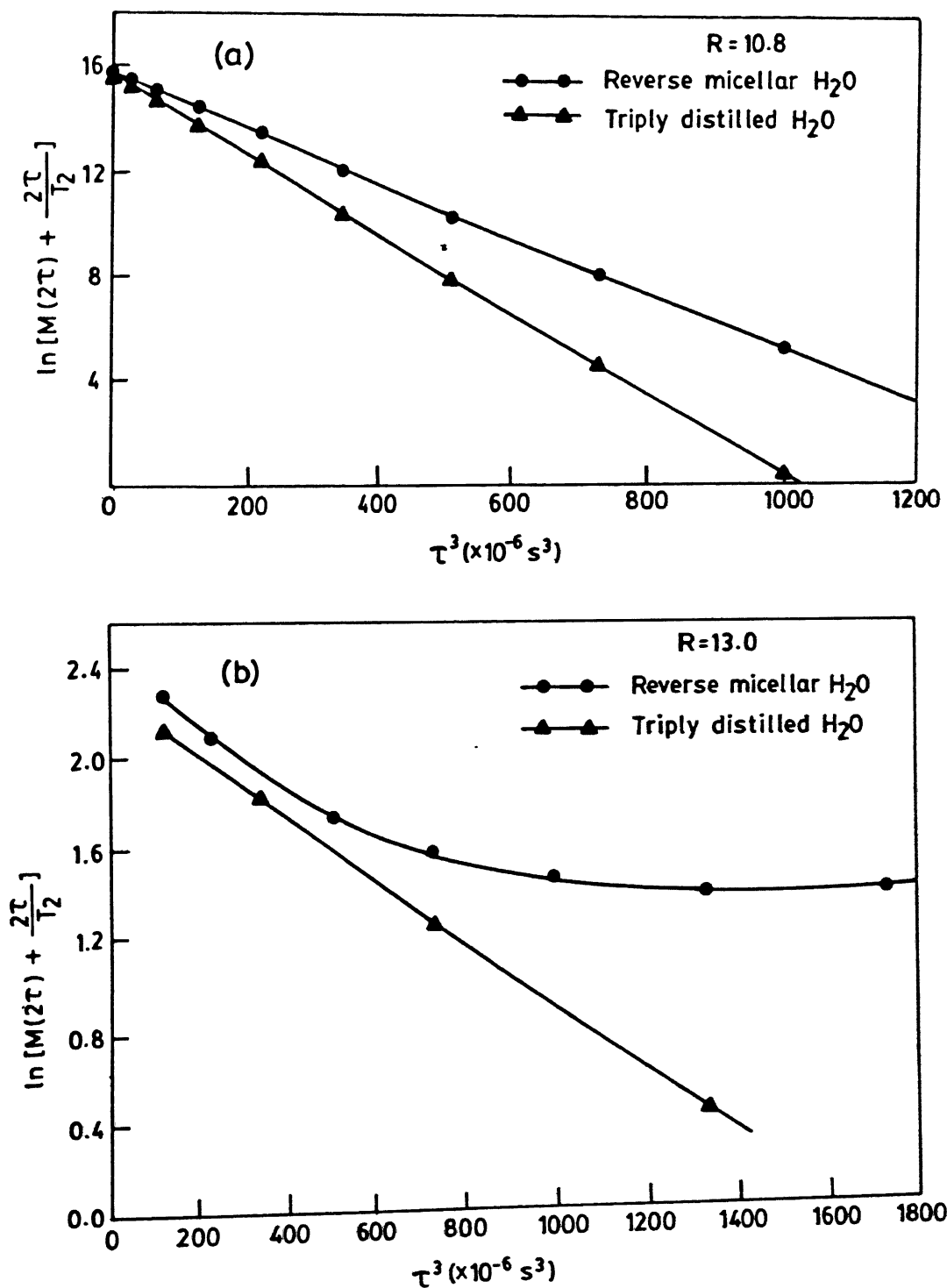


Fig.V.23

Spin echo amplitude versus τ^3 for lecithin/cyclohexane/ H_2O system.

(a) $G = 3.7 \times 10^{-2} \text{ T/m}$; $D = (-\bullet-\bullet-) = (1.61 \pm 0.02) \times 10^{-9} \text{ m}^2/\text{s}$

(b) The solid line represents the fit of eqn. [V.15] to the experimental data (o).

$G = 8.9 \times 10^{-2} \text{ T/m}$; $D = (-\bullet-\bullet-) = (1.43 \pm 0.03) \times 10^{-9} \text{ m}^2/\text{s}$

Table V.7 Variation of self-diffusion coefficient of water as a function of R for lecithin/cyclohexane/H₂O system.

R	D (10 ⁻⁹ m ² s ⁻¹)	$\frac{D}{D_0}$ (D ₀ = 2.35 X 10 ⁻⁹ m ² s ⁻¹)
1.0	2.23	0.95
2.0	2.21	0.94
4.3	2.16	0.92
6.0	1.91	0.81
8.6	1.80	0.77
10.8	1.61	0.69
13.0	1.42	0.60

The variation of relative self-diffusion coefficient D/D_0 versus R is pictorially represented in Fig. V.24. From this one sees that the water self-diffusion coefficient stays within 10% of that of free water upto an R value of 6.0, after which it decreased rather sharply. This confirms our earlier results⁽⁸⁸⁾, that in this reverse micellar system around an R value of six there is a transition from the isotropic reverse micellar to an anisotropic phase which affects the mobility of the water pool.

For water diffusion in a barrier-free system, the root mean square displacement of water molecule in, say, the x-direction, $\langle(\Delta x)^2\rangle^{1/2}$, occurring during time t is related to the self-diffusion coefficient, D, by the well-known Einstein relationship

$$\langle(\Delta x)^2\rangle^{1/2} = 2Dt$$

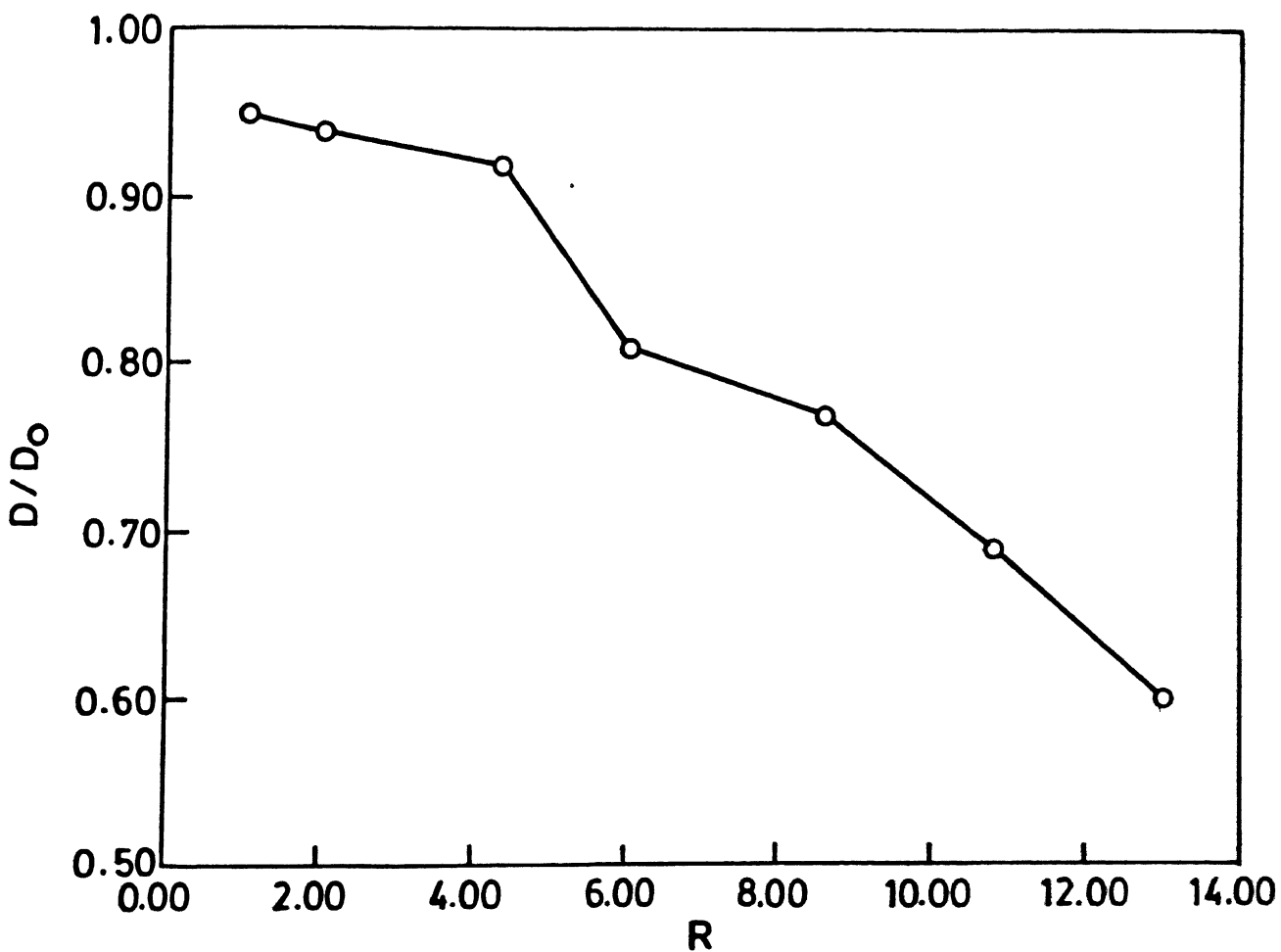


Fig.V.24

Variation of relative self-diffusion coefficient as a function of added water for lecithin/cyclohexane H_2O .

If barriers that hinder free motion are present, the measured value of D will of course be less than what it would be in the unhindered bulk fluid state. In theory, if 2τ can be made short enough (roughly less than the root mean square time for a molecule to diffuse between barriers or obstructions)^(93,94), NMR pulse techniques should yield a faithful measurement of D for the confined fluid.

Using the above analysis, if diffusion barriers are present and sufficiently close together, D becomes a function of the applied gradient and the echoes no longer decay as τ^3 ⁽⁹³⁾. For low R value cases ($R < 6$), the value of D in each case was constant when G^2 was varied by a factor of 20, and all the echo decays were linear in τ^3 to $2\tau \sim 25$ ms for the smallest gradient used. Hence, any barrier must be more than $[2D(25 \text{ ms})]^{1/2}$ apart, i.e. 10 microns apart. This is in agreement with the estimates of the upper limit of micellar size by our electron microscopy experiments published earlier⁽⁸⁸⁾.

The linear least squares fit plots of $\ln \left[M(2\tau) + \frac{2\tau}{T_2} \right]$ versus τ^3 for lecithin/ $\text{CCl}_4/\text{H}_2\text{O}$ with different R values are shown in Figs. V.25 and V.26. The self diffusion coefficients for different R values and D/D_0 ratio are given in Table V.8 and the variation of D/D_0 versus R is shown in Fig. V.27.

Fig.V.27 shows that initially added water becomes tightly bound to the interface, and is then becoming released for more free diffusion or exchange with core water thus provides a dynamical contrast to the case of the corresponding cyclohexane-containing system.

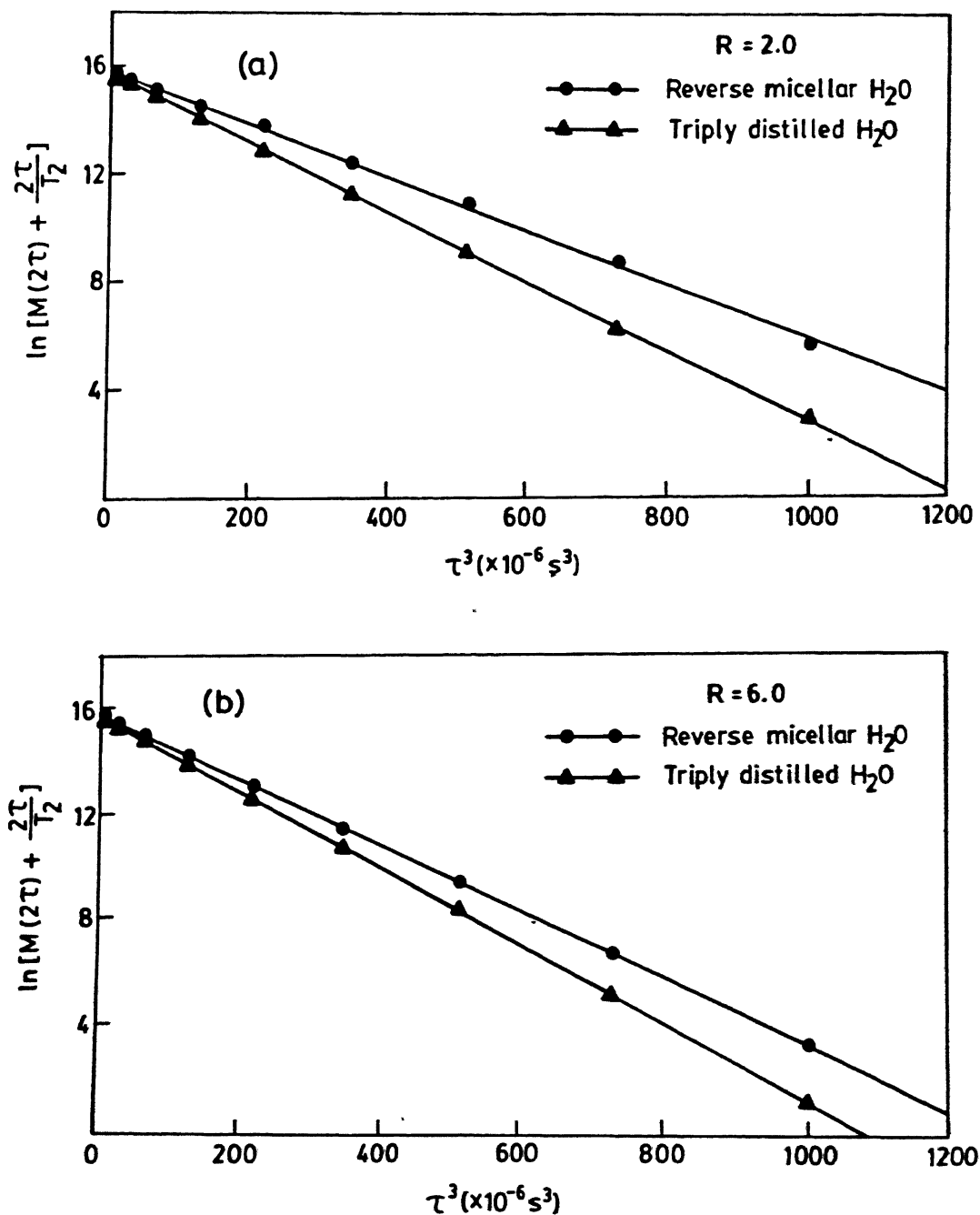


Fig.V.25 Spin echo amplitude versus τ^3 for lecithin/ $\text{CCl}_4/\text{H}_2\text{O}$ system.

- (a) $G = 3.3 \times 10^{-2} \text{ T/m}$; $D = (-\bullet-\bullet-) = (1.85 \pm 0.04) \times 10^{-9} \text{ m}^2/\text{s}$
- (b) $G = 3.6 \times 10^{-2} \text{ T/m}$; $D = (-\bullet-\bullet-) = (2.01 \pm 0.02) \times 10^{-9} \text{ m}^2/\text{s}$

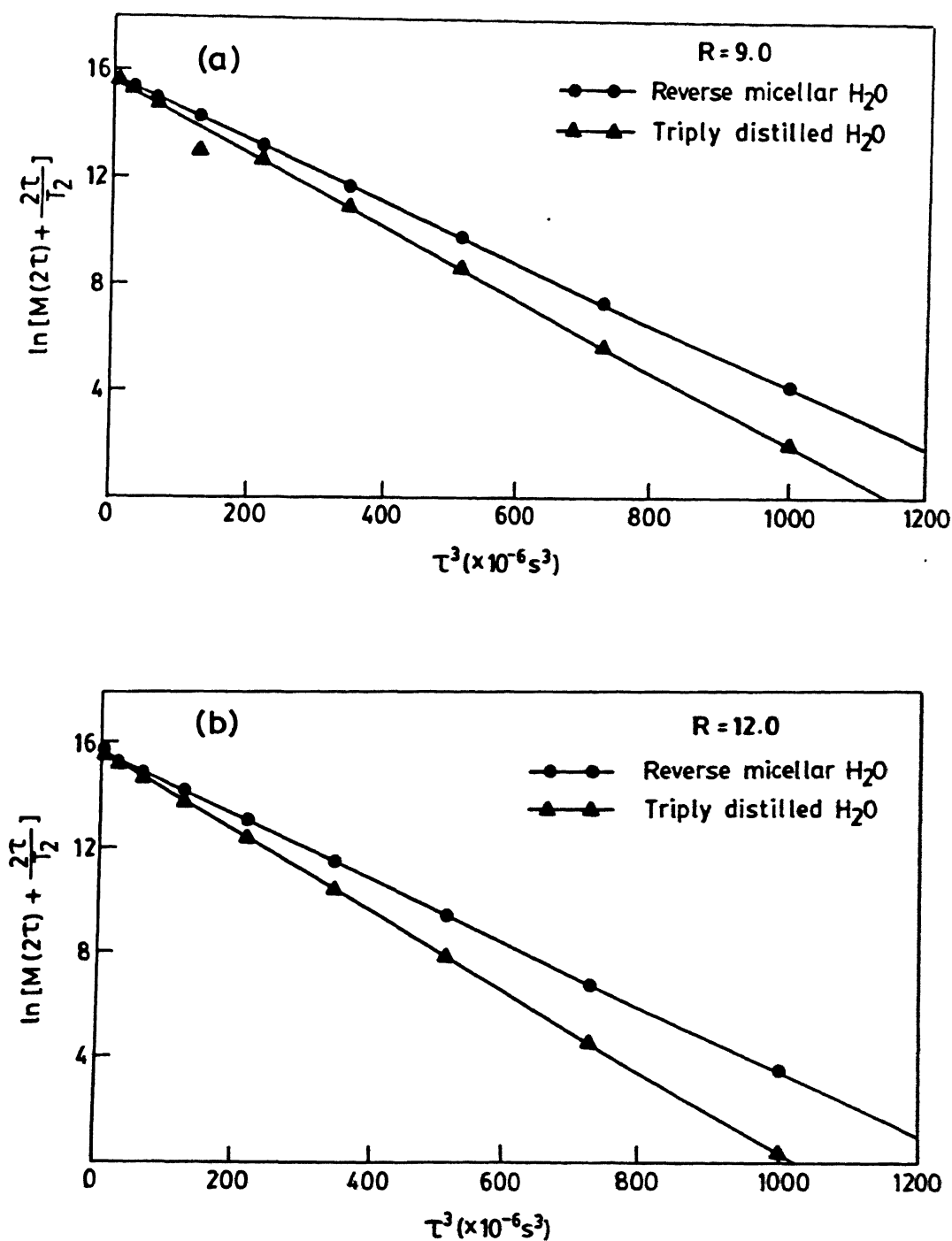


Fig.V.26 Spin echo amplitude versus τ^3 for lecithin/ $\text{CCl}_4/\text{H}_2\text{O}$ system.

- (a) $G = 3.5 \times 10^{-2} \text{ T/m}$; $D = (-\bullet-\bullet-) = (1.97 \pm 0.02) \times 10^{-9} \text{ m}^2/\text{s}$
- (b) $G = 3.7 \times 10^{-2} \text{ T/m}$; $D = (-\bullet-\bullet-) = (1.88 \pm 0.02) \times 10^{-9} \text{ m}^2/\text{s}$

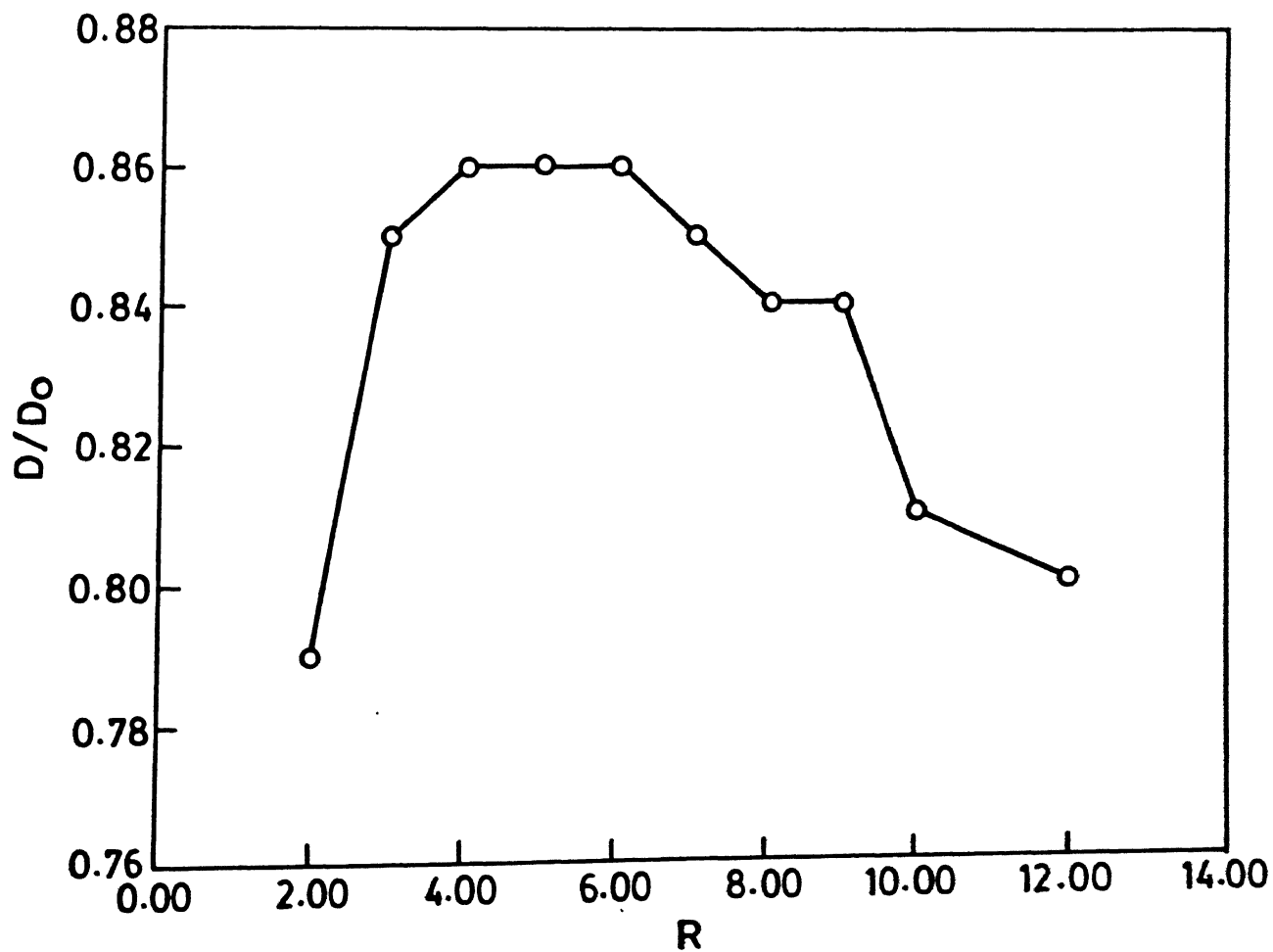


Fig.V.27

Variation of relative self-diffusion coefficient
as a function of added water for lecithin/ CCl_4 / H_2O

Table V.8 Variation of self-diffusion coefficients of water as a function of R for lecithin/ CCl_4 /water system

R	D	$\frac{D}{D_0}$
	$(10^{-9} \text{ m}^2 \text{ s}^{-1})$	$(D_0 = 2.35 \times 10^{-9} \text{ m}^2 \text{ s}^{-1})$
2	1.85	0.79
3	2.00	0.85
4	2.01	0.86
5	2.02	0.86
6	2.01	0.86
7	2.00	0.85
8	1.98	0.84
9	1.97	0.84
10	1.90	0.81
12	1.88	0.80

Although the above estimate of the diffusion of trapped water is somewhat crude, it should be mentioned here that more sophisticated NMR experiments such as the pulsed field gradient technique⁽⁷²⁾ as well as more recent experimental refinements such as (i) techniques for diffusion measurement in presence of small and large background gradients^(95,19) and (ii) methods for absolute measurement of D without recourse to a standard sample⁽⁹⁶⁾ should further improve our understanding of lecithin based reverse micellar systems.

V.8 Conclusions

1. We have demonstrated the successful construction of a versatile magnetic field gradient controller capable of generating continuous-linear, pulsed-linear and oscillating field gradient types.
2. Self-diffusion coefficients of water in lecithin based reverse micelles could not be measured using our magnetic field gradient controller owing to some practical difficulties experienced in performing PMFG spin echo experiments on the older BRUKER WP-80 FT NMR spectrometer. Nevertheless, the performance results of our gradient controller for two types of gradients have been illustrated.
3. The self-diffusion coefficients of H_2O in the lecithin/cyclohexane/ H_2O and lecithin/ CCl_4 / H_2O systems at a number of R values have been measured on a BRUKER B-KR 322s FT NMR spectrometer. The trend revealed by D/D_0 Vs R plots substantiates the earlier findings of our laboratory.

REFERENCES

1. P. Mansfield and P.G. Morris, **NMR Imaging in Biomedicine**, Supplement 2, Adv. Magn. Reson., J.S. Waugh(ed.), Academic Press, New York (1982).
2. H. Goldstein, **Classical Mechanics**, Addison-Wesley, Reading, Massachusetts (1950).
3. R. Gabillard, C.R. Acad. Sci. (Paris) **232**, 1551 (1951).
4. R. Gabillard, Rev. Sci. Paris **90**, 307 (1952).
5. H.Y. Carr and E.M. Purcell, Phys. Rev. **94**, 636 (1954).
6. R. Bradford, C. Clay, and E. Strick, Phys. Rev. **84**, 157 (1954).
7. J. Libove and J.R. Singh, J. Phys. E : Sci. Instrum. **14**, 702 (1981).
8. P.A. Bottomley, J. Phys. E : Sci. Instrum. **14**, 1052 (1981).
9. P.A. Bottomley, J. Phys. E : Sci. Instrum. **14**, 1081 (1981).
10. K.J. Wilson and C.P.G. Vallabhan, J. Phys. E : Sci. Instrum. **22**, 131 (1989).
11. R. Puvvada, S. Mekaoui, and M. Chemioul, Meas. Sci. Technol. **1**, 1247 (1990).
12. R. Kapitza, Proc. Roy. Soc. (London) **A105**, 691 (1924); *ibid*, **A115**, 658 (1927); *ibid*, **A119**, 358 (1928); *ibid* **A123**, 342 (1929); *ibid* **A131**, 224, 243 (1931); *ibid*, **A135**, 537, 556, 568 (1932).
- 13(a) S. Foner and H.H. Kolm, Rev. Sci. Instrum. **28**, 799 (1957).
- (b) D. Melville, D.L. Rayner, W.I. Khan, P.G. Mattocks, and K.M. Al-Rawi, J. Phys. E: Sci. Instrum. **14**, 611 (1981).
- (c) S. Takeyama, H. Ochimizu, S. Sasaki, and N. Miura, Meas. Sci. Technol **3** 662 (1992) and references cited therein.
14. A. G. Anderson, R.L. Garwin, E.L. Hahn, J.W. Horton, G.L. Tucker, and R.M. Walker, J. Appl. Phys. **26**, 1324 (1955).
15. D.W. McCall, D.V. Douglass, and E.W. Anderson, Ber. Bunsenges. Physik. Chem. **67**, 336 (1963).
16. E.O. Stejskal and J.E. Tanner, J. Chem. Phys. **42**, 288 (1965).
17. J.E. Tanner, Rev. Sci. Instrum. **36**, 1086 (1965).
18. B. Gross and R. Kosfeld, Messtechnik **7-8**, 171 (1969).

19. R.F. Karliceck and I.J. Lowe, J. Magn. Reson. 37, 75 (1980).
20. M.I. Hrovat, C.O. Britt, T.C. Moore, and C.G. Wade, J. Magn. Reson. 49, 411 (1982).
21. P.T. Callaghan, C.M. Trotter, and K.W. Jolley, J. Magn. Reson. 37, 247 (1980).
22. A. Kumar, D. Welte, and R. Ernst, J. Magn. Reson. 18, 69 (1975).
23. J.M.S. Hutchison, W.A. Edelstein, and G. Johnson, J. Phys. E: Sci. Instrum. 13, 947 (1980).
- 24(a) R. Turner and R.M. Bowley, J. Phys. E : Sci. Instrum. 19, 876 (1986)
- (b) T.A. Frenkiel, A. Jasinski, and P.G. Morris, J. Phys. E : Sci. Instrum. 21, 374 (1988)
- (c) T.R. Saarinen and W.S. Woodward, Rev. Sci. Instrum. 59, 761 (1988).
- (d) S. Pittard, M.E. Fry, R.E. Ellis, E.A. Moore, and W. Vennart, J. Phys. E. : Sci. Instrum. 22, 574 (1989).
- (e) G. Carlo de Nascimento, R. Emmanuel de Souza, and M. Engelsberg, J. Phys. E : Sci. Instrum. 22, 774 (1989).
- (f) P. Mansfield, P.R. Harvey, and R.J. Coxon, Meas. Sci. Technol. 2, 1051 (1991).
25. P.C. Lauterbur, Nature (London) 242, 190 (1973)
26. A.N. Garroway, P.K. Grannell, and P. Mansfield, J. Phys. C: 7, 457 (1974).
27. W.S. Hinshaw, Phys. Lett. A48, 87 (1974).
28. W.S. Hinshaw, Proceedings of the 18th Ampere Congress, Nottingham, P.S. Allen, E.R. Andrew, and C.A. Bates (eds.), North-Holland Publishing Co., Amsterdam (1975), Vol. 2, p. 433.
29. W.S. Hinshaw, J. Appl. Phys. 47, 3709 (1976).
30. F.T. Meiere and F.C. Thatcher, J. Appl. Phys. 50, 4491 (1979).
31. I. Shenberg and A. Macovski, IEEE Trans. Med. Imaging MI-4, 144 (1985).
32. P. Mansfield, J. Phys. C : 10, L55 (1977).
33. P. Mansfield and I.L. Pykett, J. Magn. Reson. 29, 355 (1978).
34. S. Ljunggren, J. Magn. Reson. 54, 165 (1983).

35. L.F. Feiner and P.R. Locher, Appl. Phys. 22, 257 (1980).
36. M.M. Tropper, J. Magn. Reson. 42, 193 (1981).
37. J. Frahm and W. Hänicke, J. Phys. E : Sci. Instrum. 17, 612 (1984).
38. A. Macovski, Magn. Reson. Med. 2, 29 (1985).
39. I. Shenberg and A. Macovski, IEEE Trans. Med. Imaging MI-4, 165 (1985).
40. S.J. Norton, IEEE Trans. Med. Imaging, MI-6, 21 (1987).
- 41(a) I. Shenberg and A. Macovski, IEEE Trans. Med. Imaging MI-5, 121 (1986).
- (b) S.D. Rand and A. Macovski, IEEE Trans. Med. Imaging MI-6, 346 (1987).
- (c) A. Maeda, K. Sano, and T. Yokoyama, IEEE Trans. Med. Imaging MI-7, 26 (1988).
- (d) S.D. Rand and A. Macovski, IEEE Trans. Med. Imaging MI-7, 99 (1988).
- (e) A. Maeda and T. Yokoyama, IEEE Trans. Med. Imaging MI-8, 8 (1989).
- (f) S.P. Cottrell, M.R. Halse, and J.H. Strange, Meas. Sci. Technol. 1, 624 (1990).
- (g) A. Zakhor, R. Weisskoff, and R. Rzedzian, IEEE Trans. Signal Process. 37, 2056 (1991).
- (h) D.C. Noll, C.M. Meyer, J.H. Pauly, D.G. Nishimura, and A. Macovski, IEEE Trans. Med. Imaging MI-10, 629 (1991).
- 42(a) P. Raghunathan, S. Krishnan, and K.R. Srivathsan, Proc. Ind. Acad. Sci. (Chem. Sci.) 95, 59 (1985).
- (b) A. Kasi Viswanathan and P. Raghunathan, Proc. Solid State Physics Symposium 34C, 441 (1991).
43. C.M. Lai, J.W. Shook, and P.C. Lauterbur, Chem. Biomed., and Environ. Instrumentation 9, 1 (1979).
- 44(a) P.C. Lauterbur, Nature (London) 242, 190 (1973).
- (b) P.C. Lauterbur, Pure Appl. Chem. 40, 149 (1974).
- (c) P.C. Lauterbur, in NMR in Biology, R.A. Dwek, I.D. Campbell, R.E. Richards, and R.J.P. Williams (eds.), Academic Press, London (1977).
45. C.M. Lai and P.C. Lauterbur, J. Phys. E :Sci. Instrum. 13, 747 (1980).

46. J.R. Fitzsimmons, *Rev. Sci. Instrum.* **53**, 1338 (1982).
47. S.S. Ray, Ph.D. Thesis, Indian Institute of Technology, Kanpur, India (1991).
48. K.J. Mysels and D. Stigter, *J. Phys. Chem.*, **57**, 104 (1953).
49. D. Stigter, R.J. Williams, and K.J. Mysels, *J. Phys. Chem.* **59** 330 (1955).
50. B. Lindman, P. Stilbs, and M.E. Moseley, *J. Colloid Interface Sci.* **83**, 569 (1980).
51. B. Lindman, N. Kamenka, T.M. Kathopoulis, B. Brun, and P.G. Nilsson, *J. Phys. Chem.* **84**, 2485 (1980).
52. B. Lindman, M.C. Puyal, N. Kamenka, B. Brun, and G. Gunnarsson, *J. Phys. Chem.* **86**, 1702 (1982).
53. P.G. Nilsson, H. Wennerström, B. Lindman, *J. Phys. Chem.* **87**, 1377 (1983).
54. B. Lindman, N. Kamenka, M.C. Puyal, B. Brun, and B. Jönsson, *J. Phys. Chem.* **88**, 53 (1984).
55. D. Chatenay, W. Urbach, C. Nicot, M. Vacher, and M. Waks, *J. Phys. Chem.* **91**, 2198 (1987).
56. M. Jansson, P. Linse, and R. Rymdén, *J. Phys. Chem.* **92**, 6689 (1988).
57. J.H. Wang, *J. Am. Chem. Soc.* **76**, 4775 (1954); T.L. James and K.T. Giller, *Biochim. Biophys. Acta* **286**, 10 (1972); E.E. Burnell, M.E. Clark, J.A.M. Hinke, and N.R. Chapman, *Biophys. J.* **33**, 1 (1981); E.D. Finch, J.F. Harmon, and B.H. Muller, *Arch. Biochem. Biophys.* **147**, 299 (1971); J.R. Hansen, *Biochim. Biophys. Acta* **230**, 482 (1971); D.C. Chang, C.F. Hazelwood, B.L. Nichols, and H.E. Roscharch, *Nature* **236**, 170 (1972); D.C. Chang, H.E. Roscharch, B.L. Nichols, and C.F. Hazelwood, *Ann. N.Y. Acad. Sci.* **204**, 434 (1973); H.E. Roscharch, D.C. Chang, C.F. Hazelwood, and B.L. Nichols, *Ann. N.Y. Acad. Sci.* **204**, 444 (1973).
58. K.P. Das, A. Ceglie, B. Lindman, and S.E. Friberg, *J. Colloid Interface Sci.* **116**, 390 (1987).
59. J.S. Anderson and K. Saddington, *J. Chem. Soc.* S381 (1949).
60. R.H. Stokes, *J. Am. Chem. Soc.* **72**, 763 (1950).
61. E.L. Hahn, *Phys. Rev.* **80**, 580 (1950).
62. M.M. Poo and R.A. Cone, *Nature (London)* **247**, 438 (1974).
63. F. Rondelez, in *Light Scattering in Liquids and Macromolecular Solutions*, V. Degiorgio, M. Corti, and M. Giglio (eds.), Plenum Press, Newyork (1980).

64. J.R. Lalanne, B. Pouligny, and E. Sein, *J. Phys. Chem.* **87**, 696 (1983).
65. F. Mazei, *Physica* **120**, 51 (1983).
66. H.J.V. Tyrrell and K.R. Harris, *Diffusion in Liquids*, Butterworths, London (1984); L. Costanbino, C.D. Volpe, O. Ortona, and V. Vitagliano, *J. Colloid Interface Sci.* **148**, 72 (1992).
67. A. Abragam, *Principles of Nuclear Magnetism*, Oxford University Press, London (1961), p. 59.
68. T.L. James, *NMR in Biochemistry*, Academic Press, New York (1975), p. 27.
69. H.Y. Carr and E.M. Purcell, *Phys. Rev.* **94**, 630 (1954).
70. S. Meiboom and D. Gill, *Rev. Sci. Instrum.* **29**, 688 (1958).
71. P.T. Callaghan, *Principles of Nuclear Magnetic Resonance Microscopy*, Clarendon Press, Oxford (1991), Chap. 3, p. 161.
72. E.O. Stejskal and E.J. Tanner, *J. Chem. Phys.* **49**, 288 (1965).
73. R.L. Vold, J.S. Waugh, M.P. Klein and D.E. Phelps, *J. Chem. Phys.* **48**, 3831 (1968).
74. T.L. James and G.G. McDonald, *J. Magn. Reson.* **11**, 58 (1973).
75. P. Stilbs and M.E. Moseley, *Chem. Scr.* **15**, 176 (1980); *ibid*, **15**, 215 (1980).
76. P. Stilbs, *J. Colloid Interface Sci.* **87**, 385 (1982); *ibid*, **94**, 463 (1983).
77. B. Lindman, N. Kamenka, M.C. Puyal, R. Rumsdén, and P. Stilbs, *J. Phys. Chem.* **88**, 5048 (1984).
78. P. Stilbs, *J. Colloid Interface sci.* **80**, 608 (1981); *ibid*, **87** 385 (1982); *ibid*, **94** 463 (1983); P. Stilbs, G. Arvidson, and G. Lindblom, *Chem. Phys. Lipids* **35**, 309 (1984).
79. P. Stilbs, *J. Colloid Interface Sci.* **89**, 547 (1982).
80. T. Bull and B. Lindman, *Mol. Cryst. Liq. Cryst.* **28**, 155 (1974); G. Lindblom, K. Larsson, L. Johansson, K. Fontell, and S. Forsén, *J. Am. Chem. Soc.* **101**, 5465 (1979).
81. P.G. Nilsson, H. Wennerström, and B. Lindman, *Chem. Scr.* **25** 67 (1985).
82. P. Stilbs, *Prog. NMR spectrosc.* **19**, 1 (1987).
83. G. Lindblom, *Acta Chem. Scand.* **B35**, 61 (1981).
84. C. Chachaty, *Prog. NMR Spectrosc.* **19**, 183 (1987).

85. K. Vos, C. Laane, and A.J.W.G. Visser, *Photochem. Photobiol.* 45, 863 (1987).
86. B. Lindman and P. Stilbs, in *Microemulsions : Structure and Dynamics*, S.E. Friberg and P. Bothorel (eds.), CRC Press, Florida (1987), Chap. 5.
87. V.V. Kumar, P.T. Manoharan, and P. Raghunathan, *J. Biosci.* 4, 449 (1982).
88. V.V. Kumar, C. Kumar, and P. Raghunathan, *J. Colloid Interface Sci.* 99, 315 (1984).
89. V.V. Kumar and P. Raghunathan, *Chem. Phys. Lipids* 41, 159 (1986).
90. R. Blinc, M. Burgar, M. Luzar, J. Pirs, I. Zupancic, and S. Zumer, *Phys. Rev. Lett.* 33, 1192 (1974).
91. D.G. Hughes, *J. Magn. Reson.* 26, 481 (1977).
92. T.L. Isenhour and P.C. Jurs, *Introduction to Computer Programming for Chemists*, Allyn and Bacon, Boston (1972), p. 278.
93. R.C. Wayne and R.C. Cotts, *Phys. Rev.* 151, 264 (1964) and references cited therein.
94. D.E. Woessner, *J. Phys. Chem.* 67, 1365 (1963).
95. W.D. Williams, E.F.W. Seymour, and R.F. Cotts, *J. Magn. Reson.* 31, 271 (1978).
96. M.I. Hrovath and C.G. Wade, *J. Chem. Phys.* 73, 2509 (1980).

CHAPTER VI

OVERALL CONCLUSIONS AND FURTHER PROSPECTS

We shall now summarize the principal findings of our work.

- (1) We have prepared a novel and potentially valuable new reverse micellar system, and have characterized it by ^1H and ^{31}P NMR spectroscopy.
- (2) From our neutron magnetic resonance measurements, we have been able to interpret our result in terms of two motionally distinct sites for D_2O molecules (i.e., 'two-site' model) present in DCC-added and DCC-free reverse micelles over a range of R-values. We have also observed a thousand fold reduction in the exchange rate of water molecules between these two sites while going to a lower temperature.
- (3) The manifestation of cross-relaxation terms, and the importance of including them in a detailed description of motional and structural parameters of aggregated structures, have been investigated with special reference to the DOC reverse micelles.
- (4) By way of advancing the overall NMR instrumentation capabilities of our laboratory, we have accomplished the construction of a versatile magnetic field gradient controller. Its performance for two types of gradients have been illustrated using water samples.
- (5) The measured self-diffusion coefficients of H_2O in egg-lecithin based reverse micelles in different organic solvents show that initially added water becomes tightly

bound to the interface, and is then becoming gradually released for more free diffusion or exchange with core water.

During the course of our studies, various other interesting experimental possibilities suggested themselves. We document some of these as further research prospects.

- (1) It would be interesting to study the phase behavior of our reverse micellar system lecithin/DCC/Cyclohexane by constructing a four component phase diagram at different temperatures.
- (2) The indication of structural changes occurring between R values of 5 and 6 in this system may be further verified visually by recording transmission electron micrographs. For example, in dissolving a suitable electron impermeable stain in the aqueous core.
- (3) The freezing points of different types of water present in the reverse micelles can be measured by performing low-temperature differential scanning calorimetry (DSC) experiments.
- (4) During the course of our theoretical investigations, we have realized the mathematical complexity of handling A_9 coupled spin systems. Further theoretical efforts at simplifying this mathematical problem may perhaps be worthwhile for a better understanding of lecithin polar head group dynamics in reverse micelles.

APPENDIX

```

C -----
C DEUTERIUM LINESHAPE SIMULATION PROGRAM
C FILE NAME NEW.F
C INPUTS:OMGAQ1,OMGAQ2,RK12,RK21,T21,T22,TAU,STEP,FINT,VARI
C OMGAQ1=QUADRUPOLEAR FREQUENCY-SITE 1
C OMGAQ2=QUADRUPOLEAR FREQUENCY -SITE 2
C RJUMP=RATE OF EXCHANGE OF MOLECULES FROM ONE SITE TO ANOTHER
C T21=T2 FOR THE SITE 1 MOLECULES
C T22=T2 FOR THE SITE 2 MOLECULES
C NSTEP=NO. OF OMEGA VALUES CHOOSSEN
C HALFDEL=ONE HALF OF THE DELDA OMEGA
C NTHETA=NO. OF THETA VALUES CHOOSSEN
C QCC=QUAD. COUPLING CONST. (E**2*Q*Q/H)
C -----
C PARAMETER XYD=500
C COMPLEX AA,BB,CC,DETS,J(2),LAMDA(2),R(2,2),RLAMDA(2,2),
1 S(2,2),S2(2,2),S3(2,2),S4(2,2),S5(2,2),SINVER(2,2),SUM,TOTAL
C REAL OMGAIN,OMGAFI,OMGAQ1,OMGAQ2,P(2),PERINB,STEP,TAU,
1 T21,T22,XAXIS(XYD),YAXIS(XYD)
C INTEGER N,LDA,LDEVEC
C COMMON/AREA1/N,LDA,LDEVEC
C OPEN(UNIT=21,FILE='XY.O')
C OPEN(UNIT=20,FILE='DLINS.OUT')
C OPEN(UNIT=19,FILE='DLINS.IN')
C READ(19,*) T21,T22,RJUMP
C READ(19,*) TAU
C READ(19,*)NSTEP,HALFDEL,NTHETA,QCC
C -----
C DO 2000 VARI=1,NSTEP
C YAXIS(VARI)=0.0
C XAXIS(VARI)=0.0
2000 CONTINUE
C N=2
C LDA=2
C LDEVEC=2
C T=2.0*TAU
C PI=4.0*ATAN(1.0)
C PIFACT=PI/180.0
C COUCON=QCC*3.14*3/4.0
C DVARI=90.0/NTHETA
C THETA=0.0
C A=RK21+1.0/T21
C B=RK12+1.0/T22
C DO 1000 LOOP=1,NTHETA
C THERAD1=THETA*PIFACT
C THERAD2=(104.0-THETA)*PIFACT
C COSTH1=COS(THERAD1)
C COH2H2=COS(THERAD2)
C COSSQ1=COSTH1*COSTH1
C COSSQ2=COSTH2*COSTH2
C OMGAQ1=COUCON*(3*COSSQ1-1)
C OMGAQ2=COUCON*(3*COSSQ2-1)
C R(1,1)=CMPLX(A,OMGAQ1)
C R(1,2)=CMPLX(-RJUMP,0.0)
C R(2,1)=CMPLX(-RJUMP,0.0)
C R(2,2)=CMPLX(B,OMGAQ2)
C -----

```

```

C      THE ECHO INTENSITY E IS COMPUTED AS:
C
C      *
C      E=1.J=1.EXP(-R TAU)(EXP(-R TAU)) P
C      EXP(R TAU)=S EXP(LAMDA TAU) S(INVERSE).
C      -----
CALL EIGEN(R,LAMDA,S,PERIND)
RLAMDA(1,1)=CEXP(-LAMDA(1)*TAU)
RLAMDA(2,2)=CEXP(-LAMDA(2)*TAU)
RLAMDA(1,2)=(0.0,0.0)
RLAMDA(2,1)=(0.0,0.0)
CALL MTMLCC(S,RLAMDA,S2)
CALL INVERS(S,SINVER,DETS)
CALL MTMLCC(S2,SINVER,S3)
CALL CMPCON(S3,S4)
CALL MTMLCC(S3,S4,S5)
P(1)=1
P(2)=1
CALL MTMLCR(S5,P,J)
OMGAZO=61.0E6
OMGAIN=OMGAZO-HALFDEL
OMGAFI=OMGAZO+HALFDEL
OMEGA=(OMGAIN-OMGAZO)
STEP=(OMGAFI-OMGAIN)/NSTEP
DO 200 MM=1,NSTEP
TOTAL=(0.0,0.0)
DO 300 I=1,2
DO 300 L=1,2
DO 300 K=1,2
AA=S(I,K)*LAMDA(K)*SINVER(K,L)
BB=OMEGA*OMEGA+LAMDA(K)*LAMDA(K)
CC=(AA/BB)*J(L)
TOTAL=TOTAL+CC
300 CONTINUE
XAXIS(MM)=OMEGA
YAXIS(MM)=REAL(TOTAL)+YAXIS(MM)
OMEGA=OMEGA+STEP
200 CONTINUE
THETA=THETA+DVARI
1000 CONTINUE
WRITE(20,10)R
10  FORMAT(1X,'R-MATRIX',//,1X,4(E11.3,E11.3))
WRITE(20,20)LAMDA
20  FORMAT(1X,'LAMDA-EIGEN VALUES',//,1X,2(E11.3,E11.3))
WRITE(20,30)S
30  FORMAT(1X,'S-EIGEN VECTORS',//,1X,4(E11.3,E11.3))
WRITE(20,40)RLAMDA
40  FORMAT(1X,'RLAMDA',//,1X,4(E11.3,E11.3))
WRITE(20,50)S2
50  FORMAT(1X,'S2',//,1X,4(E11.3,E11.3))
WRITE(20,60)SINVER
60  FORMAT(1X,'SINVER',//,1X,4(E11.3,E11.3))
WRITE(20,70)DETS
70  FORMAT(1X,'DETS',//,1X,2E11.3)
WRITE(20,80)S3
80  FORMAT(1X,'S3',//,1X,4(E11.3,E11.3))
WRITE(20,90)S4
90  FORMAT(1X,'S4',//,1X,4(E11.3,E11.3))
WRITE(20,110)S5
110 FORMAT(1X,'S5',//,1X,4(E11.3,E11.3))
WRITE(20,120)P

```

```

120  FORMAT(1X,'P',//,1X,2F3.1)
    WRITE(20,130)J
130  FORMAT(1X,'J',//,1X,2(E11.3,E11.3))
    WRITE(20,140)OMGAIN,OMGAFI
140  FORMAT(1X,'OMGAIN,OMGAFI',//,1X,2E15.4)
    DO 155 I=1,NSTEP
    WRITE(21,*)XAXIS(I),YAXIS(I)
    WRITE(20,*)XAXIS(I),YAXIS(I)
155  CONTINUE
C    WRITE(21,*)NSTEP
    WRITE(20,*)NSTEP,MM
    STOP
    END

C    -----
C    EIGEN(R,LAMDA,S,PERIND)
C    THIS GIVES EIGEN VALUES IN 'LAMDA' AND EIGENVECTORS IN 'S'
C    EIGENVECTORS ARE NORMALISED
C    IN THIS SUBROUTINE 'EVCCG' IS AN 'IMSL' ROUTINE
C    -----

    SUBROUTINE EIGEN(R,LAMDA,S,PERIND)
    COMMON/AREA1/N,LDA,LDEVEC
    COMPLEX R(2,2),LAMDA(2),S(2,2)
    INTEGER NOUT
    EXTERNAL EPICG,EVCCG,UMACH,WRCRN
    CALL EVCCG(N,R,LDA,LAMDA,S,LDEVEC)
    PERIND=EPICG(N,N,R,LDA,LAMDA,S,LDEVEC)
    CALL UMACH(2,NOUT)
C    CALL WRCRN('EVAL',1,N,LAMDA,1,0)
C    CALL WRCRN('EVEC',N,N,S,LDEVEC,0)
C    WRITE(NOUT,'(/,R,F6.3)') 'PERFORMANCE INDEX = ',PERIND
    RETURN
    END

C    -----
C    INVERS(A,AINVER)
C    TO FIND INVERSE OF A MATRIX 'A'
C    -----

    SUBROUTINE INVERS(A,AINVER,DETS)
    COMPLEX A(2,2),AINVER(2,2),DETS
    DETS=A(1,1)*A(2,2)-A(1,2)*A(2,1)
    AINVER(1,1)=(1/DETS)*A(2,2)
    AINVER(1,2)=-(1/DETS)*A(1,2)
    AINVER(2,1)=-(1/DETS)*A(2,1)
    AINVER(2,2)=(1/DETS)*A(1,1)
    RETURN
    END

C    -----
C    CMPCON(A,B)
C    TO FIND COMPLEX CONJUGATE OF A
C    -----

    SUBROUTINE CMPCON(A,B)
    COMPLEX A(2,2),B(2,2),CONJG
    DO 100 I=1,2
    DO 100 J=1,2
    B(I,J)=CONJG(A(I,J))
100  CONTINUE
    RETURN
    END

C    -----
C    MTMLCC(A,B,C)

```

C MATRIX MULTIPLICATION COMPLEX.COMPLEX

C -----
 SUBROUTINE MTMLCC(A,B,C)
 COMPLEX A(2,2),B(2,2),C(2,2)
 DO 100 I=1,2
 DO 100 J=1,2
 C(I,J)=(0.0,0.0)
 DO 100 K=1,2
 C(I,J)=C(I,J)+A(I,K)*B(K,J)
100 CONTINUE
 RETURN
 END

C -----
 MTMLCR(A,B,C)
 MATRIX MULTIPLICATION COMPLEX.REAL

 SUBROUTINE MTMLCR(A,B,C)
 COMPLEX A(2,2),C(2)
 REAL B(2)
 DO 100 I=1,2
 C(I)=(0.0,0.0)
 DO 100 K=1,2
 C(I)=C(I)+A(I,K)*B(K)
100 CONTINUE
 RETURN
 END